

Experimental Assessment with Wind Turbine
Emulator of Variable-Speed Wind Power
Generation System using Boost Chopper
Circuit of Permanent Magnet Synchronous
Generator

By

Sirichai Tammaruckwattana

A thesis submitted in partial fulfilment for the requirements of
the degree of Ph.D. (by Research) at the
Fukuoka Institute of Technology

November, 2014

ABSTRACT

This thesis verifies the performance of a Variable-Speed Wind Power Generation System (VSWPGS) using Permanent Magnet Synchronous Generator (PMSG) and Boost Chopper Circuit (BCC) experimentally. The assessments are conducted with a test bench using a Wind Turbine Emulator (WTE). The WTE reproduces the shaft torque of a wind turbine (WT) for an arbitrary wind velocity by the servo motor drives. The shaft-torque reference of servo motor drive is estimated in real time based on the blade element momentum theory (BEMT) by using windmill wing profiles, wind velocity data, and windmill rotational speed. Also the difference of inertia between the WT and the servo motor is compensated simultaneously. The WTE is newly-proposed for the experimental assessment. The tested VSWPGS using BCC has three speed control modes to the wind velocity. By combining the three control modes, the VSWPGS using BCC can extend the variable speed range more than conventional control methods. The experimental assessments shows that the VSWPGS using the BCC can reduce the costs while improving the reliability of the whole system, and has the same performance as the VSWPGS using a PWM converter of benchmark.

主論文の要旨

本論文は、永久磁石同期発電機（PMSG）を前提とする昇圧チョッパ回路（BCC）を用いる可変速風力発電システム（VSWPGS）の実機検証を行う。実機検証は、風車エミュレータ（WTE）を使用するテストベンチによって行う。WTEは、サーボモータドライブにより任意の風速に対する風車タービン（WT）の軸トルクを再現する。サーボモータドライブに与える軸トルク指令は、翼素運動量理論に基づいて、風車翼プロファイル、風速データ、そして風車回転速度からリアルタイムに演算され、同時にサーボモータとWTのイナーシャの違いも補償される。WTEは実機検証のために新規に提案するものである。実機検証するBCCを用いるVSWPGSは、風速に応じた3つの制御モードを有する。3つの制御モードを組み合わせることにより、BCCを用いるVSWPGSは、従来の制御方式よりも可変速範囲を広げることができる。実機検証により、BCCを用いたVSWPGSが、システム全体の信頼性を向上させつつコスト削減を達成し、ベンチマークであるPWMコンバータを用いるVSWPGSと同等の性能を有することを示す。

CONTENTS

| | |
|---|-------------|
| Acknowledgements..... | VIII |
| List of Abbreviations..... | IX |
| List of Figures..... | XI |
| List of Tables..... | XVII |
| | |
| Chapter 1: Introduction..... | 1 |
| 1.1 Background introduction | 1 |
| 1.2 Aims and objectives..... | 3 |
| 1.3 Structure of thesis..... | 5 |
| | |
| Chapter 2: Operation principle of the variable-speed wind power generation system..... | 7 |
| 2.1 Introduction..... | 7 |
| 2.2 Wind turbine control for grid connection..... | 8 |
| 2.2.1 Direct-coupled generator..... | 8 |
| 2.2.2 Doubly-fed induction generator (DFIG)..... | 9 |
| 2.2.3 Fully rated converter..... | 10 |

CONTENTS

| | |
|--|-----------|
| 2.2.4 AC/DC Rectifier and DC/ DC converter | 11 |
| 2.2.5 Comparison between Direct Torque Control and Field Oriented Control..... | 14 |
| 2.3 System configuration..... | 16 |
| 2.4 Boost chopper scheme..... | 16 |
| 2.5 back to back PWM converter scheme..... | 19 |
| 2.6 Summary..... | 20 |
| | |
| Chapter 3: Assessment with simulation of the variable speed wind power generation system..... | 21 |
| 3.1 Modeling method..... | 21 |
| 3.2 Windmill model..... | 22 |
| 3.3 Pitch angle control system..... | 31 |
| 3.4 Mechanical model for wind turbine..... | 32 |
| 3.5 Mechanical model for wind turbine emulator..... | 34 |
| 3.6 PMSG and converter main circuit..... | 36 |
| 3.6.1 Modeling of boost chopper method..... | 37 |
| 3.6.2 Modeling of PWM converter method..... | 51 |
| 3.7 Mechanical system..... | 52 |
| 3.8 DC link division..... | 53 |
| 3.8.1 Modeling of boost chopper method..... | 53 |
| 3.8.2 Modeling of PWM converter method..... | 57 |
| 3.9 Converter control system..... | 59 |

CONTENTS

| | |
|--|-----------|
| 3.9.1 Modeling of boost chopper method..... | 59 |
| 3.9.2 Modeling of PWM converter method..... | 62 |
| 3.10 Power system and inverter main circuit..... | 65 |
| 3.11 Inverter control system..... | 66 |
| 3.11.1 Modeling of boost chopper method..... | 67 |
| 3.11.2 Modeling of PWM converter method..... | 70 |
| 3.12 MATLAB Simulink model of the Boost chopper method..... | 71 |
| 3.12.1 PI gain of the boost chopper scheme..... | 72 |
| 3.13 MATLAB Simulink model of the PWM converter method..... | 77 |
| 3.13.1 PI gain of the PWM converter scheme..... | 78 |
| 3.14 Simulation results of the Boost chopper method..... | 83 |
| 3.15 Simulation results of the PWM converter method..... | 89 |
| 3.16 Summary..... | 94 |
| | |
| Chapter 4: Wind Turbine Emulator..... | 95 |
| 4.1 Wind turbine emulator..... | 95 |
| 4.2 Blade element momentum theory..... | 97 |
| 4.3 Airfoil profiles..... | 99 |
| 4.3.1 Fluid analysis using finite element method software ANSYS.... | 99 |
| 4.3.2 Analysis results due to the ANSYS..... | 100 |
| 4.4 Mechanical model..... | 109 |
| 4.5 System configuration of WTE..... | 110 |
| 4.6 Experimental system of real wind turbine (PWM converter scheme)..... | 111 |

CONTENTS

| | |
|---|------------|
| 4.7 Experimental system of wind turbine emulator (PWM converter scheme) | 113 |
| 4.8 Change of the wind velocity of wind turbine emulator. (PWM converter scheme)..... | 115 |
| 4.9 Experimental results of wind turbine emulator (PWM converter scheme). | 116 |
| 4.10 Simulation results of wind turbine model (PWM converter Scheme).... | 124 |
| 4.11 Natural wind velocity of real wind turbine (PWM converter scheme)... | 132 |
| 4.12 Experimental results of real wind turbine (PWM converter scheme).... | 133 |
| 4.13 Experimental results of wind turbine emulator (PWM converter scheme)..... | 137 |
| 4.14 Summary..... | 141 |
| | |
| Chapter 5: Experimental assessment of variable speed wind power generation system..... | 142 |
| 5.1 Performance evaluation scheme..... | 142 |
| 5.2 Experimental system of wind turbine emulator (Boost chopper scheme)... | 142 |
| 5.3 Experimental system of wind turbine emulator (PWM converter scheme). | 144 |
| 5.4 Phase locked loop (PLL) control system..... | 146 |
| 5.5 Laboratory prototype..... | 147 |
| 5.6 Structure of wind turbine emulator..... | 148 |
| 5.7 Structure of real wind turbine..... | 149 |
| 5.8 Experimental results of wind turbine emulator (Boost chopper scheme)... | 150 |
| 5.9 Experimental results of wind turbine emulator (PWM converter scheme). | 158 |
| 5.10 Experimental system of real wind turbine (Boost chopper scheme)..... | 166 |
| 5.11 Experimental results of real wind turbine (Boost chopper scheme)..... | 168 |
| 5.12 Experimental results of wind turbine emulator (Boost chopper scheme). | 173 |
| 5.13 The each element of the system..... | 177 |

CONTENTS

| | |
|--|------------|
| 5.13.1 Boost chopper scheme..... | 177 |
| 5.13.2 PWM converter scheme..... | 177 |
| 5.14 Summary..... | 179 |
| Chapter 6: Conclusion and Discussion..... | 180 |
| 6.1 Conclusion and Discussion..... | 181 |
| References..... | 182 |
| Appendix-A FPGA control for PWM converter..... | 192 |
| Appendix-B FPGA control for boost chopper scheme..... | 199 |
| Appendix-C Rotary Encoder Parameter..... | 207 |
| Appendix-D MWINV-4R222..... | 208 |
| Appendix-E Anemometer CYG-5103VM..... | 209 |

Acknowledgements

I would like to express my sincere thanks to my thesis adviser, Prof. Kazuhiro Ohyama for his invaluable help and constant encouragement throughout the course of this research. I am most grateful for his teaching and advice, not only the research methodologies but also many other methodologies in life.

I would also like to extend my thanks to the technicians of the laboratory of the manufacturing center department for their help in offering me the resources in research. And my thanks go to all research colleagues, in Ohyama laboratory for harmonious atmosphere.

I would also like to extend my thanks to the Royal Thai Government Scholarship for Science and Technology, Ministry of Science and Technology for their support throughout my study.

I would like to express my gratitude to the authority and all members of staff at the Fukuoka Institute of Technology for the support and opportunity they provided for me to be a student of the institution. I am proud of you all.

Finally, I wish to thank my parents for their support and encouragement throughout my study.

List of Abbreviations

| | |
|------|---|
| AC | Alternating Current |
| BEMT | Blade Element Momentum Theory |
| BCC | Boost Chopper Circuit |
| DSP | Digital Signal Processing |
| DC | Direct Current |
| FPGA | Field Programmable Gate Array |
| FEM | Finite Element Method |
| IGBT | Insulated Gate Bipolar Transistor |
| NACA | National Advisory Committee for Aeronautics |
| PMSG | Permanent Magnet Synchronous Generator |
| PWM | Pulse Width Modulation |
| WTE | Wind Turbine Emulator |

List of Symbols

| | |
|--------------------------|---|
| V_0 | rotor inflow wind speed [m/s] |
| u | wind speed before passing the rotor [m/s] |
| u_1 | wind speed after passing the rotor [m/s] |
| R | rotor radius [m] |
| Ω | rotor angular speed [rad/s] |
| θ | blade pitch angle [rad] |
| W | blade inflow wind speed [m/s] |
| ϕ | inflow angle [rad] |
| α | meeting angle [rad] |
| L | lift |
| D | drag |
| a, a' | interference factor |
| c | wind of code [m] |
| v_{au}, v_{av}, v_{aw} | armature voltages |
| i_{au}, i_{av}, i_{aw} | armature currents |
| e_{au}, e_{av}, e_{aw} | speed electromotive forces for permanent magnet field |
| R_a | armature winding resistance |
| L_a' | self-inductance of armature winding |

List of Symbols

| | |
|------------------|---|
| M_a' | mutual inductance of armature winding |
| ω_{ge} | rotor angular speed (electrical angle) |
| θ_{ge} | rotor position (electrical angle) |
| p | time derivative operator |
| R | line resistance of power system |
| L_s | line inductance of power system |
| ω_s | angular frequency of power system |
| i_{sd}, i_{sq} | dq -axis current for inverter side [A] |
| ω_s | grid system angular frequency [rad/s] |
| L_s | line inductance [H] |
| i_{sd}, i_{sq} | dq -axis current for inverter side [A] |
| V_{sd}, V_{sq} | dq -axis voltage for inverter side [V] |
| R_s | line resistance [W] |
| e_{sd} | dq transform of inverter side |
| Q | The generated torque of the wind turbine side |
| T_g | The generated torque of the generator side |
| T_1 | The shaft torque of the wind turbine side |
| T_2 | The shaft torque of the generator side |
| ω_t | The rotor rotational angular speed of wind turbine side |
| ω_g | The rotor rotational angular speed of generator side |
| B_t | The viscous friction coefficient of the wind turbine side |
| B_g | The viscous friction coefficient of the generator side |
| J_t | The moment of inertia of the wind turbine side |
| J_g | The moment of inertia of the generator side |
| T_{im} | The generated torque of the induction motor side |
| T_{1im} | The shaft torque of the induction motor side |

List of Symbols

| | |
|---------------|---|
| ω_{im} | The rotor rotational angular speed of induction motor side |
| B_{im} | The viscous friction coefficient of the induction motor side |
| J_{im} | The moment of inertia of the induction motor side |
| i_{dc1} | Current flowing through the diode bridge rectifier circuit [A] |
| D_{U1} | Diode maximum voltage side of the diode bridge rectifier circuit |
| D_{V2} | Diode minimum voltage side of the diode bridge rectifier circuit |
| L_{dc} | Inductance of the step-up chopper circuit [H] |
| r_L | Resistance of inductance itself of the step-up chopper circuit [Ω] |
| Tr | Switch of the boost chopper circuit |
| r_T | Switching resistance [Ω] |
| D | Diode of the boost chopper circuit |
| r_D | Resistance of the diode itself of the boost chopper circuit [Ω] |
| C_{dc} | DC link capacitor [F] |
| R_{dc} | DC link resistance [Ω] |
| V_{dc} | DC link voltage [V] |
| Q | generated torques for windmill |
| T_g | generated torques for PMSG sides |
| T_1 | shaft torques for windmill |
| T_2 | shaft torques for PMSG sides |
| ω_g | Rotor angular speed (mechanical angle) |
| B_t | Viscous friction coefficient for windmill |
| B_m | Viscous friction coefficient for PMSG sides |
| J_t | moments of inertia for windmill |
| J_m | moments of inertia for PMSG sides |
| n_1/n_2 | gear ratio. |
| T_g | generator torque [Nm] |
| P | stator pole |
| Φ_{fa} | stator flux [Wb] |
| i_{aq} | q -axis current [A] |
| ω_g | generator speed [rad/s] |
| T_g | generator torque [Nm] |

List of Symbols

| | |
|------------------|---|
| J_m | PMSG moment of inertia [kgm^2] |
| J_t | windmill moment of inertia [kgm^2] |
| B_m | coefficient of viscosity for PMSG [$\text{Nm}/(\text{rad/s})$] |
| B_t | coefficient of viscosity for wind turbine [$\text{Nm}/(\text{rad/s})$]. |
| i_{ad}, i_{aq} | dq -axis current [A] |
| ω_{ge} | angular velocity of the field (electrical angle) [rad/s] |
| L_a | stator inductance [H] |
| V_{ad}, V_{aq} | dq -axis voltage [V] |
| R_a | stator resistance [W] |
| v_{ad}, v_{aq} | dq -axis voltage [V] |

List of Figures

| | | |
|------------|--|----|
| Figure 2.1 | Fixed-speed wind turbine..... | 9 |
| Figure 2.2 | Doubly-fed induction generator (DFIG) wind turbine..... | 10 |
| Figure 2.3 | Fully rated converter grid connection..... | 10 |
| Figure 2.4 | Wind turbine PMSG with back to back PWM converter..... | 12 |
| Figure 2.5 | Wind turbine generator with diode bridge rectifier..... | 13 |
| Figure 2.6 | Wind turbine generator with diode bridge rectifier and boost chopper circuit..... | 14 |
| Figure 2.7 | VSWPGS using PMSG of boost chopper method | 18 |
| Figure 2.8 | VSWPGS using PMSG of PWM converter method | 20 |
| Figure 3.1 | Annular floe tube..... | 22 |
| Figure 3.2 | Velocity triangle..... | 23 |
| Figure 3.3 | Wind turbine blade shape model..... | 27 |
| Figure 3.4 | Wind turbine speed reference and electric power reference to keep maximum conversion factor..... | 28 |
| Figure 3.5 | Logic for control of wind turbine..... | 30 |
| Figure 3.6 | Timing to change control method..... | 31 |
| Figure 3.7 | Simulink and system block of wind turbine..... | 32 |

List of Figures

| | | |
|-------------|--|----|
| Figure 3.8 | Windmill turbine model..... | 33 |
| Figure 3.9 | Simulink and system block of wind turbine | 34 |
| Figure 3.10 | Windmill turbine emulator model..... | 35 |
| Figure 3.11 | Simulink and system block of wind turbine emulator..... | 36 |
| Figure 3.12 | Simulink and model Equivalent circuit of PMSG..... | 39 |
| Figure 3.13 | <i>U-phase, V-phase</i> main circuit of (conduction mode ①)..... | 41 |
| Figure 3.14 | <i>U-phase, W-phase</i> main circuit of (conduction mode ②)..... | 41 |
| Figure 3.15 | <i>V-phase, W-phase</i> main circuit of (conduction mode ③)..... | 42 |
| Figure 3.16 | <i>V-phase, U-phase</i> main circuit of (conduction mode ④)..... | 42 |
| Figure 3.17 | <i>W-phase, U-phase</i> main circuit of (conduction mode ⑤)..... | 43 |
| Figure 3.18 | <i>W-phase, V-phase</i> main circuit of (conduction mode ⑥)..... | 43 |
| Figure 3.19 | Simulink model to detect conduction mode..... | 46 |
| Figure 3.20 | Simulink and model Simplified converter main circuit of conduction mode 1..... | 49 |
| Figure 3.21 | Model of PWM converter main circuit..... | 52 |
| Figure 3.22 | Simulink and model DC link model of boost converter method..... | 54 |
| Figure 3.23 | Simulink and model Simplified DC link model of boost converter method..... | 57 |
| Figure 3.24 | Simulink and model DC link model of PWM converter method | 59 |
| Figure 3.25 | Duty ratio control system..... | 61 |
| Figure 3.26 | PWM converter control system..... | 64 |
| Figure 3.27 | System and main circuit of PWM inverter..... | 66 |

List of Figures

| | | |
|-------------|---|----|
| Figure 3.28 | Inverter control system of boost converter method..... | 69 |
| Figure 3.29 | Inverter control system of PWM converter method..... | 70 |
| Figure 3.30 | MATLAB Simulink block of the Boost chopper method..... | 71 |
| Figure 3.31 | Current control system of inverter..... | 74 |
| Figure 3.32 | MATLAB Simulink block of the PWM converter method | 77 |
| Figure 3.33 | Speed control system of the PWM converter method..... | 79 |
| Figure 3.34 | Current control system of converter..... | 82 |
| Figure 3.35 | Generated power of Boost chopper scheme..... | 84 |
| Figure 3.36 | Wind turbine Torque..... | 84 |
| Figure 3.37 | Tip speed ratio..... | 85 |
| Figure 3.38 | Rotational speed reference and Rotational speed..... | 85 |
| Figure 3.39 | Duty cycle..... | 86 |
| Figure 3.40 | d -axis and q -axis voltage for converter side..... | 86 |
| Figure 3.41 | d -axis and q -axis current for converter side..... | 87 |
| Figure 3.42 | d -axis and q -axis current for inverter side..... | 87 |
| Figure 3.43 | DC link voltage and its reference..... | 88 |
| Figure 3.44 | Generated power of PWM converter scheme..... | 90 |
| Figure 3.45 | Wind turbine Torque..... | 90 |
| Figure 3.46 | Tip speed ratio..... | 91 |
| Figure 3.47 | Rotational speed reference and Rotational speed..... | 91 |
| Figure 3.48 | q -axis current for feed-forward reference..... | 92 |
| Figure 3.49 | d -axis and q -axis voltage for converter side..... | 92 |

List of Figures

| | | |
|-------------|--|-----|
| Figure 3.50 | <i>d</i> -axis and <i>q</i> -axis current for converter side..... | 93 |
| Figure 3.51 | <i>d</i> -axis and <i>q</i> -axis current for inverter side..... | 93 |
| Figure 3.52 | DC link voltage and its reference..... | 94 |
| Figure 4.1 | Wind turbine emulator..... | 96 |
| Figure 4.2 | Wind turbine blade shape model..... | 96 |
| Figure 4.3 | Real wind turbine blade shape..... | 97 |
| Figure 4.4 | XY coordinate data of NACA4415..... | 100 |
| Figure 4.5 | The angle of attack of 0 [deg] of the wind vector illustration..... | 101 |
| Figure 4.6 | The angle of attack of 0 [deg] of the wind velocity distribution..... | 101 |
| Figure 4.7 | The angle of attack of 0 [deg] of the pressure distribution..... | 102 |
| Figure 4.8 | The angle of attack of -10[deg]..... | 102 |
| Figure 4.9 | The angle of attack of -10 [deg] of the wind vector illustration..... | 103 |
| Figure 4.10 | The angle of attack of -10 [deg] of the wind velocity distribution.... | 103 |
| Figure 4.11 | The angle of attack of -10 [deg] of the pressure distribution..... | 104 |
| Figure 4.12 | The angle of attack of +10[deg]..... | 104 |
| Figure 4.13 | The angle of attack of +10 [deg] of the wind vector illustration..... | 105 |
| Figure 4.14 | The angle of attack of +10 [deg] of the wind velocity distribution... | 105 |
| Figure 4.15 | The angle of attack of +10 [deg] of the pressure distribution..... | 106 |
| Figure 4.16 | Calculated wind turbine blade performance output result..... | 107 |
| Figure 4.17 | Windmill output torque..... | 108 |
| Figure 4.18 | Windmill output power..... | 108 |
| Figure 4.19 | Mechanical model for real wind turbine..... | 109 |

List of Figures

| | | |
|-------------|--|-----|
| Figure 4.20 | Mechanical model for wind turbine emulator..... | 110 |
| Figure 4.21 | WTE base on BEMT..... | 111 |
| Figure 4.22 | Experimental systems using the real wind turbine (PWM converter scheme)..... | 112 |
| Figure 4.23 | Experimental systems using the wind turbine emulator (PWM converter scheme)..... | 114 |
| Figure 4.24 | Wind velocity..... | 115 |
| Figure 4.25 | Generated power..... | 117 |
| Figure 4.26 | Wind turbine Torque..... | 117 |
| Figure 4.27 | Thrust..... | 118 |
| Figure 4.28 | Tip speed ratio..... | 118 |
| Figure 4.29 | Power reference..... | 119 |
| Figure 4.30 | Rotational speed Reference..... | 119 |
| Figure 4.31 | Rotational speed..... | 120 |
| Figure 4.32 | d -axis and q -axis current for converter side..... | 120 |
| Figure 4.33 | Integrated power..... | 121 |
| Figure 4.34 | q -axis current reference of feed-forward control | 121 |
| Figure 4.35 | q -axis current reference of Speed regulator..... | 122 |
| Figure 4.36 | q -axis current Reference of Power regulator..... | 122 |
| Figure 4.37 | DC link voltage and its reference..... | 123 |
| Figure 4.38 | d -axis and q -axis current for inverter side..... | 123 |
| Figure 4.39 | Generated power..... | 125 |

List of Figures

| | | |
|-------------|--|-----|
| Figure 4.40 | Wind turbine Torque..... | 125 |
| Figure 4.41 | Thrust..... | 126 |
| Figure 4.42 | Tip speed ratio..... | 126 |
| Figure 4.43 | Power reference..... | 127 |
| Figure 4.44 | Rotational speed Reference..... | 127 |
| Figure 4.45 | Rotational speed..... | 128 |
| Figure 4.46 | d -axis and q -axis current for converter side..... | 128 |
| Figure 4.47 | Integrated power..... | 129 |
| Figure 4.48 | q -axis current reference of feed-forward control | 129 |
| Figure 4.49 | q -axis current reference of Speed regulator..... | 130 |
| Figure 4.50 | q -axis current Reference of Power regulator..... | 130 |
| Figure 4.51 | DC link voltage and its reference..... | 131 |
| Figure 4.52 | d -axis and q -axis current for inverter side..... | 131 |
| Figure 4.53 | Natural wind velocity of the real wind turbine..... | 132 |
| Figure 4.54 | Generated power and system power of the real wind turbine..... | 134 |
| Figure 4.55 | Tip speed ratio of the real wind turbine..... | 134 |
| Figure 4.56 | Rotational speed Reference and Rotational speed of the real wind turbine..... | 135 |
| Figure 4.57 | d -axis and q -axis voltage reference for converter side of the real wind turbine..... | 135 |
| Figure 4.58 | DC link voltages and its reference of the real wind turbine..... | 136 |
| Figure 4.59 | d -axis and q -axis current for inverter side of the real wind turbine... | 136 |

List of Figures

| | | |
|-------------|--|-----|
| Figure 4.60 | Generated power and system power of the wind turbine emulator.... | 138 |
| Figure 4.61 | Tip speed ratio of the wind turbine emulator..... | 138 |
| Figure 4.62 | Rotational speed Reference and Rotational speed of the wind turbine emulator..... | 139 |
| Figure 4.63 | d -axis and q -axis voltage reference for converter side of the wind turbine emulator..... | 139 |
| Figure 4.64 | DC link voltage and its reference of the wind turbine emulator..... | 140 |
| Figure 4.65 | d -axis and q -axis current for inverter side of the wind turbine emulator..... | 140 |
| Figure 5.1 | Experimental systems using the wind turbine emulator (Boost chopper scheme)..... | 143 |
| Figure 5.2 | Experimental systems using the wind turbine emulator (PWM converter scheme)..... | 145 |
| Figure 5.3 | Structure of phase locked loop control system... .. | 146 |
| Figure 5.4 | Laboratory Prototype..... | 147 |
| Figure 5.5 | Structure of the wind turbine emulator..... | 148 |
| Figure 5.6 | Structure of the real wind turbine | 149 |
| Figure 5.7 | Change of wind velocity..... | 150 |
| Figure 5.8 | Rotational speed reference and Rotational speed of boost chopper scheme..... | 152 |
| Figure 5.9 | Duty control signal of boost chopper scheme..... | 152 |
| Figure 5.10 | Wind turbine torque of boost chopper scheme..... | 153 |
| Figure 5.11 | Tip speed ratio of boost chopper scheme..... | 153 |
| Figure 5.12 | Integrated power system of boost chopper scheme..... | 154 |

List of Figures

| | | |
|-------------|---|-----|
| Figure 5.13 | Power set of boost chopper scheme..... | 154 |
| Figure 5.14 | DC link voltage and its reference of boost chopper scheme..... | 155 |
| Figure 5.15 | System power of boost chopper scheme..... | 155 |
| Figure 5.16 | Pitch angle control of boost chopper scheme..... | 156 |
| Figure 5.17 | d -axis and q -axis current of boost chopper scheme..... | 156 |
| Figure 5.18 | d -axis and q -axis voltage for converter side of boost chopper scheme | 157 |
| Figure 5.19 | d -axis and q -axis voltage for inverter side of boost chopper scheme | 157 |
| Figure 5.20 | Rotational speed reference and Rotational speed of the PWM converter scheme..... | 159 |
| Figure 5.21 | q -axis current reference of feed-forward control of the PWM converter scheme..... | 159 |
| Figure 5.22 | Wind turbines Torque of the PWM converter scheme..... | 160 |
| Figure 5.23 | Tip speed ratio of the PWM converter scheme..... | 160 |
| Figure 5.24 | Integrated power system of the PWM converter scheme..... | 161 |
| Figure 5.25 | Power set of the PWM converter scheme..... | 161 |
| Figure 5.26 | DC link voltages and its reference of the PWM converter scheme.... | 162 |
| Figure 5.27 | System power of the PWM converter scheme..... | 162 |
| Figure 5.28 | Pitch angle control of the PWM converter scheme..... | 163 |
| Figure 5.29 | d -axis and q -axis current for converter side of the PWM converter scheme..... | 163 |
| Figure 5.30 | d -axis and q -axis voltage of the PWM converter scheme..... | 164 |

List of Figures

| | | |
|-------------|--|-----|
| Figure 5.31 | <i>q</i> -axis current reference of power regulator control of the PWM converter scheme..... | 164 |
| Figure 5.32 | Experimental systems using the real wind turbine (Boost chopper scheme)..... | 167 |
| Figure 5.33 | Natural wind velocity of the real wind turbine | 168 |
| Figure 5.34 | Generated power and system power of the real wind turbine | 170 |
| Figure 5.35 | Rotational speed Reference and Rotational speed of the real wind turbine | 170 |
| Figure 5.36 | Torque for wind turbine | 171 |
| Figure 5.37 | <i>d</i> -axis and <i>q</i> -axis voltage reference for converter side of the real wind turbine | 171 |
| Figure 5.38 | DC link voltages and its reference of the real wind turbine | 172 |
| Figure 5.39 | <i>d</i> -axis and <i>q</i> -axis current for converter side of the real wind turbine..... | 172 |
| Figure 5.40 | Generated power and system power of the wind turbine emulator ... | 174 |
| Figure 5.41 | Rotational speed Reference and Rotational speed of the wind turbine emulator..... | 174 |
| Figure 5.42 | Torque for wind turbine | 175 |
| Figure 5.43 | <i>d</i> -axis and <i>q</i> -axis voltage reference for converter side of the wind turbine emulator..... | 175 |
| Figure 5.44 | DC link voltages and its reference of the wind turbine emulator | 176 |
| Figure 5.45 | <i>d</i> -axis and <i>q</i> -axis current for converter side of the wind turbine emulator | 176 |

List of Table

| | | |
|-----------|---|-----|
| Table 3.1 | Conduction mode of diode bridge rectifier | 44 |
| Table 3.2 | Common parameters of boost chopper scheme and PWM converter scheme..... | 75 |
| Table 3.3 | Control parameters of boost chopper scheme | 76 |
| Table 3.4 | Control parameters of PWM converter scheme..... | 80 |
| Table 4.1 | Three-dimensional table data..... | 97 |
| Table 4.2 | Airfoil profile result..... | 98 |
| Table 5.1 | Integrated power of each mode..... | 165 |

Chapter 1

Introduction

1.1 Background

The power of the wind has been utilized for at least the past 3000 years [1]. Until the early 20th century wind power was used to provide mechanical power to pump water or to grind grain. At the beginning of modern industrialization, the use of the fluctuating wind energy resource was substituted by fossil fuel fired engines or the electrical grid, which provided a more consistent power source. In the early 1970s, with the first oil price shock, the interest in the power of the wind re-emerged. This time, however, the main focus was on wind power providing electrical energy instead of mechanical energy. This way, it became possible to provide a reliable and consistent power source by using other energy technologies, via the electrical grid, as a back-up. The first wind turbines for electricity generation had already been developed at the beginning of the 20th century. The technology was improved step by step since the early 1970s. By the end of the 1990s, wind energy has re-emerged as one of the most important sustainable energy resources. During the last decade of the 20th century, worldwide wind capacity has doubled approximately every 3 years. The costs of electricity generated from wind power have fallen to about one-sixth since the early 1980, and the trend seems to continue. Some experts predict that the cumulative capacity will be growing worldwide by about 25% per year until 2005. Wind energy technology itself also moved very fast towards new dimensions. At the end of 1989, a 300 kW wind turbine with a 30-m rotor diameter was state-of-the-art. Only 10 years

later, 1500 kW turbines with a rotor diameter of around 70 m are available from many manufacturers. The first demonstration projects using 2 MW wind turbines with a rotor diameter of 74 m was installed before the turn of the century. Four and five MW wind turbines are expected to become available in 2001 or 2002.

In the last 12 years, A Survey of Control Issues in PMSG-Based Small Wind-Turbine Systems in 2013 [2]. The penetration of the wind-turbine power generation is dramatically increased worldwide. This growing trend is stimulating the research in the power processing field aiming at optimizing the energy extraction from the wind and the energy injection into the grid [4]. Particular interest has been focused in recent years on distributed generation through small wind-turbines because of: lower impact on the landscape, lower noise level, grid codes and national laws imposing simpler grid connection and higher feed-in tariffs and capability to work in island-mode for isolated communities [5].

As power generating systems which can utilize renewable wind energy effectively, the researches of variable-speed wind generator systems which change windmill rotational frequency in proportion to the wind velocity are widely carried out [6-32]. The energy conversion efficiencies of propeller windmills change for conditions of wind velocity and windmill speed. Therefore the converter connected with a generator must control the windmill speed in proportion to the wind velocity in order to maintain the energy conversion efficiency maximum [33].

At present, the variable-speed wind generator systems using the PWM converter (PWM converter method) are introduced [34-56]. The PWM converter is costly because a lot of switching devices are used and its control system is complicated. However, the PWM converters are used for large-capacity variable-speed wind generator systems which need windmill speed control, because the vector control can be applied to realize the high-speed and high-precise generator torque control.

The converter does not need to supply the excitation energy when the permanent magnet synchronous generator (PMSG) is used as a generator [57-59]. Therefore, the wind generator system for the purpose of battery charger uses the diode bridge rectifier as a converter. It is operated mainly at the rated wind velocity since the induced voltage is enough to charge the battery [75-78]. The wind generator systems

using diode bridge rectifier (diode rectification method) can constitute low-cost converters [60-68]. However, the windmill speed control becomes difficult, since the converter cannot control the PMSG torque by itself. And, the induced voltage necessary for system interconnection cannot be obtained at low wind velocity. At present, the diode rectification method which realizes the windmill speed control and system interconnection simultaneously at low wind velocity is not reported.

This thesis will address the generator control of a small wind turbine for grid connection. The wind turbine extracts the energy from the wind through the rotor blade, which drives the generator to produce electricity.

This thesis focuses on 3-phase AC Permanent Magnet Synchronous Generator (PMSG). And the research has been focused on the development of a new turbine design to reduce the cost of wind power and to make wind turbines more economical and efficient. The investigation of wind power system involves high performance wind turbine emulators, especially for the development of optimal control solutions. For the effective utilization of renewable wind energy by power generating systems, a large number of studies are being conducted on variable-speed wind generator systems that change the windmill rotational frequency in proportion to the wind velocity. The energy conversion efficiency of propeller windmills depend on wind velocity and windmill speed. Therefore, the converter connected to the generator must control the windmill speed in proportion to the wind velocity in order to maintain the maximum energy conversion efficiency.

1.2 Aims and objectives

This thesis focuses on an experimental verification of a variable-speed wind power generation system (VSWPGS).

First, is the whole simulation system consists of models of PMSG, AC/DC converter, AC/DC rectifier, DC link, Boost chopper circuit, DC/AC inverter, and grid voltage monitoring unit, which are detailed below. The objectives of the simulation system are to develop the above mentioned mathematical and simulation models, and to verify the models through a case study simulation.

Second, is the whole experimental system model in laboratory consists of models of wind turbine emulator, PMSG, AC/DC converter, AC/DC rectifier, DC link, Boost chopper circuit, DC/AC inverter, Transformer and grid line, which are detailed below. The objectives of the experimental system are to develop the above mentioned mathematical and control circuit models, and to verify the models through a case study experimental in laboratory.

Third, is the experimental verification of a variable-speed wind power generation system using real wind turbine consists of models of real blade wind turbine, PMSG, AC/DC converter, AC/DC rectifier, DC link, Boost chopper circuit, DC/AC inverter, Anemometer, Transformer and grid line, which are detailed below. The objectives of the experimental system of a variable-speed wind power generation system using real wind turbine are to develop of a new turbine design to reduce the cost of wind power and to make wind turbines more economical and efficient. are detailed below. the experimental verification of a variable-speed wind power generation system using a permanent magnet synchronous generator and a boost chopper with three speed control modes for wind velocities. The control system is used for the VSWPGS using the diode bridge rectifier and boost chopper circuit as a converter (boost chopper scheme). The speed control mode of low wind velocity controls the windmill speed by controlling the PMSG torque with the boost chopper circuit. The boost chopper circuit can control the generator torque by adjusting the armature current of the PMSG. The speed control mode of middle wind velocity controls the windmill speed by controlling the PMSG torque with the system interconnection inverter. The system interconnection inverter can control the PMSG torque by adjusting the DC link voltage. The speed control mode over the rated wind velocity controls the windmill speed by controlling the windmill torque with the pitch angle control system. The pitch angle control system can control the windmill torque by adjusting the pitch angle. The extension of the variable-speed range is realized by using the hybrid control of three speed control modes, consequently, the system interconnection for all speed control modes. In comparison with the PWM converter scheme, the proposed control system has two advantages. First one is the cost reduction produced by reducing the number of switching devices, and second one is high reliability produced by simplifying the main circuits and control circuits.

1.3 Structure of the Thesis

This thesis is organized with following ways:

Chapter 2: Operating principle of the variable-speed wind power generation system

The structures and operation principles of the VSWPGS using PMSG used for system interconnection are described. Each control principle of VSWPGS using BCC or PWM converter handled in this thesis is explained. The differential equations describing the systems, which are necessary for modeling in simulation, are explained.

Chapter 3: Assessment with simulation of the variable-speed wind power generation system

The modeling method using MATLAB/Simulink is explained. The modelling is conducted based on the simultaneous differential equations describing each system. Also, this chapter explains the modeling method of the wind turbine (WT). The design method for control parameters of the VSWPGS using BCC or PWM converter are explained, and the parameters necessary for the simulation are shown. The simulation is conducted for the conditions of the low, medium and high wind velocity. The simulation results for each VSWPGS are shown, and the validity of the control principle for each VSWPGS is proved.

Chapter 4: Wind turbine emulator

This chapter explains the operating principle and the structure of Wind turbine emulator (WTE) based on the BEMT. Also the structures of the test benches using the WT or WTE are explained. The simulation results of the VSWPGS using PWM converter are compared with the experiment results obtained with the test bench using WTE under the same conditions of low, medium, and high wind velocities. Furthermore, under the conditions of natural winds, the experiment results obtained with the bench using WTE or WT for the VSWPGS using PWM converter are shown.

The obtained experimental results show that the proposed WTE has a sufficient performance for the experimental assessment.

Chapter 5: Experimental assessment of variable speed wind power generation system

The experimental assessment for the VSWPGS using PWM converter or BCC are conducted with the test bench using WTE under the conditions of low, medium, and high wind velocities. By comparing the experimental results of both VSWPGSs, it is shown that the VSWPGS using BCC can extend the variable speed ranges compared to conventional control methods. Also the each element of the system, which are used for experimental assessments, is considered. Then it is shown that the VSWPGS using BCC can reduce the costs and improve the reliability of the whole system, and has the same performance with the VSWPGS using PWM converter of a benchmark.

Chapter 6: Conclusion

The comprehensive discussions based on the obtained results are conducted, and the obtained research outcomes are clarified.

Chapter 2

Operation principle of the variable-speed wind power generation system

2.1 Introduction

This chapter shows the literature review of wind energy conversion system modelling a wind turbine extracts kinetic energy from the wind to drive the wind turbine rotor, which is connected to a generator producing electricity [90]. And the variable-speed wind power generation system using a permanent magnet synchronous generator (PMSG), the gearless mechanism which connects the PMSG with the windmill directly without using a speed-increasing gear is realized by adopting the multi-pole PMSG as a generator.

2.2 Wind turbine control for grid connection

In this section, the literature review on the state of the art of power converters for different types of VSWPGSs will be made. The comprehensively classified wind turbine grid connection into three classes: direct-coupled generator grid connection, doubly-fed induction generator grid connection and fully rated converter grid connection [81].

2.2.1 Direct-coupled generator grid connection

Until 2000, most wind turbines were based on cage induction generators that are directly connected to the grid, as shown in Figure 2.1. The rotational speed of the rotor is essentially fixed and the rotational speed varies only by a few percentage points. These fixed speed squirrel-cage induction generator (FSIG) wind turbines have the advantages of being simple, reliable and well proven. However, FSIG wind turbines suffer from a number of disadvantages. Firstly, fixing the rotor speed generates high mechanical loading on the structure. Secondly, FSIG wind turbines cannot maintain maximum aerodynamic efficiency. Finally, FSIG turbines are not grid friendly in terms of reactive power, low voltage ride through and flicker. For these reasons an FSIG drive train is no longer favorable for large wind turbines [82].

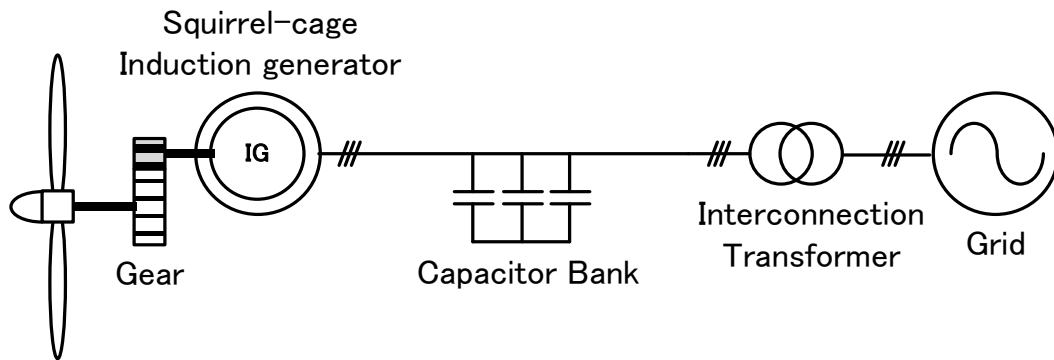


Fig 2.1 Fixed-speed wind turbine

2.2.2 Doubly-fed induction generator (DFIG) grid connection

The technology of doubly-fed induction generators is becoming more and more common due to the disadvantages of fixed speed induction generator. Variable speed DFIG is also an asynchronous generator, the common characteristics of doubly-fed and fixed-speed generator is that their stator windings can directly be connected to the grid. Power output from the stator of a DFIG can be delivered directly to the grid, and the generator rotor absorbs excitation current from the grid. As Figure 2.2 illustrated, the rotor of DFIG connects to the grid by means of power converter. The power converter is able to transfer power bi-directly, which means it can deliver power to the grid and is also able to absorb power from the grid, depending on the rotational speed of the generator [81].

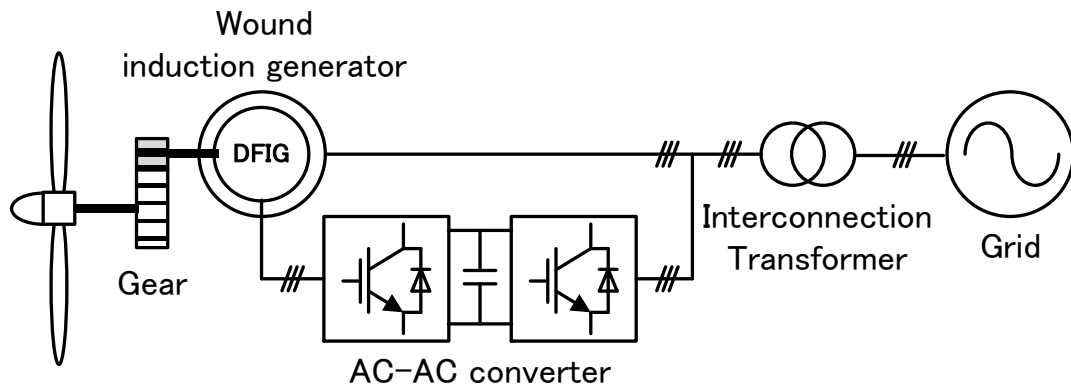


Fig 2.2 Doubly-fed induction generator (DFIG) wind turbine

2.2.3 Fully rated converter grid connection

Figure 2.3 illustrates the characteristics of wind turbine configuration with fully rated converter grid connection. The wind turbine, with or without a gearbox, is fitted with either an induction generator or a permanent magnet synchronous generator (PMSG), and is connected to the grid with a fully rated power converter [81].

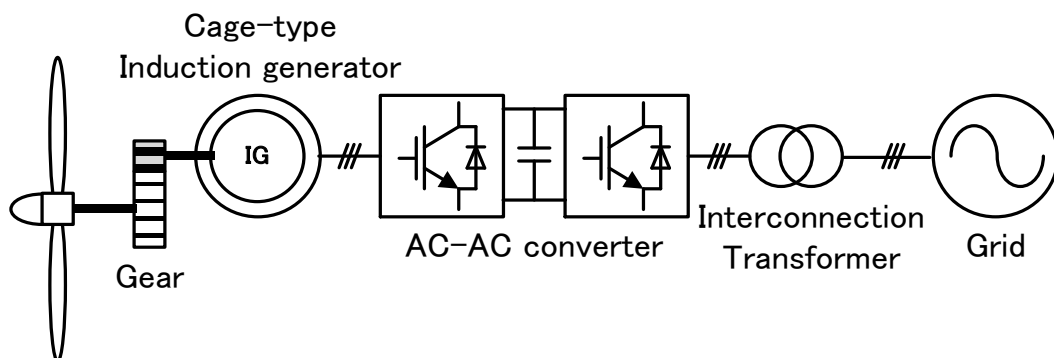


Fig 2.3 fully rated converter grid connection

The advantages of fully rated converter grid connection are:

- 1) The generator is completely decoupled from the grid, which means the power factor can be corrected by an active filter, i.e. the inverter can improve the output power quality with a unit power factor before injection to the power grid.
- 2) It allows variable-speed operation of the wind turbine, which enables maximum power point tracking (MPPT) between cut-in wind speed and rated wind speed.

In this thesis the PMSG is chosen for the wind turbine generator, and the power output from the generator is fully rated delivered to the grid through a power converter. The frequency and voltage of the power output from a PMSG varies with the rotational speed of the generator.

For this thesis, the configuration of the PMSG fully rated converter grid connection consists of AC/DC rectifier, AC/DC converter and DC/AC inverter.

2.2.4 AC/DC Rectifier and AC/ DC converter

There are a number of papers which discussed the strategy of grid connection for PMSG wind turbines. The most popular control topology is the back-to-back PWM converter as Figure 2.4 shows.

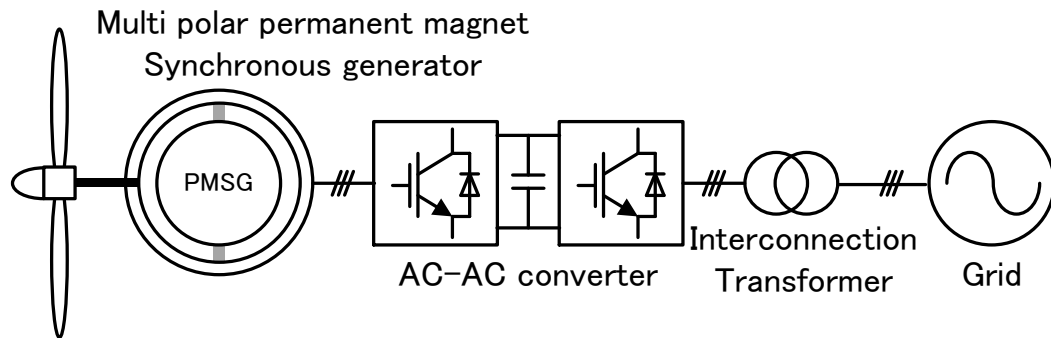


Fig 2.4 Wind turbine PMSG with back-to-back PWM converter

The characteristics of the PWM converter are that the converter utilises active devices at both the generator side for the rectifier and the grid side for the inverter [83].

The advantages of PWM converter are as follows:

- The rectifier is controllable, and
- Both rectifier and inverter bridges are composed of active IGBT devices, with the current be able to flow from either the generator to the grid or the grid to the generator.

The major disadvantage of PWM converter topology is:

- The controller is complex and expensive because it requires 12-channel Pulse Width Modulation (PWM) signals for the rectifier and the inverter. For this reason, in a practical application, the control system requires at least two or more Micro-Controller Units (MCU), Digital Signal Processor (DSP), Field Programmable Gate Array (FPGA), etc.

A simple topology for wind turbine generation was introduced by [84] and is illustrated in Figure 2.5, which consists of a diode bridge rectifier, with a DC link to an active IGBT inverter.

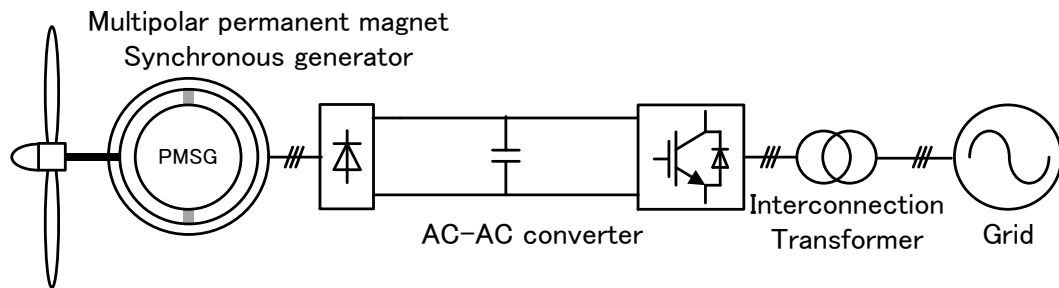


Fig 2.5 Wind turbine generator with diode bridge rectifier

Although this type of converter is simple and reliable, but the power factor of the generator is low. The other problem is that when the output voltage of the rectifier is lower than the grid, power cannot be injected to the grid.

By summarising the topology of back-to-back and diode bridge rectifier, it is possible to insert a boost circuit between the diode rectifier and the inverter, in order to solve the issue of generator power factor, as shown in Figure 2.6. There have been a number of papers describing the inclusion of Power Factor Correction (PFC) with boost chopper circuits, however only a few papers discuss it with the wind turbine controller [68], [69], [85], [86].

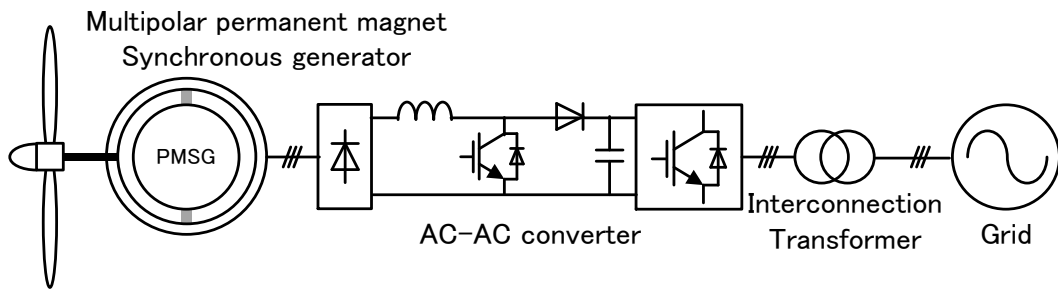


Fig 2.6 Wind turbine generator with diode bridge rectifier and boost chopper circuit

For this topology of converter, operation at relatively low wind speeds is possible due to the inclusion of the boost circuit. The boost chopper circuit can maintain the DC bus link voltage at a constant value. This topology is utilised for the converter in this thesis.

2.2.5 Comparison between Direct Torque Control and Field Oriented Control

Direct torque control (DTC) and field oriented control (FOC) are two of the most commonly applied algorithms for the control of PMSMs. The DTC approach was first developed and presented by I. Takahashi [87]. The basic principle of the DTC approach is that the stator flux linkage and the electromagnetic torque are estimated and compared with their reference values. Based on the control algorithm of mitigating the errors between the reference and estimated values, the reference torque and flux can be achieved by controlling the inverter states. The FOC approach was pioneered by F. Blaschke in 1970s [88]. The FOC approach has been and continues to be a significant factor in PMSMs control, which makes it possible that PMSMs can be controlled as easily as DC machines. In the FOC approach, the dq -axes are rotating at

the rotor electrical angular speed with the d -axis aligned with the rotor flux direction. Thus, the flux producing current component, i_{ds} , and the torque producing current component i_{qs} , are along the d -axis and q -axis, respectively. Thus, the dq -axes currents can be controlled independently by two closed loop controls in the FOC approach, which indirectly controls the speed and the torque of the PMSMs.

When choosing one control strategy of either DTC or FOC for the generator-side converter control, their merits and drawbacks need to be analyzed and compared according to the operation requirements of the direct-drive PMSG systems. The DTC approach has the advantages that the electromagnetic torque can be changed very fast by changing the reference, and no coordinate transforms and PI controllers are needed which decreases the computational effort. On the other hand, the DTC approach also presents some disadvantages such as: (1) the difficulty to control the torque at very low speed; (2) the high current and torque ripples; and (3) the high noise level at low speed. When it comes to the FOC approach, although its implementation requires large computational effort including PI control and coordinate transformations, it possesses the following merits: (1) fast speed and torque response; (2) outstanding low speed performance; and (3) low current and torque ripples.

For the application of direct-drive PMSG systems, the PMSGs are directly driven by the wind turbine without a gearbox, which means that their operation speeds are always in a relatively low range. Moreover, the torque ripples of the direct-drive PMSGs should be controlled at a low level to decrease the mechanical stresses on the wind turbine. On the basis of the analysis above, the FOC approach was found to be more suitable for the direct-drive PMSG systems than the DTC approach.

2.3 System configuration

The variable-speed wind power generation system using a permanent magnet synchronous generator (PMSG), the gearless mechanism which connects the PMSG with the windmill directly without using a speed-increasing gear is realized by adopting the multi-pole PMSG as a generator. The windmill consists of a pitch angle control system. The pitch angle control system is activated beyond the rated wind velocity, and the windmill rotational speed is maintained at the rated windmill speed. Below the rated wind velocity, the windmill rotational speed is controlled in order to maintain the maximum energy conversion efficiency below the rated wind velocity. The converter is connected to the PWM inverter for system interconnection through the DC link condenser. The PWM inverter supplies the power system with the active power obtained from the converter side

2.4 Boost converter scheme

Figure. 2.7 shows the variable speed wind power generation system using diode bridge rectifier and boost converter (boost chopper scheme). It is not possible for the boost chopper scheme to motoring the PMSG, since the diode bridge rectifier limits the direction of current. However, it does not become serious problem, since the motoring mode is not carried out in general wind generator systems. However the diode bridge rectifier cannot control the generator torque, since the armature current of PMSG changes depend on the relationship between induced voltage and DC link

voltage. This becomes problem. Then the windmill speed control scheme using the system interconnection inverter was proposed [68], [69]. The proposed scheme controls the windmill speed by adjusting the DC link voltage. The scheme decreases the number of switching devices, and can reduce the size and cost of power conversion system. However, the proposed scheme has the defect that narrows the variable-speed range, since the sufficient generator torque cannot be obtained when the induced voltage is decreases under the low range of wind velocity. Then, in this thesis, the boost chopper circuit is added to improve the variable-speed range. It is possible to control the DC link current regardless of the magnitude of the induced voltage when the boost chopper circuit is added. The generator torque can be controlled by controlling the DC link current in the low range of wind velocity, in which the diode rectification scheme cannot control the generator torque. In short, the variable-speed range from the cut-in wind velocity to the rated wind velocity, which is equivalent to the variable-speed range of PWM converter scheme, is achieved. The PWM converter scheme is explained in 2.5. However the boost chopper scheme needs to add the reactor and switching device for the diode rectification scheme of [68], [69], it has the advantage which can reduce the size and cost of a power converter in comparison with the PWM converter scheme. The inverter controls the generator torque as well as the diode rectification scheme by adjusting the DC link voltage from the wind velocity, which makes the PMSG generate the induced voltage necessary for system interconnection, to the rated wind velocity. The reduction of switching loss and load to the switching device can be reduced by turning off the chopper circuit. And, it is possible to minimize the capacity of switching device by limiting the usage

of chopper circuit to the usage in low wind velocity. Under the rated wind velocity, the windmill speed is controlled with two above-mentioned generator torque control schemes. Over the rated wind velocity, the windmill speed is controlled with the pitch angle control system by adjusting the windmill torque. And, the inverter adjusts the DC link voltage and controls the generator torque to maintain the generated output at the rated power of PMSG.

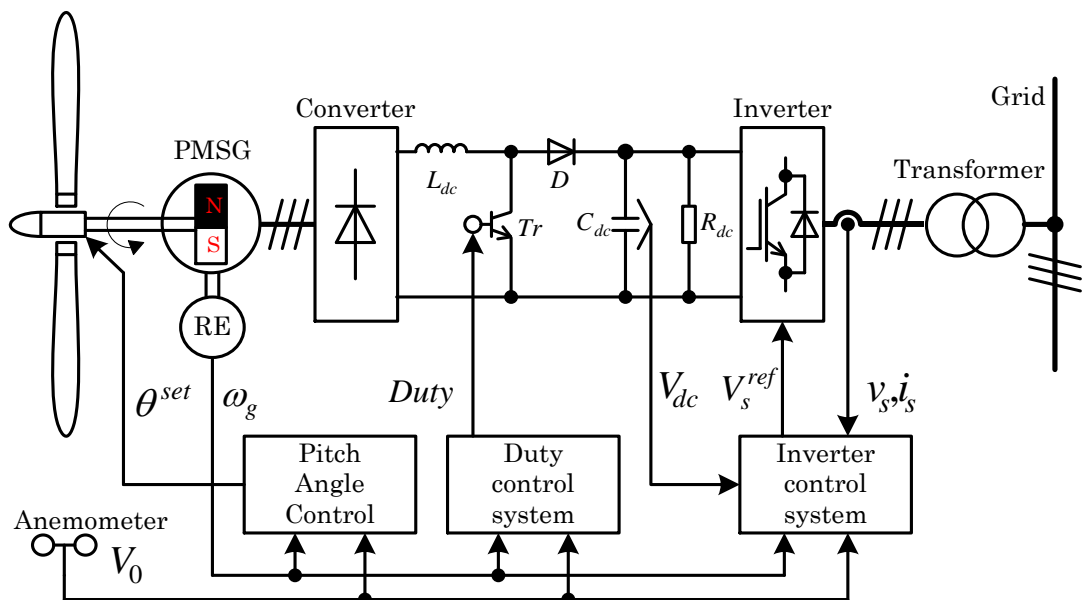


Fig. 2.7 Variable speed wind power generation system using PMSG for boost converter scheme.

2.5 back to back PWM converter scheme

Figure. 2.8 shows the variable speed wind power generation system using back to back PWM converter (PWM converter scheme). The PWM converter controls the

windmill speed by adjusting the generator torque. The PWM inverter maintains the DC link voltage to be the constant voltage necessary for system interconnection and keeps the system interconnection. The PWM converter scheme can carry out the high-speed and high-precise generator torque control from the cut-in wind velocity to the rated wind velocity, since the PWM converter scheme can apply the vector control system. Therefore, the frequency characteristics and variable-speed range of the windmill speed control become the benchmark. The similar PWM converter schemes are proposed, and the novelty for scheme itself does not exist. This research utilizes the PWM converter scheme as a comparison object to evaluate the performance of the boost chopper scheme.

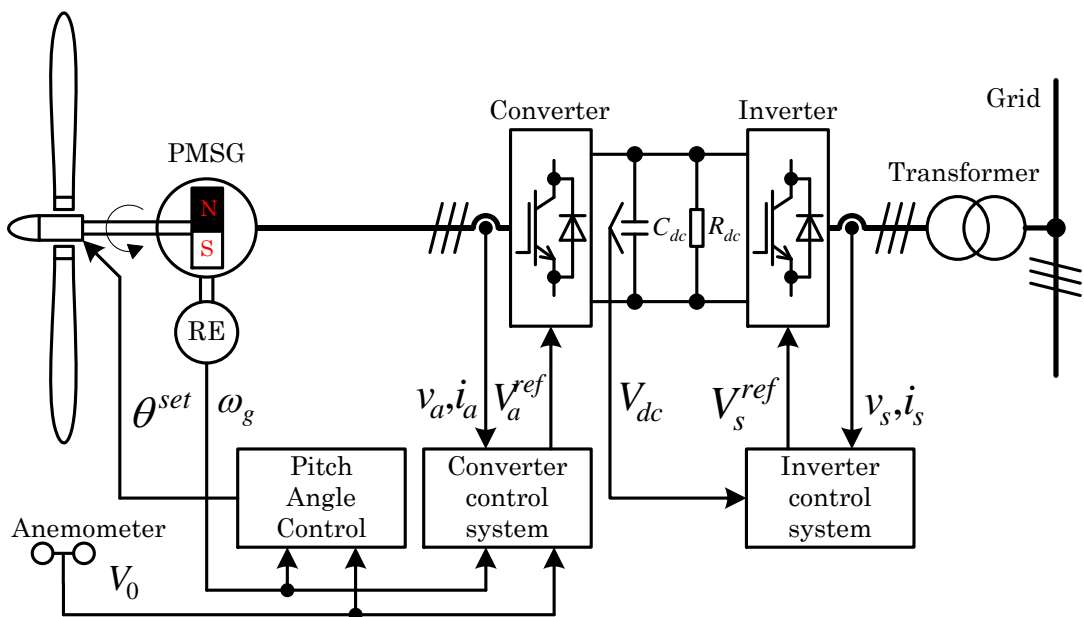


Fig. 2.8 Variable speed wind power generation system using PMSG for PWM converter scheme.

2.6 Summary

The literature review detailed in this chapter has led to a comprehensive understanding of the concepts relevant to the control of a permanent magnet synchronous generator for wind turbines with grid line connection. Also, this described system configuration of the variable-speed wind power generation system using a permanent magnet synchronous generator for the boost converter scheme and the PWM converter scheme. By this two schemes are utilized for the converter in this thesis.

Chapter 3

Assessment with simulation of the variable speed wind power generation system

3.1 Modeling method

This chapter described the control strategy and modeling for simulation using Matlab Simulink of the proposed variable-speed wind power generation system using boost converter. Also this paper described the control strategy and modeling of variable-speed wind power generation system using PWM converter. The steady state and transient responses for wind velocity changes were simulated using the Matlab Simulink.

3.2 Windmill model

The simulation assumes that wind will pass through the windmill, flowing through the cylindrical tube without interference, as shown in fig.3.1. The velocity diagram of the blade element in the position of radius r assumes fig.3.2. It is assumed that in fig. 3.1, The wind speed accelerates peripheral speed only in $w(= r\Omega a)$, and that the propeller wind turbine decelerates the inflow wind speed only in $V_0 a$. The variable definitions in fig. 3.1 and 3.2 are as follows.

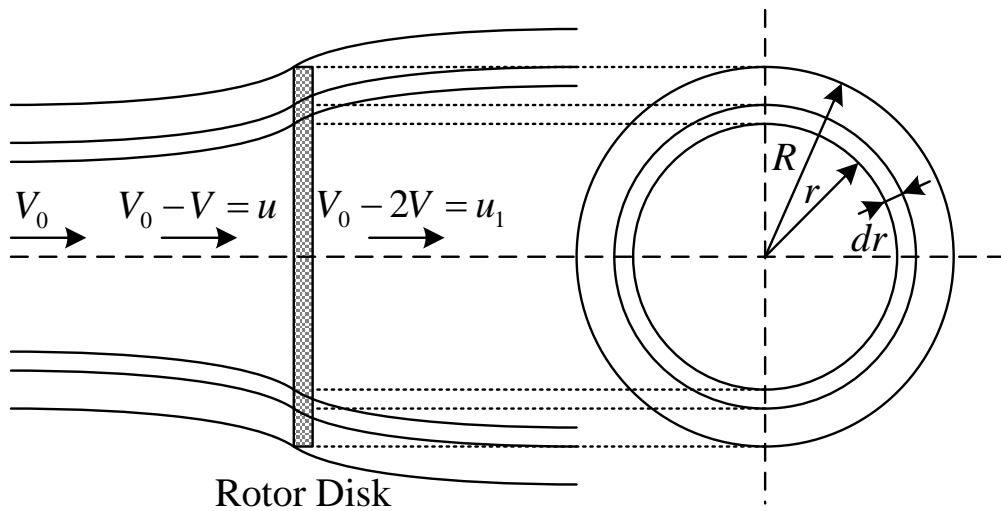


Fig. 3.1. Annular flow tube

Where, V_0 : rotor inflow wind speed [m/s], u : wind speed before passing the rotor [m/s], u_1 : wind speed after passing the rotor [m/s], R : rotor radius [m]

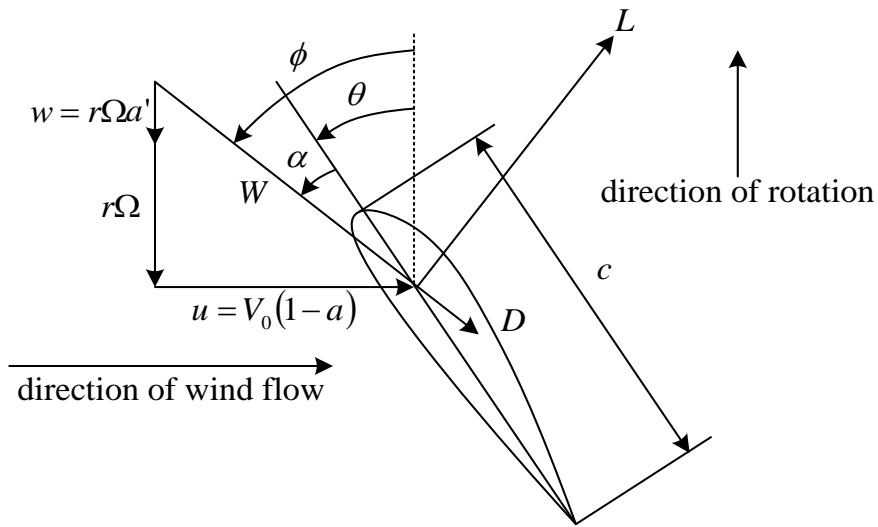


Fig. 3.2. Velocity triangle

Where, Ω : the rotor angular speed [rad/s], θ : the blade pitch angle [rad], W : the blade inflow wind speed [m/s], ϕ : the inflow angle [rad], α : the meeting angle [rad], L : the lift, D : the drag, a, a' : the interference factor, c : the wind of code [m].

The force which arises in the blade element caused by wind which passes the propeller wind turbine is defined as lift L and drag D as shown in Fig.3.2. The lift dL and drag dD which arise in the blade element of minimal width dr in the position of radius r are given in the following equation using the air density ρ , lift coefficient c_l , and coefficient c_d

$$dL = \frac{1}{2} \rho W^2 c_l c dr \dots\dots\dots(3.1)$$

$$dD = \frac{1}{2} \rho W^2 c_d c dr \dots\dots\dots(3.2)$$

The torques dQ which arises in the blade element of minimal width dr in the position of radius r is a product between radius r and the sum of the rotational direction components of lift dL and drag dD . Therefore, considering the number of blade B , torque dQ is given as.

$$dQ = \frac{1}{2} \rho W^2 r (c_l \sin \phi - c_d \cos \phi) B c d r \dots\dots\dots(3.3)$$

In addition, output power is calculated as the product of rotor rotational angle speed Ω and torque dQ .

$$dP = \Omega dQ = \frac{1}{2} \rho W^2 \Omega r (c_l \sin \phi - c_d \cos \phi) B c d r \dots\dots\dots(3.4)$$

In addition, the trust is calculated as.

$$dT = \frac{1}{2} \rho W^2 (c_l \cos \phi + c_d \sin \phi) B c d r \dots\dots\dots(3.5)$$

The lift coefficient c_l and drag coefficient c_d are functions of the meeting angle α . α is calculated using the geometrical relation in the equation.

$$\alpha = \phi - \theta \dots\dots\dots(3.6)$$

In addition, blade inflow wind speed W and inflow angle ϕ can be calculated as follows.

$$W = \sqrt{u^2 + (r\Omega + w)^2} = \sqrt{\{V_0(1-a)\}^2 + \{r\Omega(1-a')\}^2} \dots\dots\dots(3.7)$$

$$\tan \phi = \frac{u}{r\Omega + w} = \frac{V_0(1-a)}{r\Omega(1-a')} \dots\dots\dots(3.8)$$

Furthermore, torque dQ and thrust dT of the ring division from r to $r + dr$ are given using momentum conservation and Bernoulli's law in the following equations.

$$dQ = \rho u(2\pi r dr)2wr \dots\dots\dots(3.9)$$

$$dT = \rho u(2\pi r dr)2(V_0 - u) \dots\dots\dots(3.10)$$

The following equations are obtained, when the equation derived from equations. (3.5) and (3.10) and the equation derived from equations. (3.3) and (3.9) are arranged, by substituting relational expressions of $W = u/\sin\phi = (r\Omega + w)/\cos\phi$ as explained in Fig.3.2.

$$\frac{V_0 - u}{u} = \left(\frac{Bc}{8\pi r}\right)\left(\frac{c_l \cos\phi + c_d \sin\phi}{\sin^2\phi}\right) \dots\dots\dots(3.11)$$

$$\frac{w}{w + r\Omega} = \left(\frac{Bc}{8\pi r}\right)\left(\frac{c_l \sin\phi - c_d \cos\phi}{\sin\phi \cos\phi}\right) \dots\dots\dots(3.12)$$

The following equation is obtained here, when the variables of $a = V_0 - u/V_0$, $a' = w/\Omega r$, and $\sigma = Bc/2\pi r$ are defined. σ is the ratio of local ring division wind receiving area and blade area in the part.

$$\frac{a}{1-a} = \frac{c_l \cos\phi + c_d \sin\phi}{4\sin^2\phi} \sigma \dots\dots\dots(3.13)$$

$$\frac{a'}{1-a'} = \frac{c_l \sin\phi - c_d \cos\phi}{4\sin\phi \cos\phi} \sigma \dots\dots\dots(3.14)$$

The following equation is obtained when $x = r\Omega/V_0$ the local peripheral speed ratio is substituted in equations (3.8).

$$x \tan\phi = \frac{1-a}{1+a'} \dots\dots\dots(3.15)$$

The local output coefficient C_P , the local torque coefficient C_Q , and the local lift coefficient C_T are given as follows.

$$C_P = \frac{\Omega dQ}{0.5\rho V_0^3(2\pi r dr)r} = \frac{\Omega \rho u(2\pi r dr)2wr}{0.5\rho V_0^3(2\pi r dr)} = 4a'(1-a)x^2 \dots\dots\dots(3.16)$$

$$C_Q = \frac{dQ}{0.5\rho V_0^2(2\pi r dr)r} = \frac{\rho u(2\pi r dr)2wr}{0.5\rho V_0^2(2\pi r dr)r} = 4a'(1-a)x \dots\dots\dots(3.17)$$

$$C_T = \frac{dT}{0.5\rho V_0^2(2\pi r dr)r} = \frac{\rho u(2\pi r dr)2(V_0 - u)}{0.5\rho V_0^2(2\pi r dr)} = 4a(1-a) \dots\dots\dots(3.18)$$

Using these local coefficients, the propeller wind turbine output P , the torque Q , and the thrust T are given as.

$$P = 0.5\rho V_0^3 \int_0^R C_P 2\pi r dr \dots\dots\dots(3.19)$$

$$Q = 0.5\rho V_0^2 \int_0^R C_Q 2\pi r^2 dr \dots\dots\dots(3.20)$$

$$T = 0.5\rho V_0^2 \int_0^R C_T 2\pi r dr \dots\dots\dots(3.21)$$

The procedures to calculate propeller wind turbine performance with the derived equations are given below.

- (a) The blade of propeller wind turbine is divided into adequate number in a radial direction.
- (b) At each division point, the local characteristic value is calculated by the method detailed in the following.
 - ① At the division point position r , the solution of the nonlinear simultaneous equation composed of equations. (3.13), (3.14), and (3.15) is obtained. Concretely, a , a' , and ϕ are calculated by repeat calculation using the Newton method. B , c , θ , V_0 , and Ω in the nonlinear simultaneous equation are the variables given as a condition. c_l , c_d are a function of α , and the table for α is prepared. equation. (3.6).
 - ② C_P , C_Q , C_T in division point position r are calculated with equations. (3.16), (3.17), and (3.18).

(c) After obtaining the characteristic value (C_P , C_Q , C_T) at each division point, the propeller wind turbine performance (P , Q , T) is calculated with integral computation of equations. (3.19), (3.20), and (3.21).

Fig. 3.3 shows the wind shape of wind turbine. The wind turbine shape is designed for wind turbine power generation of 300 [W] rated power, rotor diameter 1.52 [m]. Table 4.1 shows the width of code [m], the angle of twist [degree], the profile of NACA in the position of distance from the rotor center to the radial direction. The app. Table 4.1 shows the data of lift coefficient and drag coefficient for meeting angle [degree] of the profile of NACA in table 4.1. The calculation program for wind turbine performance calculation based on the Rankine-Froude actuator disc theory is made with Matlab. The program made on Matlab can be referred to on Matlab Simulink as S-function. Therefore, it can be used as a propeller wind turbine model to calculate the wind turbine torque generation.

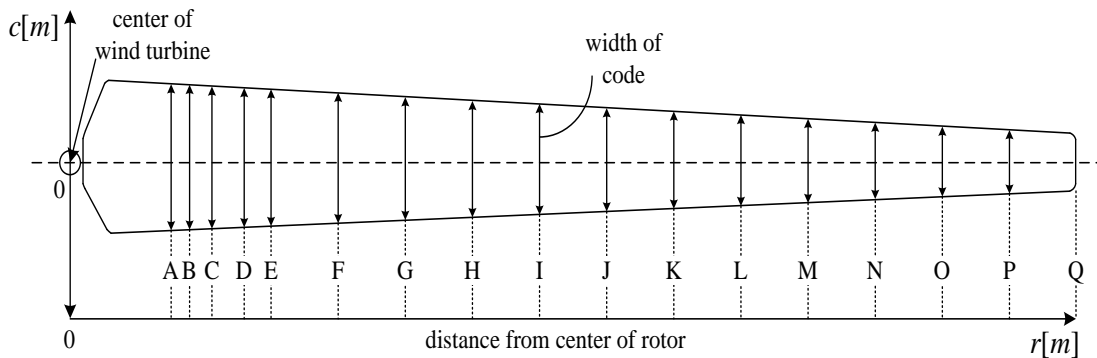


Fig. 3.3. Wind turbine blade shape model

Fig. 3.4 shows the wind turbine speed reference and electric power reference to keep maximum conversion factor. The limited value ω_g^{max} of windmill speed is set at 105%

of rated speed of PMSG. The windmill speed reference ω_g^{ref} is decided so that the tip speed ratio may become 6 until it reaches ω_g^{max} . The ω_g^{ref} and the electric power reference P^{ref} are determined in order to obtain the maximum windmill efficiency for the wind velocity under the assumption of fixed pitch angle of 10degree until the electric power reaches the rated power P^{rat} . The ω_g^{ref} is made to be ω_g^{max} , and the P^{ref} is made to be P^{rat} when the electric power is over P^{rat} .

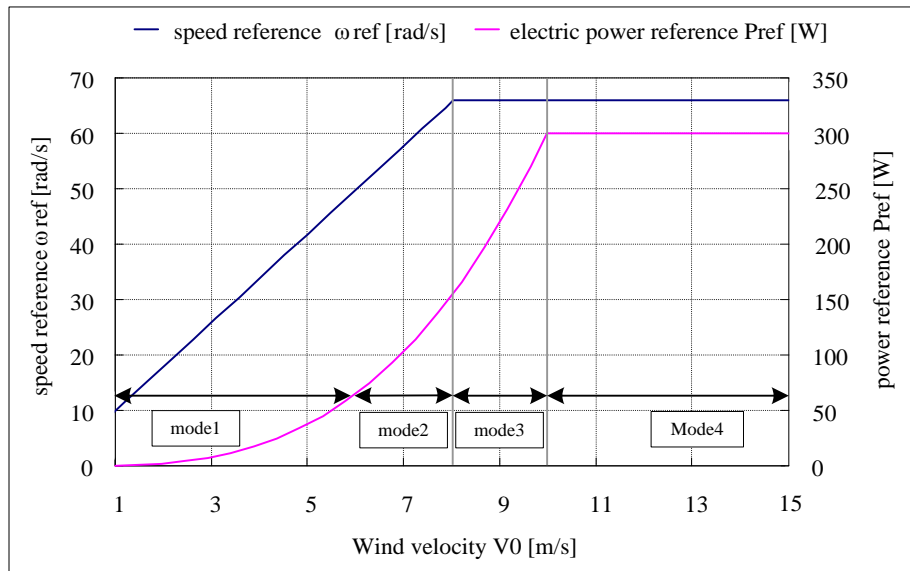


Fig. 3.4. Wind turbine speed reference and electric power reference to keep maximum conversion factor.

The P^{ref} for V_0 which is less than the wind velocity V_0^{max} corresponding to ω_g^{max} is calculated in the wind turbine performance calculation for ω_g^{ref} in advance, and the lookup table of P^{ref} for V_0 is made. The ω_g^{ref} is fixed to ω_g^{max} from V_0^{max} to the rated wind velocity V_0^{rat} (=10.50m/s) corresponding to P^{rat} . The P^{ref} for V_0 is calculated in the wind turbine performance calculation for ω_g^{max} in advance, and the lookup table of

P^{ref} for V_0 is made. In V_0 over V_0^{rat} , ω_g^{ref} is fixed to ω_g^{max} and P^{ref} is fixed to P^{rat} . The P^{ref} is decided for Instantaneous V_0 by referring the lookup table.

Fig. 3.5 shows the logic for control of wind turbine. Fig. 3.5 assumes the steady state in which the sufficient time has passed under the condition of fixed V_0 . In the real machine, the timing of changing the control methods, which are divided into mode1, mode2, mode3 and mode4, cannot be determined based on V_0 as shown in figs. 3.4 and 3.5, since V_0 always changes and the windmill output is influenced by not only V_0 but also the DC link voltage V_{dc} and ω_g [15]. Actually, the control methods are changed based on ω_g , the inverter output P , the *DRS* signal which shows the on/off condition of time ratio control system, the *SRS* signal which shows the on/off condition of speed controller, the *PRS* signal which shows the on/off condition of power controller, as shown in fig. 3.6.

| mode | mode 1 | mode 2 | mode 3 | mode 4 |
|------------------------------|---|--------------------|------------------|--|
| pitch angle | fixed pitch angle (10[deg]) | same | same | Vriable pitch angle |
| speed reference | look up table | same | ω_g^{max} | same |
| power reference | look up table | same | same | P^{rat} |
| Boost converter method | duty cycle regulator | speed regulator | same | pitch angle regulator + power regulator control with PWM inverter |
| PWM converter method | vector control + i_{aq} feedforwaed | same | same | pitch angle regulator + i_{aq} feedforward + power regulator control with PWM converter |

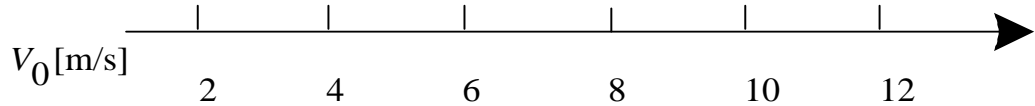


Fig. 3.5. Logic for control of wind turbine.

| rotor speed ω [rad/s] | | $\omega_g \leq \omega_g^{max}$ | | $\omega_g > \omega_g^{max}$ |
|---------------------------------|-------------------------|--------------------------------|-------|-----------------------------|
| converter output P [W] | | There is no condition | | $P > 0.9P^{rat}$ |
| Boost chopper method | Duty cycle regulator | DRS=1 | DRS=0 | DRS=0 |
| | Speed regulator | SRS=0 | SRS=1 | SRS=0 |
| | Power regulator | PRS=0 | PRS=0 | PRS=1 |
| PWM converter method | Speed regulator | SRS=1 | SRS=1 | SRS=0 |
| | Speed regulator | PRS=0 | PRS=0 | PRS=1 |

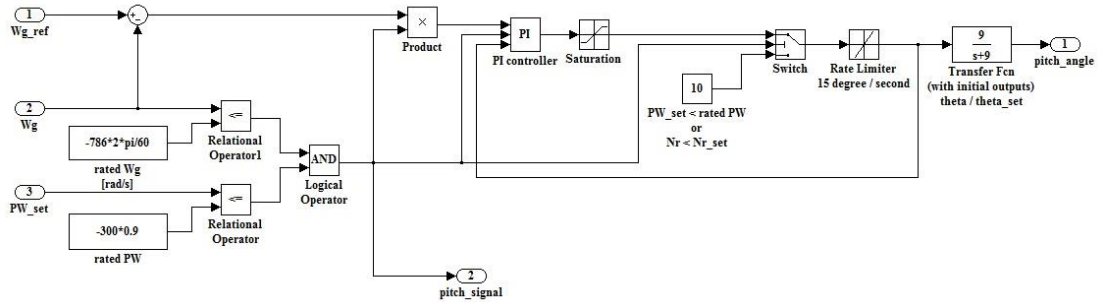
Fig. 3.6. Timing to change control method.

3.3 Pitch angle control system

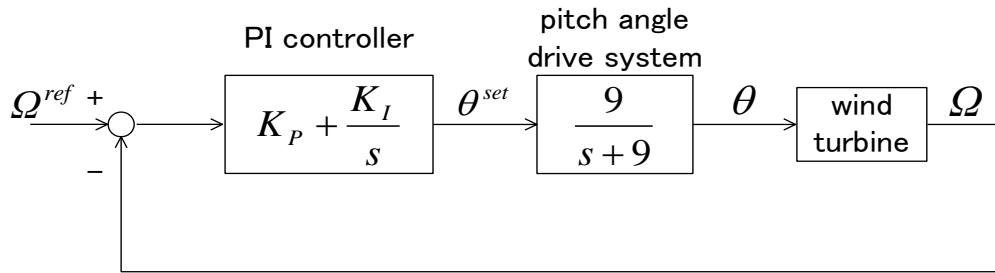
It is not possible to maintain ω_g in ω_g^{max} , because the windmill output has exceeds P^{rat} when V_0 exceeds V_0^{rat} under the condition of ω_g^{max} . Then, the windmill speed is controlled by the pitch angle control system with speed control loop. In the case of boost chopper method in this control mode, the power controller of PWM inverter adjusts V_{dc} so that P may become P^{rat} . And, in the case of PWM converter method, the q axis armature current is adjusted so that P may become P^{rat} .

Fig. 3.7 shows the Simulink and System block diagram of pitch angle control the model of pitch angle drive system describes the response of displacement servo system and hydraulic cylinder. It is described as the first-order lag element, because the hydraulic cylinder has integral characteristics, and because it becomes the

response of the closed-loop system which comprises the servo gain. The time constant of the first-order lag element is the time constant of the pitch angle control system adopted for the wind generation system.



(a) Pitch angle control system Simulink block.



(b) Pitch angle control system block.

Fig. 3.7. Simulink and System block of Pitch angle control.

3.4 Mechanical model for wind turbine

The mechanical systems of the wind turbine side and generator side in Fig.3.8 are described in the equations:

$$\left\{ J_g + J_t \left(\frac{n_2}{n_1} \right)^2 \right\} \frac{d\omega_g}{dt} = T_g - Q \frac{n_2}{n_1} - \left\{ B_g + B_t \left(\frac{n_2}{n_1} \right)^2 \right\} \omega_g \dots\dots(3.22)$$

Where, Q , T_g : The generated torque of the wind turbine side and generator side, T_1 , T_2 : The shaft torque of the wind turbine side and generator side, ω_t , ω_g : The rotor rotational angular speed of wind turbine side and generator side, B_t , B_g : The viscous friction coefficient of the wind turbine side and generator side, J_t , J_g : The moment of inertia of the wind turbine side and generator side.

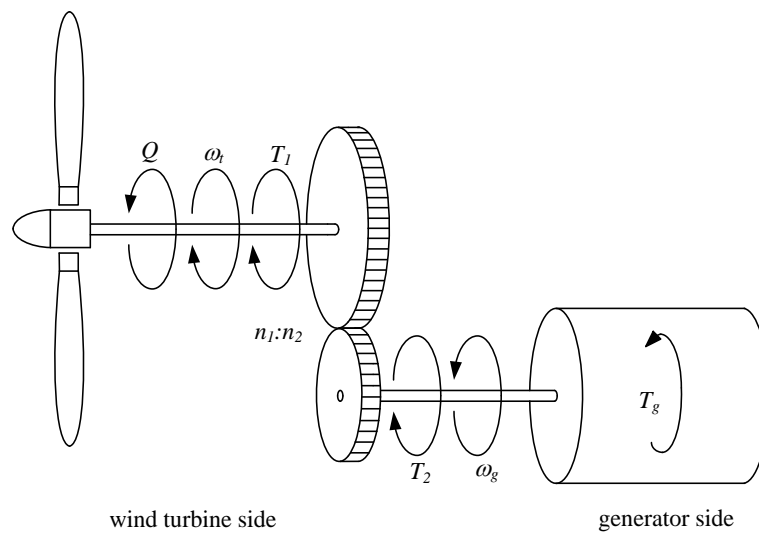


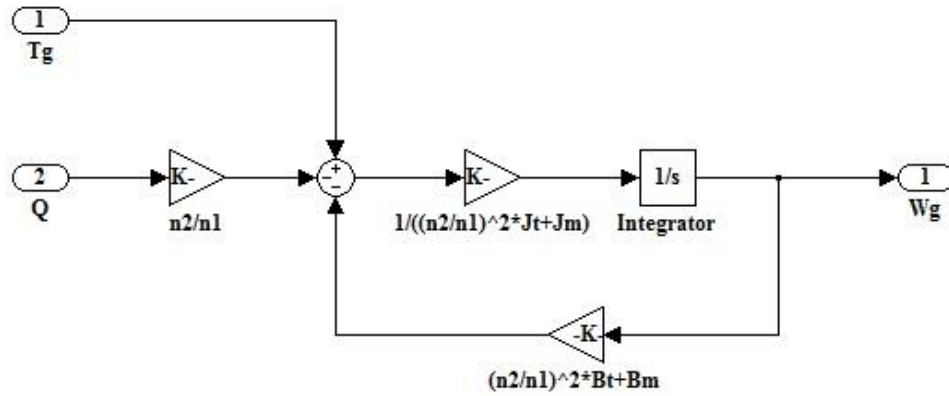
Fig. 3.8. Wind turbine model.

The following equation is obtained, when ω_t is eliminated from equations (3.22) using the gear ratio n_2/n_1 .

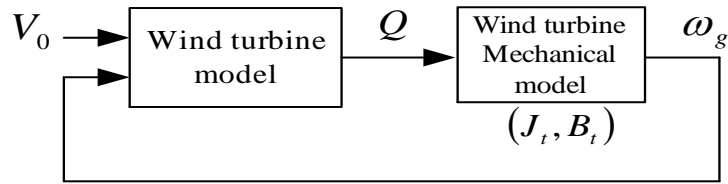
$$\omega_g = \left[T_g - Q \frac{n_2}{n_1} - \left\{ B_g + B_t \left(\frac{n_2}{n_1} \right)^2 \right\} \omega_g \right] \frac{1}{\left\{ J_g + J_t \left(\frac{n_2}{n_1} \right)^2 \right\} s} \dots (3.23)$$

Fig. 3.9 shows the Simulink and System model of the mechanical system is made on the basis of equation (3.23). The Simulink model has the inputs of the generated torque of the wind turbine side Q and the generated torque of the generator side T_g

Also, the Simulink model has the output of the rotor rotational angle speed of the generator side ω_g .



(a). Wind turbine Simulink block.



(b). Wind turbine System block.

Fig. 3.9. Simulink and System block of wind turbine.

3.5 Mechanical model for wind turbine emulator

The mechanical systems of the induction motor side and generator side in Fig.3.10. are described in the equations

$$\left\{ J_g + J_{im} \left(\frac{n_2}{n_1} \right)^2 \right\} \frac{d\omega_g}{dt} = T_g - T_{im} \frac{n_2}{n_1} - \left\{ B_g + B_{im} \left(\frac{n_2}{n_1} \right)^2 \right\} \omega_g \quad \dots(3.24)$$

Where, T_{im} : The generated torque of the induction motor side, T_{1im} : The shaft torque of the induction motor side, ω_{im} : The rotor rotational angular speed of induction motor side, B_{im} : The viscous friction coefficient of the induction motor side, J_{im} : The moment of inertia of the induction motor side. The following equation is obtained, when ω_{im} is eliminated from equations (3.24) using the gear ratio n_2/n_1 .

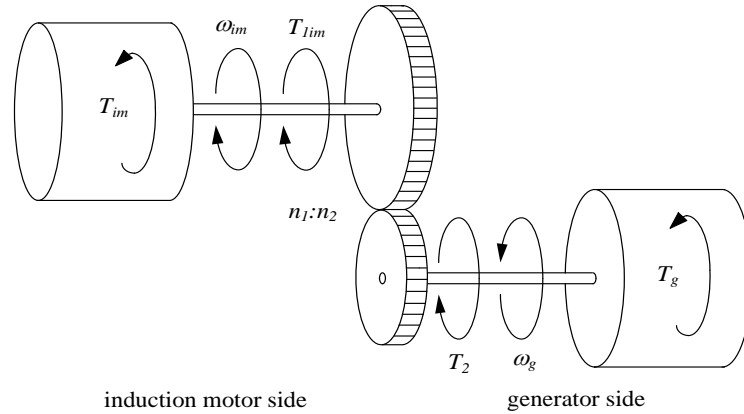
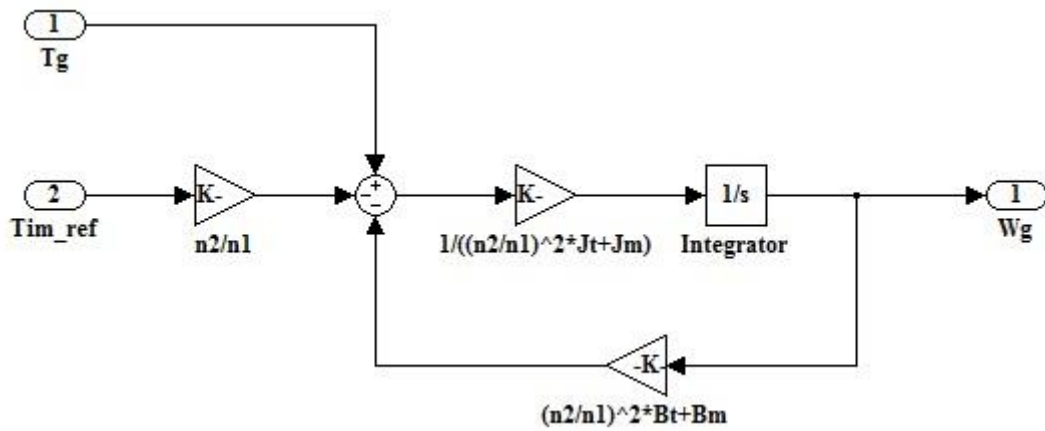


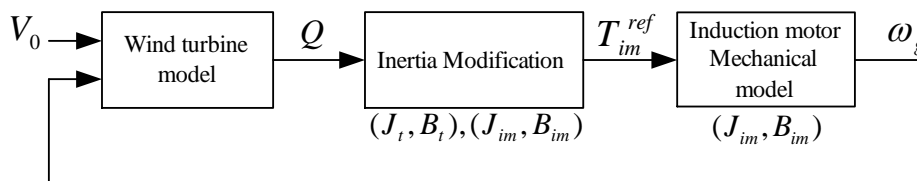
Fig. 3.10. Wind turbine emulator model.

$$\omega_g = \left[T_g - T_{im} \frac{n_2}{n_1} - \left\{ B_g + B_{im} \left(\frac{n_2}{n_1} \right)^2 \right\} \omega_g \right] \frac{1}{\left\{ J_g + J_{im} \left(\frac{n_2}{n_1} \right)^2 \right\} s} \dots\dots(3.25)$$

Fig. 3.11 shows the Simulink and System model of the mechanical system is made on the basis of equation (3.25). The Simulink model has the inputs of the generated torque of the induction motor side T_{im} and the generated torque of the generator side T_g . Also, the Simulink model has the output of the rotor rotational angular speed of the generator side ω_g .



(a) Wind turbine emulator Simulink block.



(b) Wind turbine emulator System block.

Fig. 3.11. Simulink and System block of wind turbine emulator.

3.6 PMSG and converter main circuit

In the case of boost chopper method, the phase voltage and current of PMSG are decided by the external circuit connected with the terminal of PMSG and the induced voltage e of PMSG. Therefore, it is difficult to separate the PMSG from the main circuit, when the converter model of boost chopper method is constructed. In short, PMSG cannot be described by the general voltage equation. In the meantime, in the case of PWM converter method, it is possible to separate the PMSG from the main

circuit for modeling, because the generator terminal voltage can be controlled by the PWM converter regardless of the condition of PMSG. The modeling of PMSG including the converter and main circuit for each case are described.

3.6.1 Modeling of boost chopper method

The PMSG used in this research has the features of brushless, revolving-field type, and cylindrical rotor. Though the equations from (3.26) to (3.32) are common awareness, they are explained because they must be quoted for the modeling of boost chopper method. Fig. 3.12 shows the Simulink and model equivalent circuit of PMSG. The circuit equations are described by following equations, since the armature voltage are the sum of speed electromotive forces for permanent magnet field and the induced voltages for magnetic flux excited by the armature winding [70], [71].thesis

$$\begin{bmatrix} v_{au} \\ v_{av} \\ v_{aw} \end{bmatrix} = \begin{bmatrix} R_a + pL_a' & -1/2pM_a' & -1/2pM_a' \\ -1/2pM_a' & R_a + pL_a' & -1/2pM_a' \\ -1/2pM_a' & -1/2pM_a' & R_a + pL_a' \end{bmatrix} \begin{bmatrix} i_{au} \\ i_{av} \\ i_{aw} \end{bmatrix} + \begin{bmatrix} e_{au} \\ e_{av} \\ e_{aw} \end{bmatrix} \dots\dots(3.26)$$

Where, v_{au} , v_{av} , v_{aw} : armature voltages, i_{au} , i_{av} , i_{aw} : armature currents, e_{au} , e_{av} , e_{aw} : speed electromotive forces for permanent magnet field, R_a : armature winding resistance, L_a' : self-inductance of armature winding, M_a' : mutual inductance of armature winding, ω_{ge} : rotor angular speed (electrical angle), θ_{ge} : rotor position (electrical angle), p : time derivative operator.

The magnetic flux linkages ϕ_{fau} , ϕ_{fav} , ϕ_{faw} of permanent magnet field are described by following equations. The Φ'_{fa} is the maximum value of magnetic flux linkages.

$$\phi_{fau} = \Phi'_{fa} \cos\theta_{ge} \dots\dots\dots(3.27)$$

$$\phi_{fav} = \Phi'_{fa} \cos(\theta_{ge} - 2\pi/3) \dots\dots\dots(3.28)$$

$$\phi_{faw} = \Phi'_{fa} \cos(\theta_{ge} + 2\pi/3) \dots\dots\dots(3.29)$$

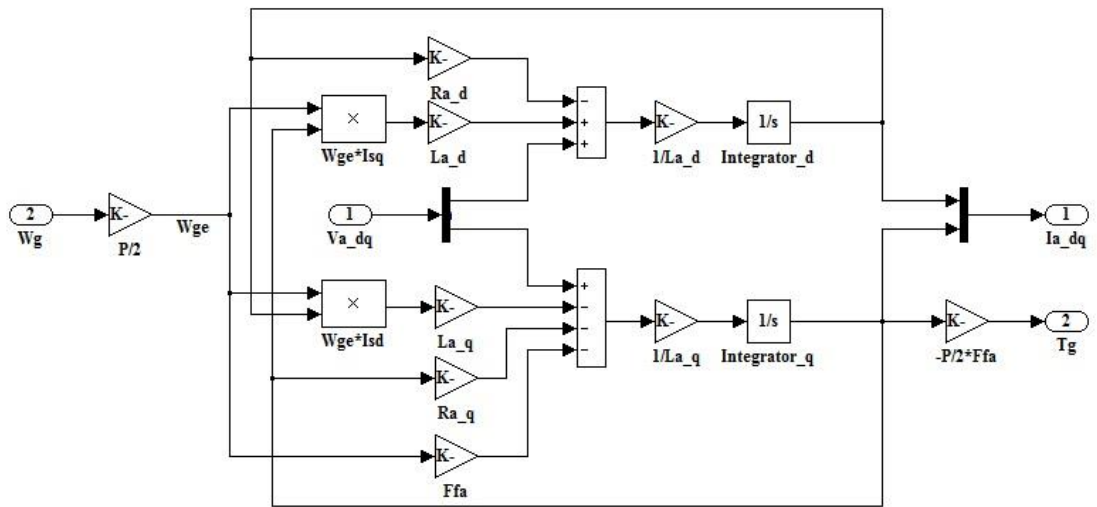
The θ_{ge} is the rotor position (electrical angle) in clockwise rotation from the u phase armature winding, as shown in fig. 3.12. The speed electromotive forces e_{au} , e_{av} , e_{aw} induced in the armature windings are obtained by differentiating the equations (3.27) – (3.29) in a time.

$$e_{au} = p\phi_{fau} = -\omega_{ge}\Phi'_{fa} \sin\theta_{ge} \dots\dots\dots(3.30)$$

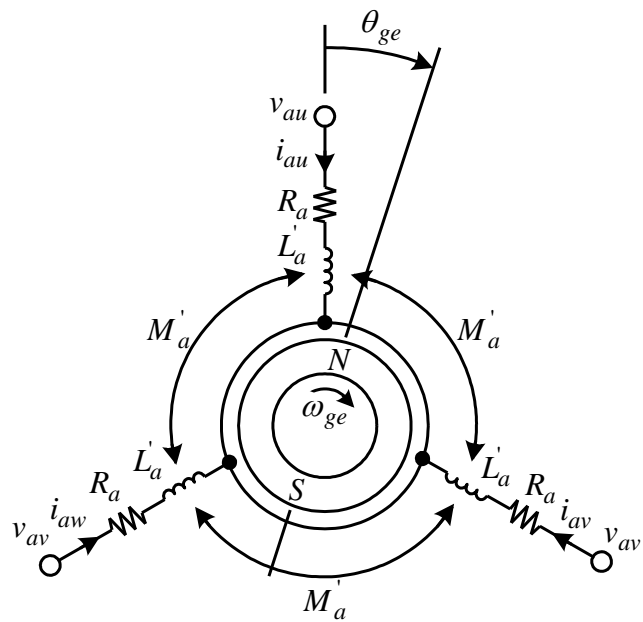
$$e_{av} = p\phi_{fav} = -\omega_{ge}\Phi'_{fa} \sin(\theta_{ge} - 2\pi/3) \dots\dots\dots(3.31)$$

$$e_{aw} = p\phi_{faw} = -\omega_{ge}\Phi'_{fa} \sin(\theta_{ge} + 2\pi/3) \dots\dots\dots(3.32)$$

The diode bridge rectifier is conducted, when the potential difference between the line voltage of PMSG and the DC link voltage V_{dc} is positive. The conducting lines are lines between the maximum phase voltage and minimum phase voltage. And after the conduction, the current keeps to conduct until the current becomes zero in spite of the magnitude of line voltage. And in the case of boost chopper circuit, two circuits of T_r on and T_r off must be considered for the condition of switch T_r .



(a) dq -axis converter of PMSG Simulink model.



(b) Model equivalent circuit of PMSG

Fig. 3.12. Simulink and model Equivalent circuit of PMSG

Fig. 3.13 shows the converter main circuit of conduction mode 1. The D_{u1} is the diode of u phase upper arm, and the D_{v2} is the diode of v phase bottom arm. The L_{dc} is the inductance component of the reactor in the boost chopper circuit, and the r_L is the resistance component of the reactor in the boost chopper circuit. The T_r is the switching device in the boost chopper circuit, and its on-resistance is r_T . The D is the diode in the boost chopper circuit, and its resistance component is r_D . The C_{dc} is the DC link condenser, and the R_{dc} is the electric discharge resistance. And fig. 3.14-3.18 shows the converter main circuits for conduction modes 2 - 6.

Where, i_{dc1} : Current flowing through the diode bridge rectifier circuit [A], D_{U1} : Diode maximum voltage side of the diode bridge rectifier circuit, D_{V2} : Diode minimum voltage side of the diode bridge rectifier circuit, L_{dc} : Inductance of the step-up chopper circuit [H], r_L : Resistance of inductance itself of the step-up chopper circuit [Ω], Tr : Switch of the boost chopper circuit, r_T : Switching resistance [Ω], D : Diode of the boost chopper circuit, r_D : Resistance of the diode itself of the boost chopper circuit [Ω], C_{dc} : DC link capacitor [F], R_{dc} : DC link resistance [Ω], V_{dc} : DC link voltage [V],

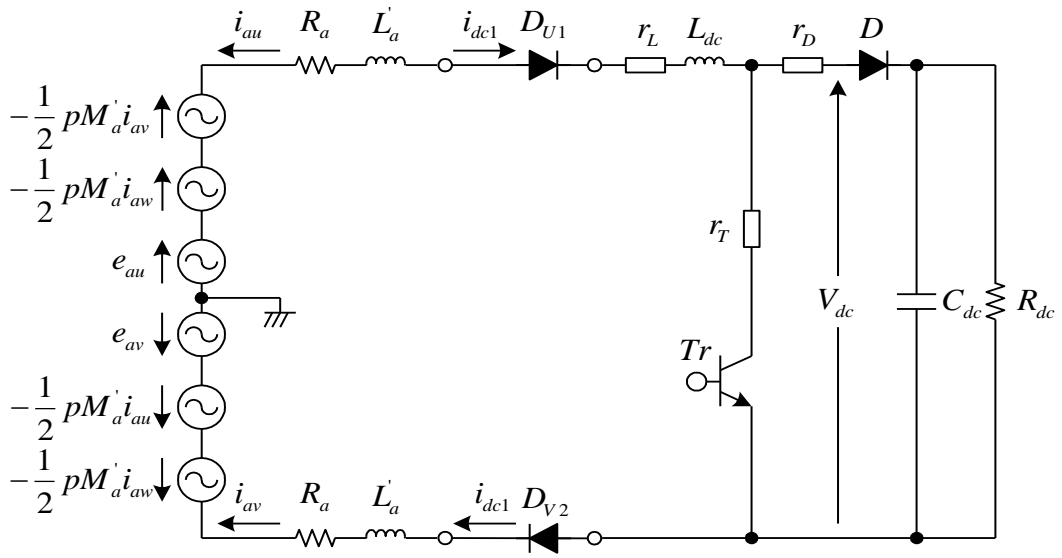


Fig. 3.13. *U*-phase, *V*-phase main circuit of (conduction mode ①)

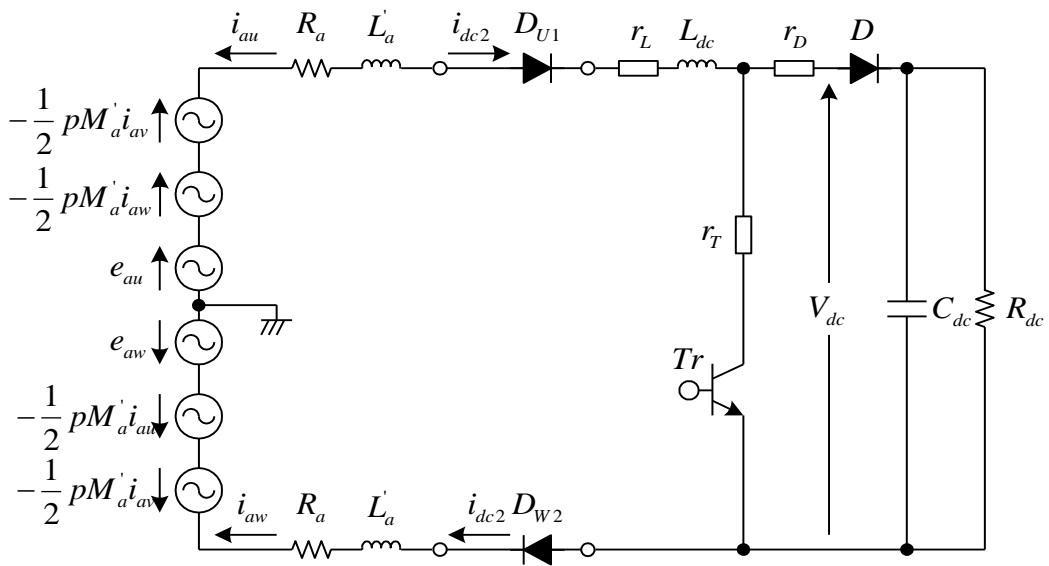


Fig. 3.14. *U*-phase, *W*-phase main circuit of (conduction mode ②)

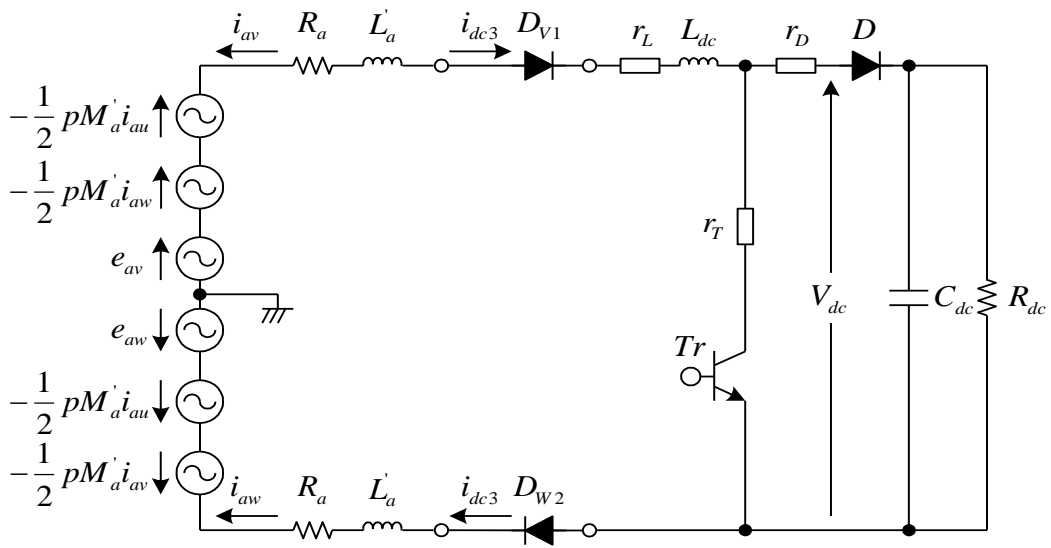


Fig. 3.15. V-phase, W-phase main circuit of (conduction mode ③)

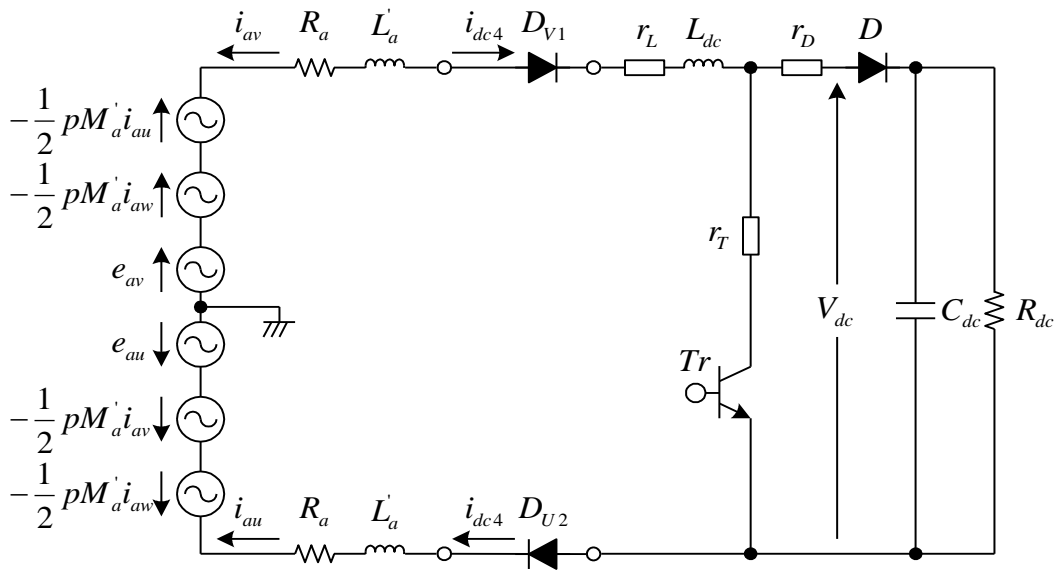


Fig. 3.16. V-phase, U-phase main circuit of (conduction mode ④)

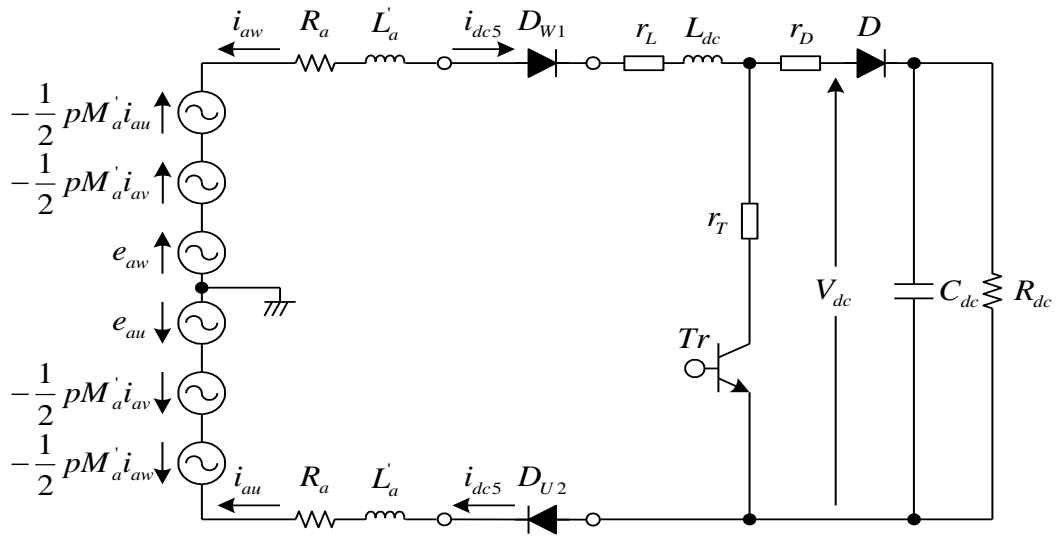


Fig. 3.17. W-phase, U-phase main circuit of (conduction mode ⑤)

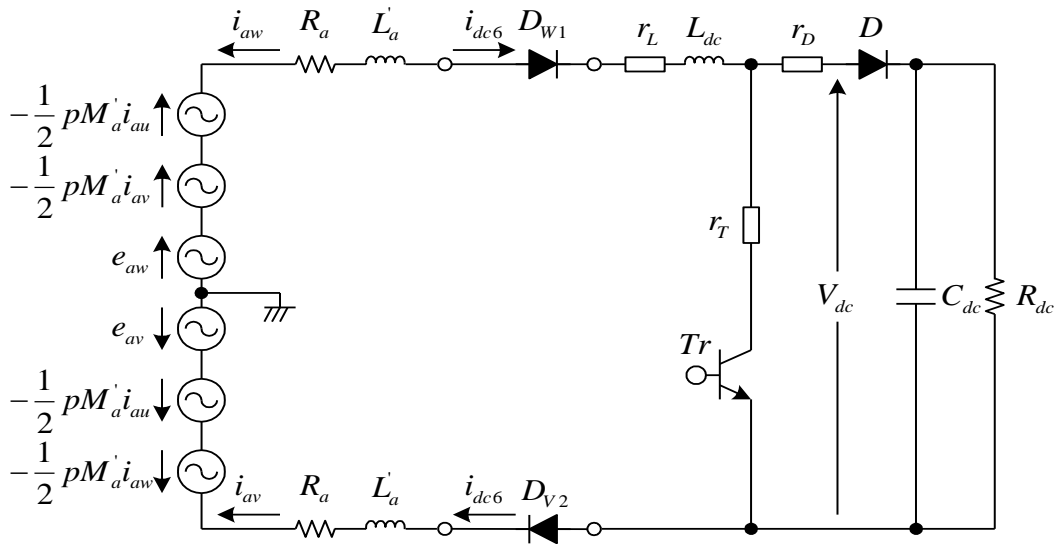


Fig. 3.18. W-phase, V-phase main circuit of (conduction mode ⑥)

Table 3.1 shows the conduction mode of diode bridge rectifier. At the each conduction mode, the forward currents, which flow the diode bridge rectifier, are defined as $i_{dc1} - i_{dc6}$. The lines between the maximum and minimum phase voltages of PMSG are conducted. Therefore, two conduction modes exist, since the v and w phases have a possibility of becoming a smallest voltage when the u phase is maximum voltage. In the same way, six conduction modes exist in total, since two conduction modes exist for each case of v and w phases are maximum voltages.

Table 3.1. Conduction mode of diode bridge rectifier

| Conduction mode | Phase of maximum voltage | Phase of minimum voltage | Phase current | | |
|-----------------|--------------------------|--------------------------|---------------|------------|------------|
| | | | i_{au} | i_{av} | i_{aw} |
| ① | U | V | $-i_{dc1}$ | i_{dc1} | 0 |
| ② | U | W | $-i_{dc2}$ | 0 | i_{dc2} |
| ③ | V | W | 0 | $-i_{dc3}$ | i_{dc3} |
| ④ | V | U | i_{dc4} | $-i_{dc4}$ | 0 |
| ⑤ | W | U | i_{dc5} | 0 | $-i_{dc5}$ |
| ⑥ | W | V | 0 | i_{dc6} | $-i_{dc6}$ |

The phase, which has the maximum sum E_a of the speed electromotive force and the induced voltage of PMSG, makes conduct the upper arm diode of diode bridge rectifier circuit. The phase, which has the minimum E_a makes conduct the bottom arm diode. The E_{au} , E_{av} , and E_{aw} are described by following equations.

$$E_{au} = e_{au} - pM'_a(i_{av} + i_{aw})/2 \dots\dots\dots (3.33)$$

$$E_{av} = e_{av} - pM'_a(i_{aw} + i_{au})/2 \dots\dots\dots (3.34)$$

$$E_{aw} = e_{aw} - pM'_a(i_{au} + i_{av})/2 \dots\dots\dots(3.35)$$

It is necessary for modeling of such behaviors to detect the phase of maximum and minimum E_a and decide the conduction modes. Fig. 3.19 shows the Simulink model to detect conduction modes. The inputs of Simulink model are E_{au} , E_{av} , and E_{aw} . The output of “max” is the E_a of maximum phase, and the output of “min” is the E_a of minimum phase. The maximum and minimum phases are detected with the relational operators by comparing the outputs of “max” and “min” with E_a of all phases. In addition, the “AND” outputs the signals CM1 - CM6 which show the on/off condition of each conduction modes.

The phase current cannot be broken until the phase current becomes zero because the armature winding has the effect of inductance even if the conduction mode changes. Then multiple conduction modes exist at same time. Therefore, the DC link current i_{dc} of the output from diode bridge rectifiers becomes the sum of currents which flow in the forward direction at all conduction modes.

$$i_{dc} = i_{dc1} + i_{dc2} + i_{dc3} + i_{dc4} + i_{dc5} + i_{dc6} \dots\dots\dots(3.36)$$

The phase currents i_{au} , i_{av} , and i_{aw} of PMSG are described by using the relationship of table 3.3 as follows.

$$i_{au} = -i_{dc1} - i_{dc2} + i_{dc4} + i_{dc5} \dots\dots\dots(3.37)$$

$$i_{av} = i_{dc1} - i_{dc3} - i_{dc4} + i_{dc6} \dots\dots\dots(3.38)$$

$$i_{aw} = i_{dc2} + i_{dc3} - i_{dc5} - i_{dc6} \dots\dots\dots(3.39)$$

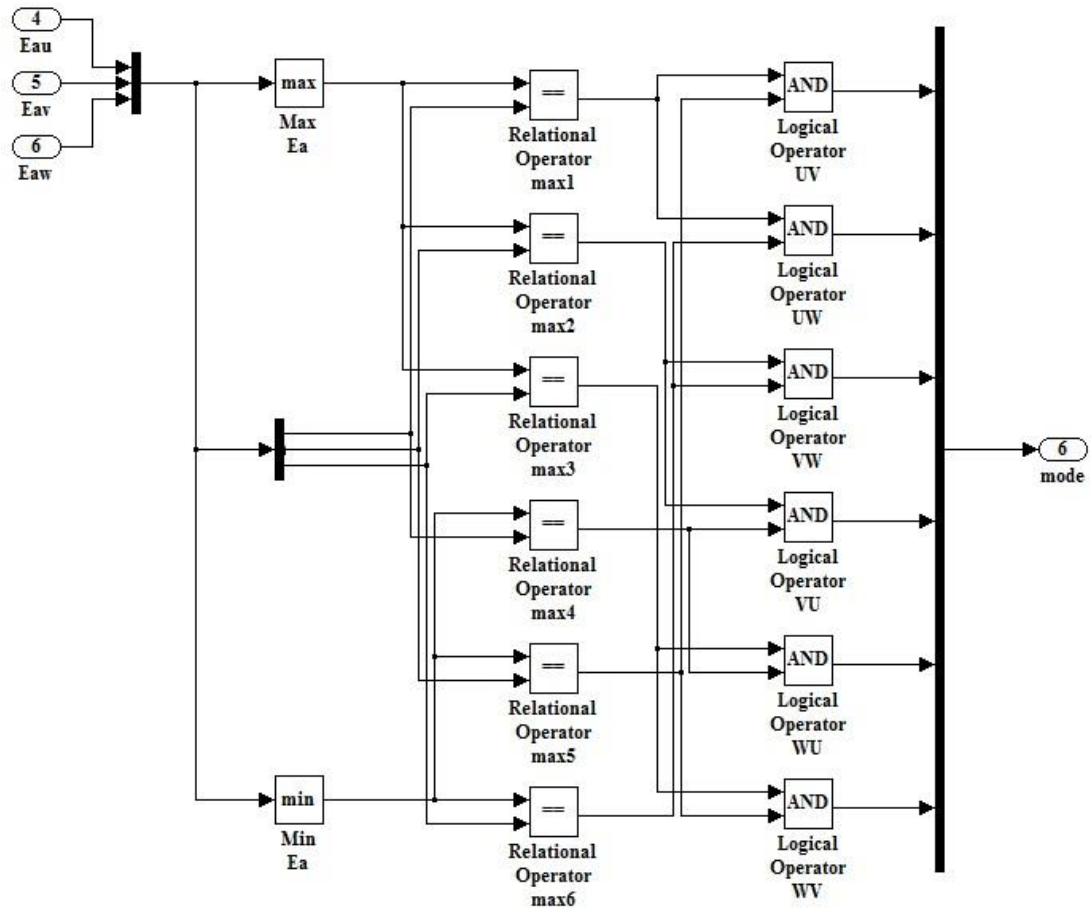


Fig. 3.19. Simulink model to detect conduction mode

The boost chopper circuit connected with diode bridge rectifier has two operating modes of T_r on and T_r off. Fig. 3.20 shows the Simulink and model simplified converter main circuits for T_r on and T_r off of conduction mode 1. The simplified main circuits for the conduction modes 2 – 6, The e_{dc1} for conduction mode 1 of fig. 3.20 and the $e_{dc2} - e_{dc6}$ for conduction modes 2 - 6 are described at the equations (3.40) - (3.45). The $e_{dc1} - e_{dc6}$ are the sums of speed electromotive forces generated by

permanent magnet field and the induced voltages generated by mutual inductances between each line.

$$e_{dc1} = e_{au} - e_{av} - pM'_a(i_{av} - i_{au})/2 \dots\dots\dots(3.40)$$

$$e_{dc2} = e_{au} - e_{aw} - pM'_a(i_{aw} - i_{au})/2 \dots\dots\dots(3.41)$$

$$e_{dc3} = e_{av} - e_{aw} - pM'_a(i_{aw} - i_{av})/2 \dots\dots\dots(3.42)$$

$$e_{dc4} = e_{av} - e_{au} - pM'_a(i_{au} - i_{av})/2 \dots\dots\dots(3.43)$$

$$e_{dc5} = e_{aw} - e_{au} - pM'_a(i_{au} - i_{aw})/2 \dots\dots\dots(3.44)$$

$$e_{dc6} = e_{aw} - e_{av} - pM'_a(i_{av} - i_{aw})/2 \dots\dots\dots(3.45)$$

The following equation is obtained from the equivalent circuit for T_r on of fig. 3.20 (a).

$$(2R_a + r_L + r_T)i_{dcl}^{on} + (2L'_a + L_{dc})p i_{dcl}^{on} = e_{dcl} \dots\dots\dots(3.46)$$

The calculation for T_r on needs to be started from the final value for T_r off as an initial value. The Simulink model for T_r on is constructed with the following equation derived from the equation (3.46).

$$i_{dcl}^{on} = \frac{e_{dcl}}{(2L'_a + L_{dc})s + 2R_a + r_L + r_T} + i_{dcl}^{on}(0-) \dots\dots\dots(3.47)$$

The conditions to conduct the diode D_{u1} and D_{u2} for T_r on are described by following equations using relational and logical operators.

$$e_{dcl} - (2L'_a + L_{dc})p i_{dcl}^{on} > 0 \text{ OR } i_{dcl}^{on} > 0 \dots\dots\dots(3.48)$$

The following equation is obtained from the equivalent circuit for T_r off of fig. 3.20 (b).

$$(2R_a + r_L + r_D)i_{dc1}^{off} + (2L'_a + L_{dc})\frac{d}{dt}i_{dc1}^{off} = e_{dc1} - V_{dc}^{off} \dots\dots\dots(3.49)$$

The calculation for T_r off needs to be started from the final value for T_r on as an initial value. The Simulink model for T_r off is constructed with the following equation derived from the equation (3.50).

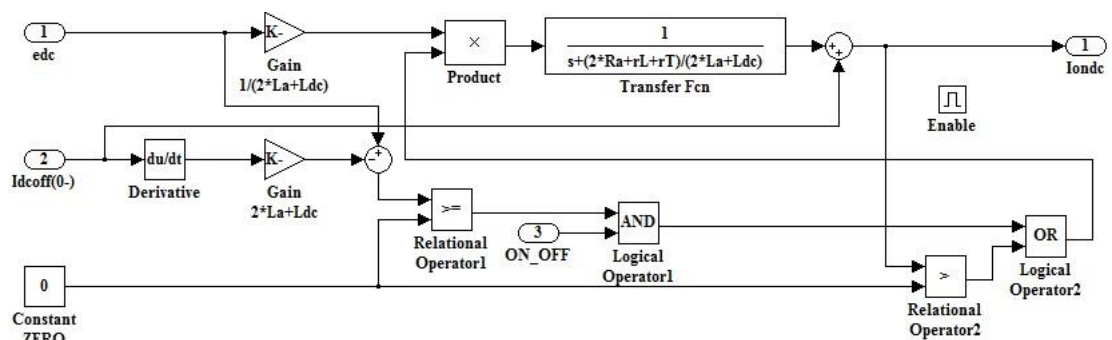
$$i_{dc1}^{off} = \frac{(e_{dc1} - V_{dc}^{off})}{(2L'_a + L_{dc})s + 2R_a + r_L + r_D} + i_{dc1}^{off}(0-) \dots\dots\dots(3.50)$$

The conditions to conduct the diode D_{u1} and D_{u2} for T_r off are described by following equations using relational and logical operators.

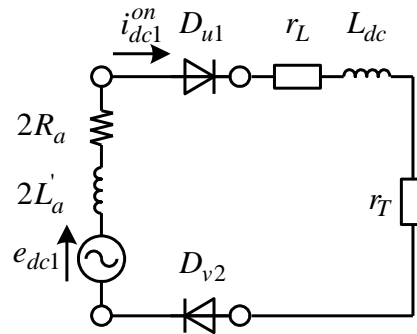
$$e_{dc1} - V_{dc}^{off} - (2L'_a + L_{dc})p i_{dc1}^{off} > 0 \text{ OR } i_{dc1}^{off} > 0 \dots\dots\dots(3.51)$$

The generated torque T_g of PMSG is described with the pole number P , flux linkage Φ_{fa} , and torque current i_{aq} in dq synchronous rotating frame as follows.

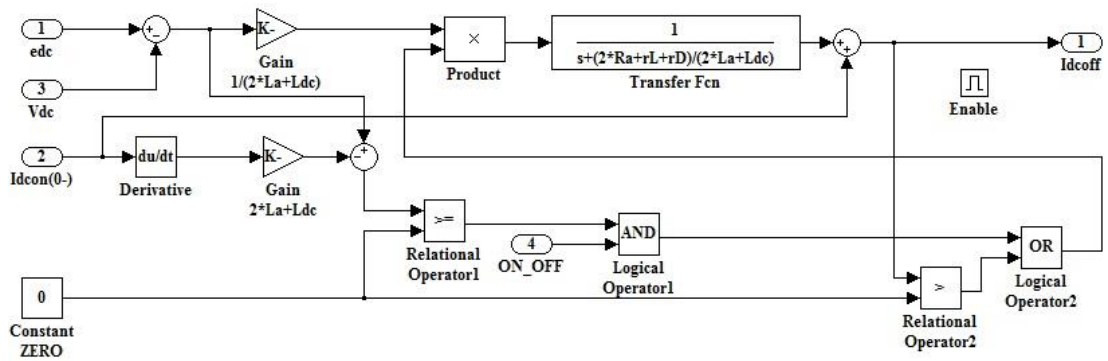
$$T_g = P\Phi_{fa}i_{aq} \dots\dots\dots(3.52)$$



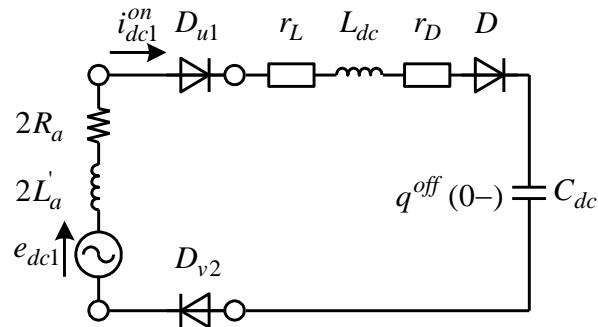
(a) T_r on Simulink block



(b) T_r on. model



(c) T_r off Simulink block



(d) T_r off. model

Fig. 3.20. Simulink and model simplified converter main circuit of

(Conduction mode ①)

The generated power P_g of PMSG is described with the armature voltage v_a and armature current i_a as follows.

$$P_g = v_{ad}i_{ad} + v_{aq}i_{aq} \dots\dots\dots(3.53)$$

The time ratio B_d of T_r on and T_r off is renewed at the switching frequency of 1kHz. The current i_{dc1} for T_r on is calculated with equation (3.47), and the i_{dc1} for T_r off is calculated with equation (3.50). The “Enabled Subsystem” can realize the switching of calculation formulas in MATLAB Simulink. And, the final values just before the switching mode of T_r on and T_r off changes are used as the initial values immediately after the switching mode changes. In MATLAB Simulink, the “Switch block” triggered by B_d can realizes these procedures.

The two operating modes of T_r on and T_r off of the boost chopper circuit exist for six conduction modes of diode bridge rectifier. The Simulink block becomes the complicated Subsystem which has the Subsystems of two operating modes in the Subsystems of six conduction modes. And, the calculations become large-scale including the calculations as follows, the speed electromotive forces e_{au} , e_{av} , e_{aw} of equations (3.30) - (3.32), the detection of conduction modes of fig. 3.19 including E_{au} , E_{av} , E_{aw} of equations (3.33) - (3.35), the DC link current i_{dc} of equation (3.36) which is outputted from the diode bridge rectifier, the phase currents i_{au} , i_{av} , i_{aw} of equations (3.37) - (3.39), the e_{dc1} - e_{dc6} of equations (3.40) - (3.45) which are the sums of the speed electromotive forces by permanent magnet field and the induced voltages by

mutual inductances between each lines, the generated torque T_g of PMSG of equation (3.52), and the generated output P_g of equation (3.53).

3.6.2 Modeling of PWM converter method

The Simulink model of PMSG is constructed by utilizing the voltage equations of (3.42) and (3.43) in dq synchronous rotating frame [71], [72]. Though the following equations of (3.54) and (3.55) are common awareness, the description is carried out to clarify the condition of simulation.

$$i_{ad} = (v_{ad} - R_a i_{ad} + \omega_{ge} L_a i_{aq} - e_{ad}) / s L_a \dots\dots\dots(3.54)$$

$$i_{aq} = (v_{aq} - R_a i_{aq} - \omega_{ge} L_a i_{ad} - e_{aq}) / s L_a \dots\dots\dots(3.55)$$

The Simulink model of PMSG is constructed with equations of (3.54) and (3.55). The inputs are v_a and rotor angular speed ω_{ge} (electrical angle), and the output are i_a , T_g , and P_g . The switching behaviors of IGBT in the PWM converter are not considered, and the output voltage limitation caused by the DC link voltage V_{dc} is considered. The sufficient accuracy is obtained by the analysis in fundamental wave, since the switching frequency of 2kHz is used in the practical wind generator system. And, the calculation considering switching behaviors increases the simulation time by about 10 times in comparison with the case of the calculation not considering switching behaviors. It is needed to avoid the increase in the simulation time when the wind generator system is evaluated, since examinations for a few minutes are carried out.

Fig. 3.21 shows the model of PWM converter main circuit. The V_a^{ref} is used as V_a , and the limiter of $\pm V_{dc}/2$ is applied after converting V_a^{ref} to the three-phase value. The output voltage restriction caused by V_{dc} is considered by this limiter, and the behaviors for starting and V_{dc} changes become more realistic.

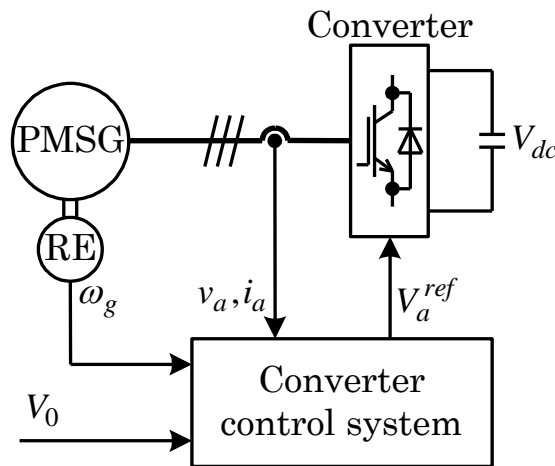


Fig. 3.21. Model of PWM converter main circuit

3.7 Mechanical systems

The modeling of mechanical system is constructed by utilizing the equations of (3.25) the equation deduced in (3.25) is described again. by equation (3.56).

$$\left\{ \left(\frac{n_2}{n_1} \right)^2 J_t + J_m \right\} p \omega_g + \left\{ \left(\frac{n_2}{n_1} \right)^2 B_t + B_m \right\} \omega_g = Q - \left(\frac{n_2}{n_1} \right) T_g \quad \dots \dots \dots (3.56)$$

Where, Q , T_g : generated torques for windmill and PMSG sides, T_1 , T_2 : shaft torques for windmill and PMSG sides, ω_g : Rotor angular speed (mechanical angle), B_t , B_m : Viscous friction coefficient for windmill and PMSG sides, J_t , J_m : moments of inertia

for windmill and PMSG sides, and n_1/n_2 : gear ratio. The Simulink model is constructed by using the following equation deduced from the equation (3.57).

$$\omega_g = \frac{Q - (n_2/n_1)T_g}{((n_2/n_1)^2 J_t + J_m)s + (n_2/n_1)^2 B_t + B_m} \dots\dots\dots(3.57)$$

The gear ratio n_1/n_2 becomes 1, since the gearless is achieved by adopting the multipole PMSG. The Simulink model is made based on the equation (3.57). The inputs are Q and T_e , and output is ω_g .

3.8 DC link division

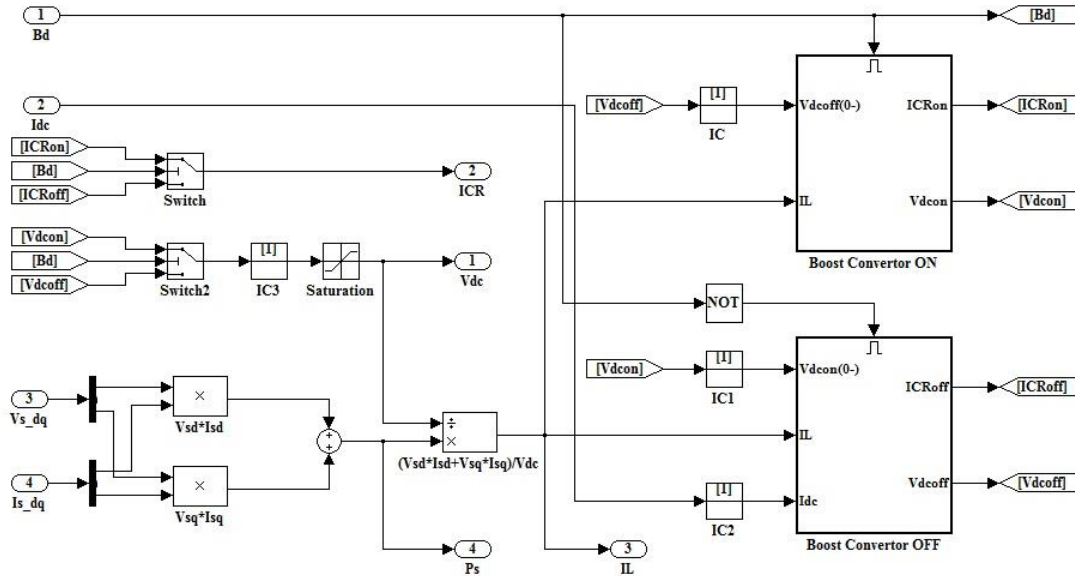
The DC link division is the junction of converter and inverter. Though the circuit structure of boost chopper method and PWM converter method in the DC link division is same, it is necessary to use the different model since the different converter is connected to the DC link division.

3.8.1 Modeling of boost chopper method

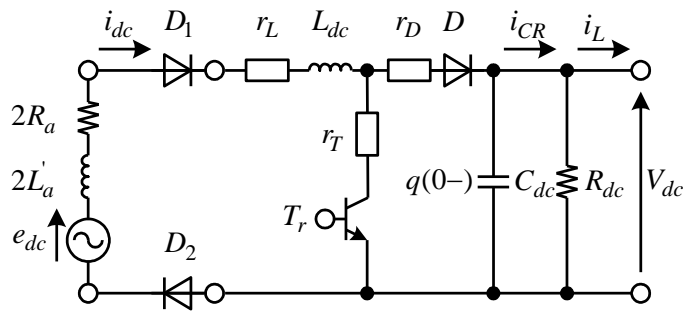
Fig. 3.22 shows the Simulink and model DC link model of boost converter method. The DC link current i_{dc} charging the DC link condenser C_{dc} from PMSG is described by equation (3.36). The current i_L which flows from the DC link division to the system side is calculated with the following equation, since the electric power $V_{dc}i_L$

which pass the DC link division is equal to the electric power $v_{sd}i_{sd}+v_{sq}i_{sq}$ which passes the inverter.

$$i_L = (v_{sd}i_{sd} + v_{sq}i_{sq})/V_{dc} \dots\dots\dots(3.58)$$



(a) DC link model of boost converter method Simulink block



(b) Model DC link model of boost converter method

Fig. 3.22. Simulink and model DC link model of boost converter method

Fig. 3.23 shows the Simulink and model simplified DC link model of boost converter method for T_r on and T_r off. In the case of boost chopper method, the converter main

circuit connected to C_{dc} changes for the conditions of T_r . The transition from T_r off to T_r on must be considered, when the behavior for T_r on is considered. The $q^{on}(0-)$ in fig. 3.23(a) is the electric charge charged in C_{dc} just before switching from T_r off to T_r on. The following equation is obtained from fig. 3.23(a).

$$V_{dc}^{on} = R_{dc}(i_{CR}^{on} - i_L) = -\frac{1}{C_{dc}} \int i_{CR}^{on} dt + \frac{q^{on}(0-)}{C_{dc}} \dots\dots\dots(3.59)$$

The calculation for T_r on needs to start from the last value for T_r off as an initial value. The Simulink model for T_r on is constructed by using the following equation deduced from equation (3.60).

$$V_{dc}^{on} = (-i_{CR}^{on})/sC_{dc} + V_{dc}^{on}(0-) \dots\dots\dots(3.60)$$

$$i_{CR}^{on} = (V_{dc}^{on} + R_{dc}i_L)/R_{dc} \dots\dots\dots(3.61)$$

The transition from T_r on to T_r off must be considered, when the behavior in T_r off is considered. The $q^{off}(0-)$ in figure 3.23(b) is the electric charge charged in C_{dc} just before switching from the T_r on to the T_r off. The following equation is obtained from fig. 3.23(b).

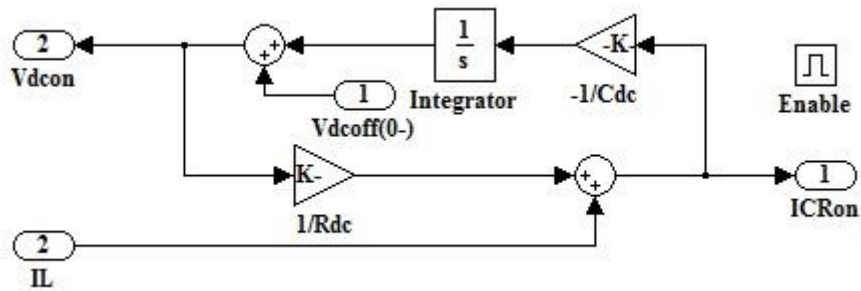
$$V_{dc}^{off} = R_{dc}(i_{CR}^{off} - i_L) = \frac{1}{C_{dc}} \int (i_{dc}^{off} - i_{CR}^{off}) dt + \frac{q^{off}(0-)}{C_{dc}} \dots\dots\dots(3.62)$$

The calculation for T_r off needs to start from the last value for T_r on as an initial value. The Simulink model for T_r off is constructed by using the following equation deduced from equation (3.62).

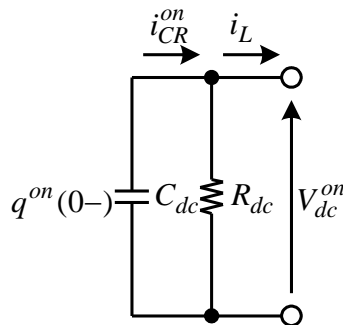
$$V_{dc}^{off} = (i_{dc}^{off} - i_{CR}^{off})/sC_{dc} + V_{dc}^{off}(0-) \dots\dots\dots(3.63)$$

$$i_{CR}^{off} = (V_{dc}^{off} + R_{dc}i_L) / R_{dc} \dots\dots\dots(3.64)$$

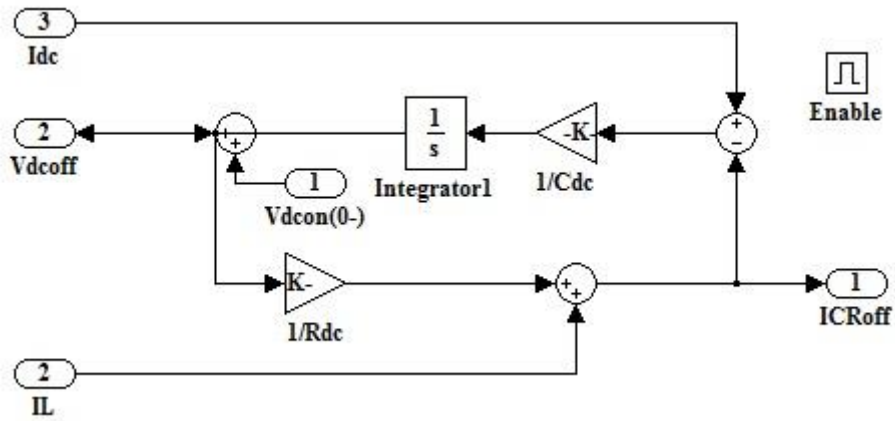
The DC link voltage V_{dc} for T_r on is calculated by equation (3.60), and V_{dc} for T_r off is calculated by equation (3.63). The “Enabled Subsystem” can realize the switching of calculation formula in MATLAB Simulink. And, the final values just before the switching mode of T_r on and T_r off changes are used as the initial values immediately after the switching mode changes. In MATLAB Simulink, the “Switch block” triggered by B_d can realizes these procedures. The Simulink block is composed of the subsystems for two operating modes and the current i_L of equation (3.58) which flows from the DC link division to the system side.



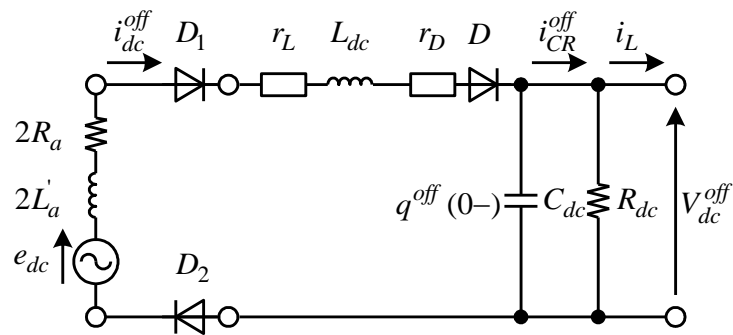
(a) T_r on. Simulink block



(b) T_r on. model



(a) T_r off. Simulink block



(c) T_r off. model

Fig. 3.23. Simulink and model Simplified DC link model of boost converter method

3.8.2 Modeling of PWM converter method

Though the equations (3.65) - (3.68) of 3.8.2 are the common awareness [19], they are explained to clarify the condition of simulation. Fig. 3.24 shows the Simulink and DC link model of PWM converter method. The current i_{dc} which flows from the PMSG to the DC link division is calculated by following equation. The equation is deduced

since the electric power $V_{dc}i_{dc}$ which pass the converter is equal to the electric power $v_{ad}i_{ad}+v_{aq}i_{aq}$ which pass the DC link division.

$$i_{dc} = -(v_{ad}i_{ad} + v_{aq}i_{aq})/V_{dc} \dots\dots\dots(3.65)$$

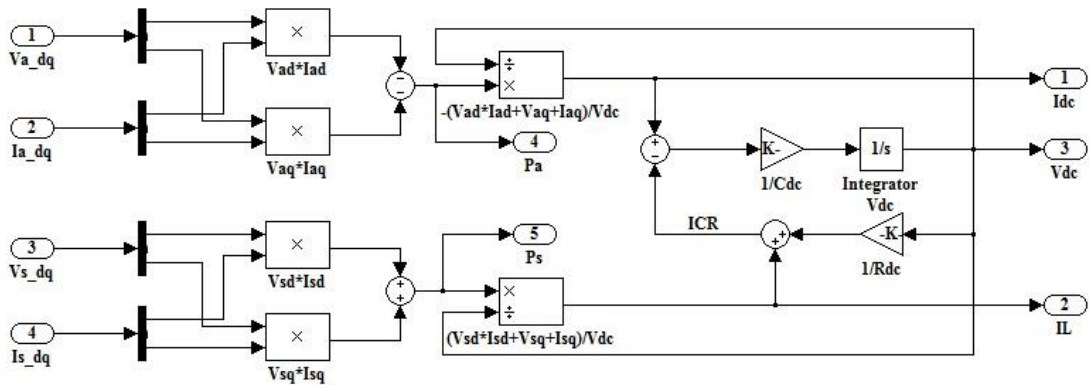
The current i_L which flows from the DC link division to the system side is described by the equation (3.58) as well as the boost chopper method. And the following equation is deduced from fig. 3.24.

$$V_{dc} = R_{dc}(i_{CR}^{on} - i_L) = \frac{1}{C_{dc}} \int (i_{dc} - i_{CR}) dt \dots\dots\dots(3.66)$$

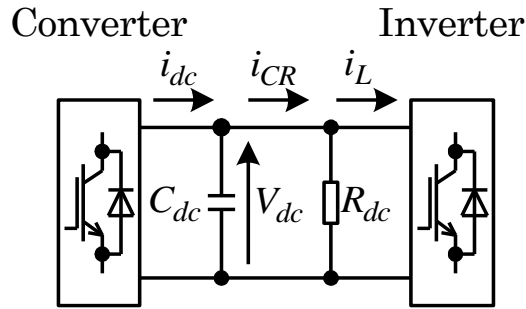
The Simulink model is constructed with the following equations deduced from the equation (3.66).

$$V_{dc} = (i_{dc} - i_{CR})/sC_{dc} \dots\dots\dots(3.67)$$

$$i_{CR} = V_{dc}/R_{dc} + i_L \dots\dots\dots(3.68)$$



(a) DC link model of PWM converter method Simulink block



(b) DC link model of PWM converter method

Fig. 3.24. Simulink and DC link model of PWM converter method

3.9 Converter control system

Since the circuit of converter division is completely different between the boost chopper method and the PWM converter method, it is necessary for converter control systems to utilize different control logics. The control logics and modeling for both methods are explained in this section.

3.9.1 Modeling of boost chopper method

In the boost chopper method, the speed of PMSG is controlled by adjusting the current i_{dc} which flows from the PMSG to the DC link division or adjusting the generated torque T_g of PMSG. It was shown that T_g can be controlled by adjusting the DC link voltage V_{dc} or adjusting i_{dc} [15]. And, the adjustable range of V_{dc} necessary for adjusting T_g becomes always under the voltage which enables the system

interconnection in the operating range of low windmill speed for low wind velocity. This operating range is corresponding to mode 1 of fig. 3.4 and fig. 3.5. Then, the i_{dc} which corresponds to T_g necessary for controlling speed of PMSG is flowed to the DC link division direction with the boost chopper circuit driven by the duty ratio control system of fig. 3.25. The V_{dc} is maintained at 100V which is necessary for the system interconnection by the inverter, when the duty control system is activated. The duty is estimated by the PI controller. The input of PI controller is the deviation between the windmill angular speed reference ω_g^{ref} and the windmill angular velocity ω_g .

$$Duty = (K_P + K_I/s) (\omega_g^{ref} - \omega_g) \dots\dots\dots(3.69)$$

Where, the K_P is the proportional gain, and the K_I is the integral gain. The *Duty* is the ratio of T_r on period for switching period of 100% and it is estimated in the range of 0 - 100%. In addition, the duty B_d correspondent to switching frequency of 1 kHz, which is used for actual switching of T_r , is estimated based on the *Duty*. The experimental model is constructed by the equation (3.69) and the ‘‘Pulse Generator block’’ which estimates the B_d based on the *Duty*.

The *Duty* becomes 0 or the switching stops when the windmill speed is comparatively high and the sum e_{dc} of the speed electromotive force by permanent magnet field and the induced voltage by mutual inductances is over 100V, since V_{dc} is maintained at 100V by the inverter. These operation ranges are corresponding to the mode 2 - mode 4, and only rectification by the diode bridge rectifier and reactor is carried out.

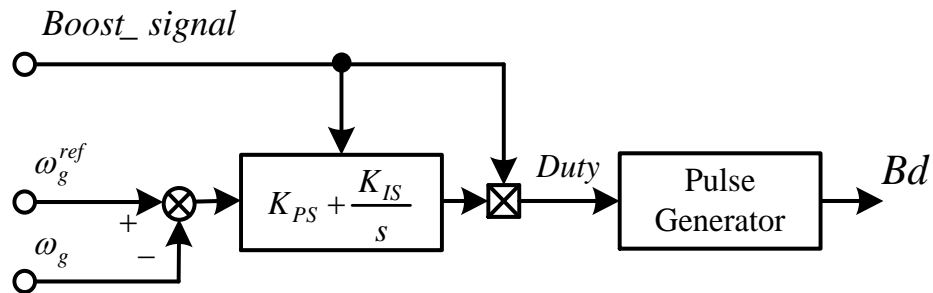


Fig. 3.25. Duty ratio control system

The duty control system is activated when the pitch angle control, the speed control with the inverter described in 3.3, and the electric power control. The pitch angle control system will have been turned on when the pitch angle reference is over the rated wind velocity, the rotational speed is controlled by regulating the wind turbine torque. The wind turbine torque is regulated by the pitch angle control system as follows

$$\theta^{ref} = \left(K_p + \frac{K_I}{s} \right) (\omega_g^{ref} - \omega_g) \dots\dots\dots(3.70)$$

3.9.2 Modeling of PWM converter method

The PWM converter method controls the speed of PMSG and electric power by adjusting the torque current i_{aq} of PMSG or generated torque T_g of PMSG. The i_{aq} can be controlled by vector control system. Fig. 3.26 shows the PWM converter control system. In the operating range which corresponds to mode1 - mode3 in figs. 3.4 and 3.5, the speed control of PMSG is used jointly with the feed-forward control of torque current. In the operating range which corresponds to mode4, the pitch angle control system carries out the speed control of PMSG, and the converter control system carries out the electric power control and torque current feed-forward control. In the operating range under rated wind velocity which corresponds to mode1 - mode3, the torque current reference $i_{aq_PI}^{ref}$ for controlling speed of PMSG is estimated by the PI controller which uses the deviation of windmill angular speed reference ω_g^{ref} and windmill angular speed ω_g as the input.

$$i_{aq_PI}^{ref} = (K_P + K_I/s)(\omega_g^{ref} - \omega_g) \dots\dots\dots(3.71)$$

And the torque current reference $i_{aq_FF}^{ref}$ of torque current feed-forward control is estimated by following equation.

$$i_{aq_FF}^{ref} = P^{ref} / P\Phi_{fa}\omega_g^{ref} \dots\dots\dots(3.72)$$

The torque current reference i_{aq}^{ref} given to the current control system is the sum of current references estimated by equations (3.71) and (3.72).

$$i_{aq}^{ref} = i_{aq_PI}^{ref} + i_{aq_FF}^{ref} + i_{aq_P}^{ref} \dots\dots\dots(3.73)$$

In the operating range over the rated wind velocity which corresponds to mode4, the torque current reference $i_{aq_PI}^{ref}$ for controlling electric power of PMSG is estimated by the PI controller which uses the deviation of electric power reference P_s^{ref} corresponds to the rated power of 300W and electric power P_s as the input.

$$i_{aq_P}^{ref} = (K_P + K_I/s)(P_s^{ref} - P_s) \dots\dots\dots(3.74)$$

And the torque current reference $i_{aq_FF}^{ref}$ of torque current feed-forward control is estimated by equation (3.72). The torque current reference $i_{aq_FF}^{ref}$ is the sum of equations (3.74) and (3.72).

$$i_{aq}^{ref} = i_{aq_P}^{ref} + i_{aq_FF}^{ref} \dots\dots\dots(3.75)$$

The switching between the speed control at operating ranges of mode1 - mode3 under the rated wind velocity and the electric power control at operating range of mode4 over the rated wind velocity is synchronized with on/off of the pitch angle control, since the pitch angle control system is activated when the wind velocity exceed the rated value. The current control in dq synchronous rotating frame is carried out for the torque current reference i_{aq}^{ref} for controlling speed and electric power of PMSG and the magnetic flux current reference i_{ad}^{ref} . The i_{ad}^{ref} is set for 0 in order to maintain the power factor of 1. The high-speed current control becomes possible by using the current control in dq synchronous frame, since the decoupling control system can be adapted easily. The current controller considering the decoupling control system is described as following equations.

$$V_{ad}^{ref} = (K_P + K_I/s)(i_{ad}^{ref} - i_{ad}) - \omega_{ge} L_a i_{aq} \dots\dots\dots(3.76)$$

$$V_{aq}^{ref} = (K_P + K_I/s)(i_{aq}^{ref} - i_{aq}) + \omega_{ge} L_a i_{ad} + \omega_{ge} \Phi_{fa}^{ref} \dots\dots\dots(3.77)$$

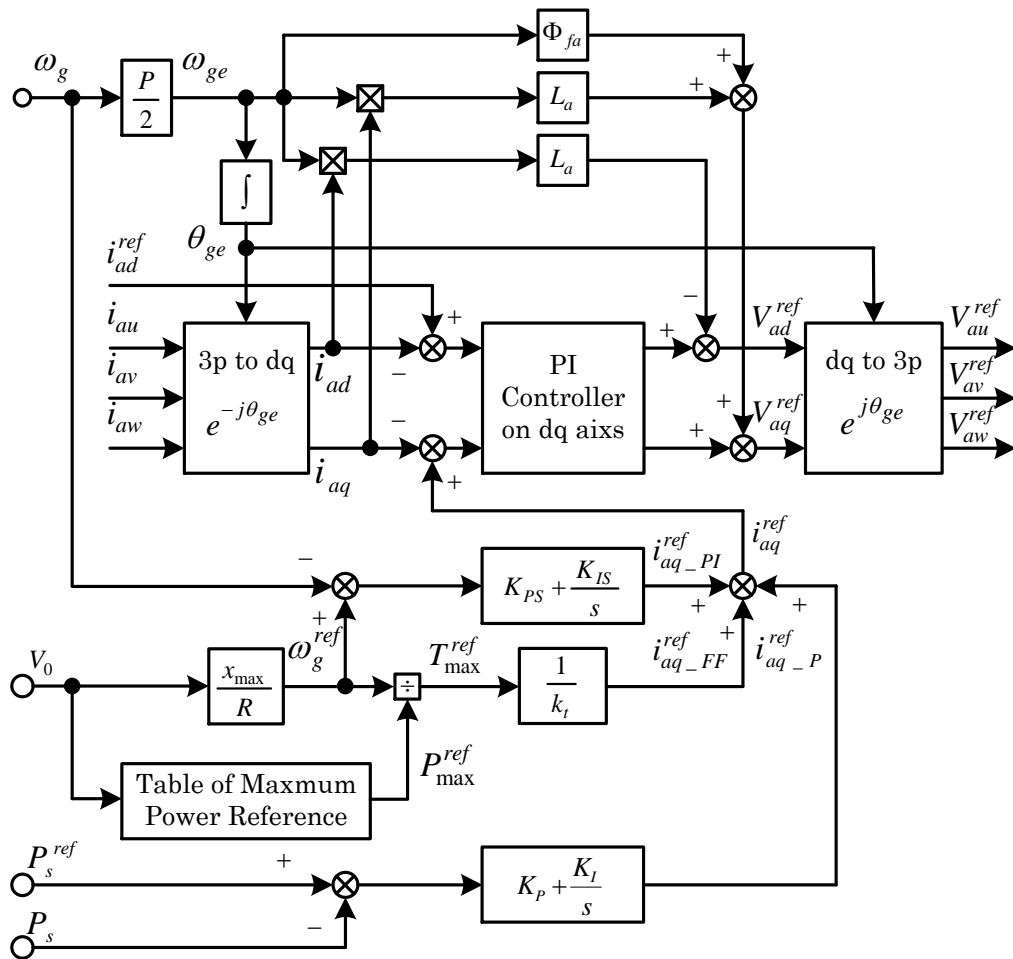


Fig. 3.26. PWM converter control system

3.10 Power system and inverter main circuit

The switching behavior of IGBT in the PWM inverter is not considered as well as the PWM converter. Only the limitation of output voltage given by the DC link voltage V_{dc} is considered. Though the equations (3.78) - (3.79) explained in 3.10 is the common awareness [72], the explanation is carried out to clarifying the condition of simulation. Fig. 3.27 shows the system and main circuit of PWM inverter. The following equations in dq synchronous rotating frame is obtained by converting the circuit equations deduced from fig. 3.27 from three-phase values to dq values.

$$i_{sd} = (-R_s i_{sd} + \omega_s L_s i_{sq} + v_{sd} - e_{sd}) / sL_s \dots\dots\dots(3.78)$$

$$i_{sq} = (-\omega_s L_s i_{sd} - R_s i_{sq} + v_{sq} - e_{sq}) / sL_s \dots\dots\dots(3.79)$$

Where, R : line resistance of power system, L_s : line inductance of power system, and ω_s : angular frequency of power system.

The Simulink model of power system is constructed from the equations (3.78) and (3.79). And the electric power P_s of power system, which is used as the feedback value for the converter and inverter control systems, is described by following equation.

$$P_s = v_{sd} i_{sd} + v_{sq} i_{sq} \dots\dots\dots(3.80)$$

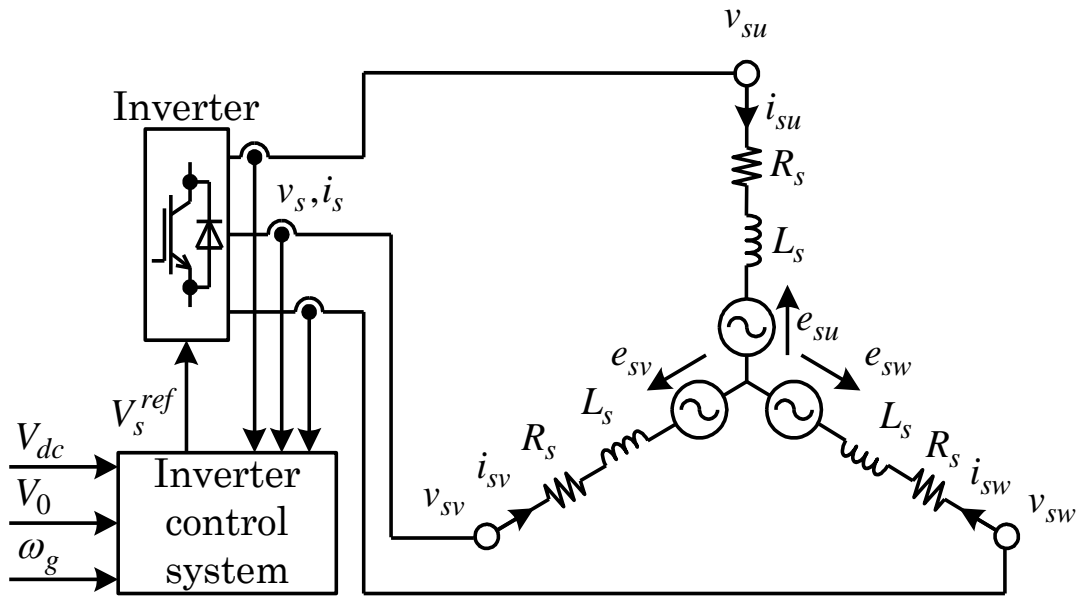


Fig. 3.27. system and main circuit of PWM inverter.

3.11 Inverter control system

The inverter control system using vector control carry out the system interconnection of generated power of PMSG as the effective power by controlling d axis current i_{sd} which corresponds to active power, and maintains the power factor at 1 by controlling q axis current i_{sq} which corresponds to reactive power. Though it is common in both methods that the vector control is used and the power factor is maintained at 1 by controlling i_{sq} to 0, the explanations of each method are carried out individually since the estimation methods for i_{sd}^{ref} are different.

3.11.1 Modeling of boost chopper method

Fig. 3.28 shows the inverter control system of boost converter method. In the boost chopper method, the speed control is carried out by using the duty control system, when the sum e_{dc} of the speed electromotive force by permanent magnet field and induced voltage by mutual inductances is under voltage which enables the system interconnection. The inverter control system controls the DC link voltage V_{dc} to be the constant voltage of 100V necessary for system interconnection. The i_{sd}^{ref} is estimated by following equation.

$$i_{sd}^{ref} = (K_P + K_I/s)(V_{dc}^{ref} - V_{dc}) \dots\dots\dots(3.81)$$

The speed control using duty control system cannot be carried out when e_{dc} exceeds 100V, since the boost chopper system cannot step-down. The condition of T_r off continues when e_{dc} exceeds 100V, and the converter main circuit is almost same with the circuit composed of the diode bridge rectifier. This operating range is correspondent to mode2 - mode4 of figs. 3.4 and 3.5. The speed control is carried out by the inverter control system in mode2 and mode3 that are under the rated wind velocity in mode2 - mode4. The generated torque T_g of PMSG can be controlled by adjusting the DC link voltage V_{dc} as described in 3.9.1. Then, the DC link voltage reference $V_{dc_w}^{ref}$ for controlling windmill speed ω_g is estimated by using following equation.

$$V_{dc_w}^{ref} = (K_P + K_I/s)(\omega_g^{ref} - \omega_g) \dots\dots\dots(3.82)$$

In mode4 which exceeds the rated wind velocity, the speed control is carried out by the pitch angle control system, and the electric power control is carried out by the inverter control system. The DC link voltage reference $V_{dc_P}^{ref}$ for controlling the electric power P_s of power system is estimated by using following equation, since the T_g can be controlled by adjusting V_{dc} .

$$V_{dc_P}^{ref} = (K_P + K_I/s)(P_s^{ref} - P_s) \dots\dots\dots(3.83)$$

The $V_{dc_P}^{ref}$ of equation (3.83) is estimated when the pitch angle control system is on. The V_{dc}^{const} is set at 100V necessary for system interconnection. The DC link voltage reference V_{dc}^{ref} is obtained by adding $V_{dc_w}^{ref}$ to V_{dc}^{const} and reducing and $V_{dc_P}^{ref}$ from V_{dc}^{const} .

$$V_{dc}^{ref} = V_{dc}^{const} + V_{dc_w}^{ref} - V_{dc_P}^{ref} \dots\dots\dots(3.84)$$

The I_{sd}^{ref} for controlling V_{dc} is estimated with following equation.

$$i_{sd}^{ref} = (K_P + K_I/s)(V_{dc}^{ref} - V_{dc}) \dots\dots\dots(3.85)$$

The current control in dq synchronous rotating frame is carried out. The d axis current reference I_{ad}^{ref} is estimated with equation (3.85), and q axis current reference I_{aq}^{ref} is set at 0 in order to maintain the power factor of power system at 1. The high-speed current control becomes possible by using the current control in dq synchronous rotating frame, since the decoupling control system can be adapted easily. The current controller considering the decoupling controller is described as following equations.

$$V_{sd}^{ref} = (K_P + K_I/s)(i_{sd}^{ref} - i_{sd}) + e_{sd} - \omega_s L_s i_{sq} \dots\dots\dots(3.86)$$

$$V_{sq}^{ref} = (K_P + K_I/s)(i_{sq}^{ref} - i_{sq}) + \omega_s L_s i_{sd} \dots\dots\dots(3.87)$$

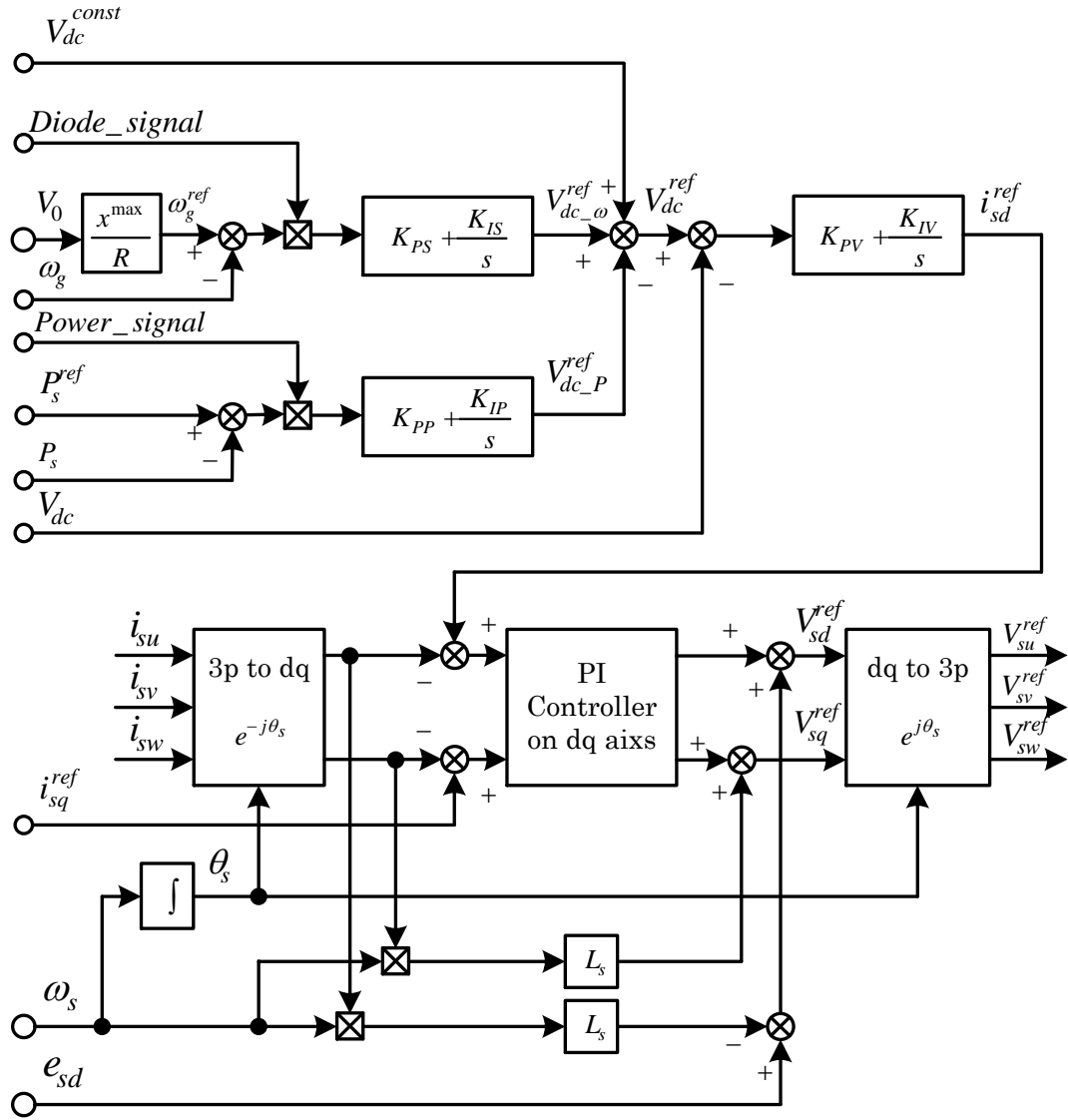


Fig. 3.28. Inverter control system of boost converter method.

3.11.2 Modeling of PWM converter method

Fig. 3.29 shows the inverter control system of PWM converter method. The PWM converter method carries out the speed control and electric power control of PMSG in the converter side. In the PWM converter method, the DC link voltage V_{dc} is controlled at constant of 100V in order to carry out speed control and electric power control of PMSG, while the system interconnection is carried out in the operating ranges of mode1 - mode4. The d axis current reference i_{sd}^{ref} of equation (3.85) is estimated by using the constant DC link voltage reference V_{dc}^{ref} of 100V. And the i_{sq}^{ref} is set at 0 in order to maintain the power factor of power system at 1. The current controller is composed of equations (3.86) and (3.87).

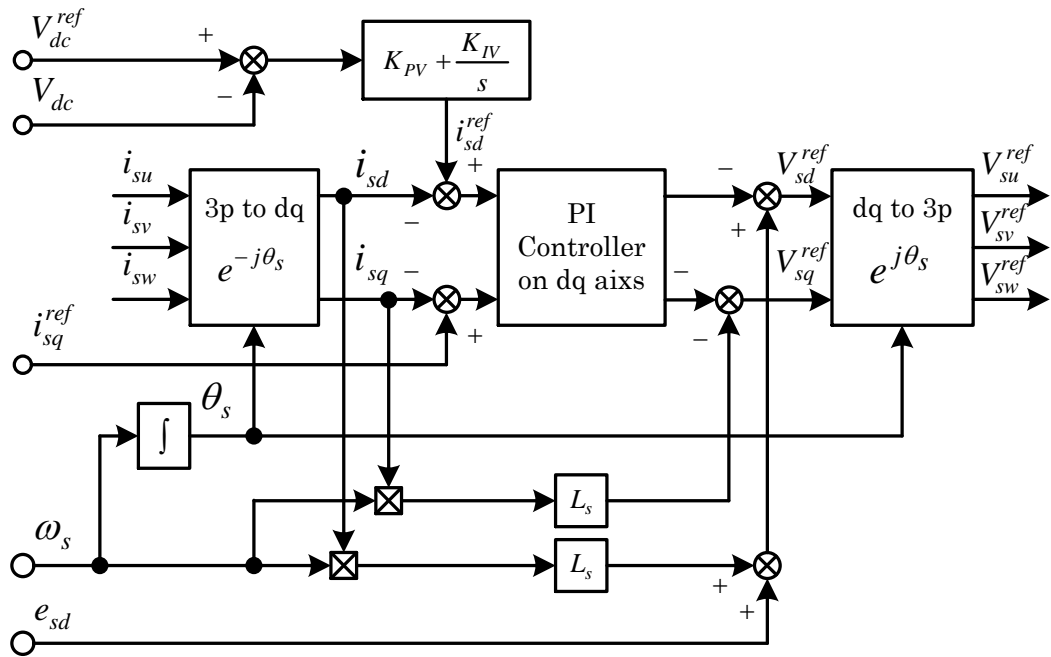


Fig. 3.29. Inverter control system of PWM converter method.

3.12 MATLAB Simulink model of the Boost chopper method

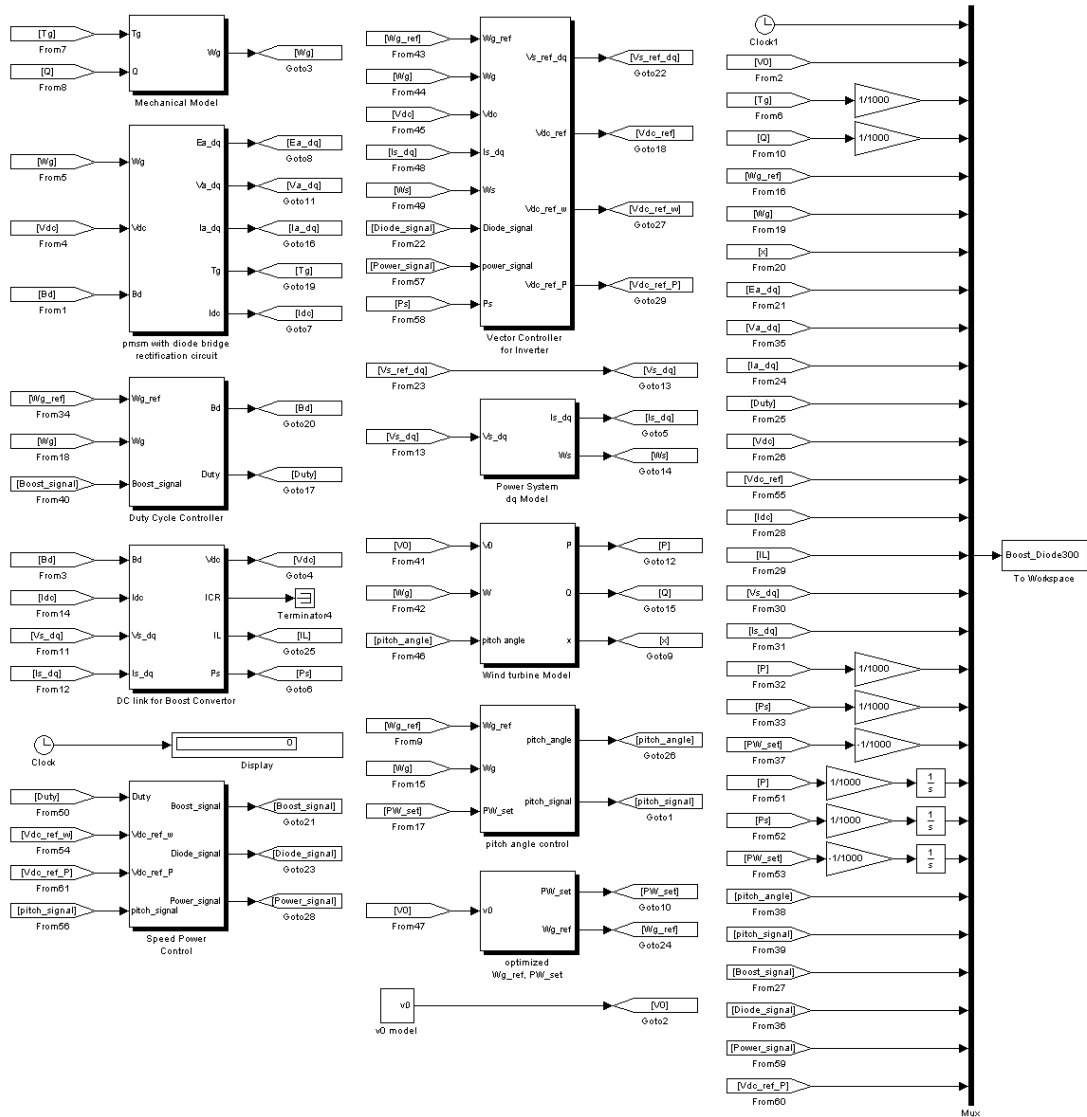


Fig. 3.30. MATLAB Simulink block of the Boost chopper method

3.12.1 PI gain of the boost chopper scheme

In the boost chopper scheme, it is not possible to describe the generated torque T_g of PMSG as the function of *Duty* and DC link voltage V_{dc} that are actuation variables of speed controller. In short, the gain design using the arrangement of pole and zero based on the classical control theory cannot be applied, since the plant cannot be described by the transfer function of single input and single output. Then, it is necessary for the boost chopper scheme to design the PI gain of speed controller by trial-and-error considering the simulation results. The PI gains of speed controller in duty control system and inverter control system are selected to be the values which seem to be optimum after examining the integrated values of generated electric power P_g and responses at the wind velocity given the sinusoidal minute fluctuation of 0.5m/s amplitude and 0.2Hz frequency for each operating points. And, the 1/10 moment of inertia is used in the simulation to shorten the calculation time. The PI gain is designed to be more optimum by considering the relative comparison. The appropriate designed value must be obtained, since the frequency which is higher than the frequency of actual wind velocity is used.

The gain design of current control system for inverter is explained. The equations (3.88) and (3.89) of *dq*-axis currents i_{sd} and i_{sq} are derived from the *dq* model of current controller for inverter side.

$$i_{sd} = \left(\frac{1}{R_s + sL_s} \right) (-v_{sd} + \omega_s L_s i_{sq} + e_{sd}) \dots\dots\dots(3.88)$$

$$i_{sq} = \left(\frac{1}{R_s + sL_s} \right) (-v_{sq} - \omega_s L_s i_{sd}) \dots\dots\dots(3.89)$$

Where, i_{sd} , i_{sq} : dq -axis current for inverter side [A], ω_s : grid system angular frequency [rad/s], L_s : line inductance [H], i_{sd} , i_{sq} : dq -axis current for inverter side [A], V_{sd} , V_{sq} : dq -axis voltage for inverter side [V], R_s : line resistance [W], and e_{sd} : dq transform of inverter side.

The equations (3.90) and (3.91) are derived from the decoupling circuits. The v_{sd}' and v_{sq}' are the outputs of current PI controllers.

$$v_{sd} = -v_{sd}' + \omega_s L_s i_{sq} + e_{sd} \dots\dots\dots(3.90)$$

$$v_{sq} = -v_{sq}' - \omega_s L_s i_{sd} \dots\dots\dots(3.91)$$

Where, V_{sd} , V_{sq} : dq -axis voltage for inverter side [V], e_{sd} : dq transform of inverter side.

The V_{sd} and V_{sq} shown by the equations of (3.90) and (3.91) achieve non-interference. Therefore the decoupled d -axis model of current controller is obtained by substituting the equation (3.90) to the equation (3.88). And the decoupled q -axis model of current controller is obtained by substituting the equation (3.91) to the equation (3.89).

$$i_{sd} = \frac{1}{R_s + pL_s} v_{sd}' \dots\dots\dots(3.92)$$

$$i_{sq} = \frac{1}{R_s + pL_s} v_{sq}' \dots\dots\dots(3.93)$$

The transfer functions of plants for each current control system are same because of equations (3.92) and (3.93). The outputs of current PI controllers are dq -axis voltage references. However these are treated as real voltages since the inverter behavior is assumed to be ideal in the design procedure. Therefore the current control system of inverter is shown in Fig. 3.31.

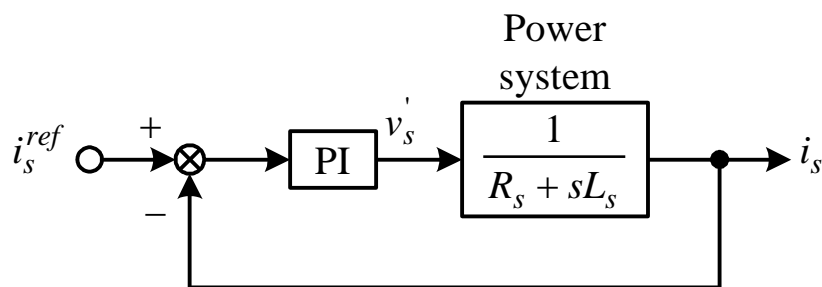


Fig. 3.31. Current control system of inverter.

The proportional gain K_{P_s} and integral gain K_{I_s} of the current PI controller is designed with the MATLAB sisotool. The power system parameters shown in Table 3.2 are used for calculating the transfer function of plant. Table 3.3 shows the parameters of the boost converter system. The gain of the PI current controller of PWM vector control inverter is designed in order to obtain the wind velocity frequency of 500 rad/s and the damping ratio $\zeta=0.8$

Table 3.2 shows the common parameters of boost converter scheme and PWM converter scheme. The parameters of permanent magnet synchronous generator

(PMSG), mechanical systems, DC link division, electric power system, and windmill turbines are common as shown in table 3.2, since the same models are used.

Table 3.2. Common parameters of boost chopper scheme and PWM converter scheme.

| Permanent Magnet Synchronous Generator | |
|--|-------------------|
| Rated power | 300[W] |
| Rated voltage | 200[V] |
| Pole number | 16 |
| Stator resistance | 1.419[Ω] |
| Stator inductance | 0.4741[mH] |
| Mutual inductance | 0.2139[mH] |
| Stator flux | 0.07293[Wb] |
| Gear ratio | 1 |
| DC link | |
| Resistance | 1000[Ω] |
| Capacitance | 1[F] |
| Power system | |
| Line resistance | 0.01[Ω] |
| Line inductance | 0.0001[H] |
| Transformer | |
| Output: | |
| Type | S3P-240-10 |
| Number of phase | 3 phase |
| Output voltage | 0 ~ 240[V] |
| Voltage fluctuation rate | 5% or less |
| Allowable current | 20[A] |
| Capacity | 3.46[KVA] |
| Input: | |
| Input voltage | 200[V] |
| Input frequency | 50/60[Hz] |

Table 3.3 shows the control parameters for the boost chopper scheme. The control parameters of the boost converter and duty control system are designed with the simulations using the implemented Simulink models. The control parameters of vector control system applied in the inverter side are designed with the conventional scheme considering the arrangement of pole and zero based on the control theory.

Table 3.3. Control parameters of boost chopper scheme.

| Boost Convertor System | |
|--|-------------|
| Inductance of boost convertor circuit | 1[mH] |
| Duty Cycle controller | |
| Proportional gain of speed regurator | 20 |
| Integral gain of speed regurator | 100 |
| Switching frequency | 1[kHz] |
| Vector controller for Invertor | |
| Proportional gain of DC link voltage regurator | -100 |
| Integral gain of DC link voltage regurator | -500 |
| Proportional gain of speed regurator | 1 |
| Integral gain of speed regurator | 500 |
| Proportional gain of maxmum power regurator | 0.000001 |
| Integral gain of maxmum power regurator | 0.001 |
| Proportional gain of d axis current regurator | 6.24/206 |
| Integral gain of d axis current regurator | 6.24 |
| Proportional gain of q axis current regurator | 6.24/206 |
| Integral gain of q axis current regurator | 6.24 |
| Setting of phase voltage | 100/sqrt(3) |
| DC link voltage reference | 35 |
| Pitch angle control | |
| Proportional gain of speed regurator | 5 |
| Integral gain of speed regurator | 10 |

3.13 MATLAB Simulink model of the PWM converter method

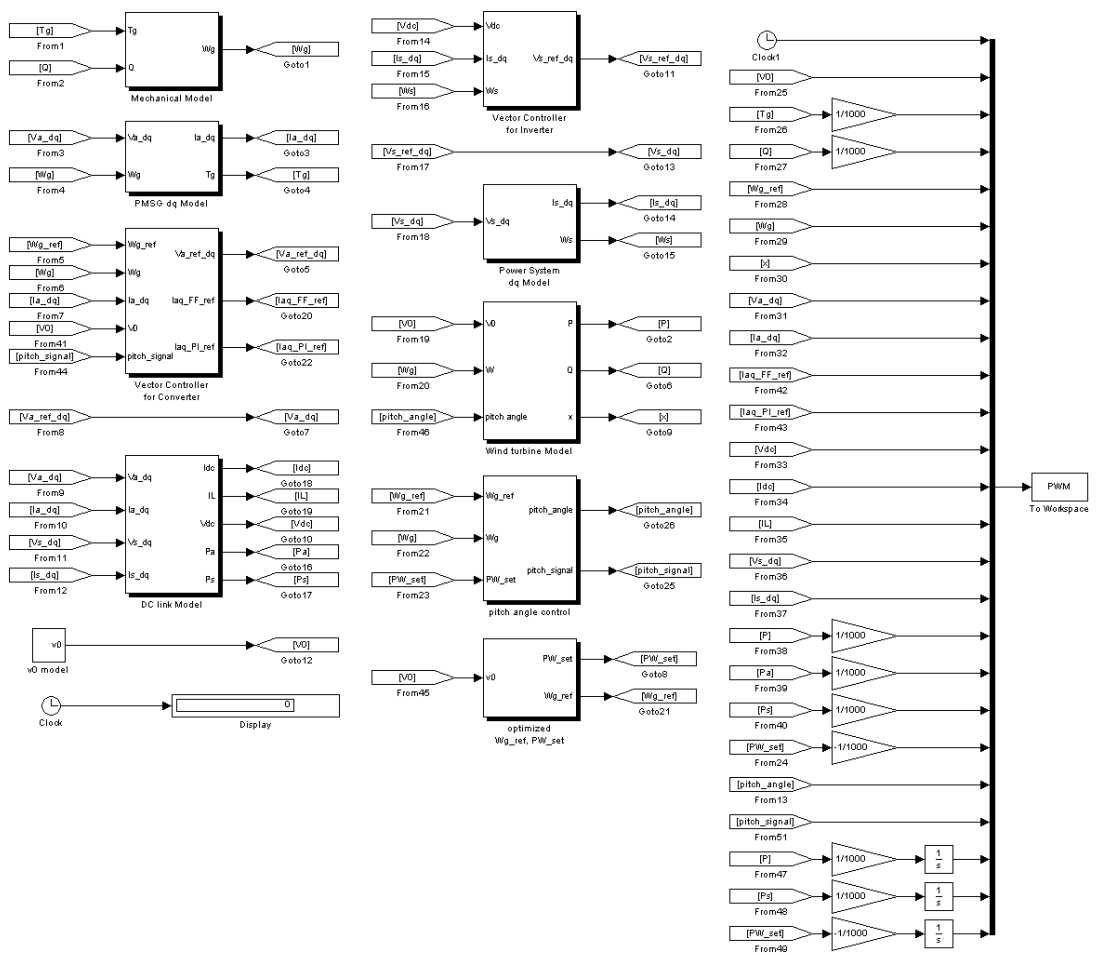


Fig. 3.32. MATLAB Simulink block of the PWM converter method

3.13.1 PI gain of the PWM converter scheme

It is possible for the PWM converter scheme to describe the generated torque T_g of PMSG as a function of torque current i_{aq} , since the vector control is carried out. Therefore, it is possible to describe the plants as transfer functions of single input and single output including mechanical system and design the gain by using the arrangement of pole and zero based on the classical control theory. Fig. 3.33 shows the speed control system of PWM converter scheme.

The PI gain of speed PI controller the vector control is applied to the converter control system. Therefore the generated torque T_g of PMSG is proportional to q -axis current i_{aq} .

$$T_g = P\Phi_{fa}i_{aq} \dots\dots\dots (3.94)$$

Where, T_g : generator torque [Nm], P : stator pole, Φ_{fa} : stator flux [Wb], i_{aq} : q -axis current [A].

The mechanical system considering the PMSG and wind turbine is described with following equation since the $n_1/n_2=1$.

$$\omega_g = \frac{T_g}{\left\{ J_m + J_t \left(\frac{n_2}{n_1} \right)^2 \right\} s + \left\{ B_m + B_t \left(\frac{n_2}{n_1} \right)^2 \right\}} \dots\dots\dots (3.95)$$

Where, ω_g : generator speed [rad/s], T_g : generator torque [Nm], J_m : PMSG moment of inertia [kgm²], J_t : windmill moment of inertia [kgm²], B_m : coefficient of viscosity for PMSG [Nm/(rad/s)], B_t : coefficient of viscosity for wind turbine [Nm/(rad/s)].

The inertia is the sum of J_m for PMSG and J_t for wind turbine. Also the coefficient of viscosity friction is the sum of B_m for PMSG and B_t for wind turbine. The plant is series block diagrams of equations (3.94) and (3.95) as shown in Fig. 3.36. It is described in time-lag of first order system.

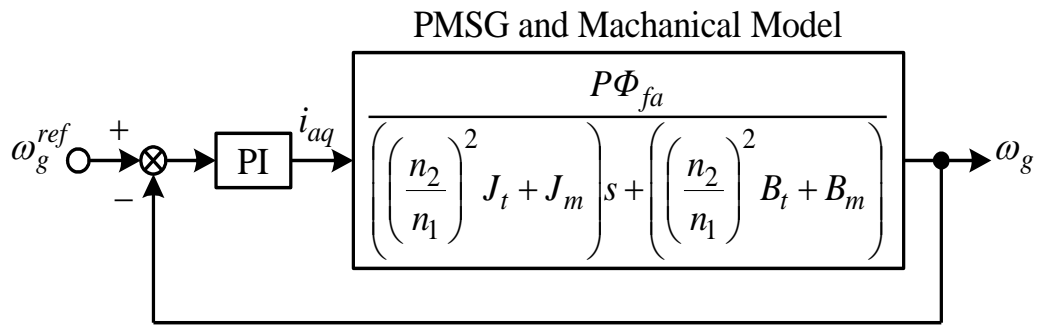


Fig. 3.33. Speed control system of the PWM converter scheme.

The output of PI controller is q -axis current reference i_{aq}^{ref} . The current control loop of minor loop is omitted, since the bandwidth of current control loop is wider than that of speed control loop. Therefore the i_{aq}^{ref} is used as i_{aq} . The proportional gain K_{PS} and integral gain K_{IS} of the speed PI controller is designed with the MATLAB sisotool. The generator parameters shown in Table 3.2 are used for calculating the transfer function of plant. Table 3.4 shows the parameters of the PWM converter system. The gain of the PI speed controller is designed in order to obtain the wind velocity frequency of 5 rad/s and the damping ratio ζ of 0.8.

Table 3.4 shows the control parameters of PWM converter scheme. The control parameters of vector control system applied in the converter and inverter sides are designed with the conventional scheme considering the arrangement of pole and zero.

Table 3.4. Control parameters of PWM converter scheme.

| PWM Converter System | |
|--|-------------|
| Vector controller for Converter | |
| Proportional gain of speed regulator | 100/3.12 |
| Integral gain of speed regulator | 100 |
| Proportional gain of maximum power regulator | 0.000001 |
| Integral gain of maximum power regulator | 0.001 |
| Proportional gain of d axis current regulator | 225/315 |
| Integral gain of d axis current regulator | 225 |
| Proportional gain of q axis current regulator | 225/315 |
| Integral gain of q axis current regulator | 225 |
| Setting of stator flux | 0.07293 |
| Vector controller for Inverter | |
| Proportional gain of DC link voltage regulator | -5 |
| Integral gain of DC link voltage regulator | 100 |
| Proportional gain of d axis current regulator | 25/357 |
| Integral gain of d axis current regulator | 25 |
| Proportional gain of q axis current regulator | 25/357 |
| Integral gain of q axis current regulator | 25 |
| Setting of phase voltage | 100/sqrt(3) |
| DC link voltage reference | 35 |
| Pitch angle control | |
| Proportional gain of speed regulator | 5 |
| Integral gain of speed regulator | 10 |

The PI gain of current controller used in converter the equations (3.96) and (3.97) of dq axis currents i_{ad} and i_{aq} are derived from the dq model of PMSG.

$$i_{ad} = \left(\frac{1}{R_a + sL_a} \right) (\omega_{ge} L_a i_{aq} + v_{ad}) \dots\dots\dots(3.96)$$

$$i_{aq} = \left(\frac{1}{R_a + sL_a} \right) \{ -\omega_{ge} (L_a i_{ad} + \Phi_{fa}) + v_{aq} \} \dots\dots\dots(3.97)$$

where, i_{ad} , i_{aq} : dq -axis current [A], ω_{ge} : angular velocity of the field (electrical angle)

[rad/s], L_a : stator inductance [H], V_{ad} , V_{aq} : dq -axis voltage [V], R_a : stator resistance [W], Φ_{fa} : stator flux [Wb].

The equations (3.98) and (3.99) are derived from the decoupling circuits. The v_{ad}' and v_{aq}' are the outputs of current PI controllers.

$$v_{ad} = v_{ad}' - \omega_{ge} L_a i_{aq} \dots\dots\dots(3.98)$$

$$v_{aq} = v_{aq}' + \omega_{ge} L_a i_{ad} + \omega_{ge} \Phi_{fa} \dots\dots\dots(3.99)$$

where, v_{ad} , v_{aq} : dq -axis voltage [V]. The v_{ad} and v_{aq} shown by the equations of (3.98) and (3.99) achieve the non-interference. Therefore the decoupled d -axis model of PMSG is obtained by substituting the equation (3.98) to the equation (3.96). And the decoupled q -axis model of PMSG is obtained by substituting the equation (3.99) to the equation (3.97).

$$i_{ad} = \frac{1}{R_a + pL_a} v_{ad}' \dots\dots\dots(3.100)$$

$$i_{aq} = \frac{1}{R_a + pL_a} v_{aq}' \dots\dots\dots(3.101)$$

The transfer functions of plants for each current control system are same because of equations (3.100) and (3.101). The outputs of current PI controllers are dq -axis voltage references. However these are treated as real voltages, since the inverter behavior is assumed to be ideal in the design procedure. Therefore the current control system of converter current is shown in Fig. 3.34.

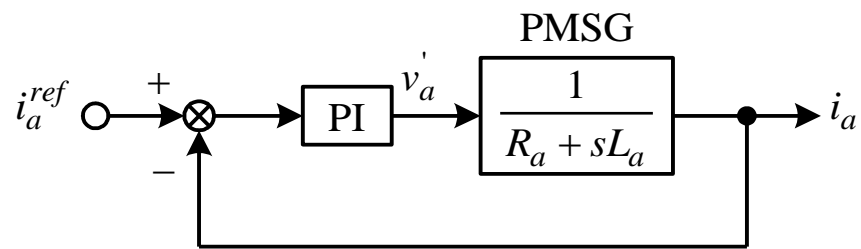


Fig. 3.34. Current control system of the converter.

The proportional gain K_{Pa} and integral gain K_{Ia} of the current PI controller is designed with the MATLAB sisotool. The generator parameters shown in Table 3.2 are used for calculating the transfer function of plant. Table 3.4 shows the parameters of the PWM converter system. The gain of the PI current controller of PWM vector control converter is designed in order to obtain the wind velocity frequency of 500 rad/s and the damping ratio $\zeta=0.8$.

3.14 Simulation results of Boost chopper scheme

Fig. 3.35- 4.43 shows the simulation results. The simulation models for the permanent magnet synchronous generator wind generation system using the boost converters are implemented by using MATLAB/Simulink. The simulation models consider the natural wind, the main circuits, the converter and inverter control systems, and the pitch angel control system. The simulation results are similar to the simulation results of fig. 3..44- 3.52.

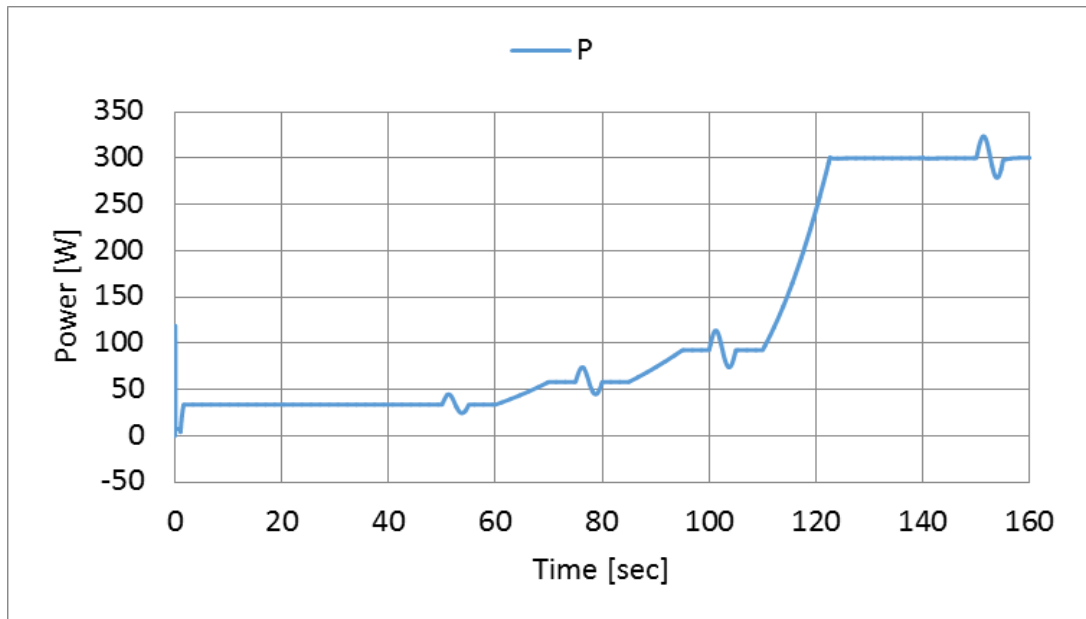


Fig. 3.35. Generated power

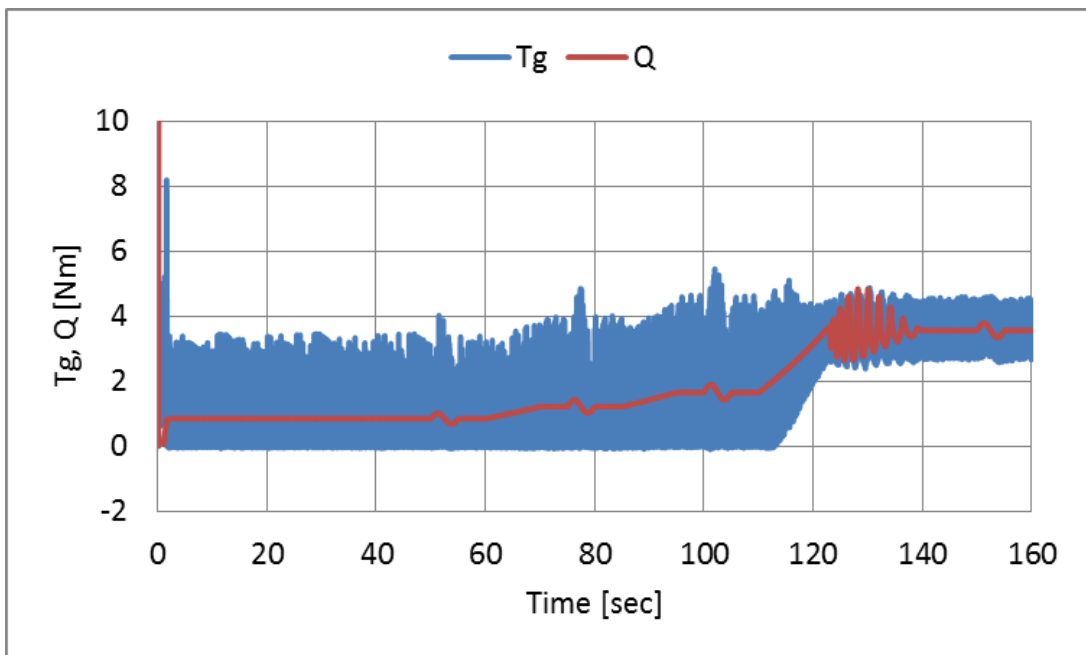


Fig. 3.36. Wind turbine Torque

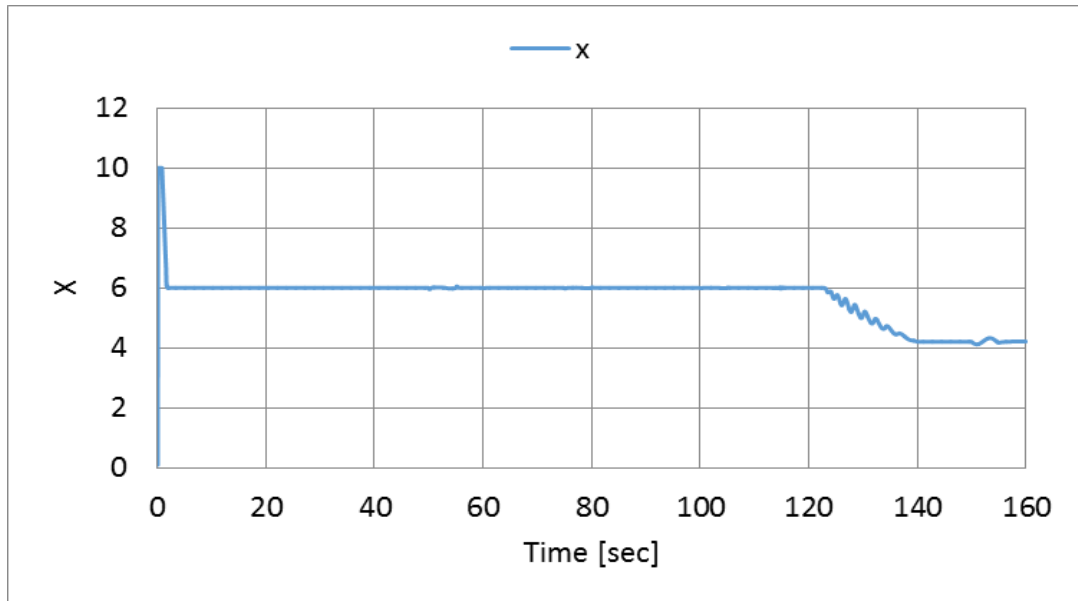


Fig. 3.37. Tip speed ratio

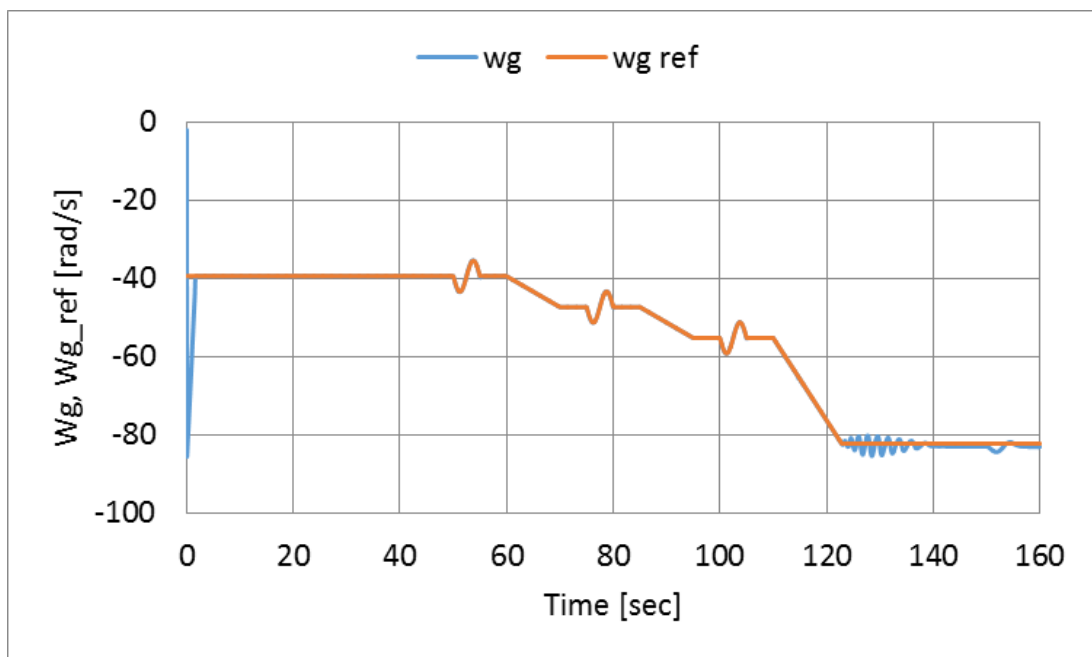


Fig. 3.38. Rotational speed reference and Rotational speed

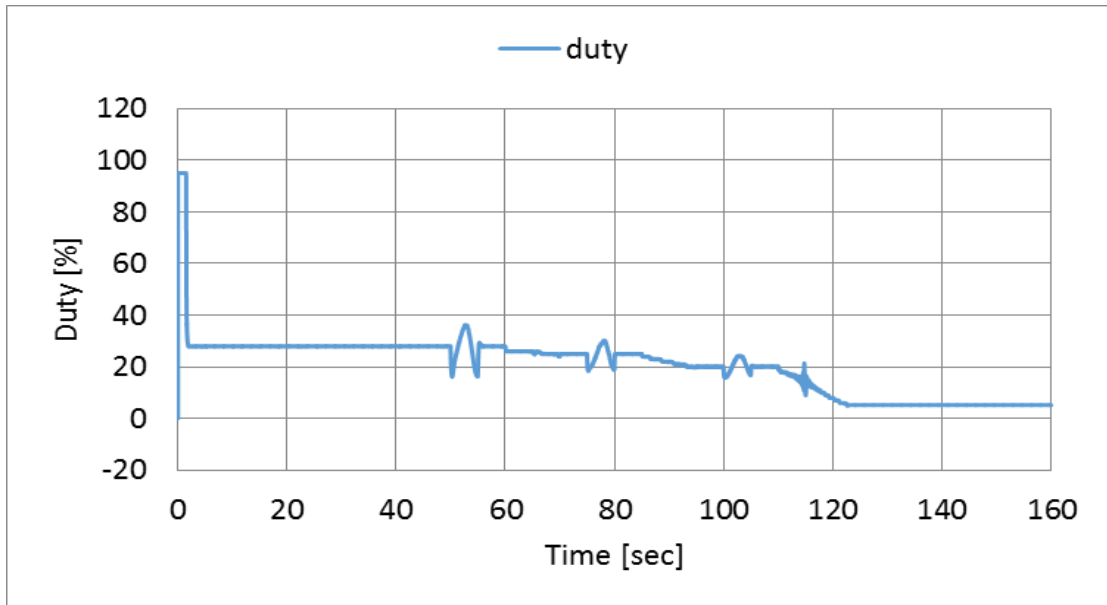


Fig. 3.39. Duty cycle

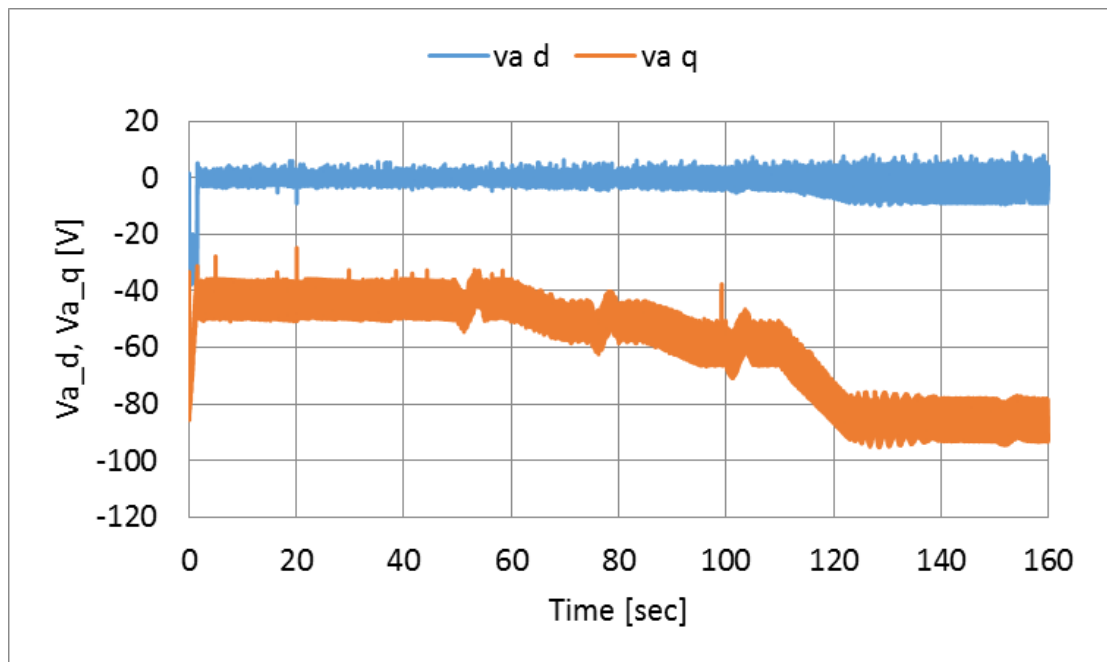


Fig. 3.40. *d*-axis and *q*-axis voltage for converter side

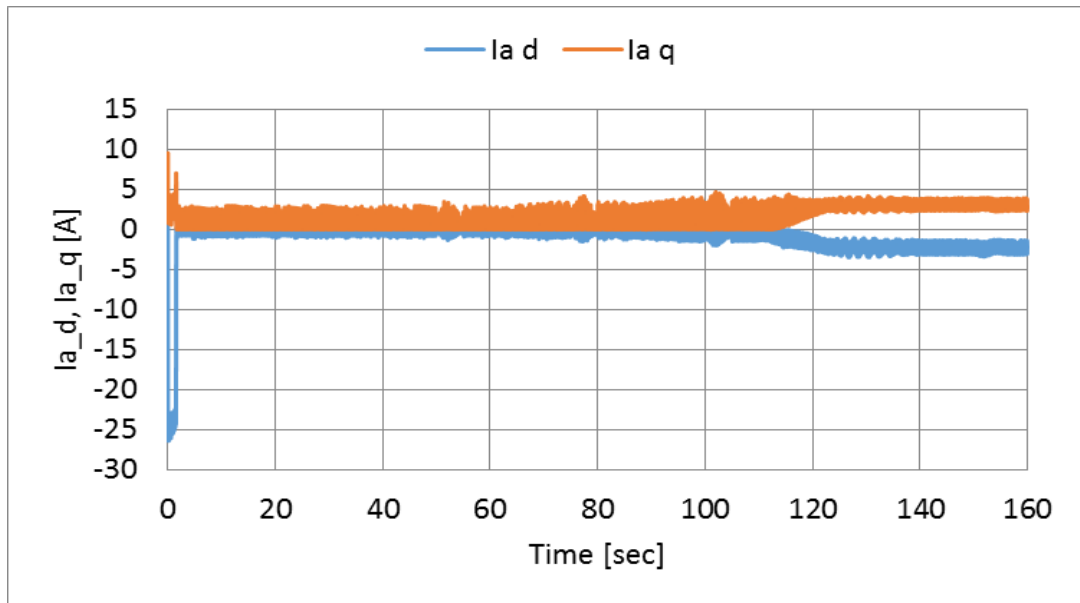


Fig. 3.41. . d -axis and q -axis current for converter side

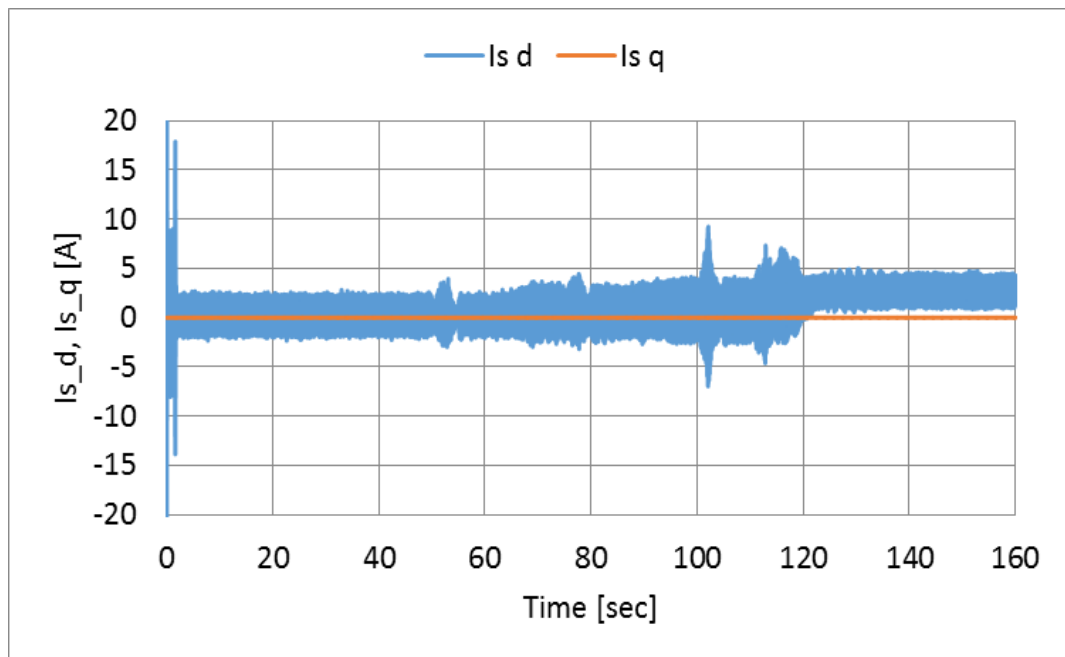


Fig. 3.42. d -axis and q -axis current for inverter side

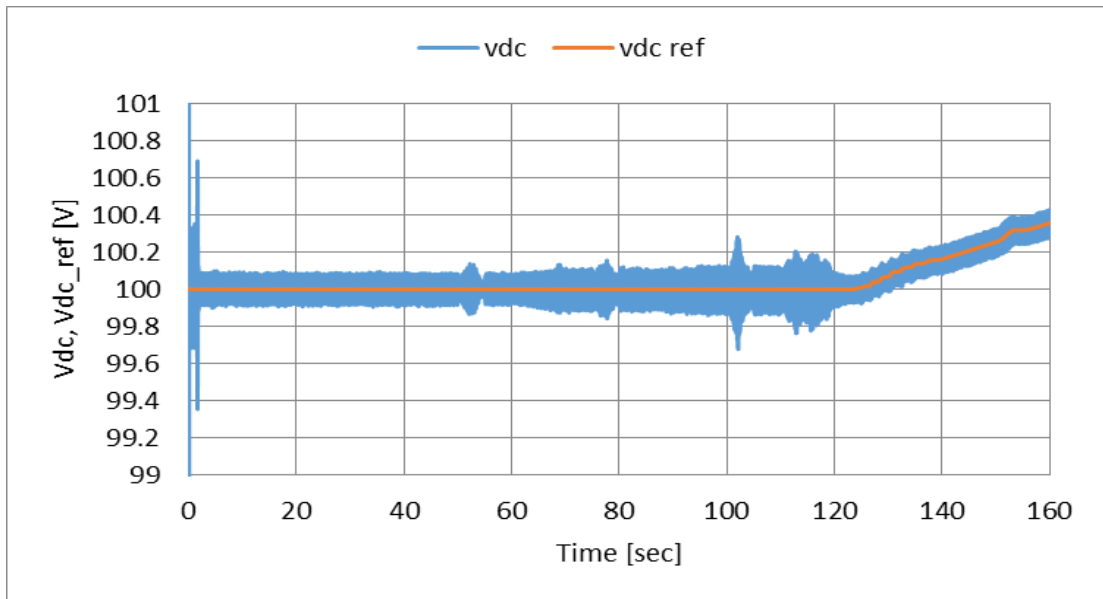


Fig. 3.43. DC link voltage and its reference

3.15 Simulation results of PWM converter scheme

Fig. 3.44- 3.52 shows the simulation results. The simulation models for the permanent magnet synchronous generator wind generation system using the PWM converters are implemented by using MATLAB/Simulink. The simulation models consider the natural wind, the main circuits, the converter and inverter control systems, and the pitch angle control system. The simulation results are similar to the simulation results of fig. 3.35- 3.43.

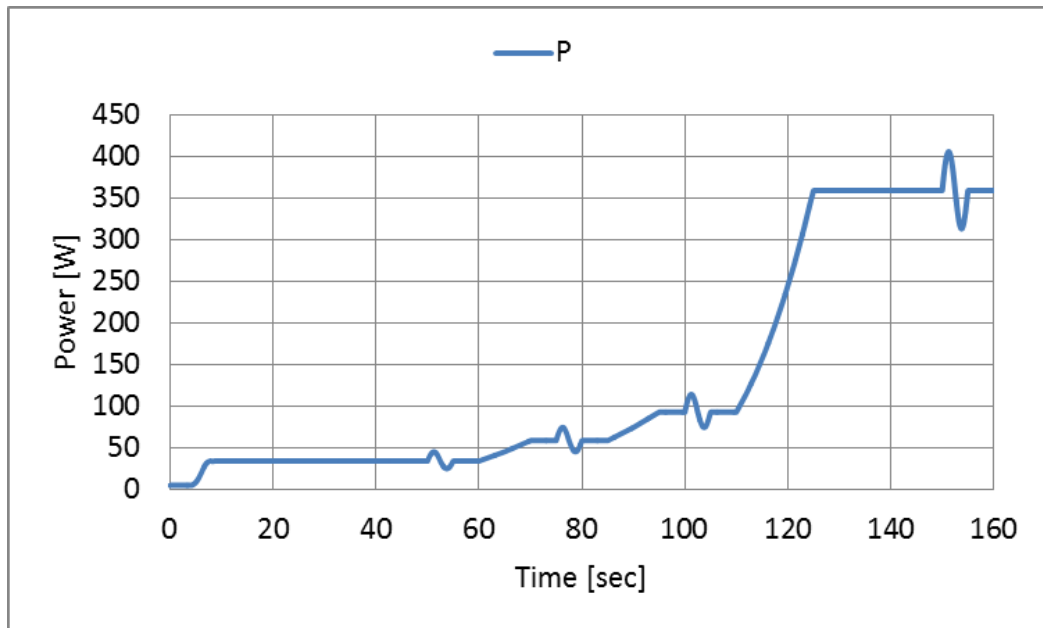


Fig. 3.44. Generated power

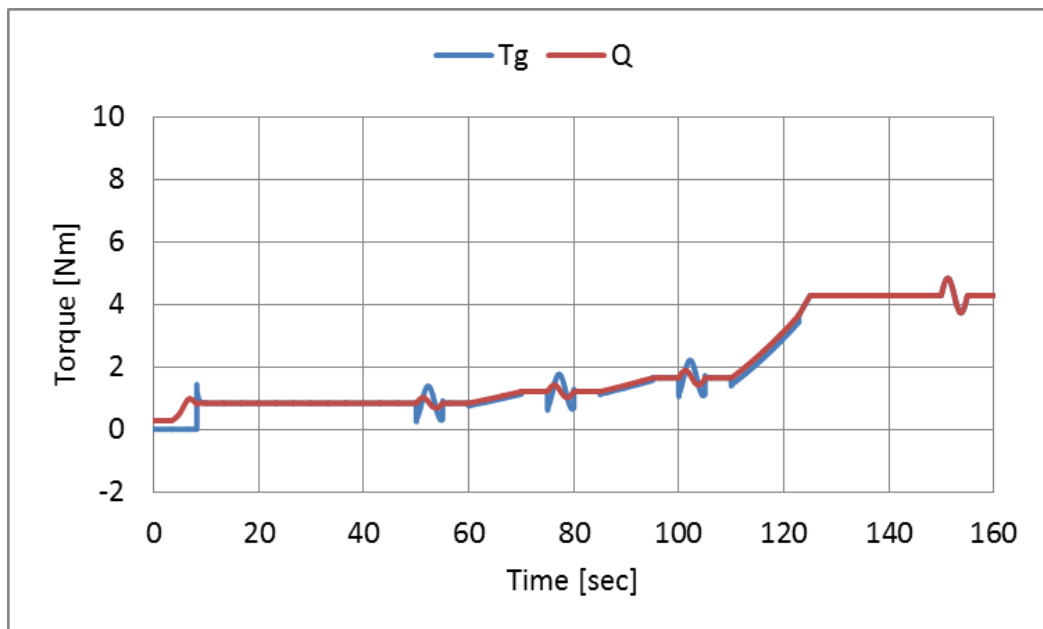


Fig. 3.45. Wind turbine Torque

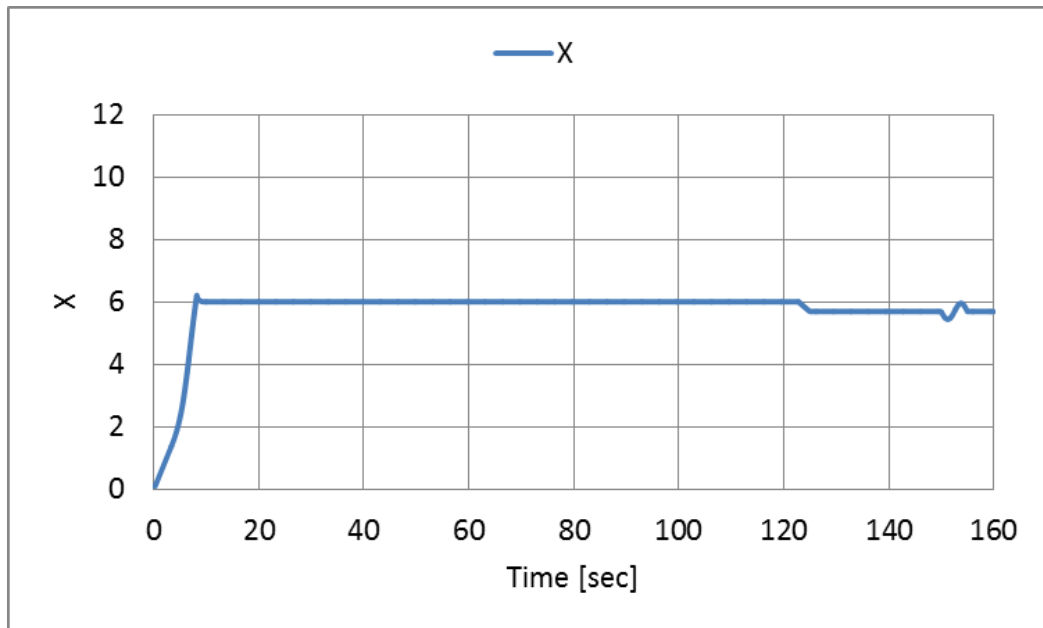


Fig. 3.46. Tip speed ratio

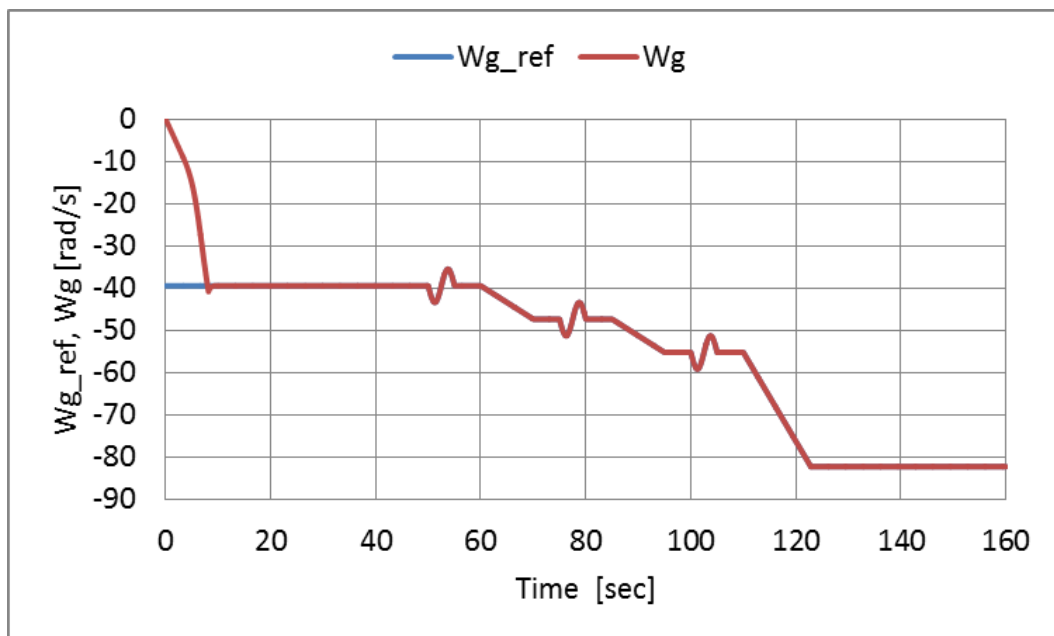


Fig. 3.47. Rotational speed reference and Rotational speed

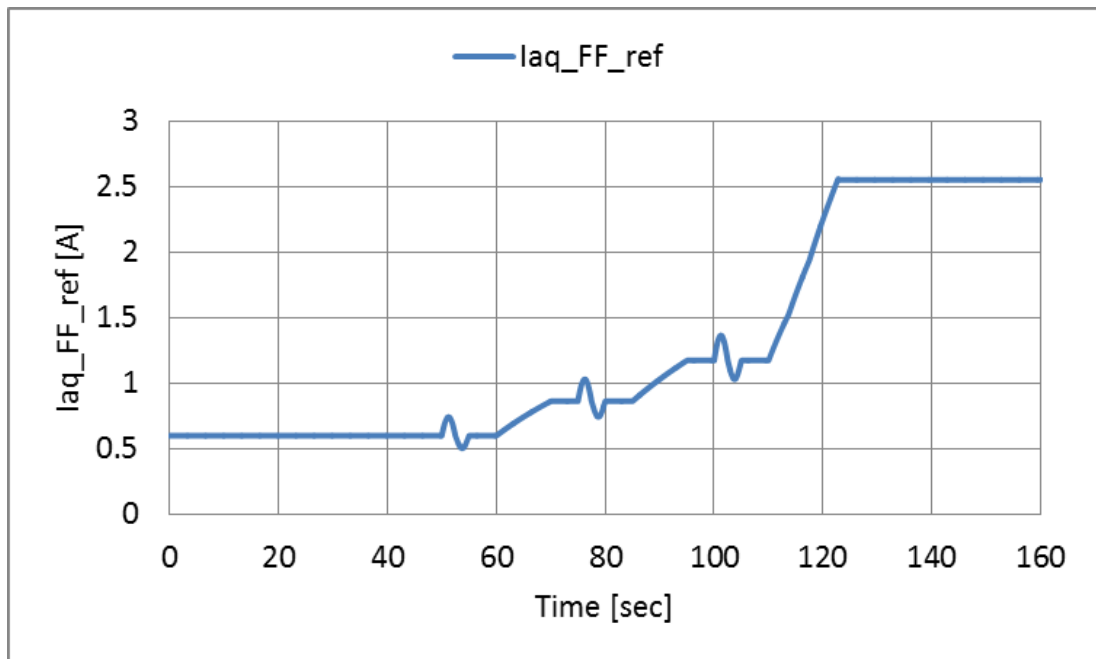


Fig. 3.48. Duty cycle

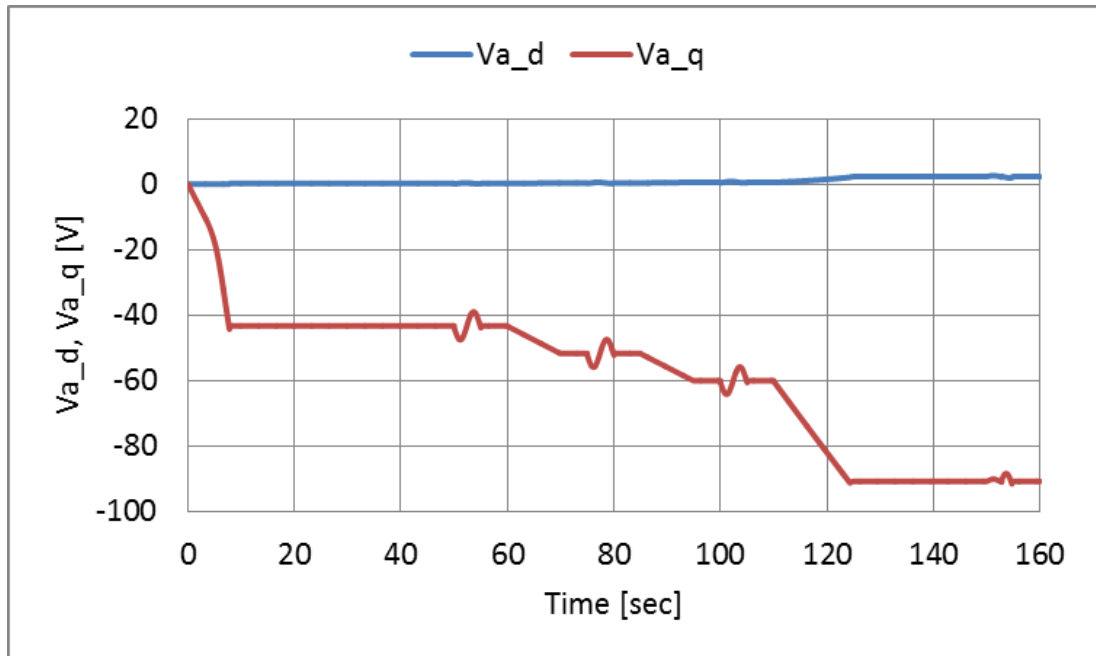


Fig. 3.49. d -axis and q -axis voltage for converter side

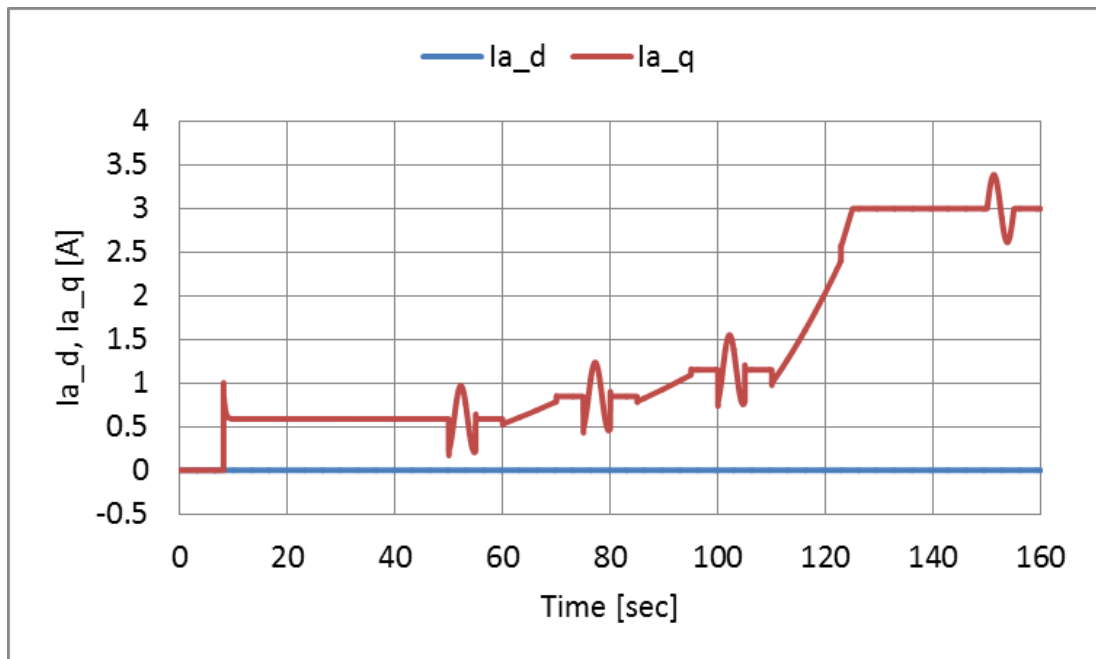


Fig. 3.50. . d -axis and q -axis current for converter side

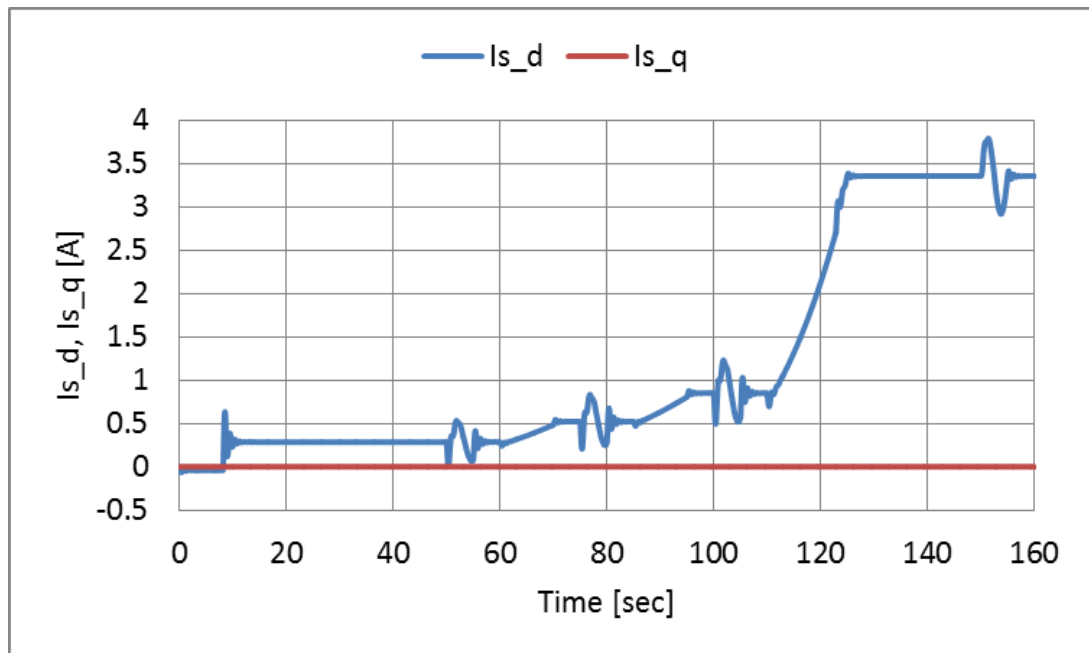


Fig. 3.51. d -axis and q -axis current for inverter side

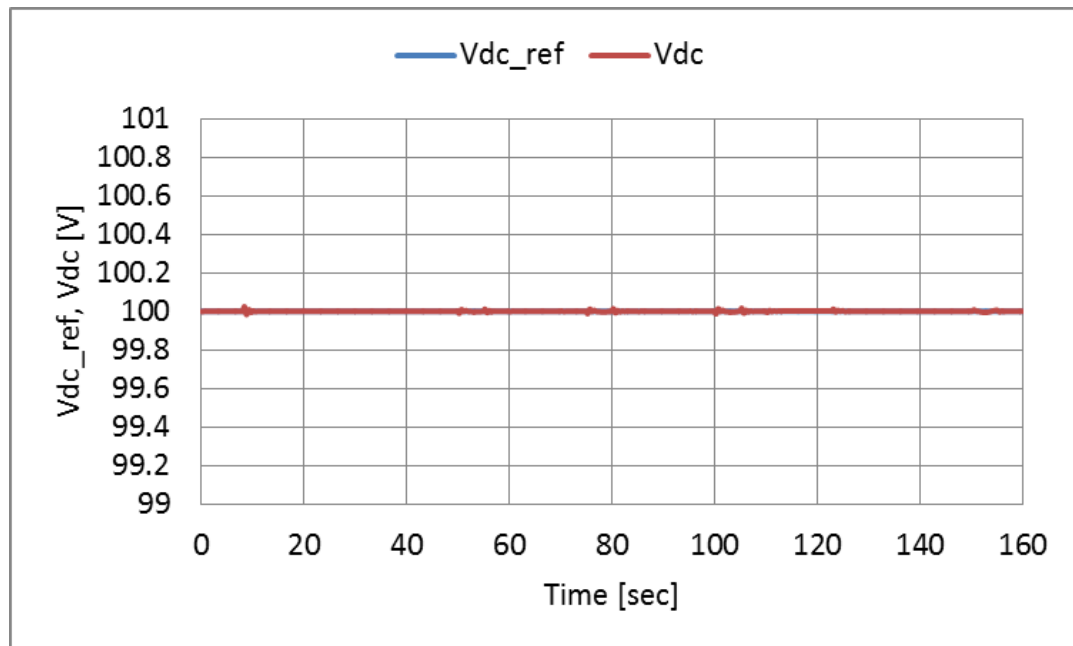


Fig. 3.52. DC link voltage and its reference

3.13 Summary

The principles of an inverter based on PWM converter control system are presented in detail, and a number of mathematical models are given. An inverter based PWM converter system has been modelled using MATLAB/Simulink and Figure 3.28-3.32 demonstrates that the PWM algorithm was successfully implemented.

Chapter 4

Wind Turbine Emulator

4.1 Wind turbine emulator

Fig. 4.1 shows the basic structure of the wind turbine emulator. The wind turbine model is based on the blade element momentum theory (BEMT) [76]. The wind turbine model consists of the three-dimensional table data of wind turbine characteristics and the mechanical model considering the difference between real wind turbine and induction motor. The 3D table data are composed of the torque Q for V_0 and ω_r . The 3D data are calculated by applying the wind turbine parameters of Fig. 4.2 to the BEMT in advance. The wind velocity V_0 [m/s] is given as a condition of emulation. The windmill rotational speed ω_r [rad/s] is detected with the rotary encoder (RE). The wind velocity V_0 and ω_r are used as inputs of the three-dimensional table.

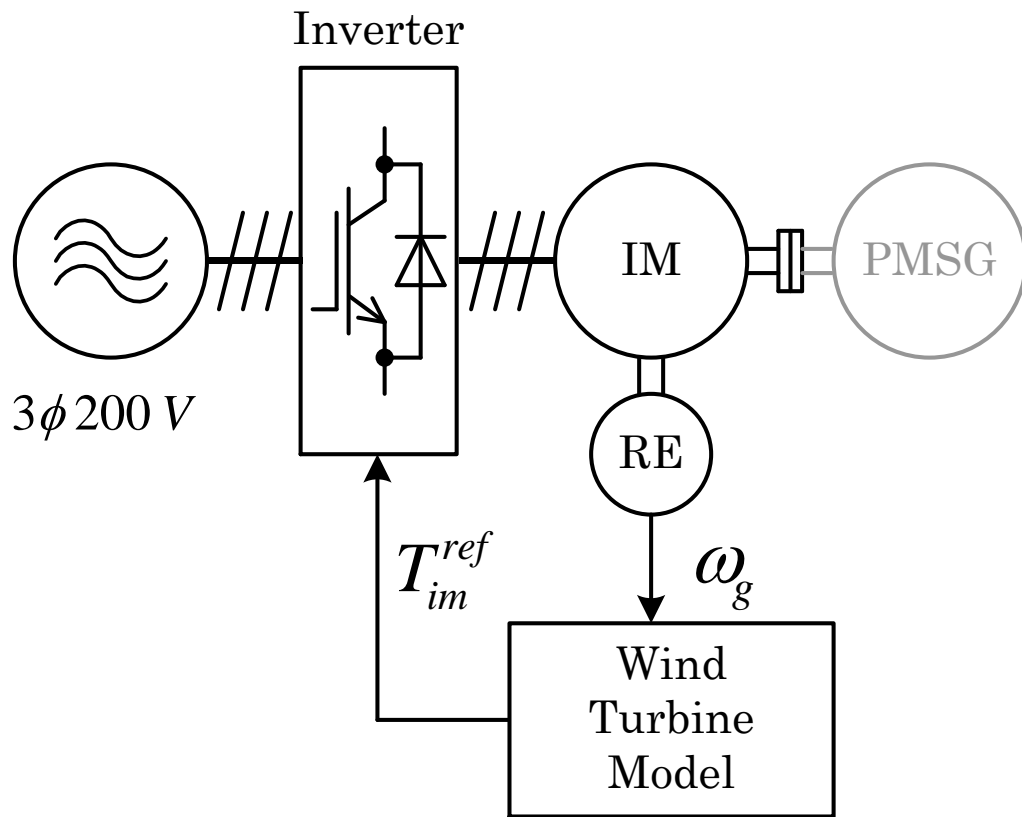


Fig. 4.1. Wind turbine emulator.

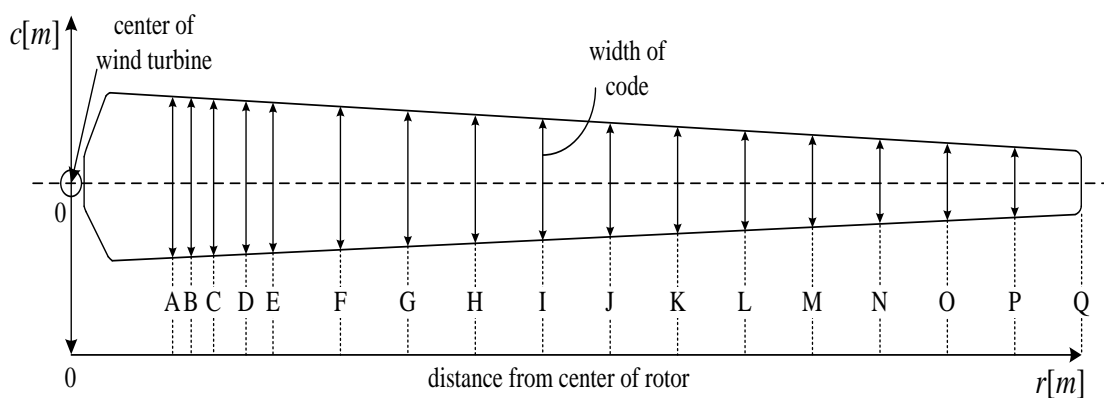


Fig. 4.2. Wind turbine blade shape model

Table 4.1 Three-dimensional table data

| | | | | | | | | | |
|--|----------|-------|-------|----------|-------|-------|-------|-------|-------|
| code number | A | B | C | D | E | F | G | H | I |
| r [m]: distance from center of rotor | 0.08 | 0.10 | 0.12 | 0.14 | 0.16 | 0.21 | 0.26 | 0.31 | 0.36 |
| c [m]: width of code | 0.096 | 0.094 | 0.093 | 0.092 | 0.090 | 0.085 | 0.080 | 0.076 | 0.071 |
| β [deg]: angle of twist | — | — | — | 2.4 | 4.4 | 5.6 | 5.6 | 5.6 | 5.6 |
| profile of NACA | — | | | NACA4415 | | | | | |
| | J | K | L | M | N | O | P | Q | |
| | 0.41 | 0.46 | 0.51 | 0.56 | 0.61 | 0.66 | 0.71 | 0.76 | |
| | 0.066 | 0.062 | 0.058 | 0.053 | 0.048 | 0.044 | 0.040 | 0.035 | |
| | 5.8 | 5.8 | 5.8 | 5.8 | 5.9 | 5.9 | 6.0 | 6.0 | |
| | NACA4415 | | | | | | | | |

4.2 Blade element momentum theory

From section at 3.2 The windmill model used in this research is the small wind turbine using 3 blades of NACA4415. The rotor diameter is 1.52 [m]. The cross sections of real wind turbine blade are shown in Fig. 4.3. The wind turbine blade is divided into 17 points from A to Q, and the all points are analyzed with the fluid analysis with finite element method software ANSYS. The results are obtained as the pressure applied to the nodes of model. The lift and drag coefficients of wind turbine blade are derived from the results, since they are required for the blade element momentum theory is shown in table 4.2.



Fig. 4.3. Real wind turbine blade shape

Table 4.2 Airfoil profile result

| NACA4415(numberE) | | | NACA4415(numberH) | | | NACA4415(numberL) | | | NACA4415(numberP) | | |
|-------------------|-------------|-------------|-------------------|-------------|-------------|-------------------|-------------|-------------|-------------------|-------------|-------------|
| α | c_l | c_d | α | c_l | c_d | α | c_l | c_d | α | c_l | c_d |
| 1 | 0.225024725 | 0.028443495 | 1 | 0.536879124 | 0.056488784 | 1 | 0.190444441 | 0.024290411 | 1 | 0.204506021 | 0.028952689 |
| 2 | 0.262529754 | 0.028899429 | 2 | 0.622935437 | 0.056696127 | 2 | 0.225304916 | 0.024712506 | 2 | 0.240157789 | 0.029838411 |
| 3 | 0.300034783 | 0.029355364 | 3 | 0.708991751 | 0.056903471 | 3 | 0.260165391 | 0.025134601 | 3 | 0.275809557 | 0.030724134 |
| 4 | 0.337539813 | 0.029811298 | 4 | 0.795048064 | 0.057110815 | 4 | 0.295025866 | 0.025556696 | 4 | 0.311461326 | 0.031609857 |
| 5 | 0.375044842 | 0.030267233 | 5 | 0.881104378 | 0.057318159 | 5 | 0.329886341 | 0.025978791 | 5 | 0.347113094 | 0.032495580 |
| 6 | 0.412549872 | 0.030723168 | 6 | 0.967160692 | 0.057525503 | 6 | 0.364746816 | 0.026400887 | 6 | 0.382764863 | 0.033381303 |
| 7 | 0.444471540 | 0.033539486 | 7 | 1.032313504 | 0.063900988 | 7 | 0.390030301 | 0.029483946 | 7 | 0.409895688 | 0.036184181 |
| 8 | 0.476393209 | 0.036355804 | 8 | 1.097466316 | 0.070276474 | 8 | 0.415313786 | 0.032567006 | 8 | 0.437026513 | 0.038987059 |
| 9 | 0.508314877 | 0.039172122 | 9 | 1.162619128 | 0.076651959 | 9 | 0.440597271 | 0.035650065 | 9 | 0.464157338 | 0.041789937 |
| 10 | 0.540236546 | 0.041988440 | 10 | 1.227771940 | 0.083027445 | 10 | 0.465880756 | 0.038733125 | 10 | 0.491288163 | 0.044592815 |
| 11 | 0.572158215 | 0.044804758 | 11 | 1.292924752 | 0.089402931 | 11 | 0.491164241 | 0.041816185 | 11 | 0.518418988 | 0.047395693 |
| 12 | 0.594339752 | 0.049792194 | 12 | 1.320981368 | 0.101193912 | 12 | 0.502888839 | 0.047609013 | 12 | 0.527515078 | 0.054451345 |
| 13 | 0.616521289 | 0.054779630 | 13 | 1.349037985 | 0.112984893 | 13 | 0.514613438 | 0.053401842 | 13 | 0.536611168 | 0.061506997 |
| 14 | 0.638402826 | 0.059767067 | 14 | 1.377094601 | 0.124775875 | 14 | 0.526338036 | 0.059194671 | 14 | 0.545707259 | 0.068562649 |
| 15 | 0.660884363 | 0.064754503 | 15 | 1.405151218 | 0.136566856 | 15 | 0.538062635 | 0.064987500 | 15 | 0.554803349 | 0.075618301 |
| 16 | 0.683065901 | 0.069741940 | 16 | 1.433207834 | 0.148357838 | 16 | 0.549787234 | 0.070780329 | 16 | 0.563899440 | 0.082673954 |
| 17 | 0.693783593 | 0.079128418 | 17 | 1.442582479 | 0.171666609 | 17 | 0.554558059 | 0.079125062 | 17 | 0.564496724 | 0.094299276 |
| 18 | 0.704501286 | 0.088514897 | 18 | 1.451957124 | 0.194975380 | 18 | 0.559331884 | 0.087469885 | 18 | 0.565094009 | 0.105924598 |
| 19 | 0.715218978 | 0.097901375 | 19 | 1.461331769 | 0.218284151 | 19 | 0.564105709 | 0.095814708 | 19 | 0.565691293 | 0.117549920 |
| 20 | 0.725936671 | 0.107287854 | 20 | 1.470706414 | 0.241592922 | 20 | 0.568879534 | 0.104159531 | 20 | 0.566288579 | 0.129175242 |
| 21 | 0.736654364 | 0.116674333 | 21 | 1.480081059 | 0.264901695 | 21 | 0.573656360 | 0.112504444 | 21 | 0.566885863 | 0.140500564 |
| 22 | 0.741374267 | 0.129851647 | 22 | 1.494690921 | 0.296828341 | 22 | 0.574679419 | 0.124461466 | 22 | 0.575629984 | 0.157591953 |
| 23 | 0.746094170 | 0.143028961 | 23 | 1.509300784 | 0.328754987 | 23 | 0.575702479 | 0.136418488 | 23 | 0.578725464 | 0.174383342 |
| 24 | 0.750814074 | 0.156206275 | 24 | 1.523910646 | 0.360681634 | 24 | 0.576725538 | 0.148375511 | 24 | 0.580020044 | 0.191174731 |
| 25 | 0.755533977 | 0.169383589 | 25 | 1.538520509 | 0.392608280 | 25 | 0.577748598 | 0.160332533 | 25 | 0.584374105 | 0.207966120 |
| 26 | 0.760253881 | 0.182560904 | 26 | 1.553130371 | 0.424534927 | 26 | 0.578771658 | 0.172239556 | 26 | 0.588746166 | 0.224757510 |
| 27 | 0.891200527 | 0.251760318 | 27 | 1.564648658 | 0.471831030 | 27 | 0.583490531 | 0.177592198 | 27 | 0.596633553 | 0.247359820 |
| 28 | 1.022147173 | 0.320959733 | 28 | 1.576166945 | 0.519127133 | 28 | 0.588209405 | 0.182944840 | 28 | 0.604520941 | 0.269962130 |
| 29 | 1.153093819 | 0.390159147 | 29 | 1.587685232 | 0.566423236 | 29 | 0.592928279 | 0.188297482 | 29 | 0.612408328 | 0.292564410 |
| 30 | 1.284040465 | 0.459358562 | 30 | 1.599203519 | 0.613719339 | 30 | 0.597647153 | 0.193650124 | 30 | 0.620295716 | 0.315166751 |
| 31 | 1.414987111 | 0.528557977 | 31 | 1.610721806 | 0.661015442 | 31 | 0.602366027 | 0.199002767 | 31 | 0.628183104 | 0.337769062 |
| 32 | 1.448722335 | 0.583770300 | 32 | 1.633140598 | 0.729852059 | 32 | 0.591536801 | 0.231417065 | 32 | 0.637463850 | 0.364873994 |
| 33 | 1.482457559 | 0.638982623 | 33 | 1.655559388 | 0.798688676 | 33 | 0.580707575 | 0.263831363 | 33 | 0.646744596 | 0.391978927 |
| 34 | 1.516192783 | 0.694194946 | 34 | 1.677978178 | 0.867525293 | 34 | 0.569878349 | 0.296245661 | 34 | 0.656025342 | 0.419083860 |
| 35 | 1.549928007 | 0.749407269 | 35 | 1.700396968 | 0.936361910 | 35 | 0.559049123 | 0.328659959 | 35 | 0.665306088 | 0.446188793 |
| 36 | 1.583663231 | 0.804619592 | 36 | 1.722815755 | 1.005198528 | 36 | 0.591536801 | 0.361074257 | 36 | 0.674586834 | 0.473293726 |
| 37 | 1.616042734 | 0.880762624 | 37 | 1.733866500 | 1.085146436 | 37 | 0.594831103 | 0.385743247 | 37 | 0.685873672 | 0.507823560 |
| 38 | 1.648422237 | 0.956905657 | 38 | 1.744917244 | 1.165064344 | 38 | 0.598125405 | 0.410412237 | 38 | 0.697160510 | 0.542353395 |
| 39 | 1.680801739 | 1.033048690 | 39 | 1.755967989 | 1.245042251 | 39 | 0.601419708 | 0.435081227 | 39 | 0.708447348 | 0.576883230 |
| 40 | 1.713181242 | 1.109191722 | 40 | 1.767018733 | 1.324990159 | 40 | 0.604714010 | 0.489750217 | 40 | 0.719734186 | 0.611413065 |
| 41 | 1.745560745 | 1.185334755 | 41 | 1.778069478 | 1.404938067 | 41 | 0.608008313 | 0.484419207 | 41 | 0.731021025 | 0.645942900 |
| 42 | 1.789618553 | 1.296947143 | 42 | 1.805012176 | 1.506627401 | 42 | 0.612739421 | 0.508601519 | 42 | 0.740372742 | 0.683474290 |
| 43 | 1.833676360 | 1.408559531 | 43 | 1.831954873 | 1.608316736 | 43 | 0.617470529 | 0.532783831 | 43 | 0.749724460 | 0.721005680 |
| 44 | 1.877734168 | 1.520171919 | 44 | 1.858897571 | 1.710006070 | 44 | 0.622201638 | 0.556966143 | 44 | 0.759076178 | 0.758537070 |
| 45 | 1.921791975 | 1.631784307 | 45 | 1.885840268 | 1.811695405 | 45 | 0.626932746 | 0.581148455 | 45 | 0.768427896 | 0.796068460 |
| 46 | 1.965849783 | 1.743396695 | 46 | 1.912782966 | 1.913384739 | 46 | 0.631663855 | 0.605330768 | 46 | 0.777779614 | 0.833599851 |
| 47 | 2.018201592 | 1.896431143 | 47 | 1.967468680 | 2.031811082 | 47 | 0.634450404 | 0.636214302 | 47 | 0.783955997 | 0.873832340 |
| 48 | 2.070553402 | 2.049465590 | 48 | 2.022154394 | 2.150237426 | 48 | 0.637236953 | 0.667097836 | 48 | 0.790132380 | 0.914064830 |
| 49 | 2.122905211 | 2.202500038 | 49 | 2.076840109 | 2.268663769 | 49 | 0.640023502 | 0.697981370 | 49 | 0.796308764 | 0.954297319 |
| 50 | 2.175257021 | 2.355534485 | 50 | 2.131525823 | 2.387090113 | 50 | 0.642810051 | 0.728864904 | 50 | 0.802485147 | 0.994529809 |
| 51 | 2.227608830 | 2.508568933 | 51 | 2.186211537 | 2.505516456 | 51 | 0.645596600 | 0.759748439 | 51 | 0.808661531 | 1.034762299 |

4.3 Airfoil profiles

The lift coefficient c_l and drag coefficient c_d are the characteristic of airfoil. They are required in order to perform the wind turbine blade performance calculations. The airfoil profile calculation using the finite element method software "ANSYS" is described as the method for obtaining the airfoil characteristics.

In this research, the shape of the wind turbine blade airfoil profile NACA4415 is used. The NACA4415 is one of the NACA4 character systems. In the United States, the extensive wind tunnel tests for airfoil series with varying systematically were carried out to obtain the airfoil characteristics. The NACA4 character-based wing is the first tested one, and windmills based on the NACA4 are often used since the design procedure is simple.

4.3.1 Fluid analysis using finite element method software ANSYS

The lift coefficient c_l and drag coefficient c_d of designed blade shape are calculated with the fluid analysis using finite element method software ANSYS. The cross section of designed blade shape is represented with NACA4415 as shown in Fig. 4.4. The XY coordinate data of NACA4415 are used in fluid analysis. Which was explained in 4.3.2 shows the calculated results of fluid analysis. The c_l and c_d are derived from the calculated results of L and D indirectly by equations in (3.1) and (3.2).

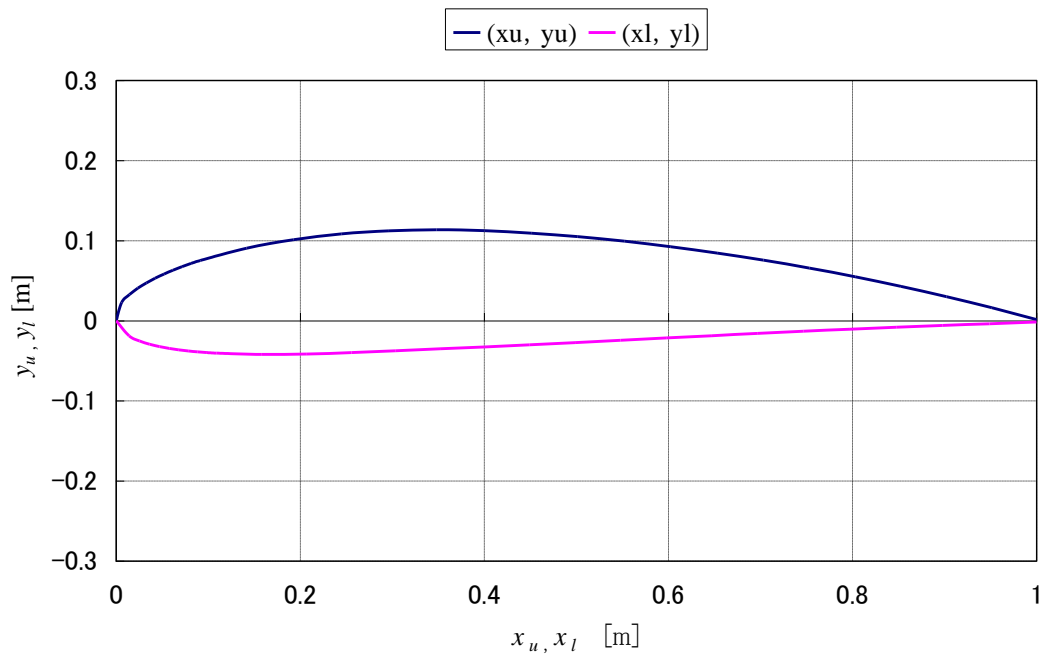


Fig. 4.4. XY coordinate data of NACA4415.

4.3.2 Analysis results due to the ANSYS

The fluid analysis using finite element method software ANSYS is executed to calculate the state of the pressure applied to the airfoil. Fig.4.5-4.15. shows the wind vector illustration, wind velocity distribution, and pressure distribution for the airfoil of NACA4415 when the meeting angles are 0, -10, +10[deg.].

The angle of attack of 0 [deg]

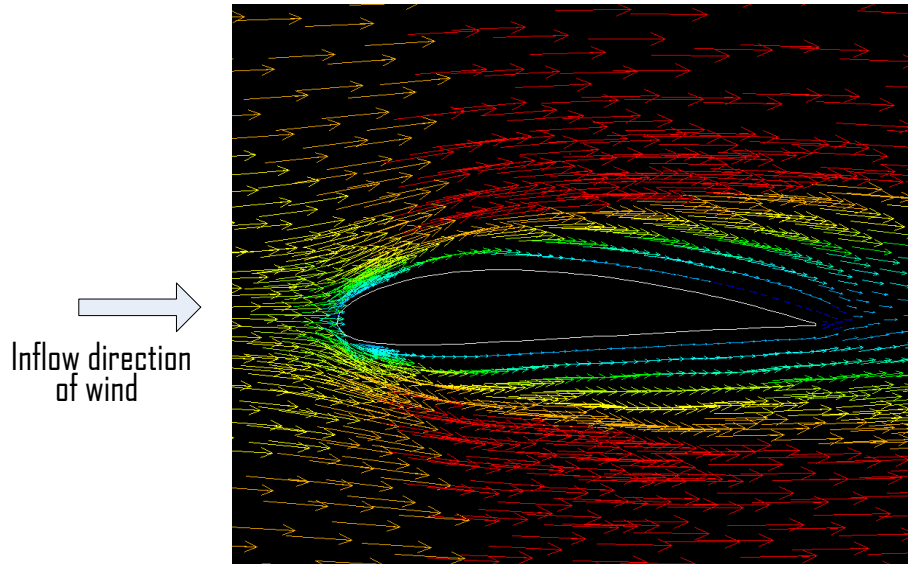


Fig 4.5. The angle of attack of 0 [deg] of the wind vector illustration

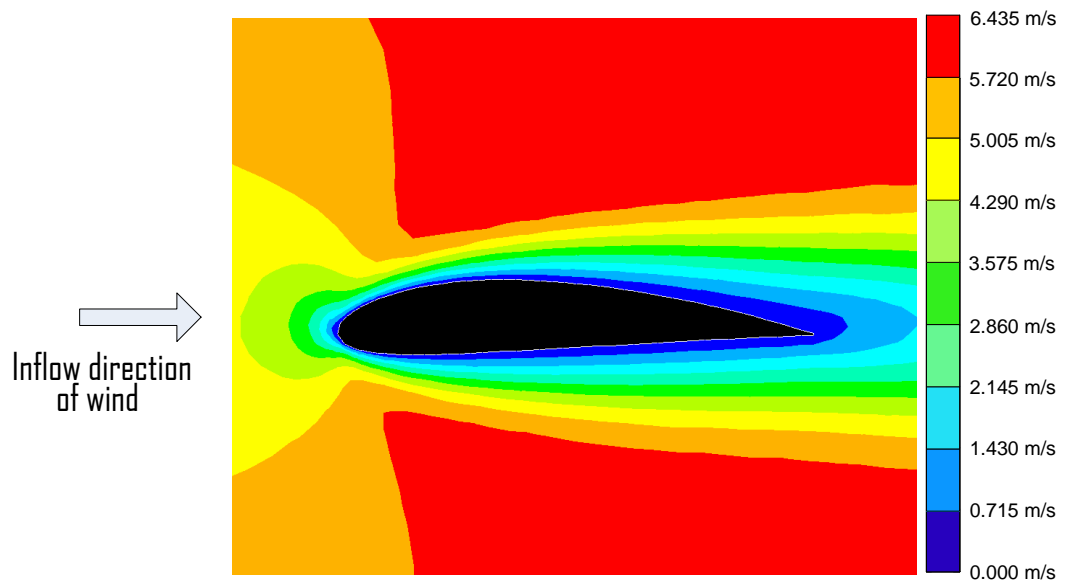


Fig 4.6. The angle of attack of 0 [deg] of the wind velocity distribution

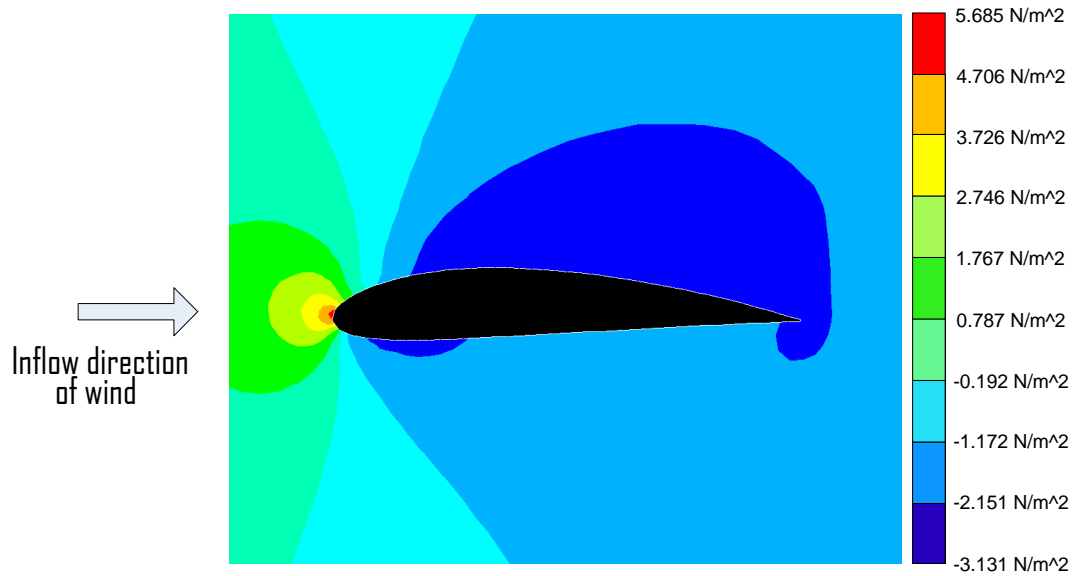


Fig 4.7. The angle of attack of 0 [deg] of the pressure distribution

The angle of attack of -10 [deg]

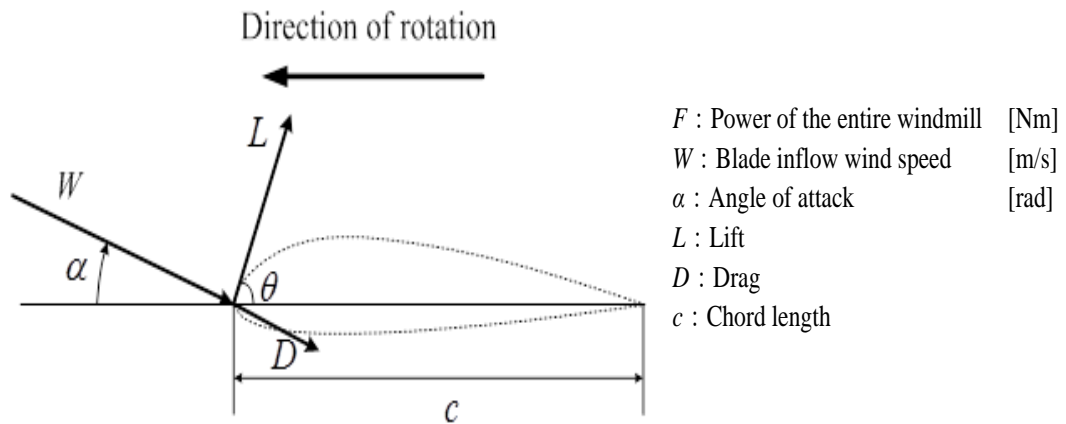


Fig 4.8. The angle of attack of -10 [deg]

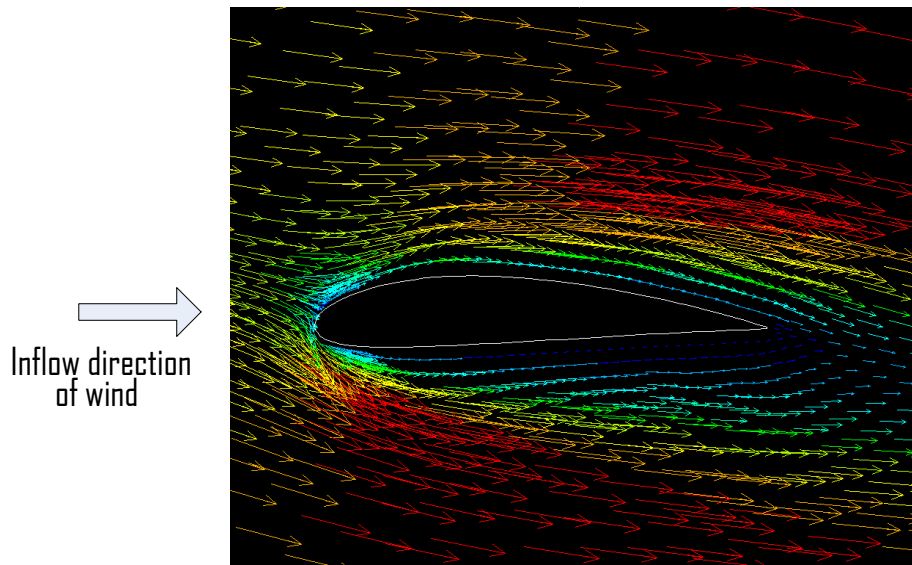


Fig 4.9. The angle of attack of -10 [deg] of the wind vector illustration

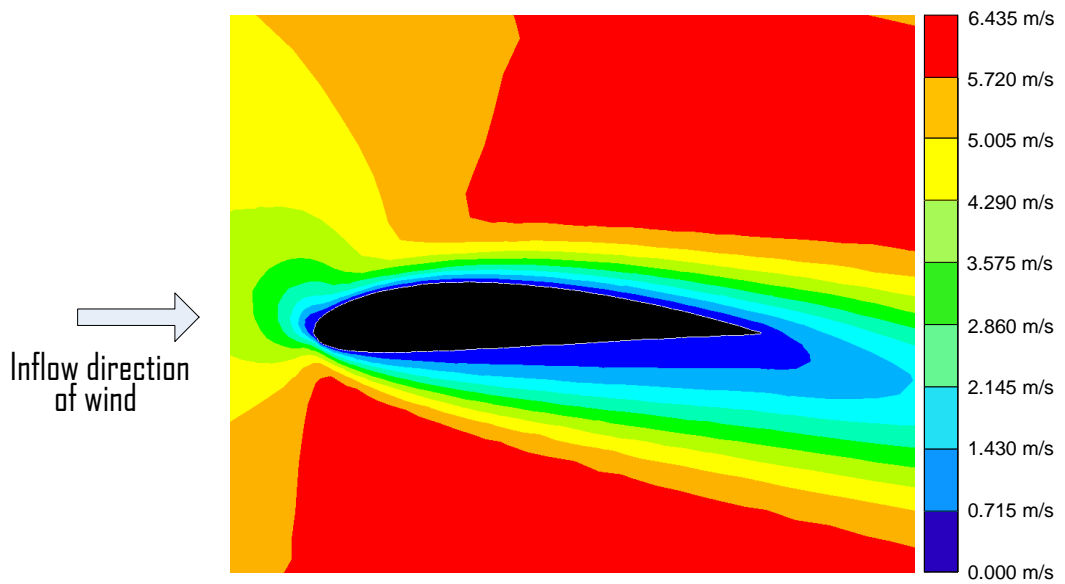


Fig 4.10. The angle of attack of -10 [deg] of the wind velocity distribution

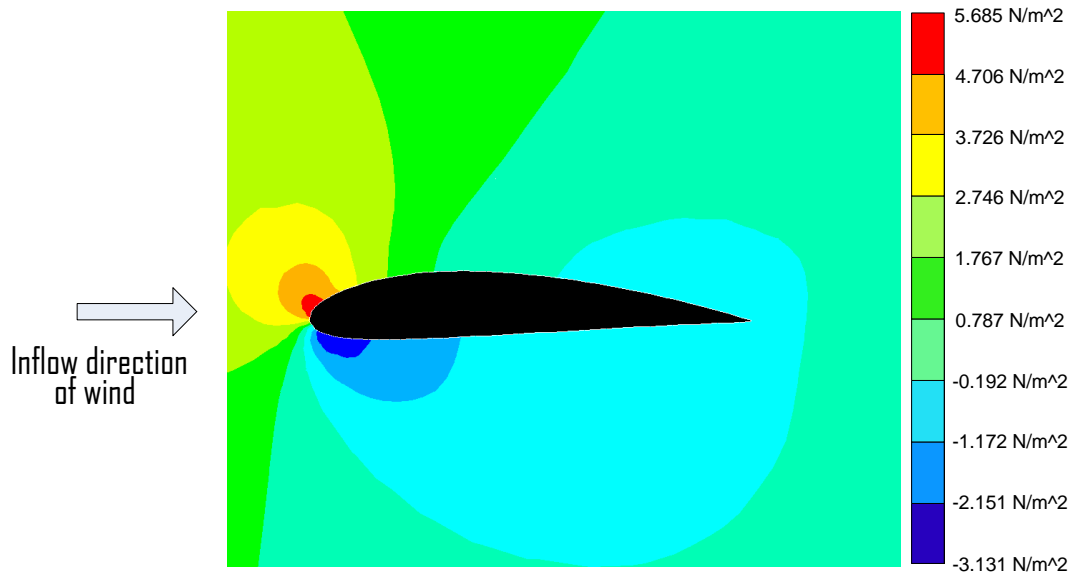


Fig 4.11. The angle of attack of -10 [deg] of the pressure distribution

The angle of attack of +10 [deg]

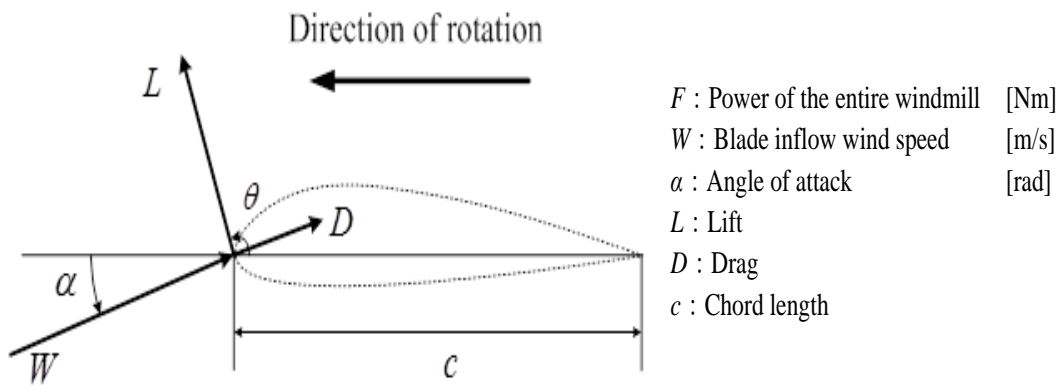


Fig 4.12. The angle of attack of +10 [deg]

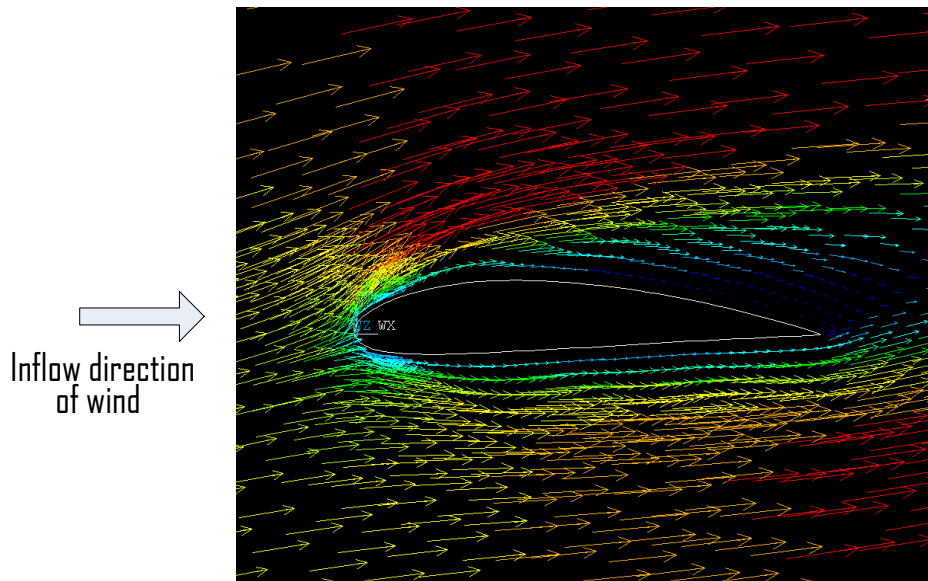


Fig 4.13. The angle of attack of +10 [deg] of the wind vector illustration

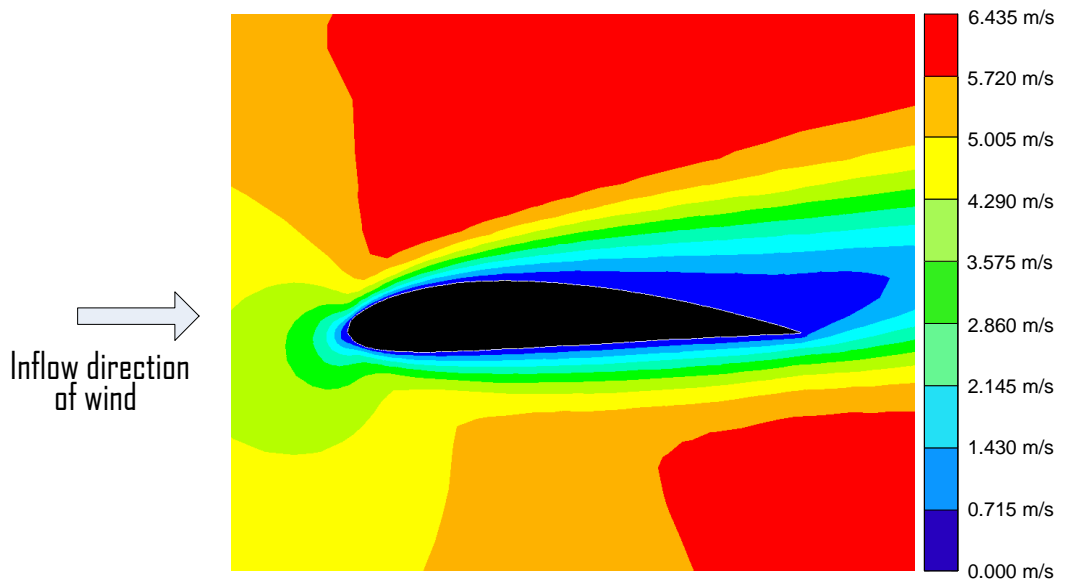


Fig 4.14. The angle of attack of +10 [deg] of the wind velocity distribution

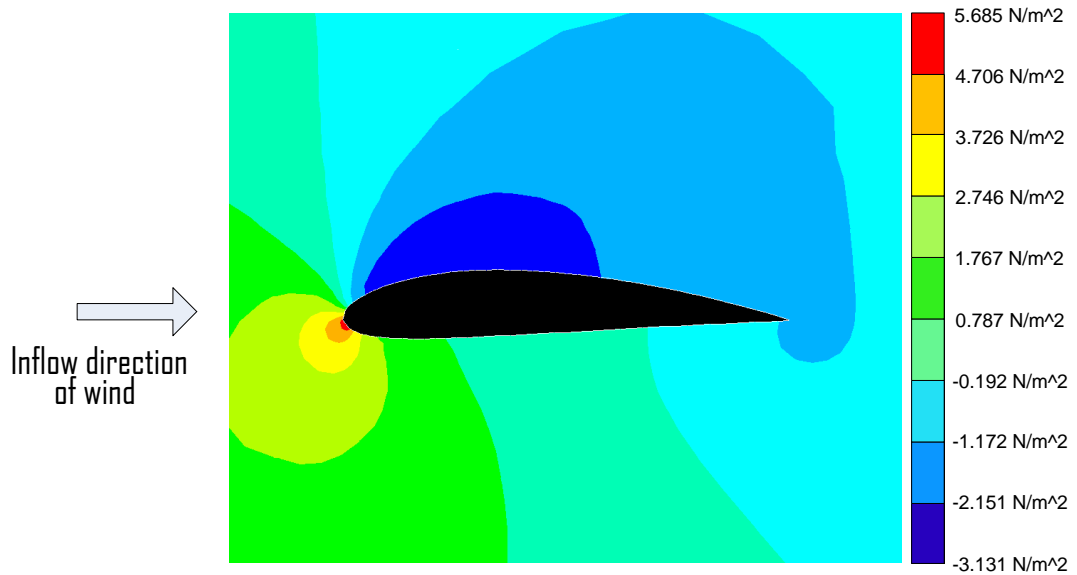


Fig 4.15. The angle of attack of +10 [deg] of the pressure distribution

The c_l and c_d are obtained by the fluid analysis using finite element method for each point and each meeting angle from 0 to 51 degrees. The concrete numeric data are not shown in circumstances of the space. Fig. 4.16, 4.17 and 4.18 shows the calculated three dimensional data and the wind turbine blade performance calculated output data.

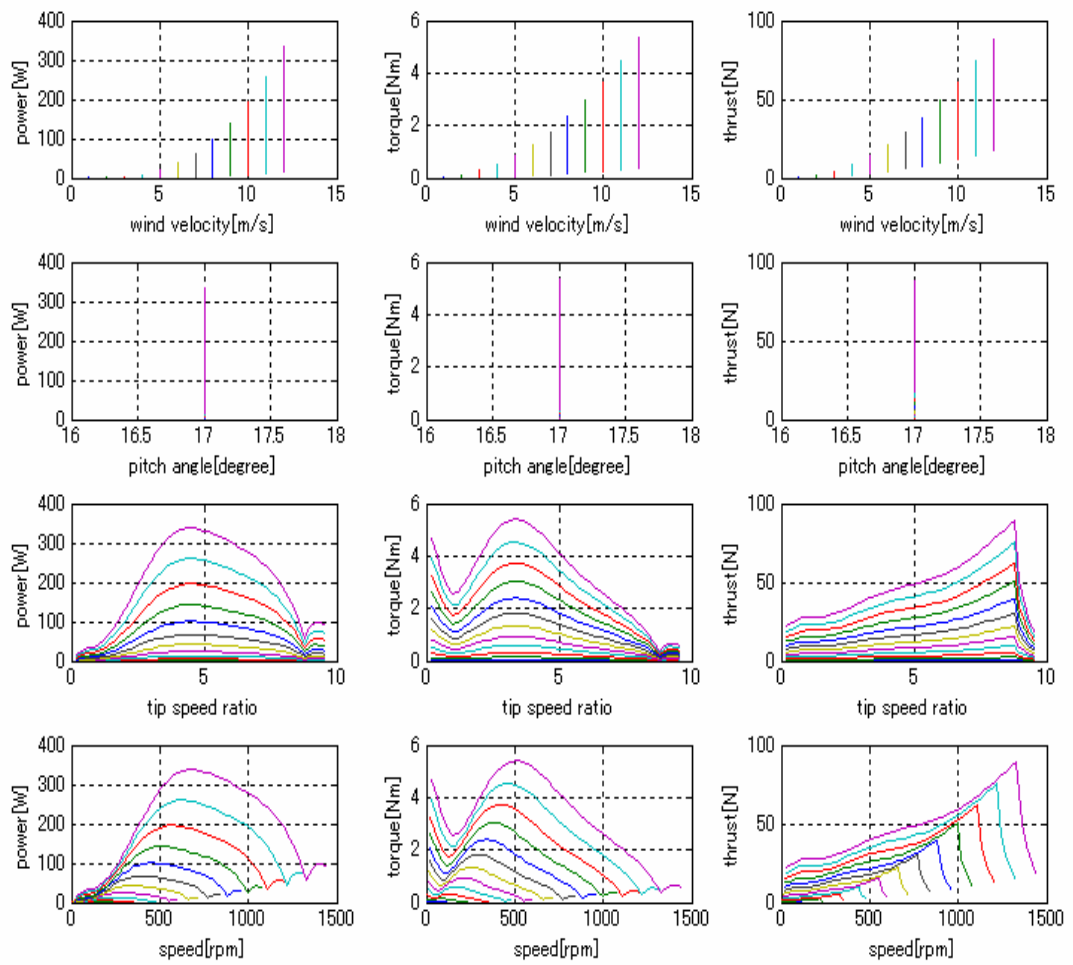


Fig. 4.16. Calculated wind turbine blade performance output result.

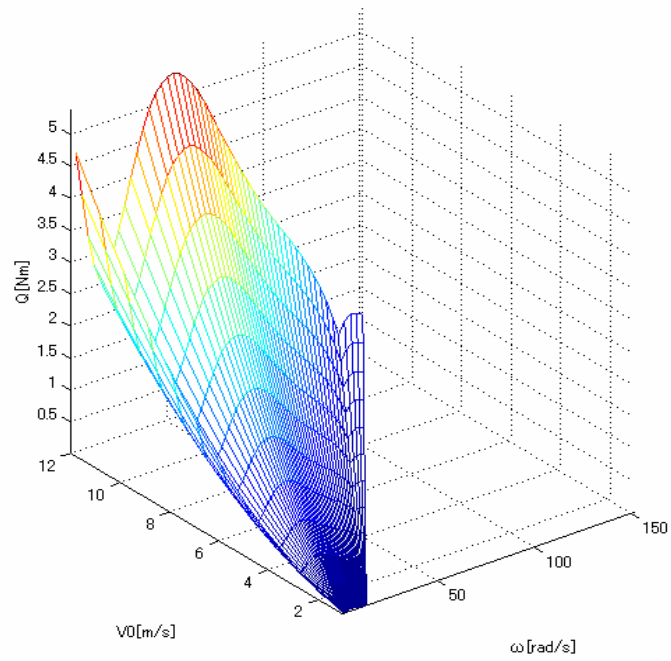


Fig.4.17. Windmill output torque.

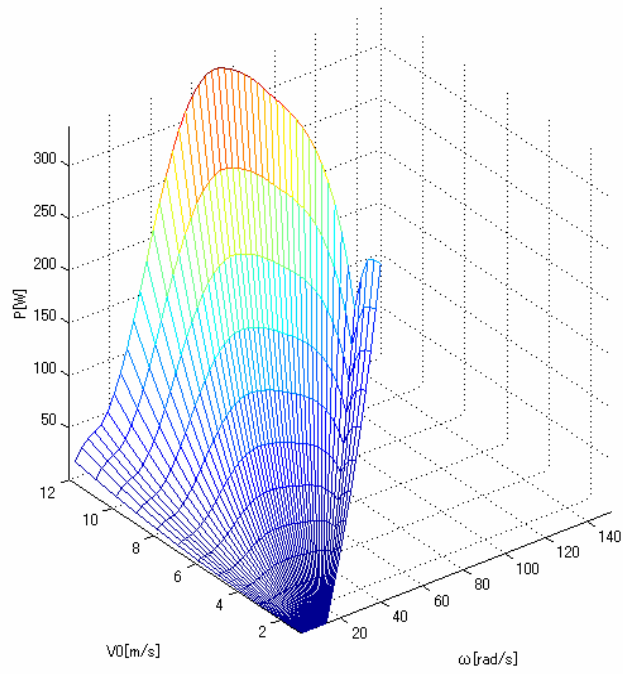


Fig 4.18. Windmill output power.

4.4 Mechanical model

The mechanical systems of the real wind turbine side and generator side in Fig. 4.19 are described in the equations

$$\left\{ J_g + J_t \left(\frac{n_2}{n_1} \right)^2 \right\} \frac{d\omega_g}{dt} = T_g - Q \frac{n_2}{n_1} - \left\{ B_g + B_t \left(\frac{n_2}{n_1} \right)^2 \right\} \omega_g \dots\dots\dots(4.1)$$

Where, Q, T_g : The generated torque of the wind turbine side and generator side, T_1, T_2 : The shaft torque of the wind turbine side and generator side, ω_t, ω_g : The rotor rotational angular speed of wind turbine side and generator side, B_t, B_g : The viscous friction coefficient of the wind turbine side and generator side, J_t, J_g : The moment of inertia of the wind turbine side and generator side.

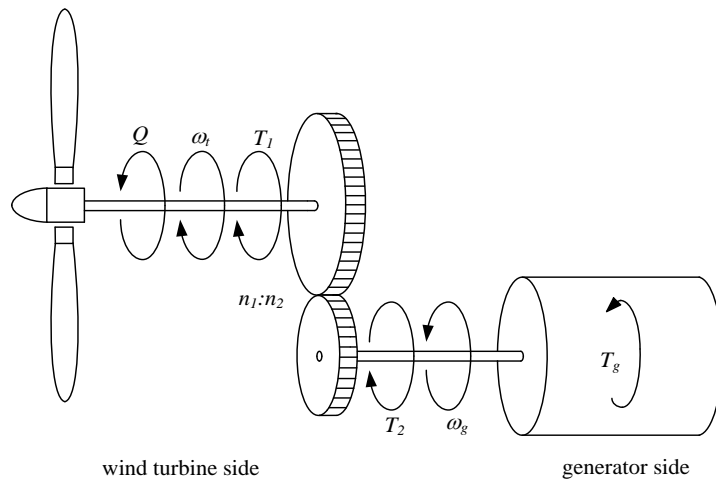


Fig. 4.19. Mechanical model for real wind turbine

The WTE uses an induction machine as a wind turbine. The mechanical systems of the induction motor side and generator side in Fig. 4.20 are described in the equations

$$\left\{ J_g + J_{im} \left(\frac{n_2}{n_1} \right)^2 \right\} \frac{d\omega_g}{dt} = T_g - T_{im} \frac{n_2}{n_1} - \left\{ B_g + B_{im} \left(\frac{n_2}{n_1} \right)^2 \right\} \omega_g \dots\dots\dots(4.2)$$

Where, T_{im} : The generated torque of the induction motor side, T_{lim} : The shaft torque

of the induction motor side, ω_{im} : The rotor rotational angular speed of induction motor side, B_{im} : The viscous friction coefficient of the induction motor side, J_{im} : The moment of inertia of the induction motor side.

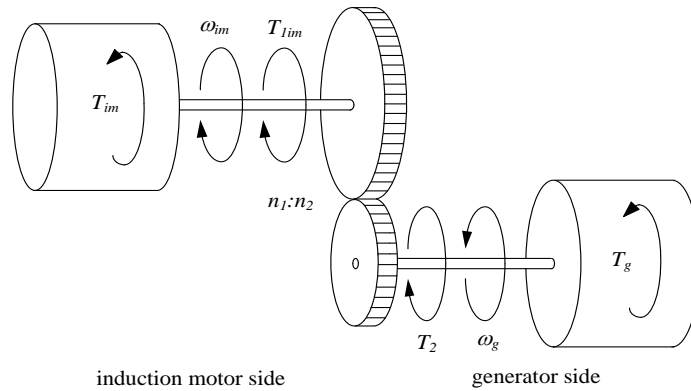


Fig. 4.20. Mechanical model for wind turbine emulator.

The moment of inertia and coefficient of viscosity are different between the real wind turbine and induction motor. The differences affect the transient and steady state responses. It is important to compensate the differences since the V_0 always change. The difference can be compensated by following equation.

$$T_{im}^{ref} = \frac{J_{im}}{J_t} (Q - B_t \omega_t) + B_{im} \omega_t \quad \dots \dots \dots (4.3)$$

Where, T_{im}^{ref} : torque reference of induction motor [Nm].

4.5 System configuration of WTE

The system configuration of WTE is shown in Fig. 4.21. The equation (4.3) is used to compensate the difference of moment of inertia and coefficient of viscosity between induction motor and wind turbine. All estimations are executed with the dSPACE control system. The T_{im}^{ref} is estimated for V_0 and ω_g . The inverter applies the vector control to an induction motor. The induction motor generates the electric torque corresponding to the T_{im}^{ref} instantaneously.

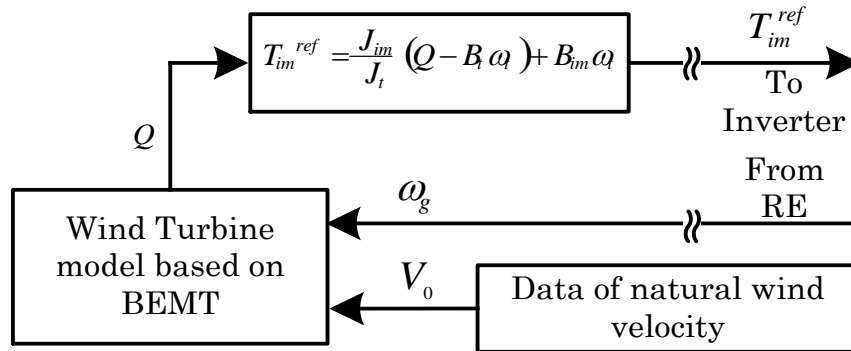


Fig. 4.21. WTE base on BEMT.

4.6 Experimental system of real wind turbine (PWM converter scheme)

Fig. 4.22 shows the experimental system using the real wind turbine of the PWM converter scheme. The wind turbine side, the natural wind velocity data is given by the real time data of anemometer (CYG-5103VM, CLIMATEC Japan). The rotational speed of PMSG is estimated in the DSP by using the signals from the rotary encoder (RE, E6C3-CWZ3XH, Omron Japan). Also, the digital signal processing (DSP) unit calculates the wind turbine torque reference from the wind velocity data and rotational speed of the induction motor (IM). The natural wind velocity data is given by the real data of anemometer from real time. The rotational speed of IM is estimated in the DSP by using the signals from the rotary encoder (RE). The torque of IM is controlled by the off-the-shelf inverter. The IM is operated based on the wind turbine torque reference sent from a DSP through the D/A board (DS2102). After the wind turbine emulator is activated, the PMSG starts to rotate, and the converter control system starts to control the windmill rotational speed for the maximum power point tracking. The PWM signals for controlling the CNV, and INV are sent from a DSP to the short-circuit prevention circuit (FPGA) through a digital I/O board (DS4002). The PWM signals are sent to the CNV and INV through the optical circuit.

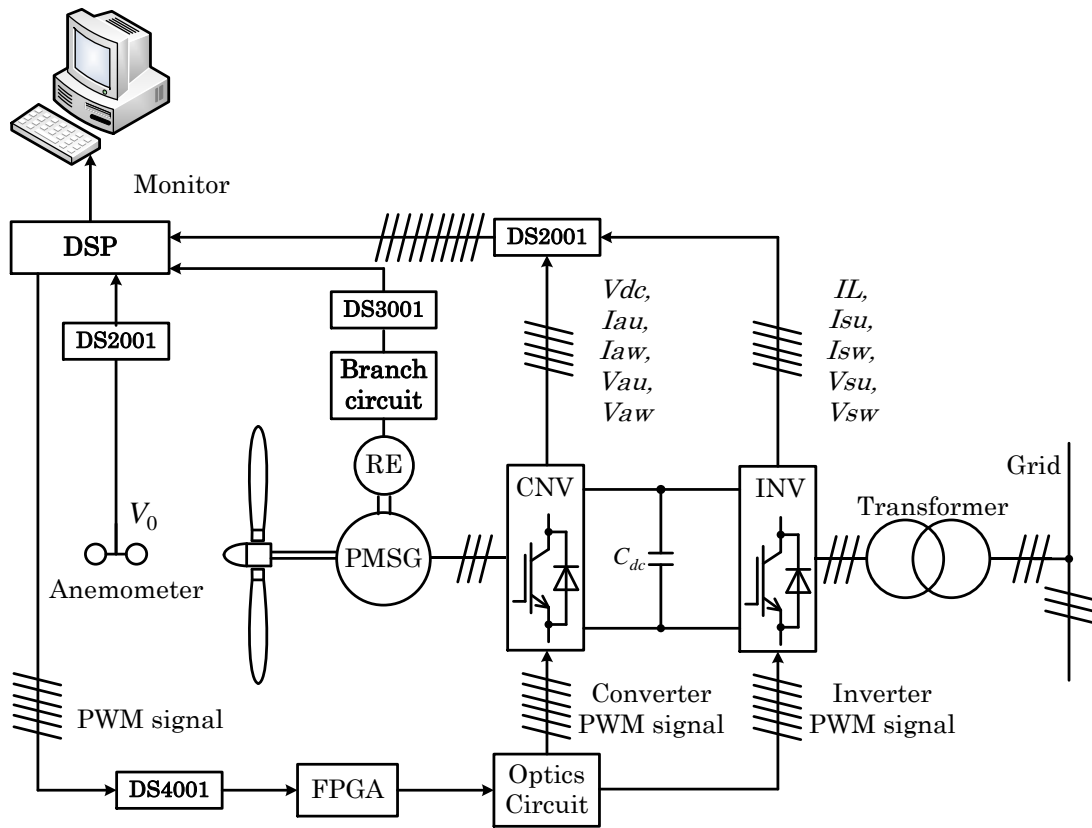


Fig. 4.22. Experimental system using the real wind turbine (PWM converter scheme)

4.7 Experimental system of wind turbine emulator

(PWM converter scheme)

Fig. 4.23 shows the experimental system of the PWM converter scheme. The digital signal processing (DSP) unit calculates the wind turbine torque reference from the wind velocity data and rotational speed of the induction motor (IM). The wind velocity data or the natural wind velocity data is given by the stored data in a PC. The rotational speed of IM is estimated in the DSP by using the signals from the rotary encoder (RE). The torque of IM is controlled by the off-the-shelf inverter. The IM is operated based on the wind turbine torque reference sent from a DSP through the D/A board (DS2102). After the wind turbine emulator is activated, the PMSG starts to rotate, and the converter control system starts to control the windmill rotational speed for the maximum power point tracking. The PWM signals for controlling the CNV, and INV are sent from a DSP to the short-circuit prevention circuit (FPGA) through a digital I/O board (DS4002). The PWM signals are sent to the CNV and INV through the optical circuit.

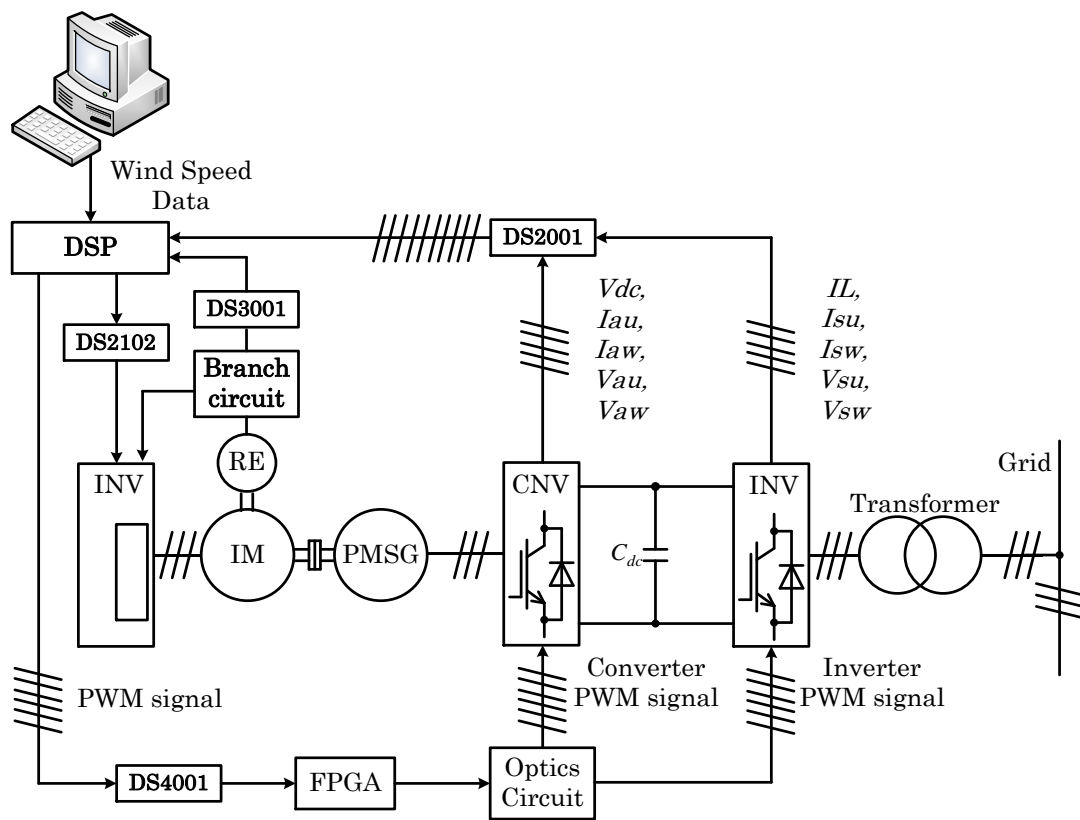


Fig. 4.23. Experimental system using the wind turbine emulator (PWM converter scheme)

4.8 Change of the wind velocity of wind turbine emulator. (PWM converter scheme)

Fig. 4.24 shows the change of the wind velocity V_0 [m/s]. The change of wind velocity includes the ranges of low wind velocity, middle wind velocity, and high wind velocity. The high wind velocity means the wind velocity that exceeds the rated value. All ranges include the change of wind velocity.

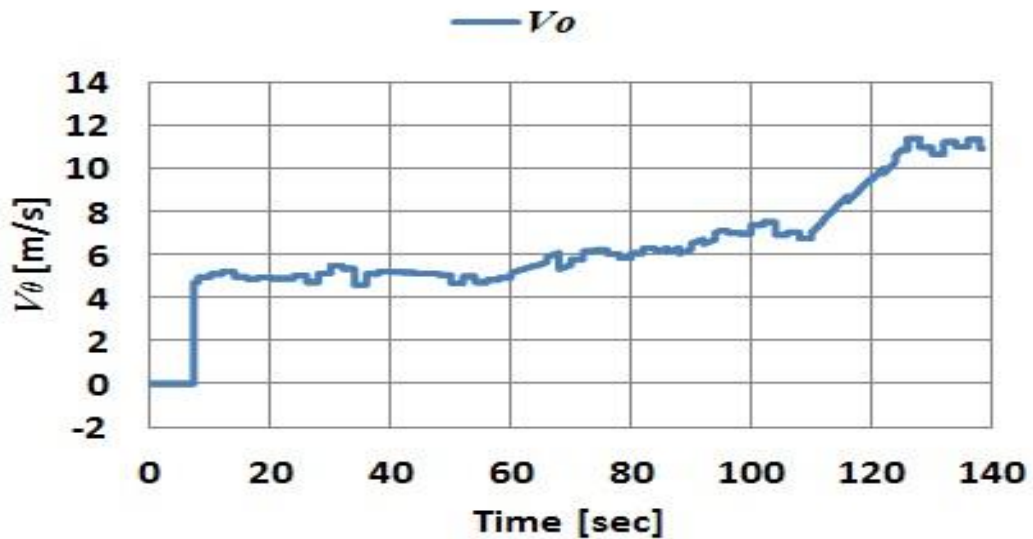


Fig. 4.24. Wind velocity.

4.9 Experimental results of wind turbine emulator

(PWM converter scheme)

Fig. 4.25- 4.38 shows the experimental results. The windmill rotational speed reaches the windmill rotational speed reference, and the power generation starts after 5 [sec] when the wind velocity is 5[m/s]. In this region of low wind velocity, that windmill rotational speed can be controlled to keep the tip speed ratio at optimized value. The speed control is carried out with the converter and inverter control systems even when the variations of wind velocity causes. The generated power is sent to the power system by the inverter.

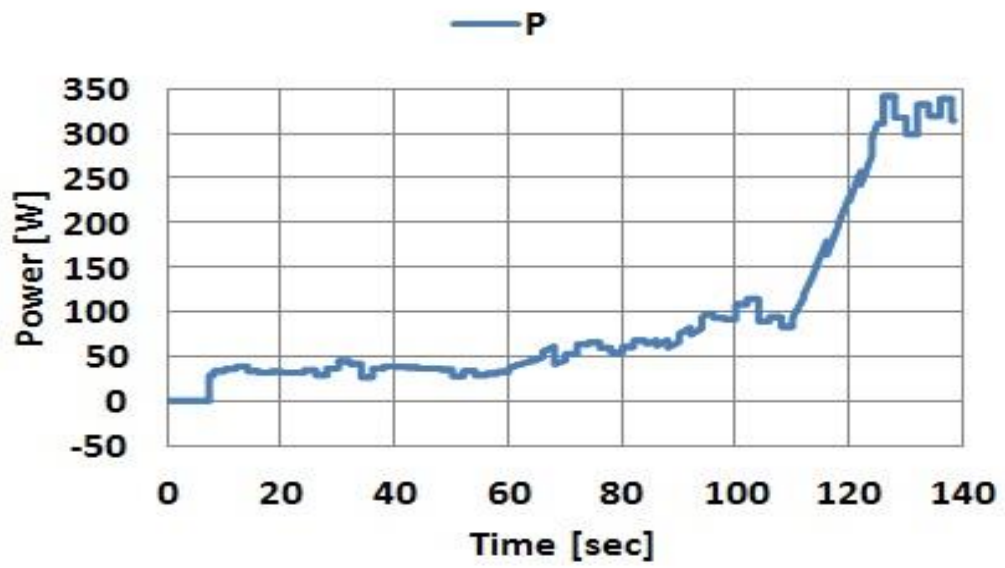


Fig. 4.25. Generated power

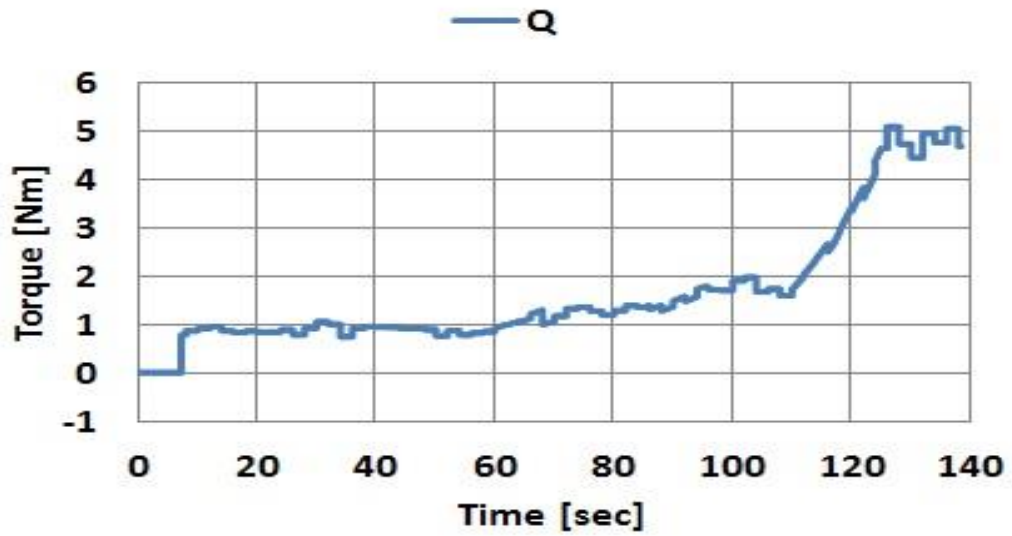


Fig. 4.26. Wind turbine Torque

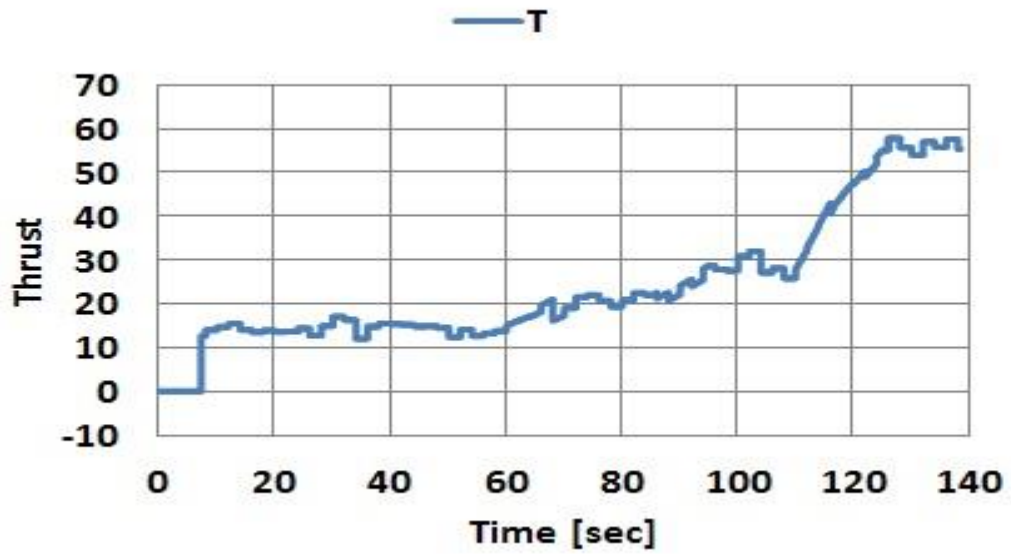


Fig. 4.27. Thrust

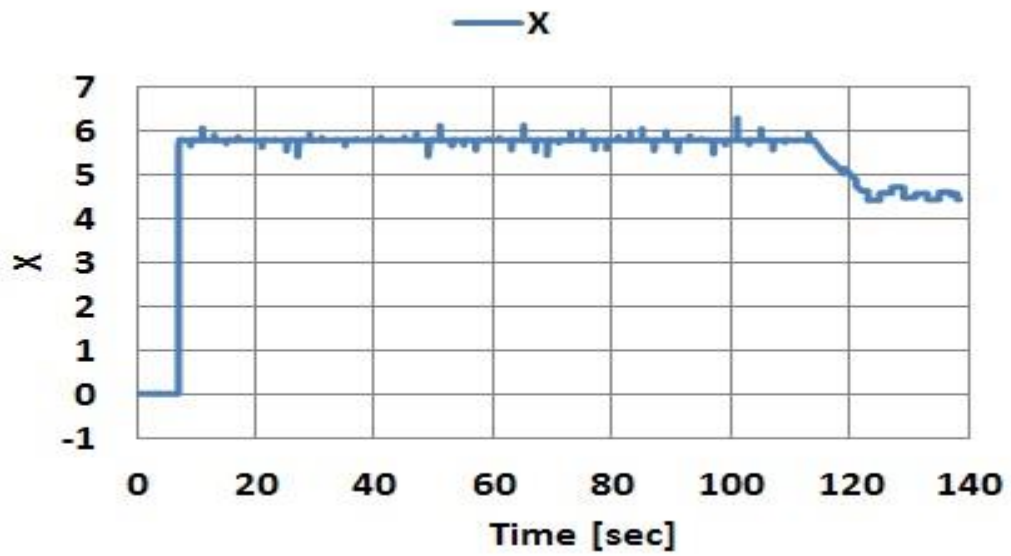


Fig. 4.28. Tip speed ratio



Fig. 4.29. Power reference

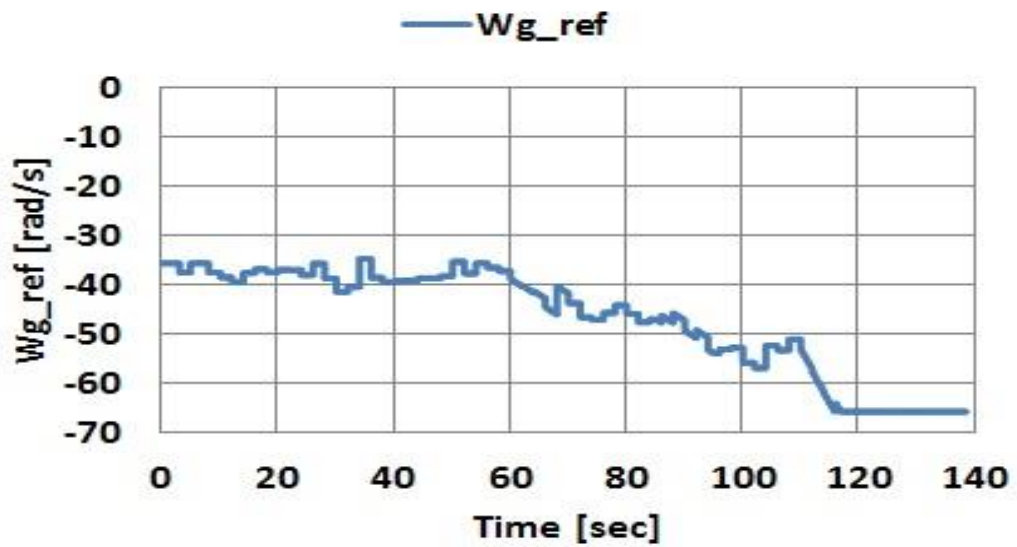


Fig. 4.30. Rotational speed Reference

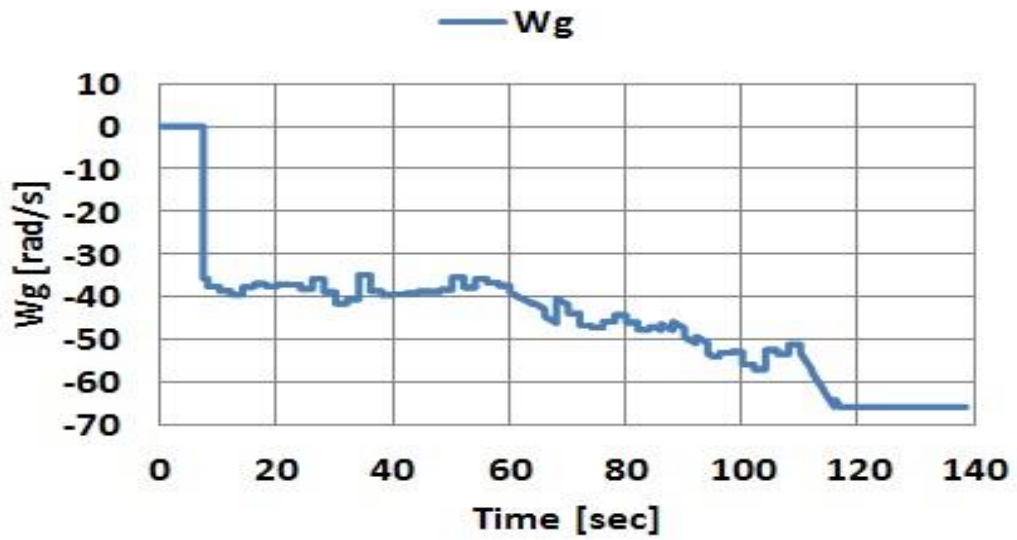


Fig. 4.31. Rotational speed

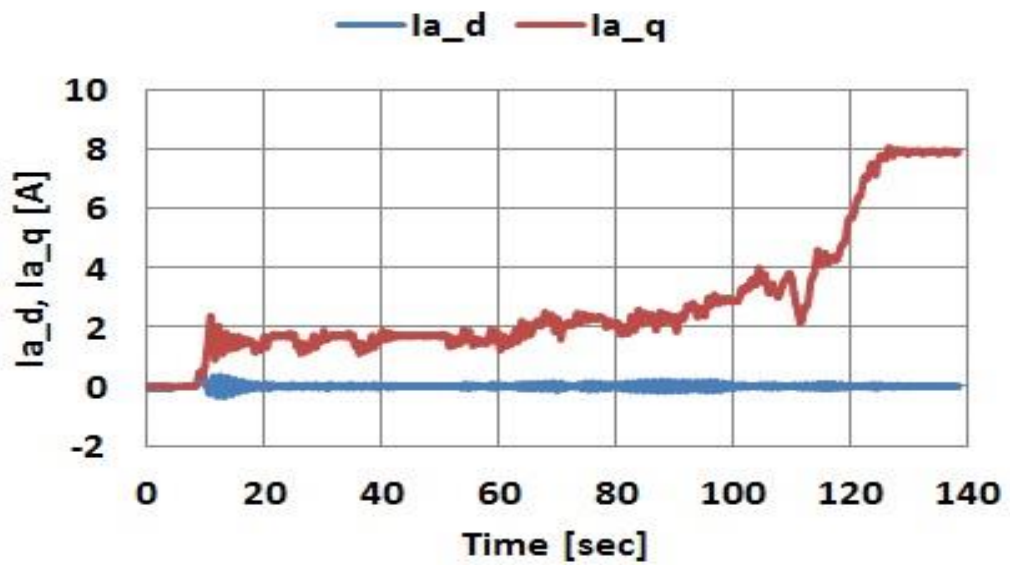


Fig. 4.32. d -axis and q -axis current for converter side

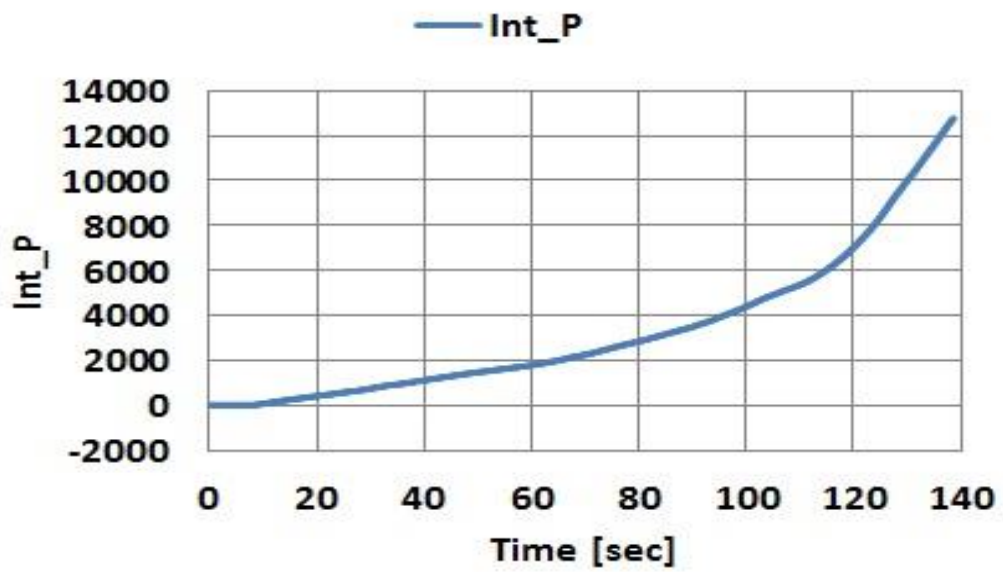


Fig. 4.33. Integrated power

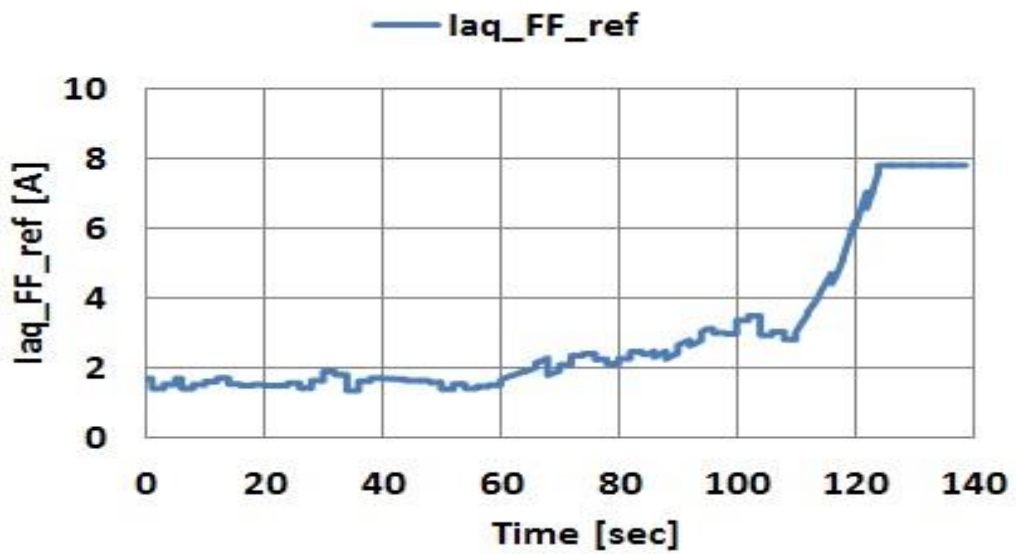


Fig. 4.34. q -axis current reference of Feed forward control

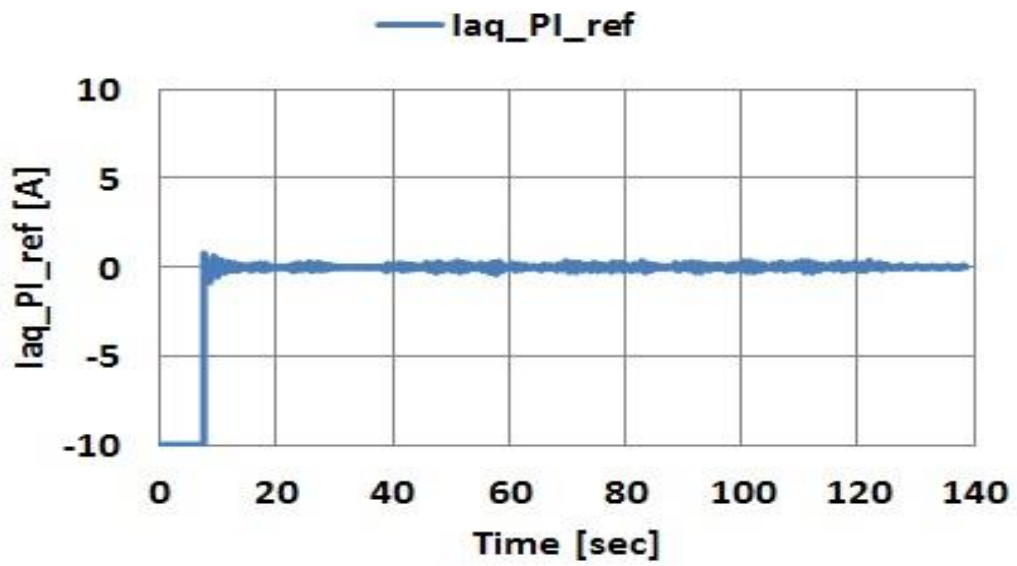


Fig. 4.35. q -axis current reference of Speed regulator

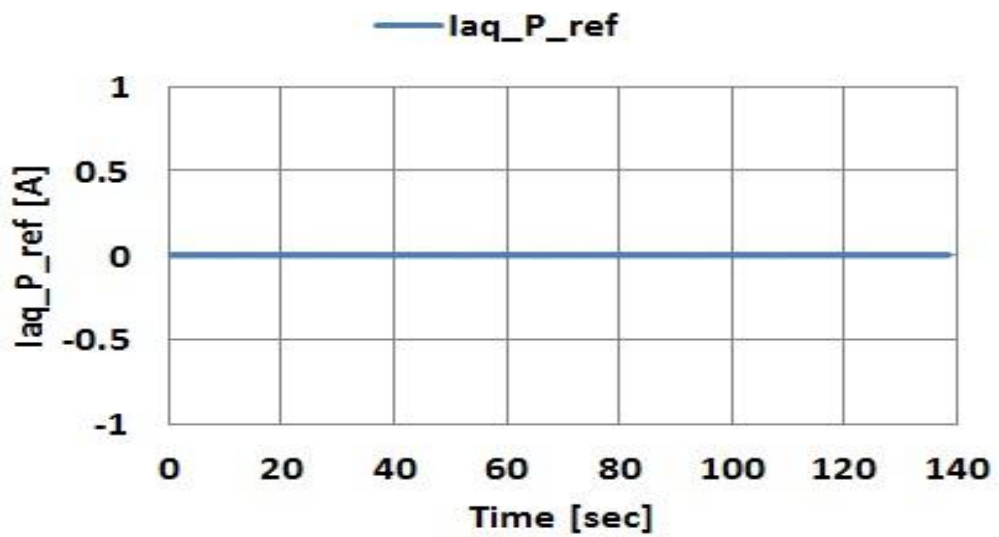


Fig. 4.36. q -axis current Reference of Power regulator

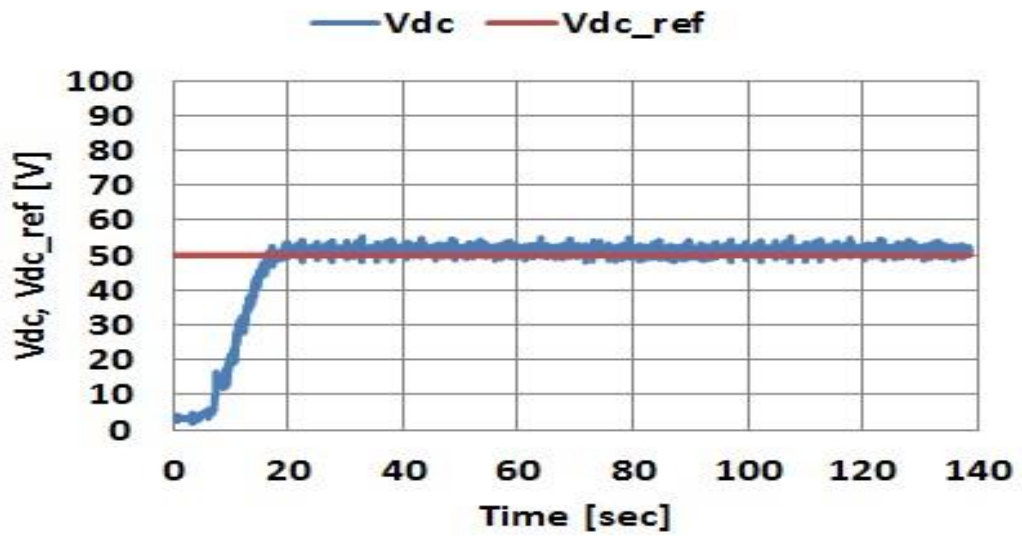


Fig. 4.37. DC link voltage and its reference

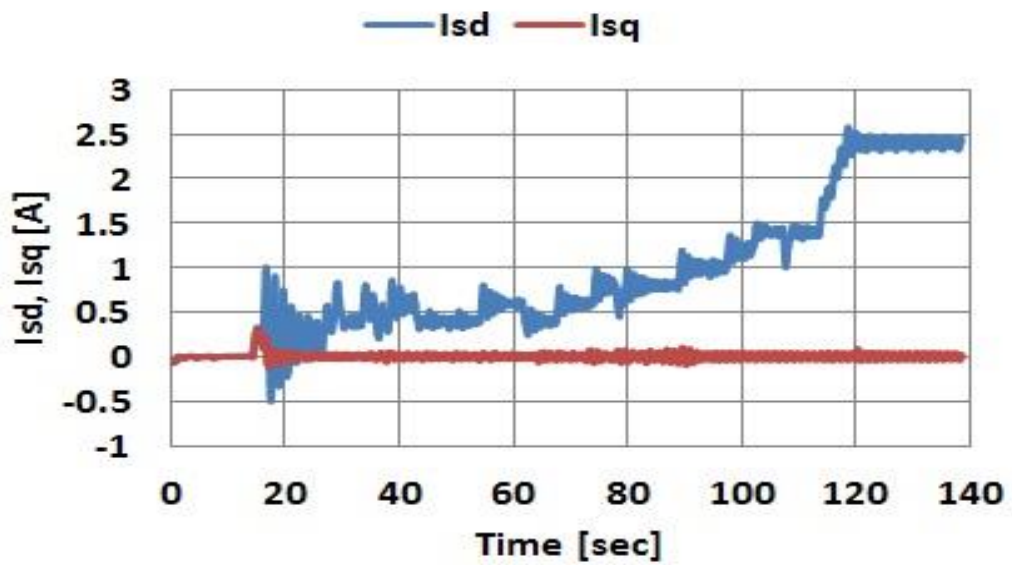


Fig. 4.38. *d*-axis and *q*-axis current for inverter side

4.10 Simulation results of wind turbine model

(PWM converter scheme)

Fig. 4.39- 4.52 shows the simulation results. The simulation models for the permanent magnet synchronous generator wind generation system using the PWM converters are implemented by using MATLAB/Simulink. The simulation models consider the natural wind, the main circuits, the converter and inverter control systems, and the pitch angle control system. The simulation results are similar to the experimental results of fig. 4.25- 4.38.

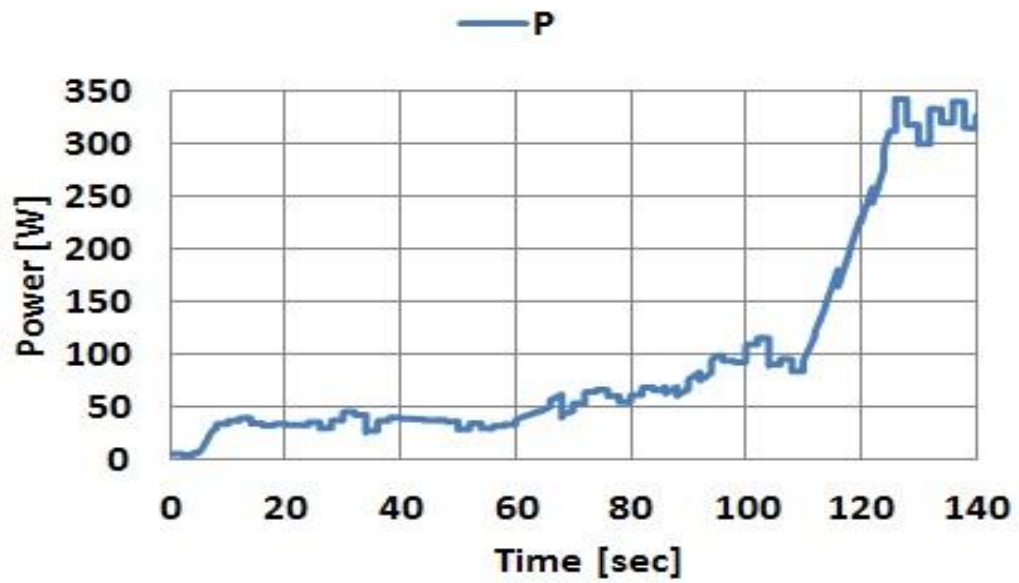


Fig. 4.39. Generated power

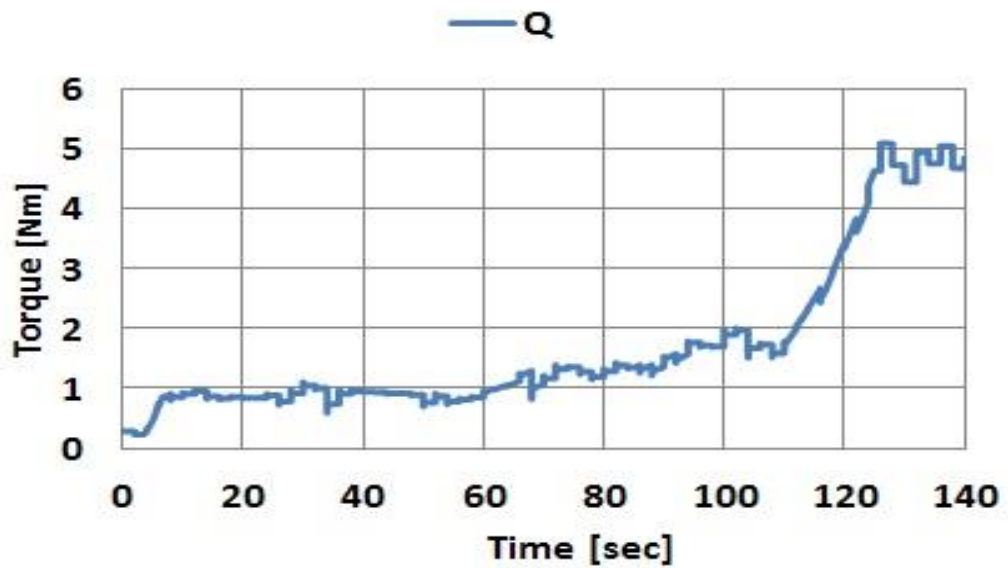


Fig. 4.40. Wind turbine Torque

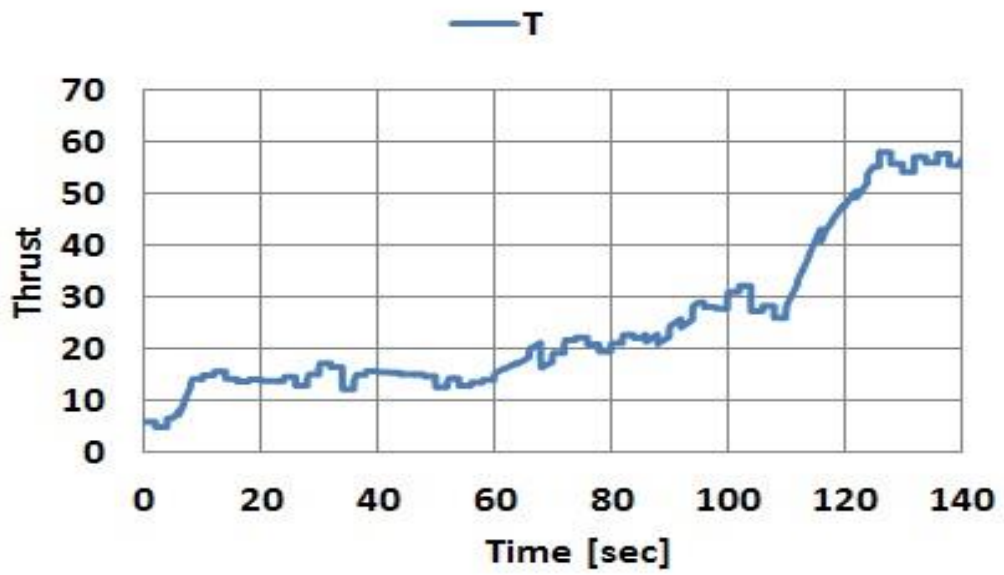


Fig. 4.41. Thrust

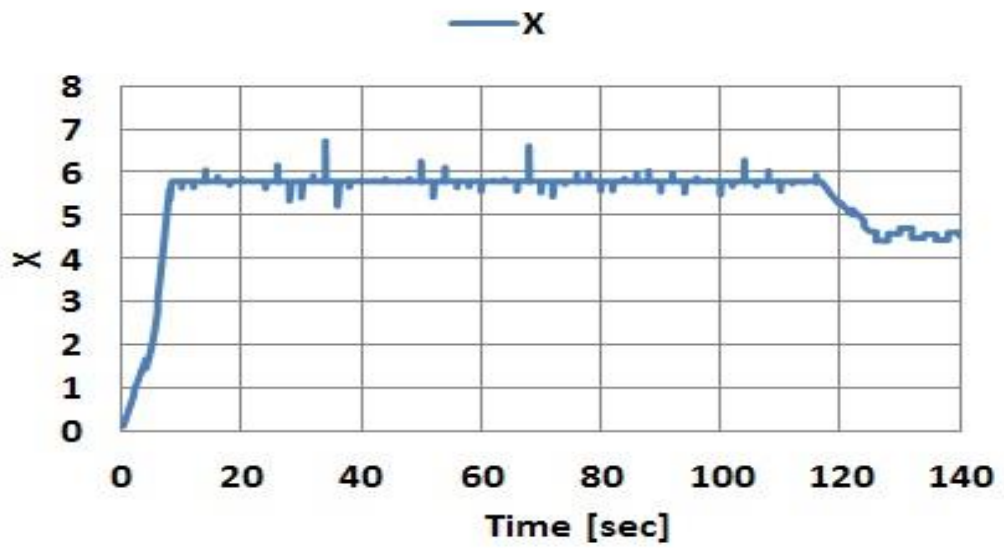


Fig. 4.42. Tip speed ratio

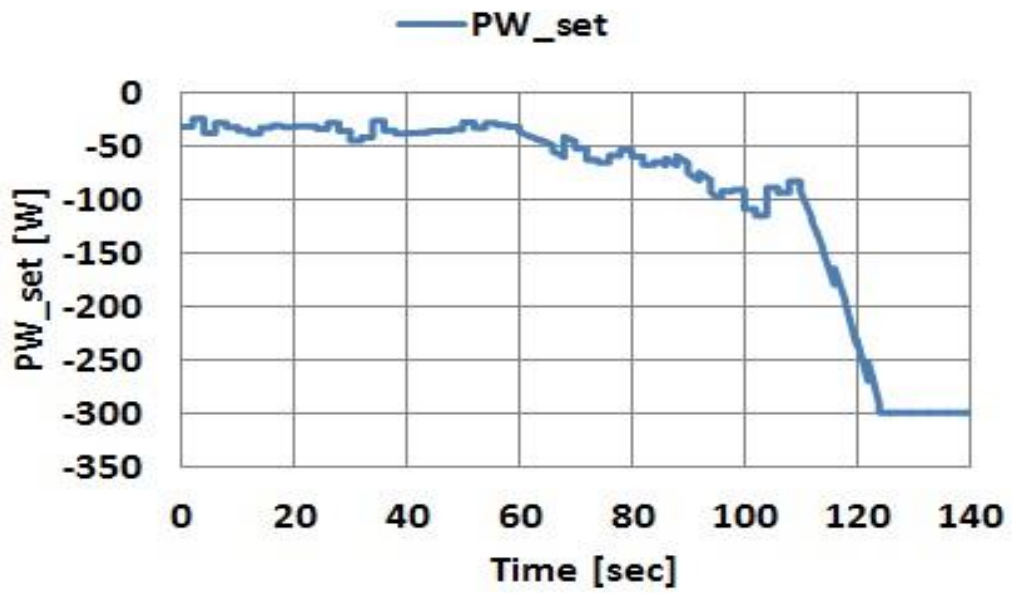


Fig. 4.43. Power reference

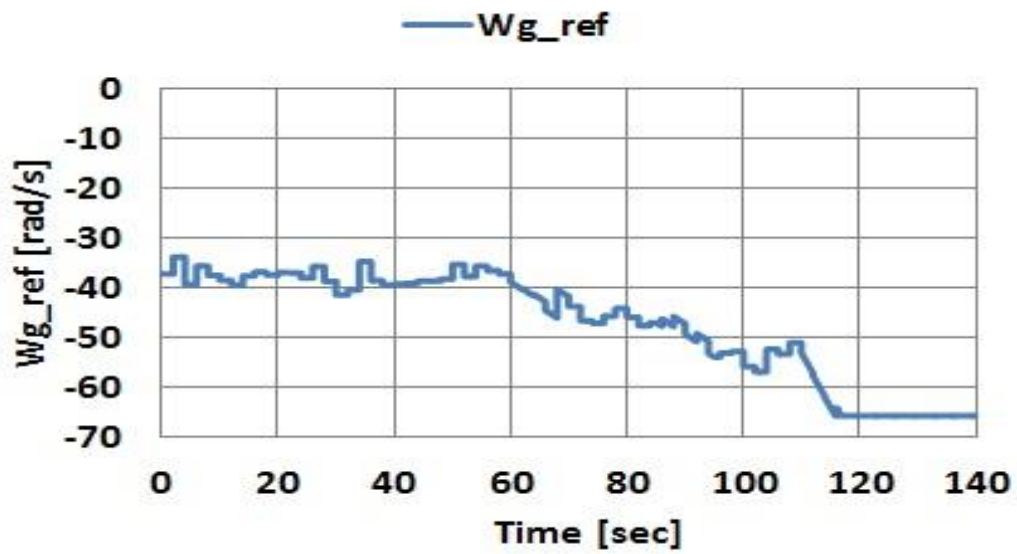


Fig. 4.44. Rotational speed reference

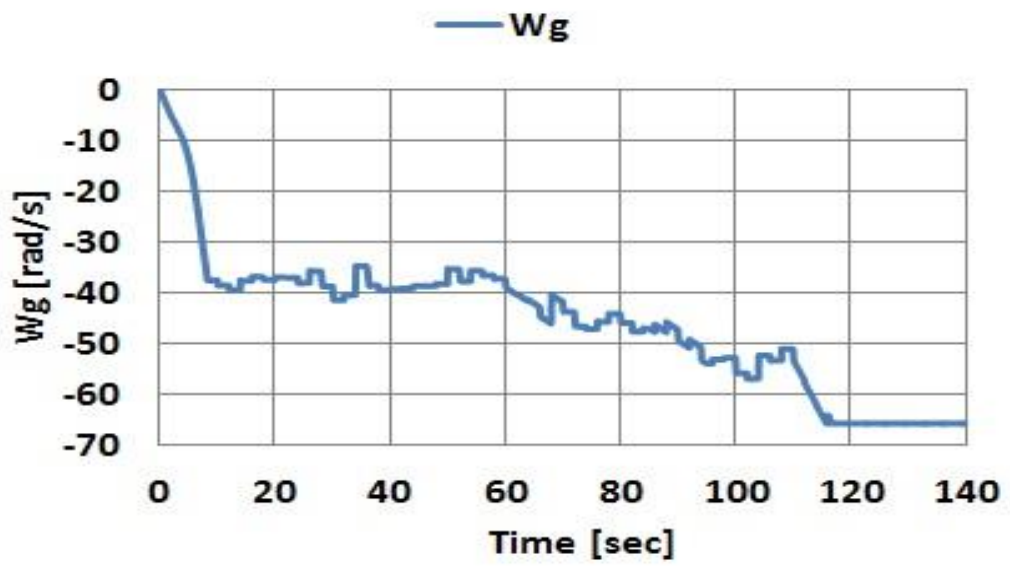


Fig. 4.45. Rotational speed

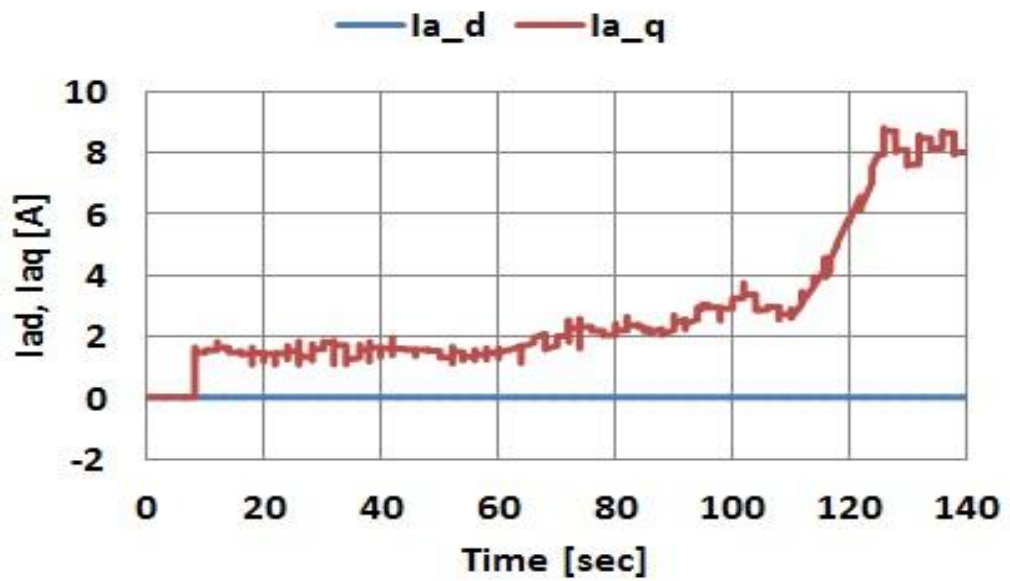


Fig. 4.46. d -axis and q -axis current for converter side

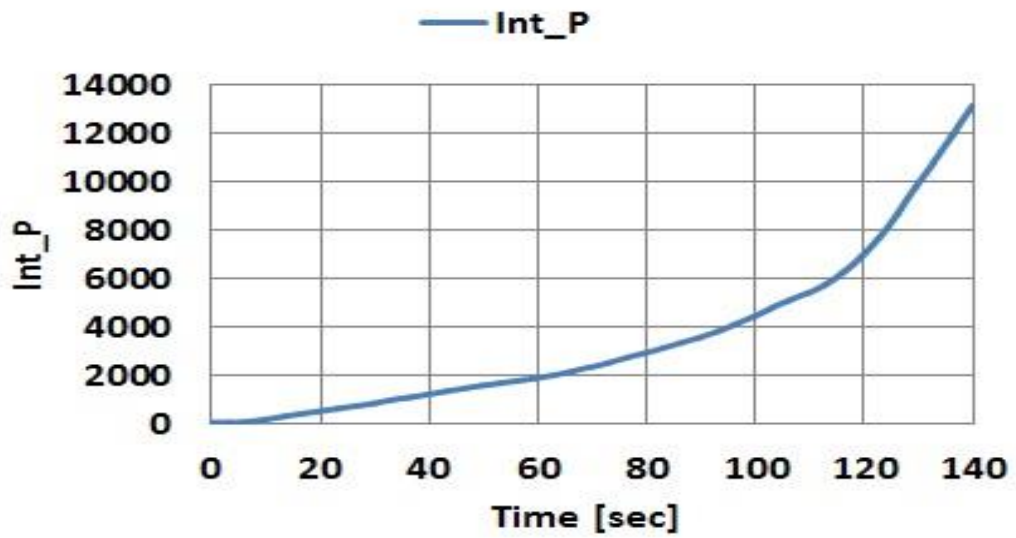


Fig. 4.47. Integrated power

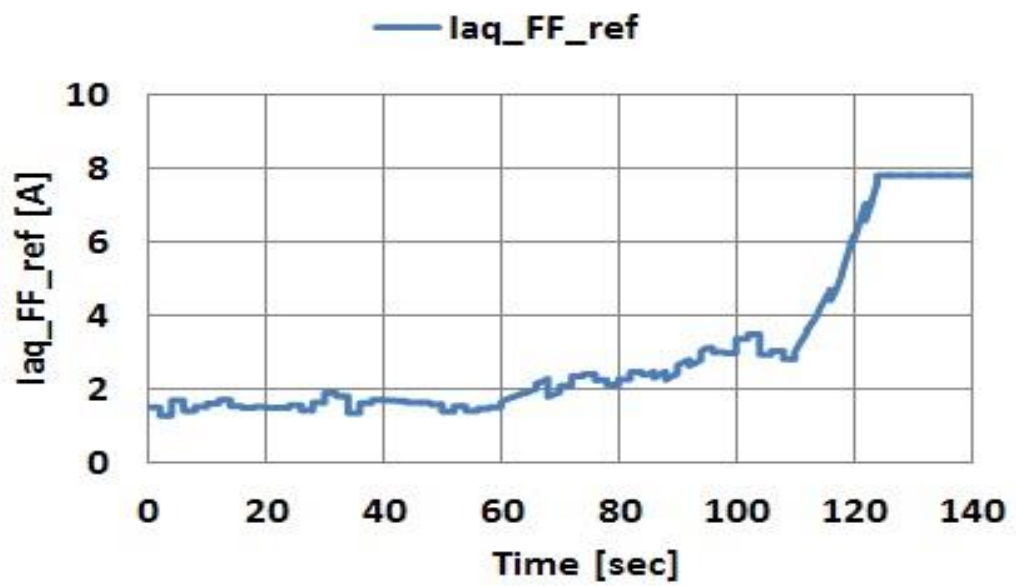


Fig. 4.48. q -axis current reference of feed forward control

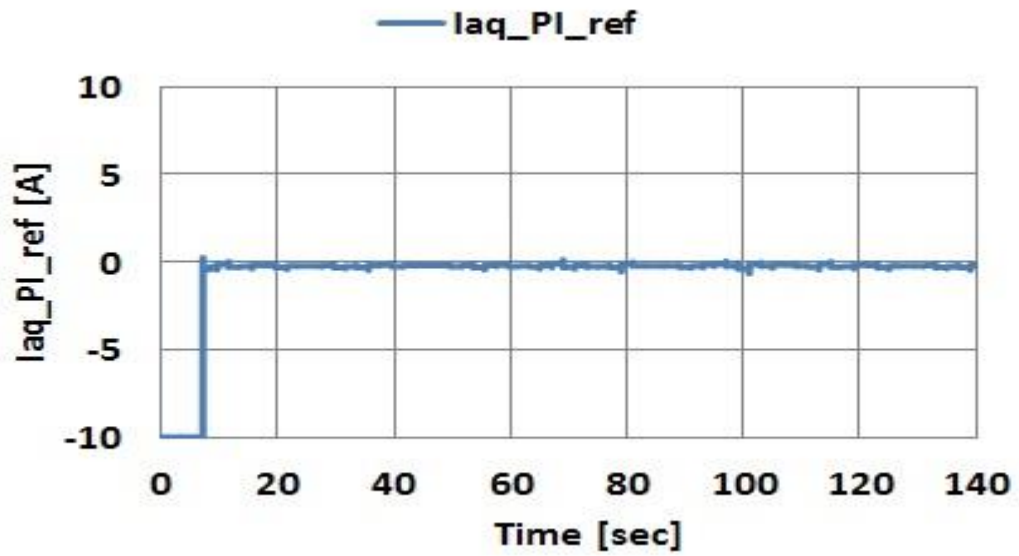


Fig. 4.49. q -axis current reference of speed regulator

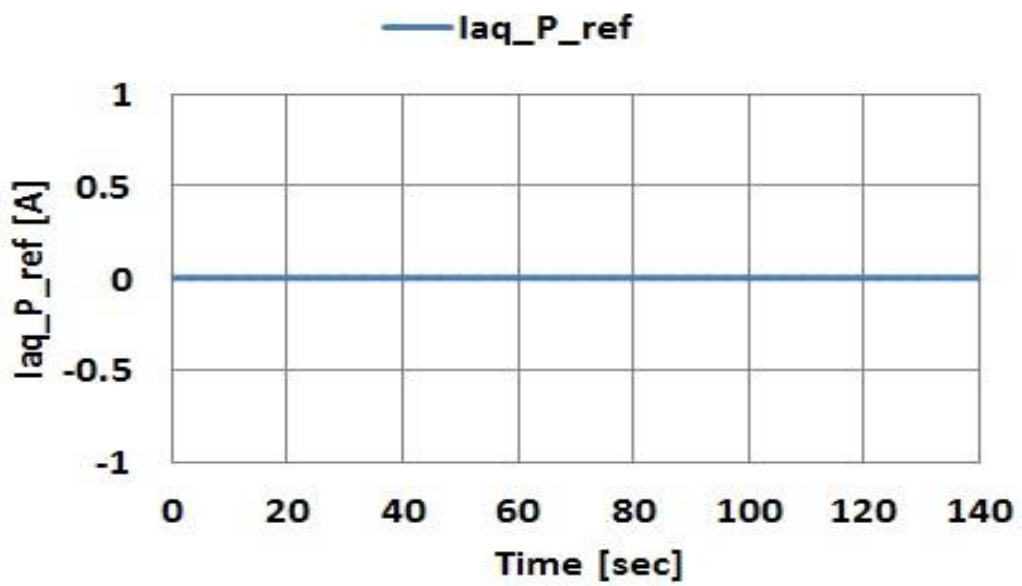


Fig. 4.50. q -axis current reference of power regulator

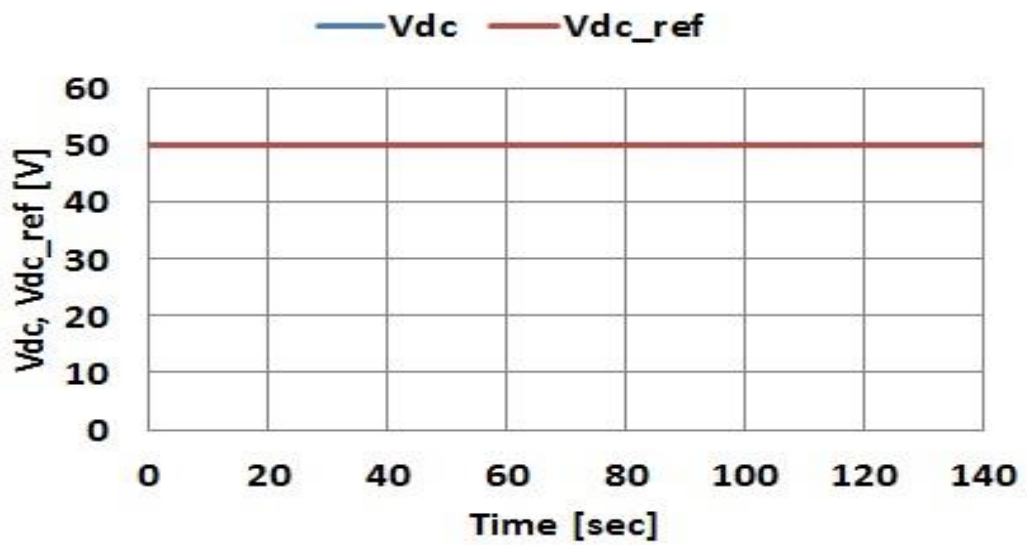


Fig. 4.51. DC link voltage and its reference

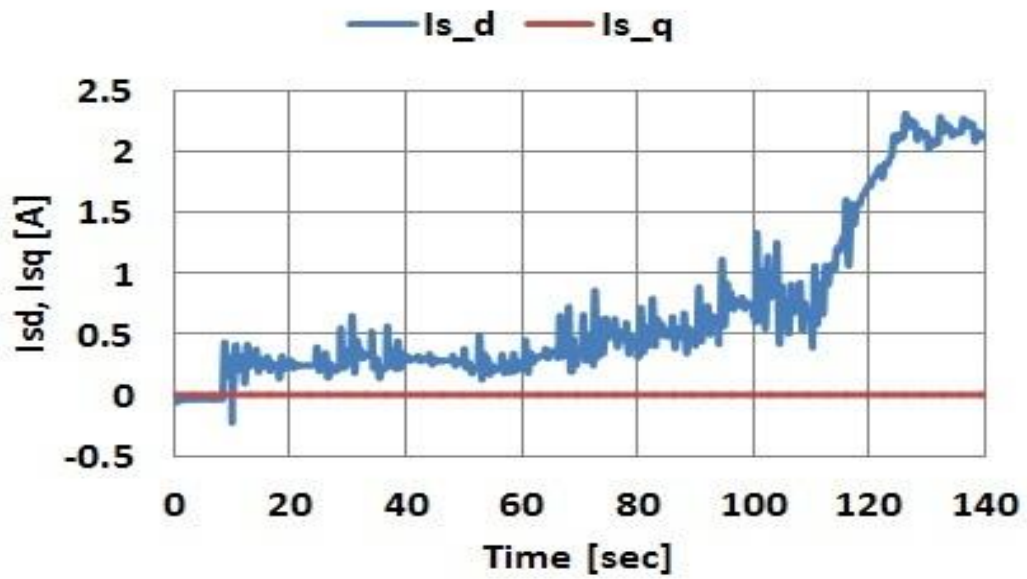


Fig. 4.52. *d*-axis and *q*-axis current for inverter side

4.11 Natural wind velocity of real wind turbine.

(PWM converter scheme)

Fig. 4.53 shows the change of the natural wind velocity V_0 [m/s] not user filter is given by the real time data of anemometer (CYG-5103VM, CLIMATEC Japan). The change of natural wind velocity includes the ranges of low wind velocity, middle wind velocity, and high wind velocity. The high wind velocity means the wind velocity that exceeds the rated value. All ranges include the change of wind velocity. The PWM converter scheme (of real wind turbine) and PWM converter scheme (of wind turbine emulator) are tested for the same change of the wind velocity, and the control performances of both schemes are discussed.

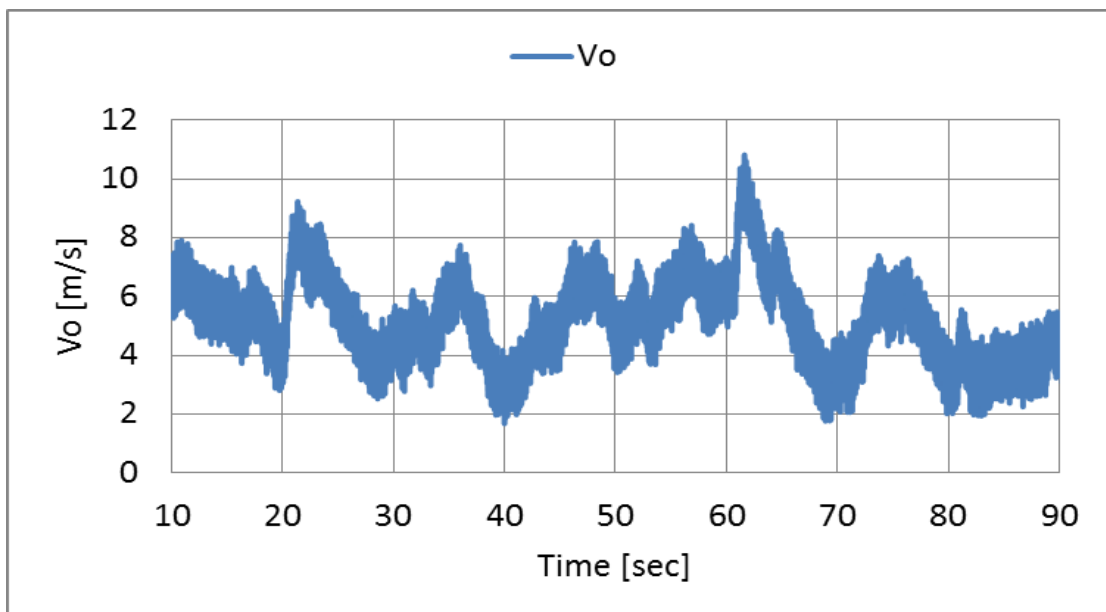


Fig. 4.53. Natural wind velocity of the real wind turbine

4.12 Experimental results of real wind turbine.

(PWM converter scheme)

Fig. 4.54-4.59 shows the experimental results of the variable speed wind power generation system (VSWPGS) using the real wind turbine. The anemometer is set up near the real wind turbine to avoid the detecting error. And the direction of nacelle is fixed, and the wind in front of the wind turbine is considered. The speed control is carried out with the converter. The windmill rotational speed ω_r is tracking the windmill rotational speed reference ω_r^{ref} , and the power generation is executed properly for the natural wind velocity V_0 . The tip speed ratio x is controlled to be around 5.8. It means the maximum power point control is successful. The q axis stator voltage reference V_{ag}^{ref} is regulated to control the q stator current i_{aq} . The i_{aq} characterize the torque of generator and output power. The generated power P_g is sent to the power system by the inverter. The inverter controls the DC link voltage V_{dc} to be constant V_{dc}^{ref} of 100V. The V_{dc} rises when the P_g comes into the DC link capacitor C_{dc} , since the C_{dc} is charged. The active current i_{sq} is controlled to keep the V_{dc} at V_{dc}^{ref} . The power transferred to the power system P_s is tracking the P_g with time lag and attenuations, since the filtering effects of C_{dc} and the power loss of inverter exist.

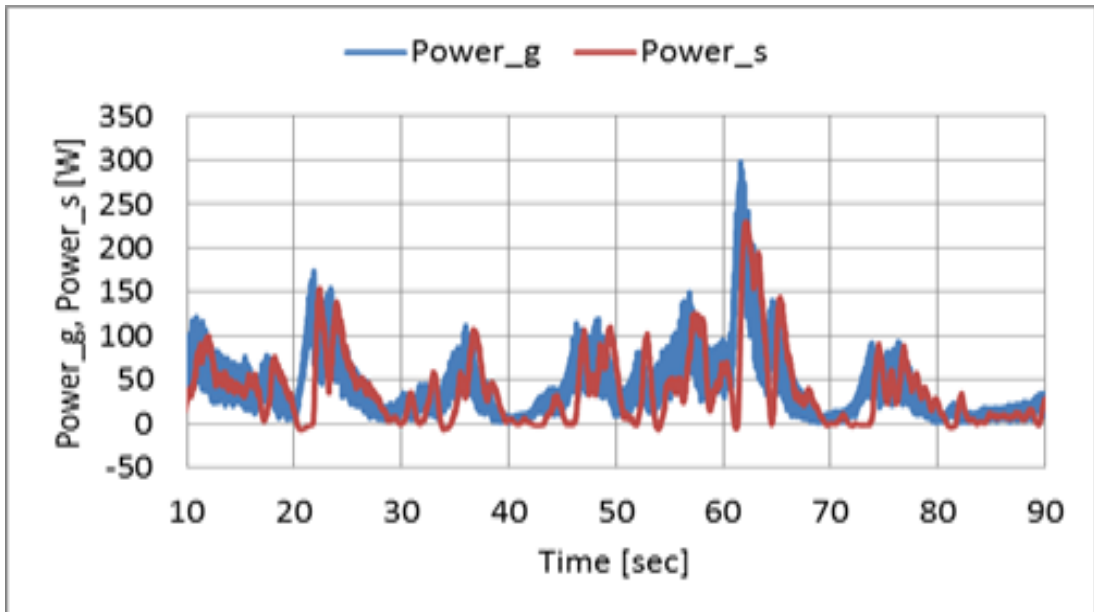


Fig. 4.54. Generated power and system power of the real wind turbine

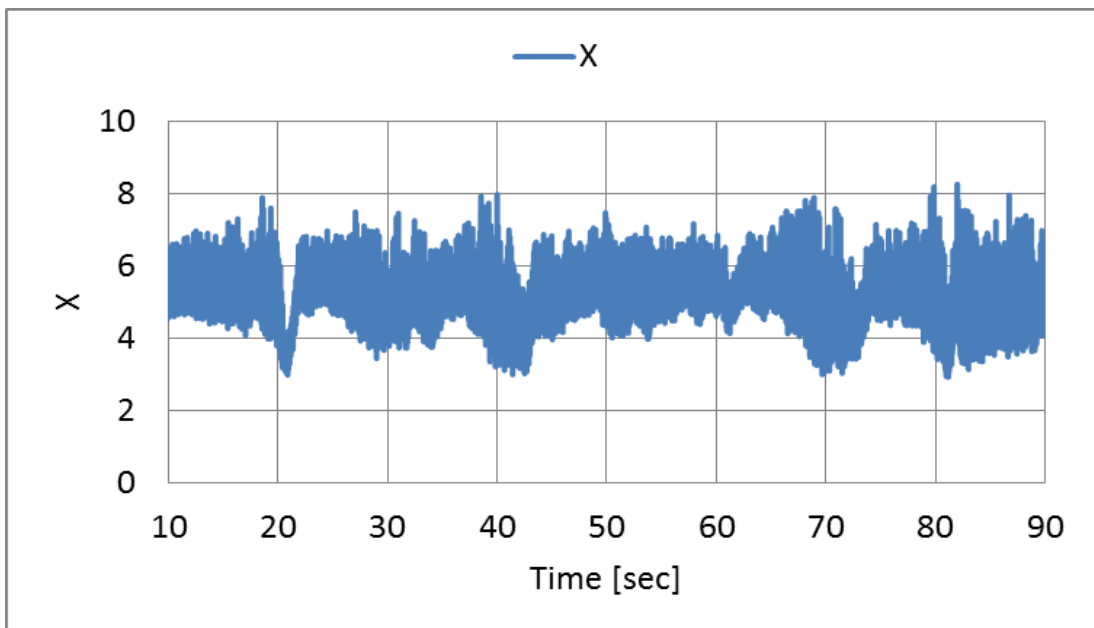


Fig. 4.55. Tip speed ratio of the real wind turbine

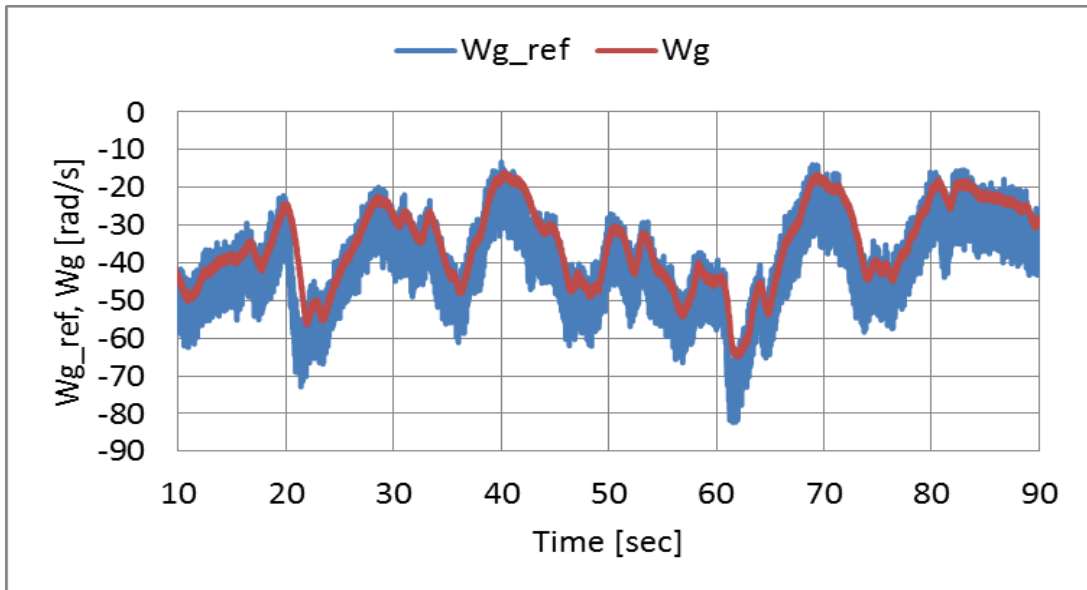


Fig. 4.56. Rotational speed Reference and Rotational speed of the real wind turbine

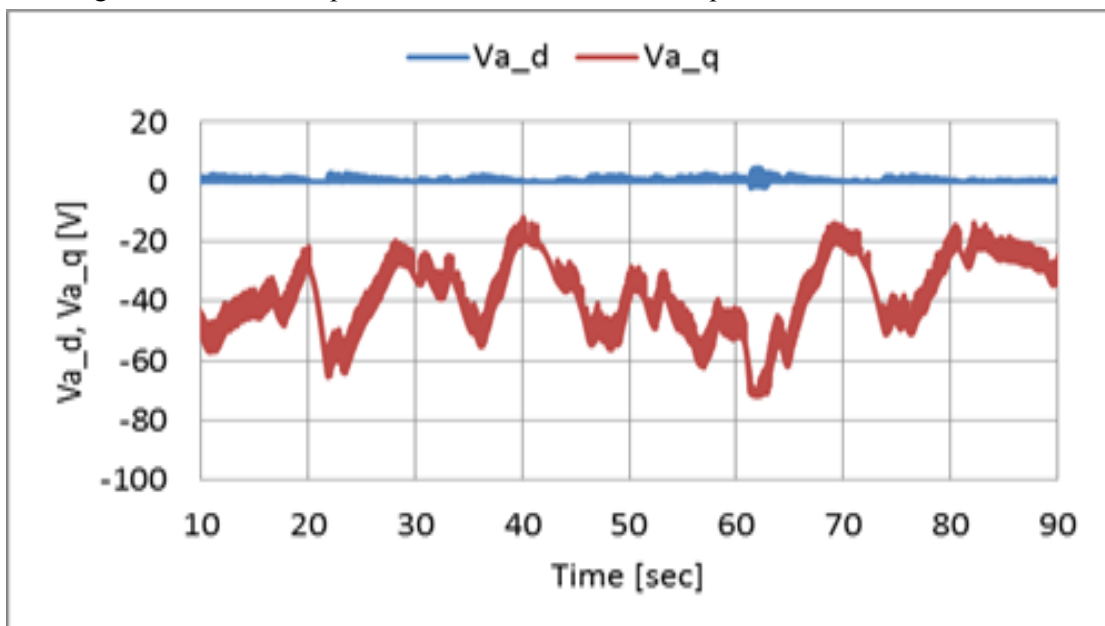


Fig. 4.57. d -axis and q -axis voltage reference for converter side of the real wind turbine

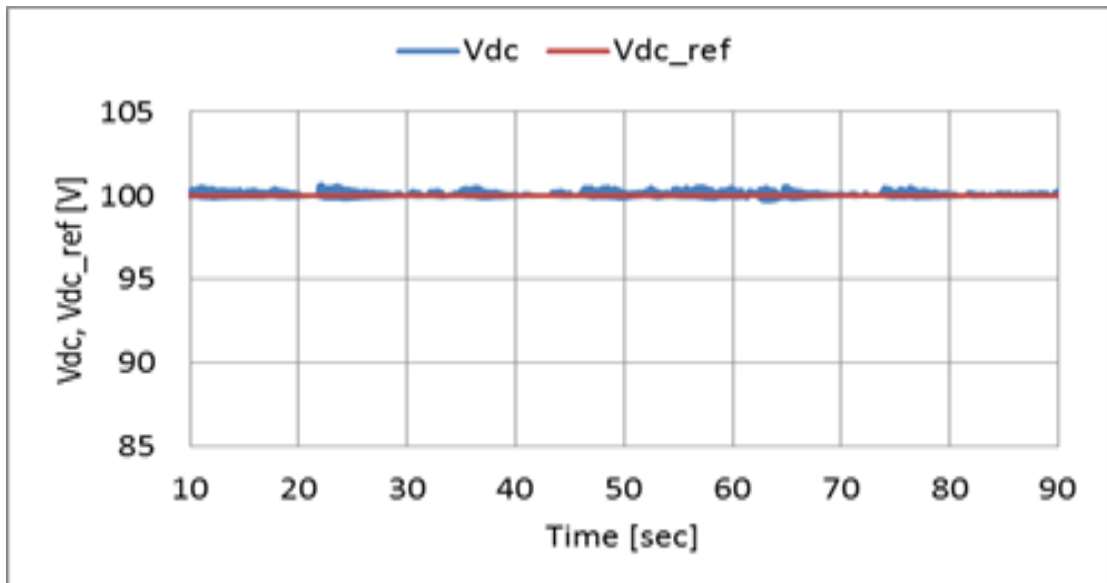


Fig. 4.58. DC link voltage and its reference of the real wind turbine

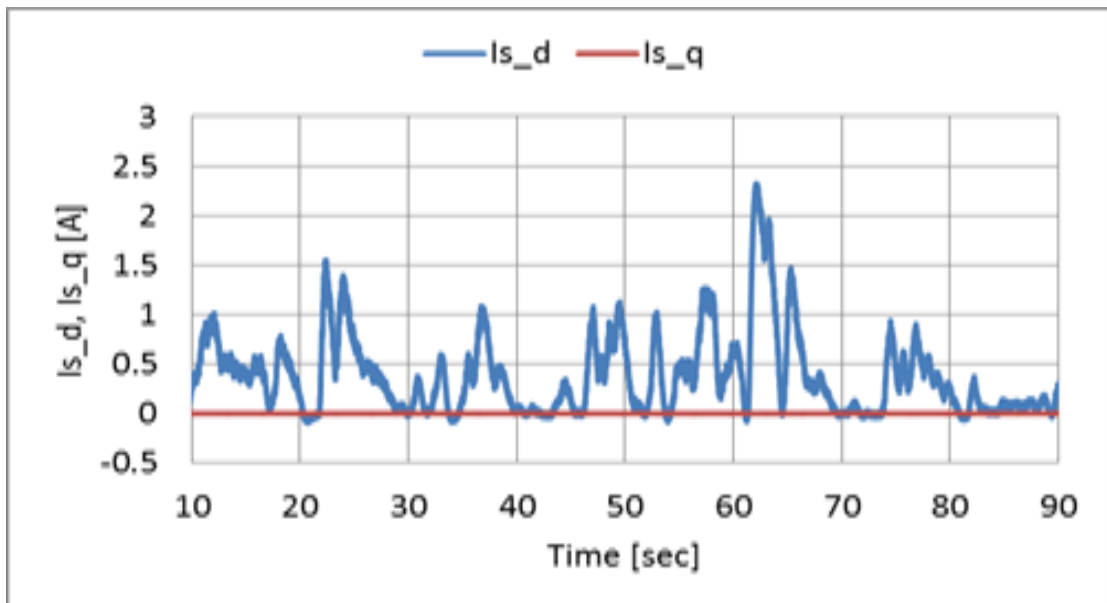


Fig. 4.59. d -axis and q -axis current for inverter side of the real wind turbine

4.13 Experimental results of wind turbine emulator

(PWM converter scheme)

Fig. 4.60-4.65 shows the experimental results of the variable speed wind power generation system using wind turbine emulator. The same V_0 is used for the wind turbine emulation. All of the results agree very well with the results for the real wind turbine of Fig. 4.54-4.59. It is obvious that the proposed wind turbine emulator can represent the behavior of real wind turbine for arbitrary wind velocities.

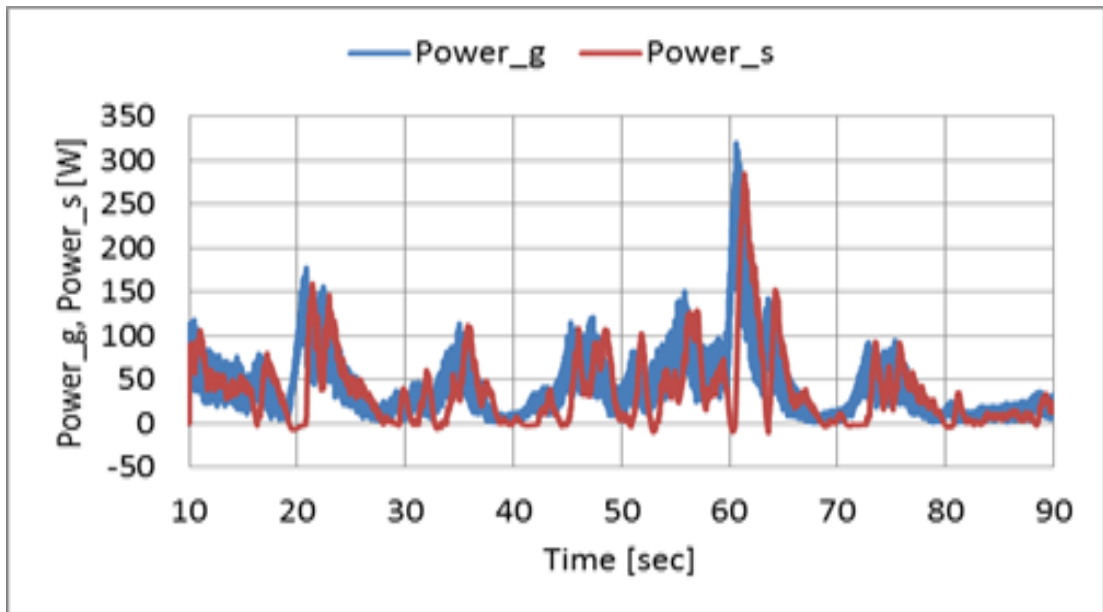


Fig. 4.60. Generated power and system power of the wind turbine emulator

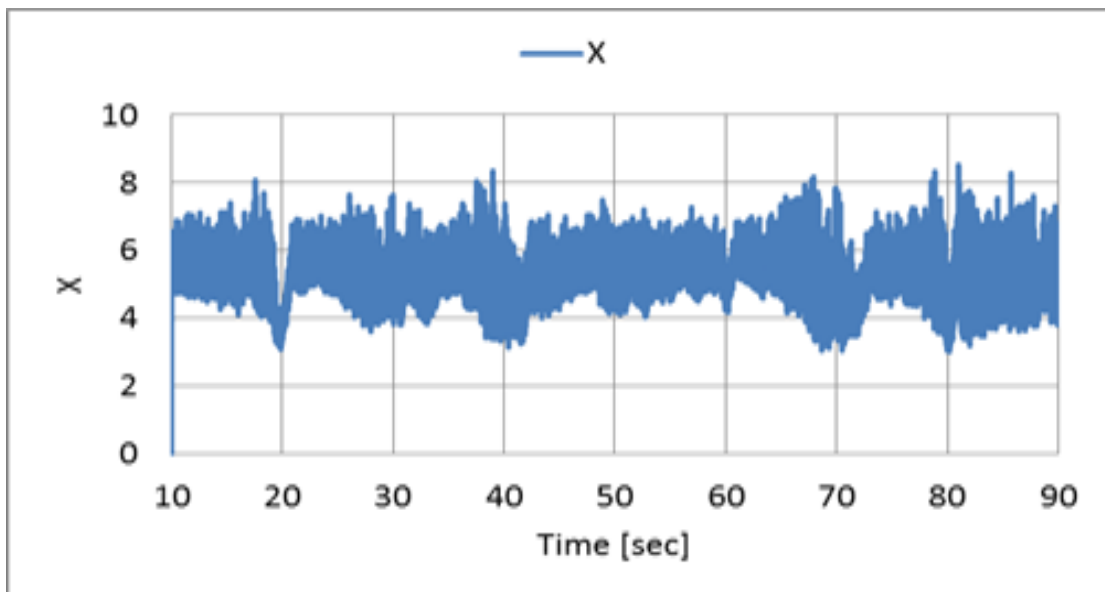


Fig. 4.61. Tip speed ratio of the wind turbine emulator

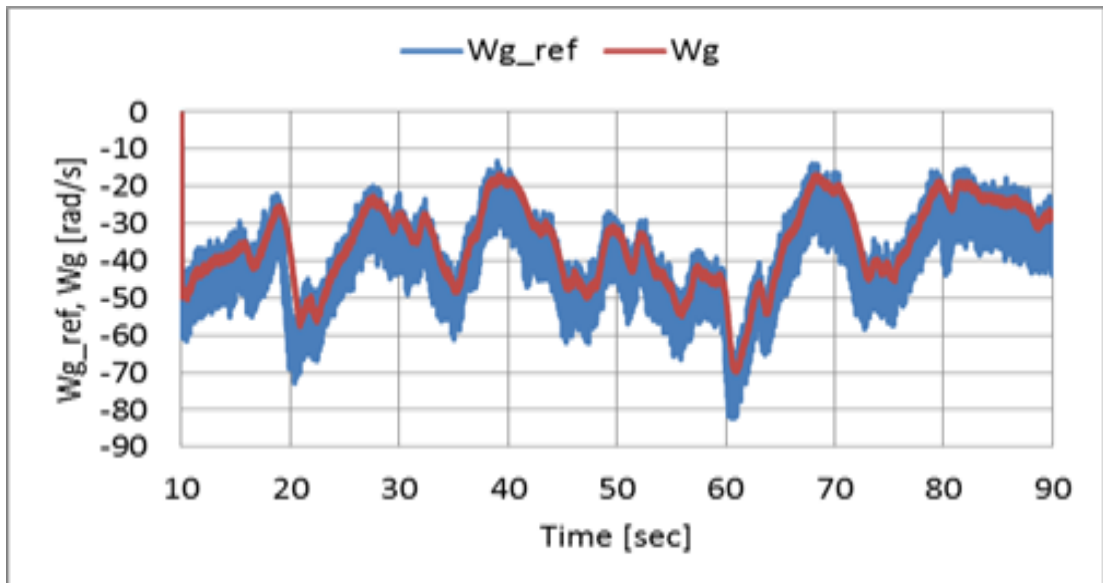


Fig. 4.62. Rotational speed Reference and Rotational speed of the wind turbine emulator

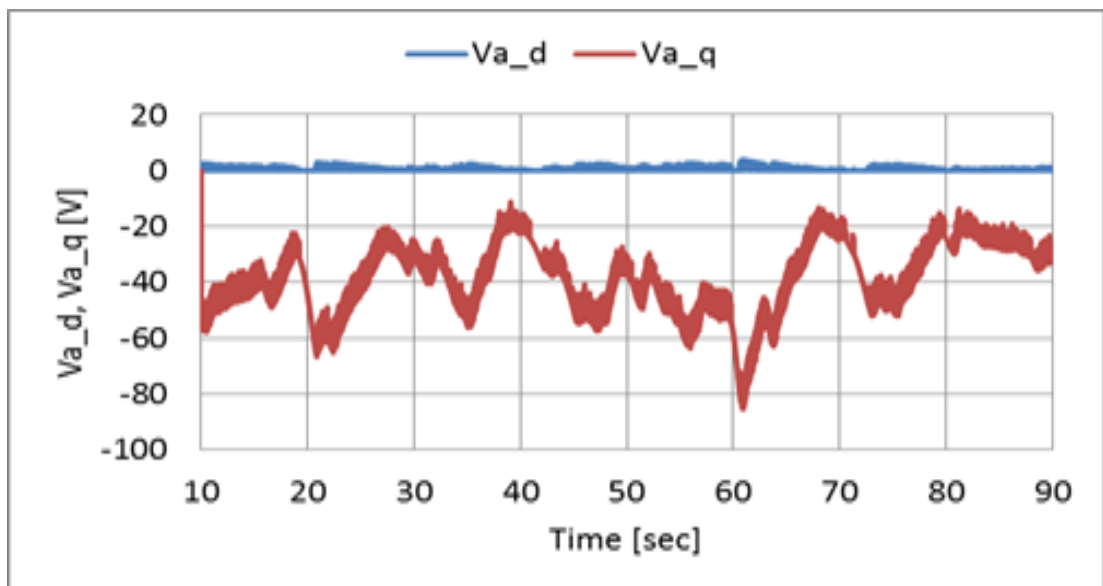


Fig. 4.63. d -axis and q -axis voltage reference for converter side of the wind turbine emulator

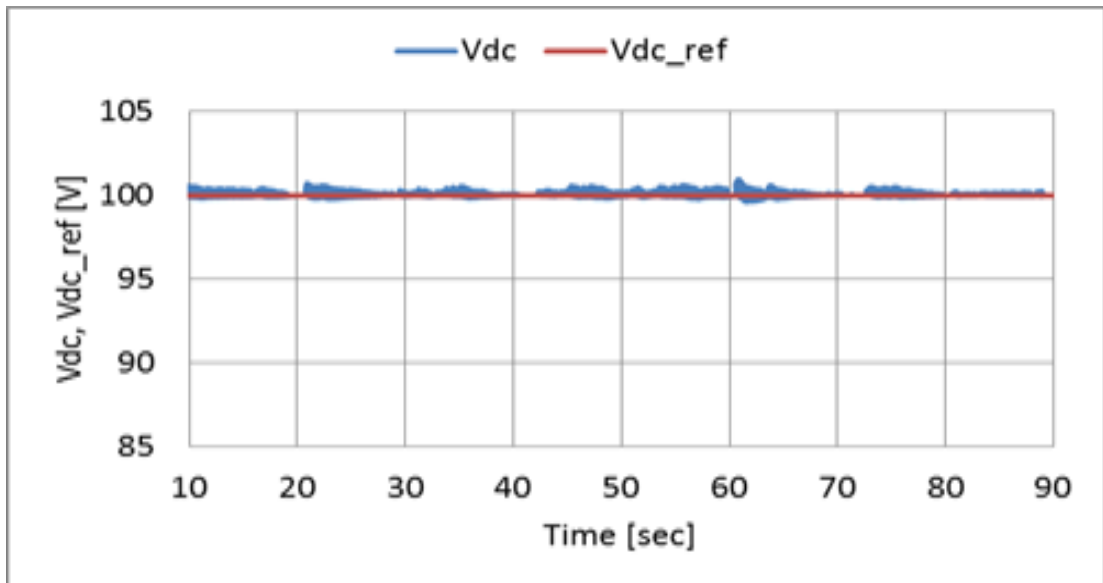


Fig. 4.64. DC link voltage and its reference of the wind turbine emulator

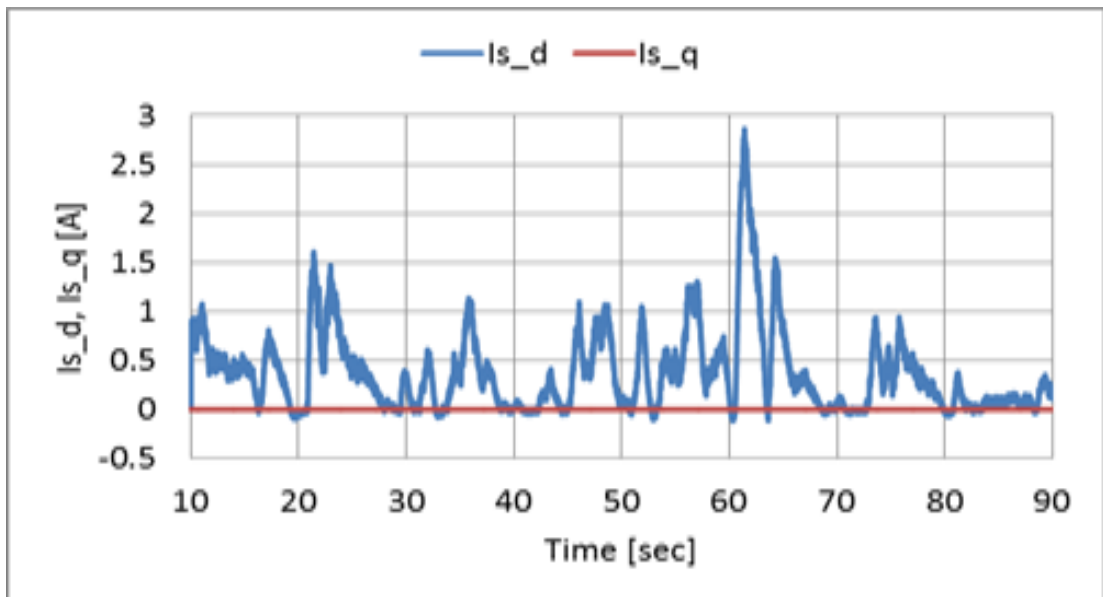


Fig. 4.65. *d*-axis and *q*-axis current for inverter side of the wind turbine emulator

4.14 Summary

This chapter explains the operating principle and the structure of WTE based on the BEMT. Also the structures of the test benches using the WT or WTE are explained. The simulation results of the VSWPGS using PWM converter are compared with the experiment results obtained with the test bench using WTE under the same conditions of low, medium and high wind velocities. Furthermore, under the conditions of natural winds, the experiment results obtained with the bench using WTE or WT for the VSWPGS using PWM converter are shown. The obtained experimental results are validated, and they show that the proposed WTE for the experimental assessment has a sufficient performance.

Chapter 5

Experimental assessment of variable speed wind power generation system

5.1 Performance evaluation scheme

The implementation of the boost chopper scheme is evaluated with the experimental study using MATLAB Simulink models and DSP control system. The experimental systems for the boost chopper scheme are implemented. The experimental systems consider the windmill, the main circuits used in each scheme, the converter and inverter control systems, and the pitch angle control system. This research verifies the fundamental implementation of the boost chopper scheme by comparing with the implementation of the PWM converter scheme.

5.2 Experimental system of wind turbine emulator

(Boost chopper scheme)

Fig. 5.1 shows the experimental system of the boost chopper scheme. The digital signal processing (DSP) unit calculates the wind turbine torque reference from the wind velocity data and rotational speed of the induction motor (IM). The wind

velocity data or the natural wind velocity data is given by the stored data in a PC. The rotational speed of IM is estimated in the DSP by using the signals from the rotary encoder (RE). The torque of IM is controlled by the off-the-shelf inverter. The IM is operated based on the wind turbine torque reference sent from a DSP through the D/A board (DS2102). After the wind turbine emulator is activated, the PMSG starts to rotate, and the converter control system starts to control the windmill rotational speed for the maximum power point tracking. The Duty and PWM signals for controlling the Duty, and INV are sent from a DSP to the short-circuit prevention circuit (FPGA) through a digital IO board (DS4002). The PWM signals are sent to the CNV and INV through the optical circuit.

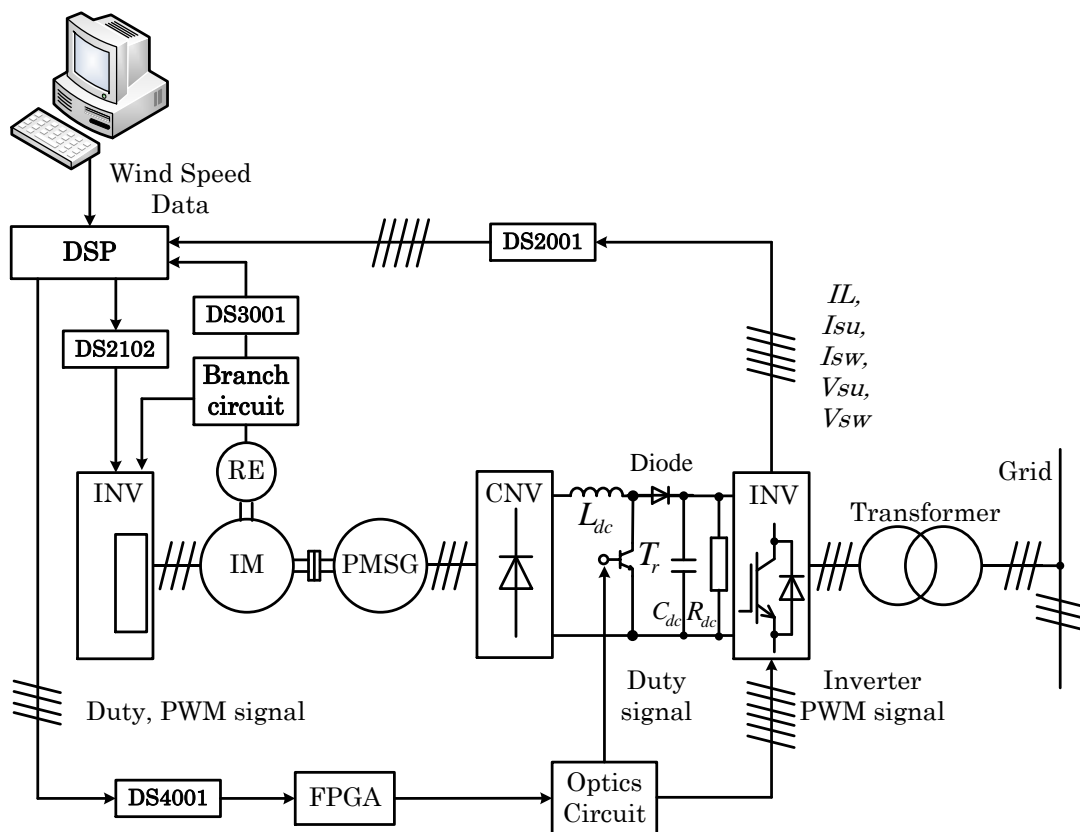


Fig. 5.1. Experimental system using the wind turbine emulator (Boost chopper scheme)

5.3 Experimental system of wind turbine emulator

(PWM converter scheme)

Fig. 5.2 shows the experimental system of the PWM converter scheme. The digital signal processing (DSP) unit calculates the wind turbine torque reference from the wind velocity data and rotational speed of the induction motor (IM). The wind velocity data or the natural wind velocity data is given by the stored data in a PC. The rotational speed of IM is estimated in the DSP by using the signals from the rotary encoder (RE). The torque of IM is controlled by the off-the-shelf inverter. The IM is operated based on the wind turbine torque reference sent from a DSP through the D/A board (DS2102). After the wind turbine emulator is activated, the PMSG starts to rotate, and the converter control system starts to control the windmill rotational speed for the maximum power point tracking. The PWM signals for controlling the CNV, and INV are sent from a DSP to the short-circuit prevention circuit (FPGA) through a digital I/O board (DS4002). The PWM signals are sent to the CNV and INV through the optical circuit.

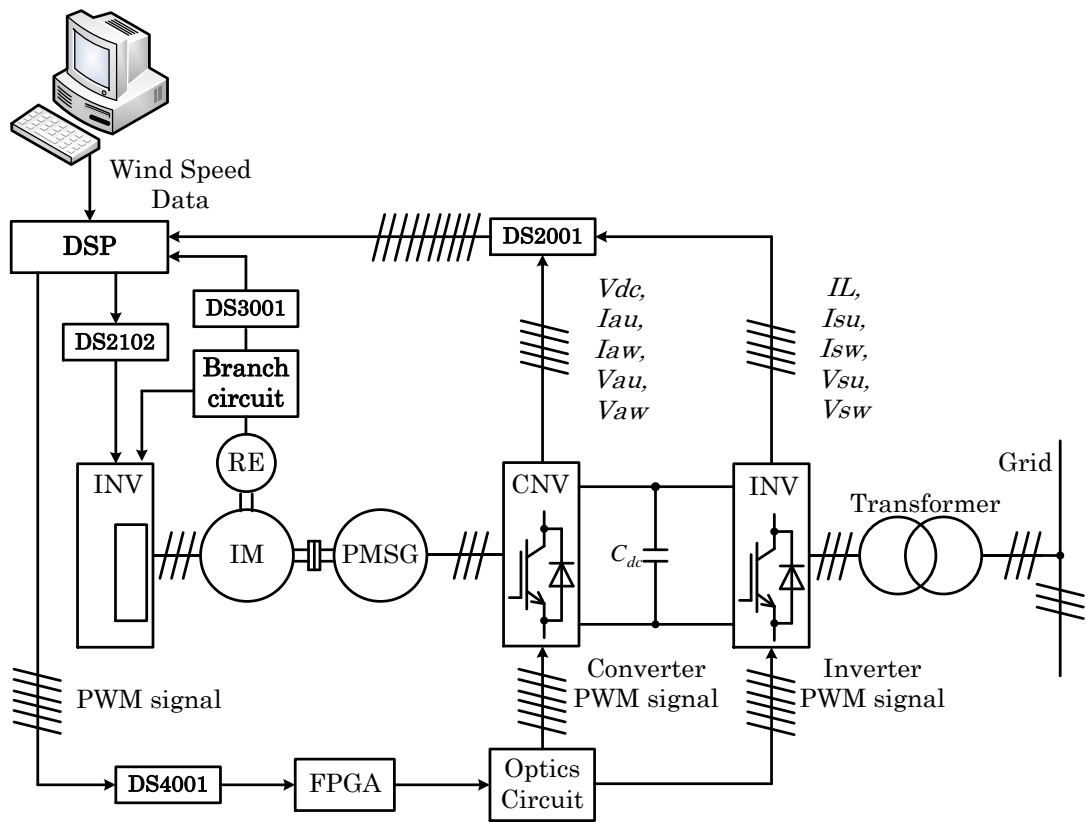


Fig. 5.2. Experimental system using the wind turbine emulator (PWM converter scheme)

5.4 Phase locked loop (PLL) control system

Fig. 5.3 shows the structure of phase locked loop (PLL) control system. This PLL control system is provided in the library of SymPowerSystems. This circuit consists the three-phase input signal is converted to a $dq0$ rotating frame (Park transform) using the angular speed of an internal oscillator. The quadrature axis signal V_q is proportional to the phase difference between the grid system voltages of V_{su} , V_{sv} , and V_{sw} and the internal oscillator rotating frame. The V_q is filtered with the “Variable frequency mean value block”. The Proportional-Integral-Derivative (PID) controller, with an optional automatic gain control, keeps the phase difference to 0 by acting on a controlled oscillator. The PID output, corresponding to the angular velocity ω_s , is filtered and converted to the frequency f_s in hertz, which is used by the mean value.

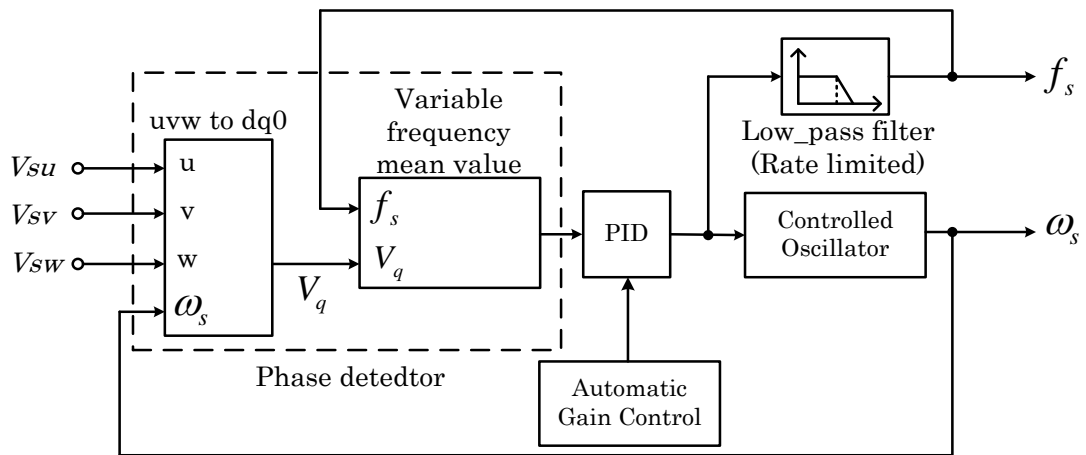


Fig. 5.3. Structure of phase locked loop control system.

5.5 Laboratory prototype

Fig. 5.4. shows the laboratory prototype. It consists of PC: computer, dSPACE: digital signal processing, D/A: digital/analog board, I/O: digital input/output board, Inverter: Yaskawa VARISPEED-G5, RE: rotary encoder, IM: induction motor, PMSG: permanent magnet synchronous generator, CNV: Myway MWINV for converter side, Boost: boost converter circuit, Diode: diode bridge rectification circuit, INV: Myway MWINV for inverter side, FPGA: FPGA controller board, Sensor: voltage and current sensor boards, TF: 3 phase transformer, Gridline.

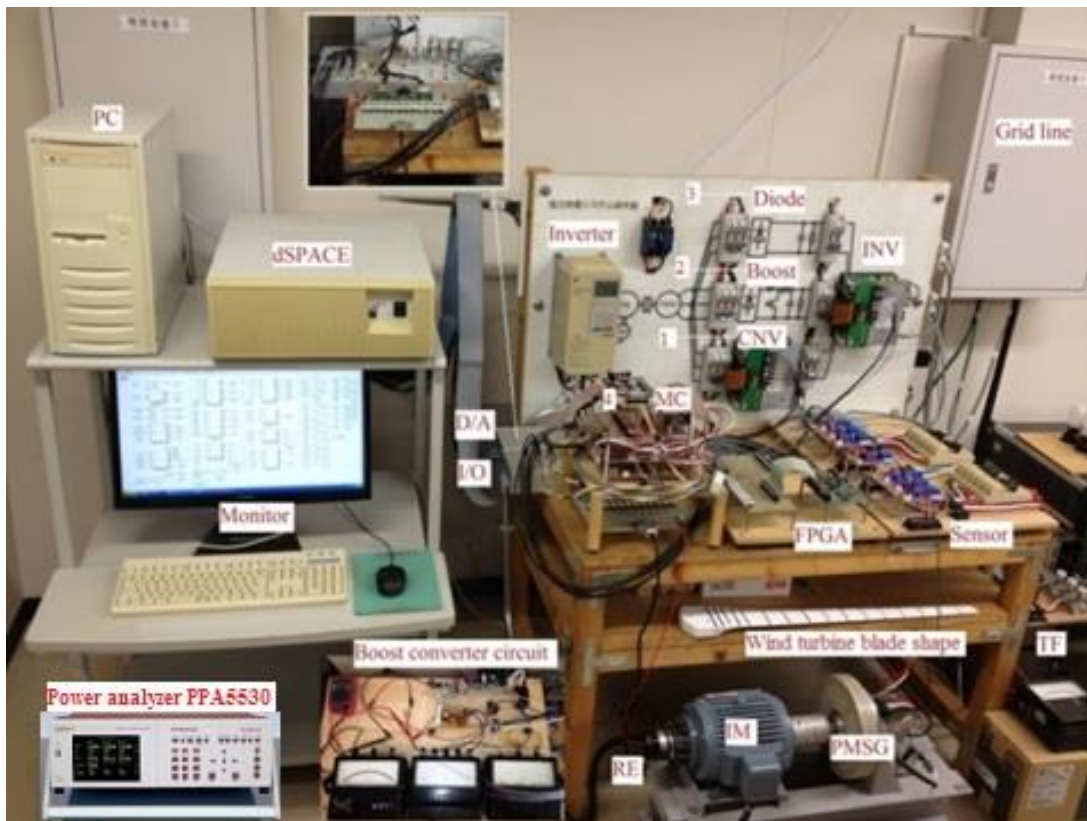


Fig. 5.4. Laboratory Prototype.

5.6 Structure of wind turbine emulator

Fig. 5.5 Show the structure of the wind turbine emulator. The inverter applies the vector control to induction motor and the induction motor generates the electric torque. The rotational speed of PMSG is estimated in the DSP by using the signals from the rotary encoder (RE).

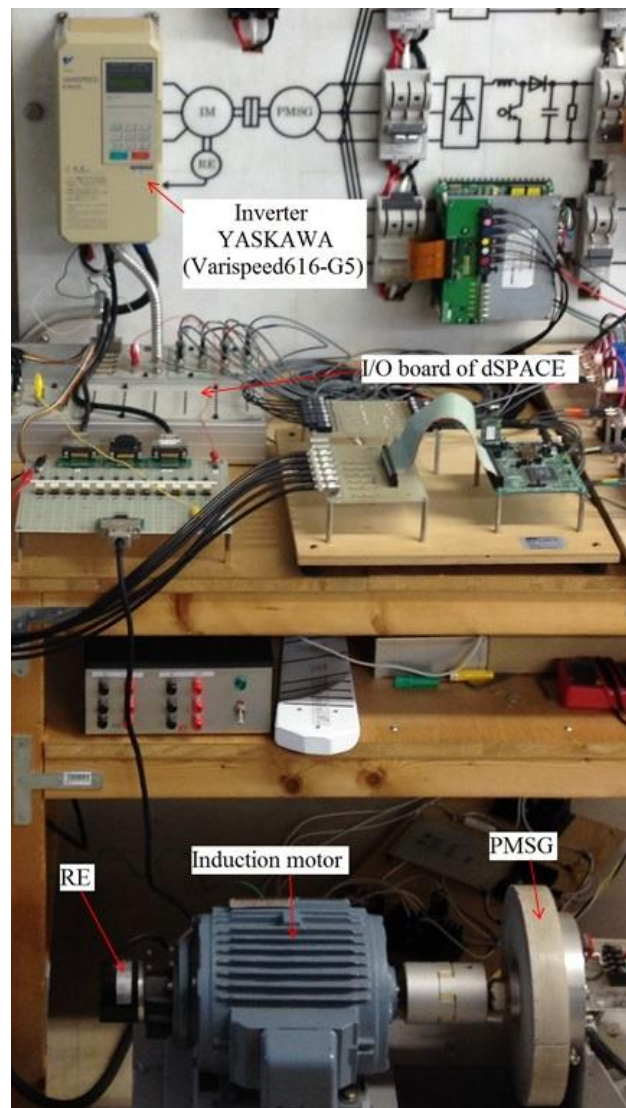


Fig. 5.5. Structure of the wind turbine emulator.

5.7 Structure of real wind turbine

Fig. 5.6 shows the structure of the real wind turbine (RWT). The 3 same blades, the rotary encoder (E6C3-CWZ3XH, Omron Japan) with the resolution ratio of 3600p/r to measure the rotor position of the RWT and the permanent magnet synchronous generator (PMSG). The anemometer (CYG-5103VM, CLIMATEC Japan) with the output of 0-1V/0 - 50m/s to measure the wind velocity V_0 were used for the real time experiment of RWT. In this paper, the experiment results were obtained when the directions of wind turbine and anemometer were fixed.

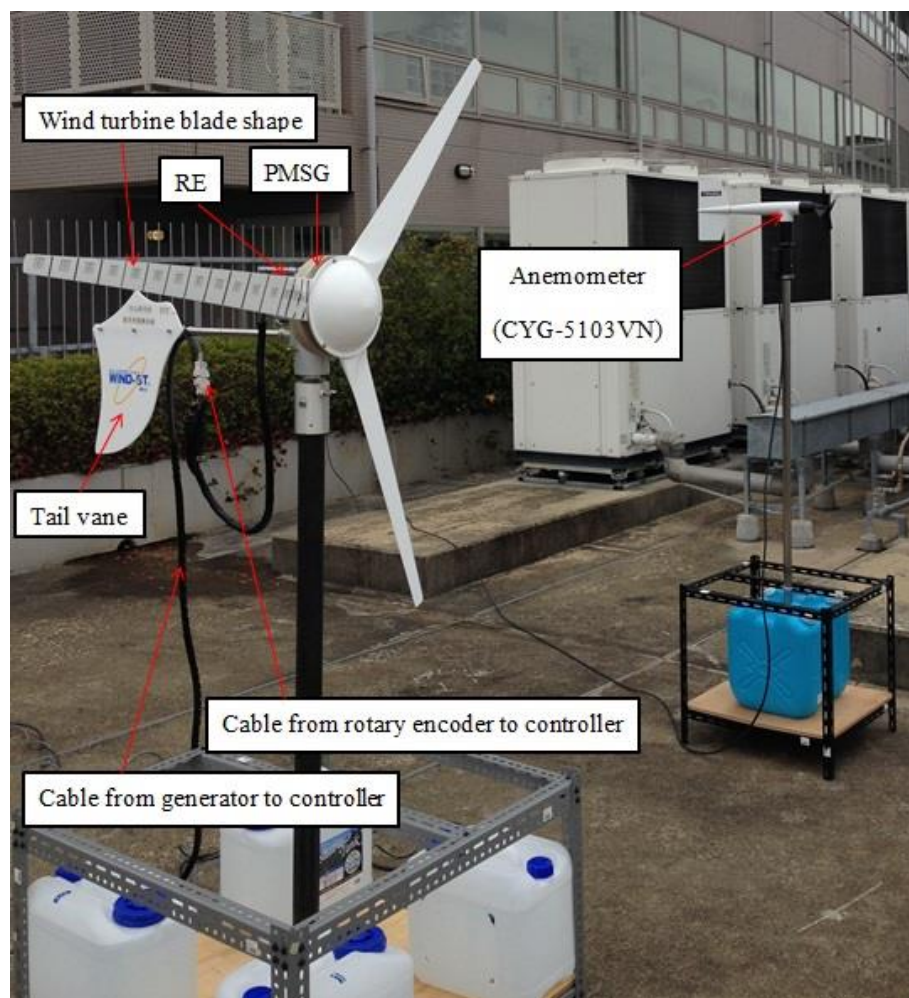


Fig. 5.6. Structure of the real wind turbine.

5.8 Experimental results of wind turbine emulator

(Boost chopper scheme)

Fig. 5.7 shows the change of the wind velocity V_0 [m/s] includes each mode shown in fig. 3.5 of chapter 3. The change of wind velocity includes the ranges of low wind velocity at 5m/s which corresponds to mode1, and the wind velocity at 6m/s which corresponds to the switching point between mode2 and mode3, middle wind velocity at 7m/s which corresponds to mode2 and mode3, and high wind velocity at 11m/s which corresponded to mode4. The high wind velocity means the wind velocity that exceeds the rated value. All ranges include the sinusoidal change of amplitude: 0.5 [m/s] and 0.2 [Hz], the boost chopper scheme (of wind turbine emulator) and PWM converter scheme (of wind turbine emulator) are tested for the same change of the wind velocity, and the control performances of both schemes are discussed.

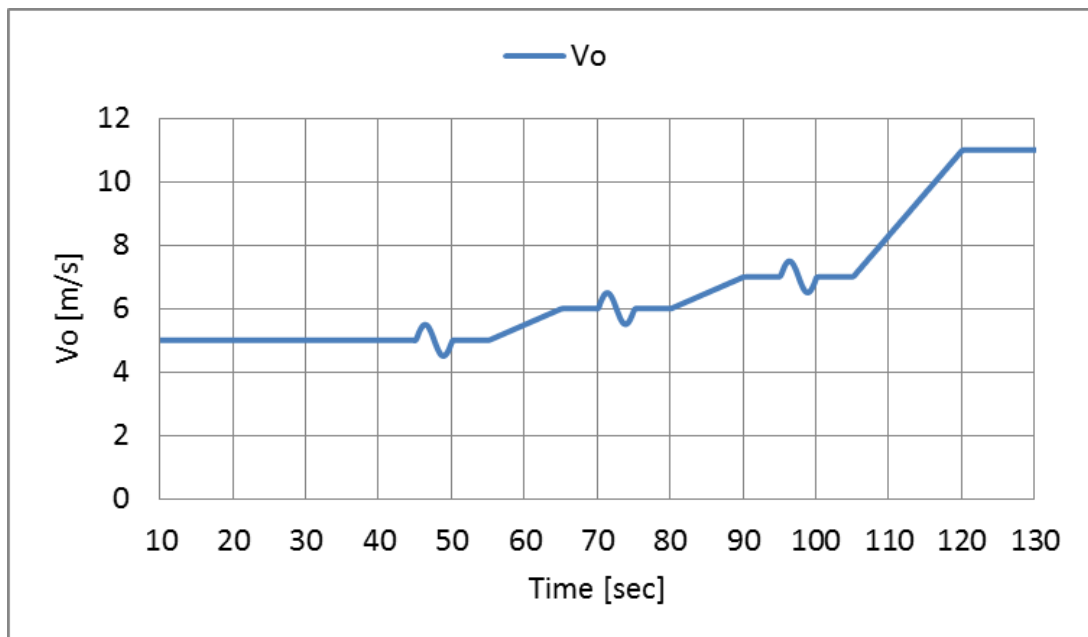


Fig. 5.7. Change of wind velocity

Figs. 5.8–5.19 show the experimental results of the boost chopper scheme. The system activates at 5m/s which exceeds cut-in wind velocity of 3m/s, and the power generation has been started after about 9 seconds in which windmill speed ω_g reaches to the windmill rotational speed reference ω_g^{ref} . In the wind velocity of 5 m/s which corresponds to mode1, the speed control is carried out by the duty control system. It can be confirmed by the windmill speed ω_g and Duty shown in fig. 5.15-5.20 that the speed control is well carried out. In the wind velocity of 6m/s which corresponds to the switching point of mode2 and mode3, it can be confirmed by the ω_g , Duty, and DC link voltage V_{dc} shown in fig. 5.21-5.26 that the speed control is carried out while the speed control system is smoothly switched. In the wind velocity of 7m/s which corresponds to mode3, the speed control is carried out by adjusting V_{dc} with the inverter control system. It can be confirmed by the ω_g and V_{dc} that the speed control is well carried out. In wind velocity of 11m/s which corresponds to mode4, the speed control is carried out by the pitch angle control system, and the electric power control is carried out by the inverter control system. It can be confirmed by the ω_g , V_{dc} , and pitch angle θ shown in fig. 5.27-5.38 that the ω_g is controlled at of the rated speed and the generated power P_s shown in fig. 5.27-5.38 is controlled at the rated power of 300W.

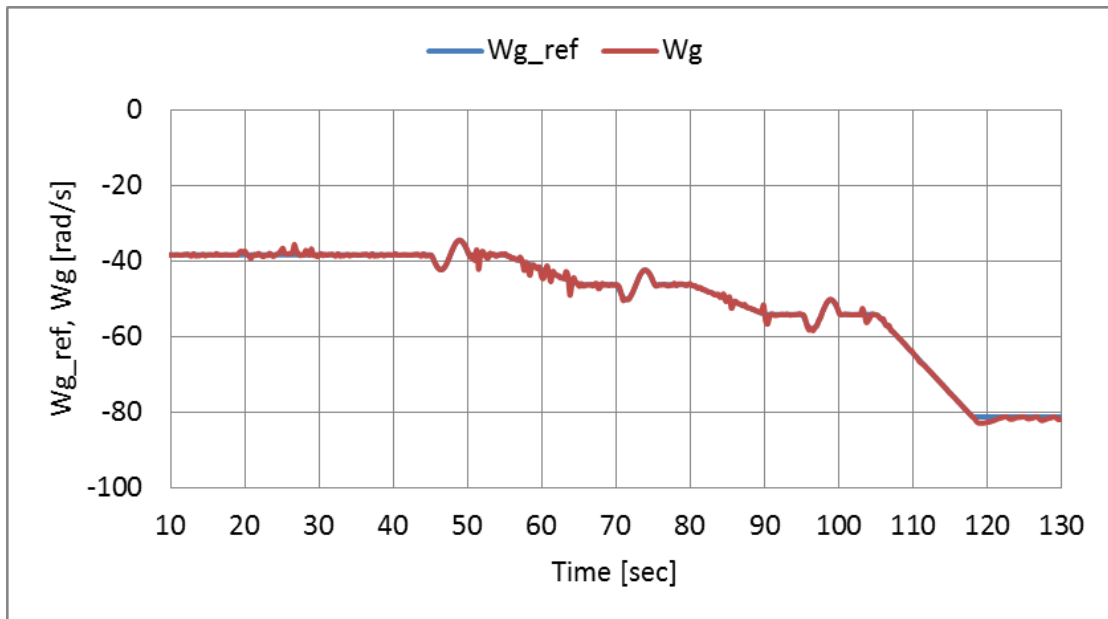


Fig. 5.8. Rotational speed reference and Rotational speed of boost chopper scheme

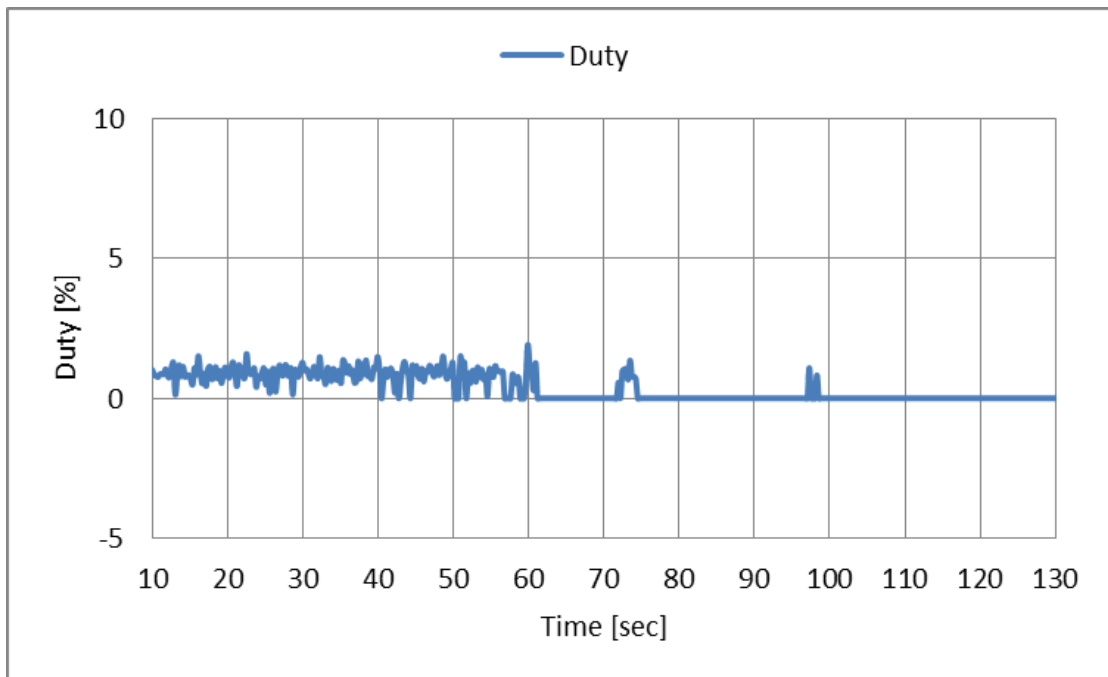


Fig. 5.9. Duty control signal of boost chopper scheme

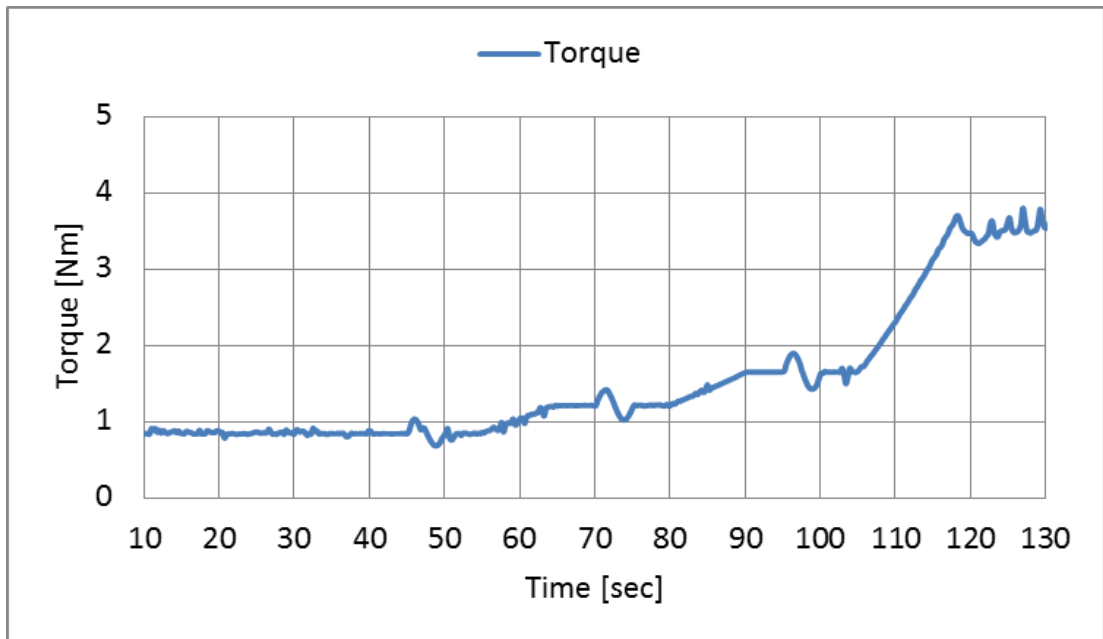


Fig. 5.10. Wind turbine torque of boost chopper scheme

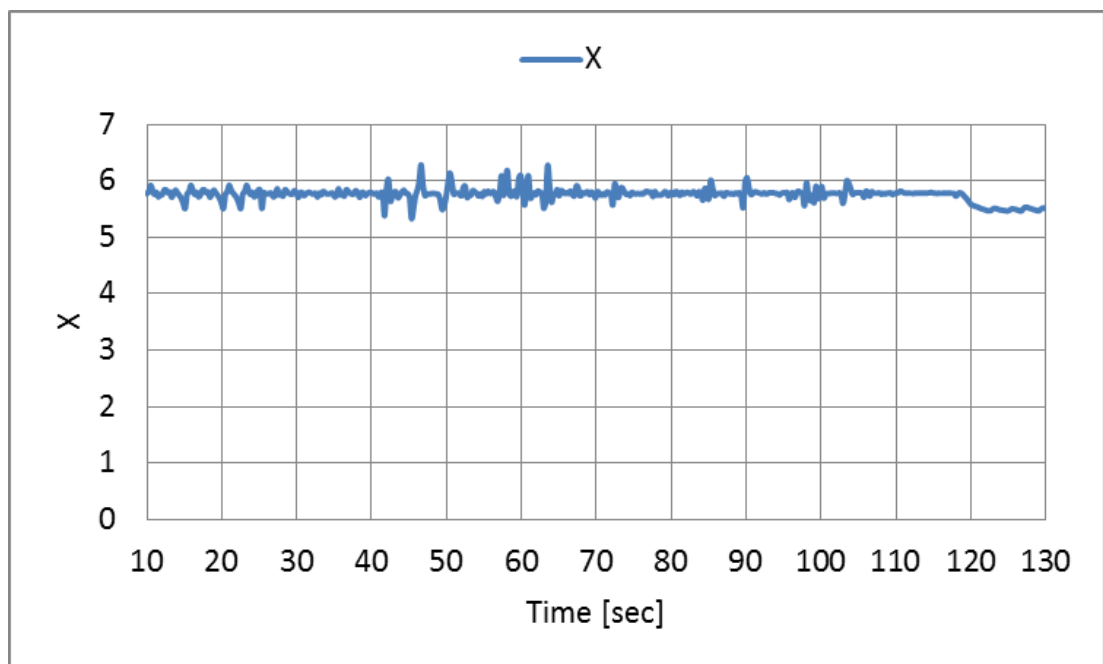


Fig. 5.11. Tip speed ratio of boost chopper scheme

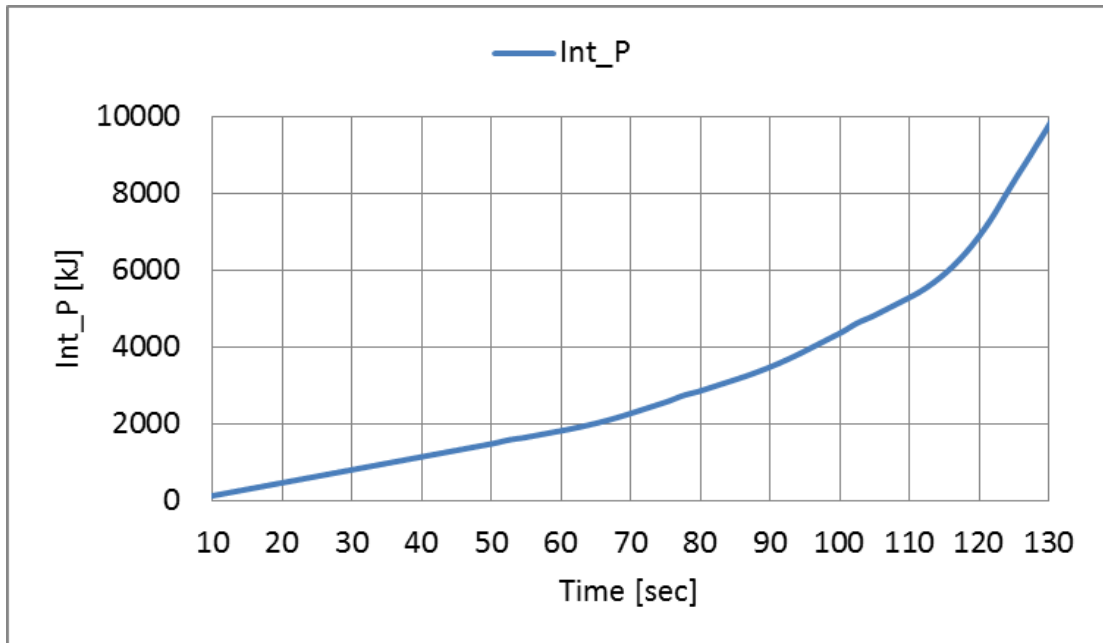


Fig. 5.12. Integrated power system of boost chopper scheme

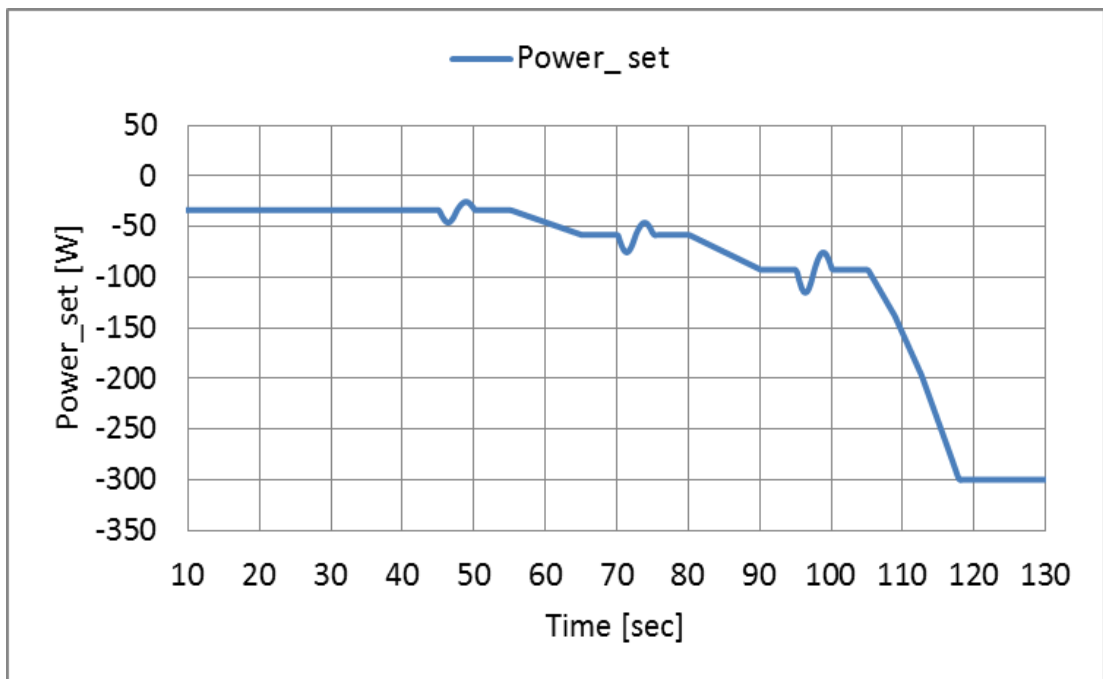


Fig. 5.13. Power set of boost chopper scheme

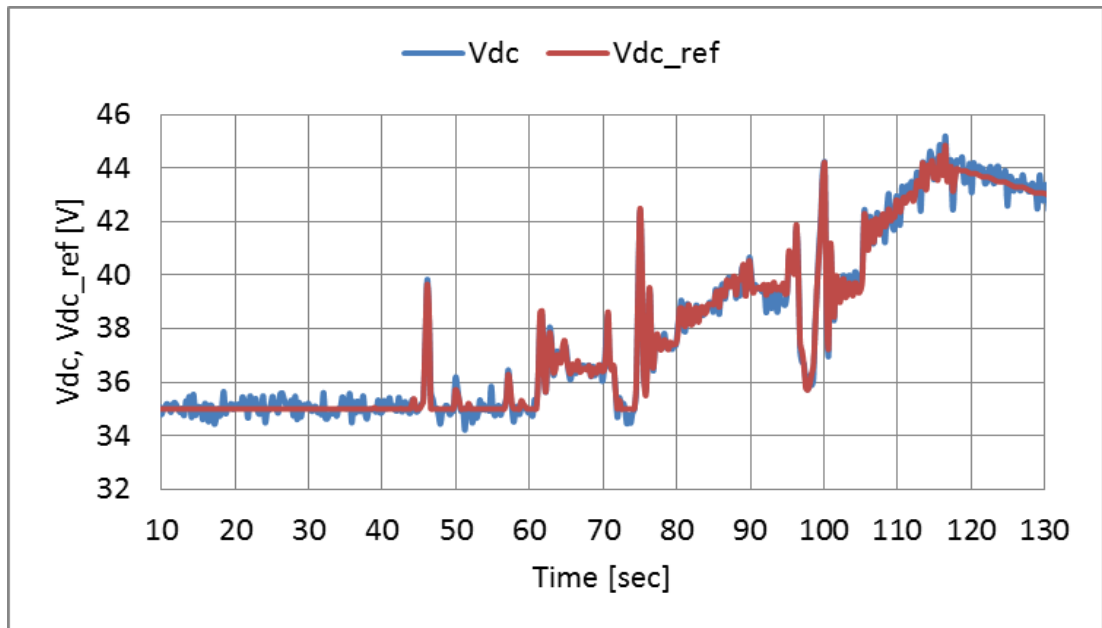


Fig. 5.14. DC link voltage and its reference of boost chopper scheme

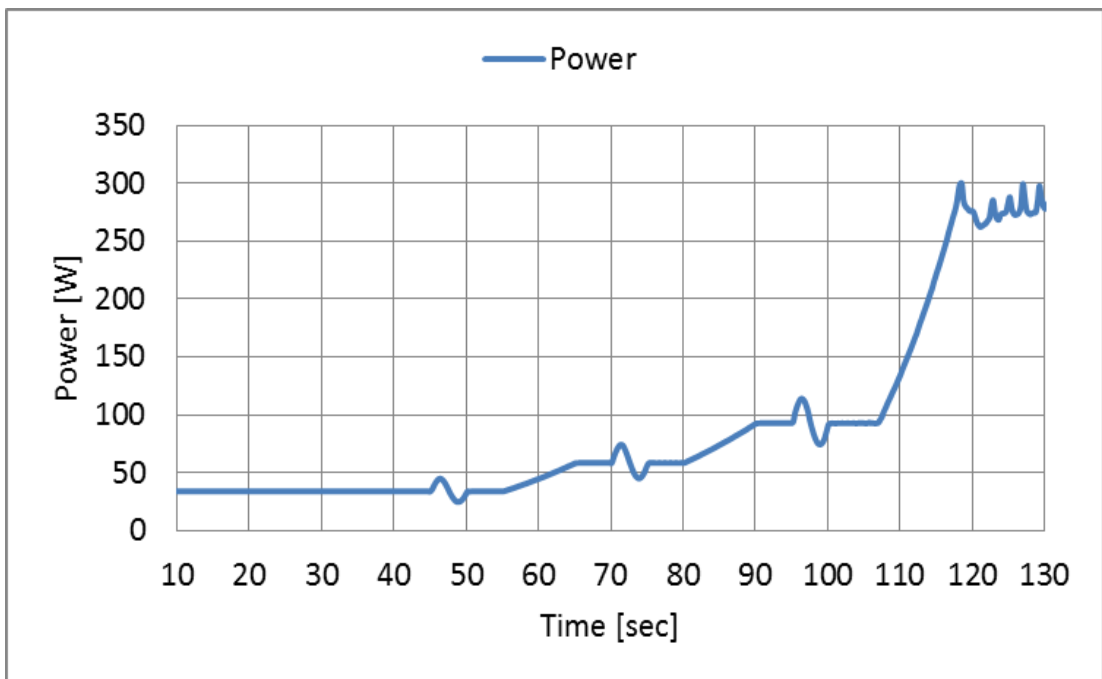


Fig. 5.15. System power of boost chopper scheme

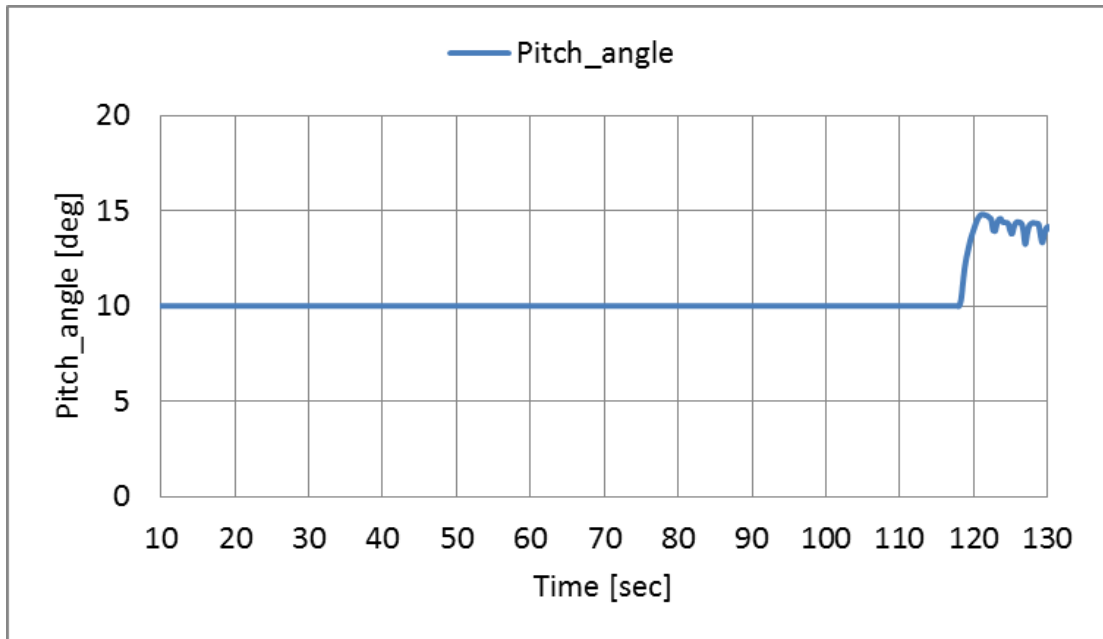


Fig. 5.16. Pitch angle control of boost chopper scheme

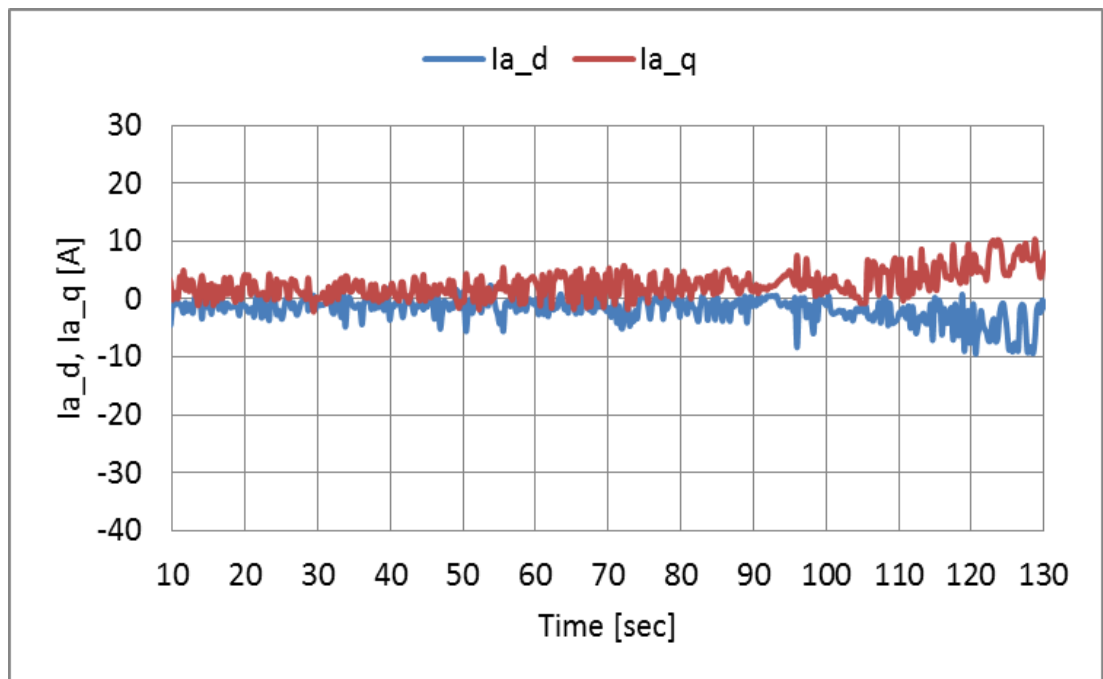


Fig. 5.17. *d*-axis and *q*-axis current of boost chopper scheme

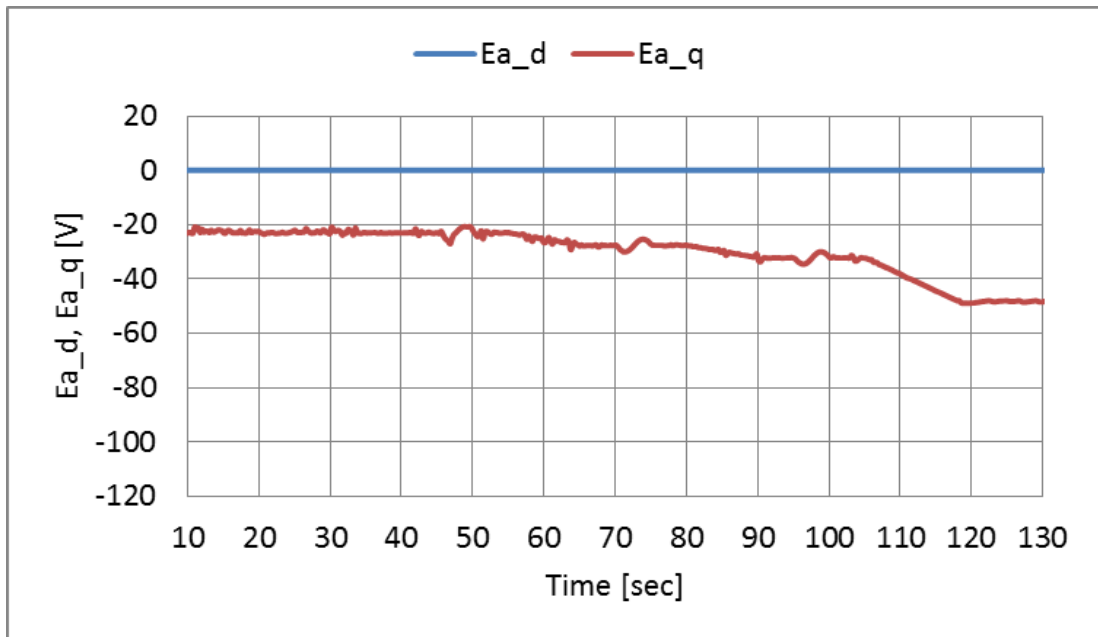


Fig. 5.18. d axis and q axis voltage for converter side of boost chopper scheme

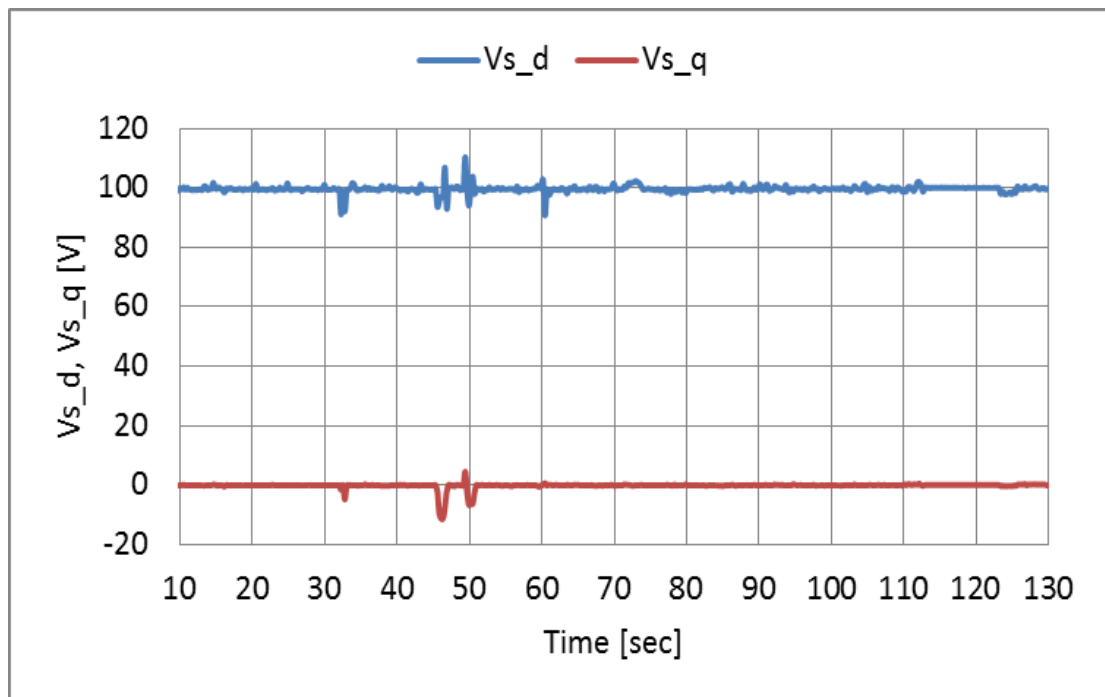


Fig. 5.19. d axis and q axis voltage for inverter side of boost chopper scheme

5.9 Experimental results of wind turbine emulator

(PWM converter scheme)

Figs. 5.20 - 5.31 show the experimental results of PWM converter scheme. The system activates at wind velocity of 5m/s which exceeds cut-in wind velocity of 3m/s, and the power generation has been started after about 11 seconds in which ω_g reaches in ω_g^{ref} as well as the boost chopper scheme. The system is operated under the rated wind velocity which corresponds to mode1 - mode3 until about 115 seconds. It can be confirmed that the ω_g follows ω_g^{ref} . However, the response of PWM converter scheme has been retarded for the increase of ω_g^{ref} corresponds to the increase of wind velocity, since the restriction of torque current reference i_{aq}^{ref} has been established so that PMSG may not carry out the motoring. The operating range which exceeds the rated wind velocity corresponds to mode4 starts after 115 seconds. The pitch angle control system starts around 118 seconds, and the speed controller of converter control system stops simultaneously, and the maximum electric power tracking control is activated. The sinusoidal change of wind velocity is superimposed in this operating range. The ω_g is maintained at of rated speed by speed control by pitch angle control system and the electric power control by converter control system and the generated output P_s is maintained at the rated power of 300W.

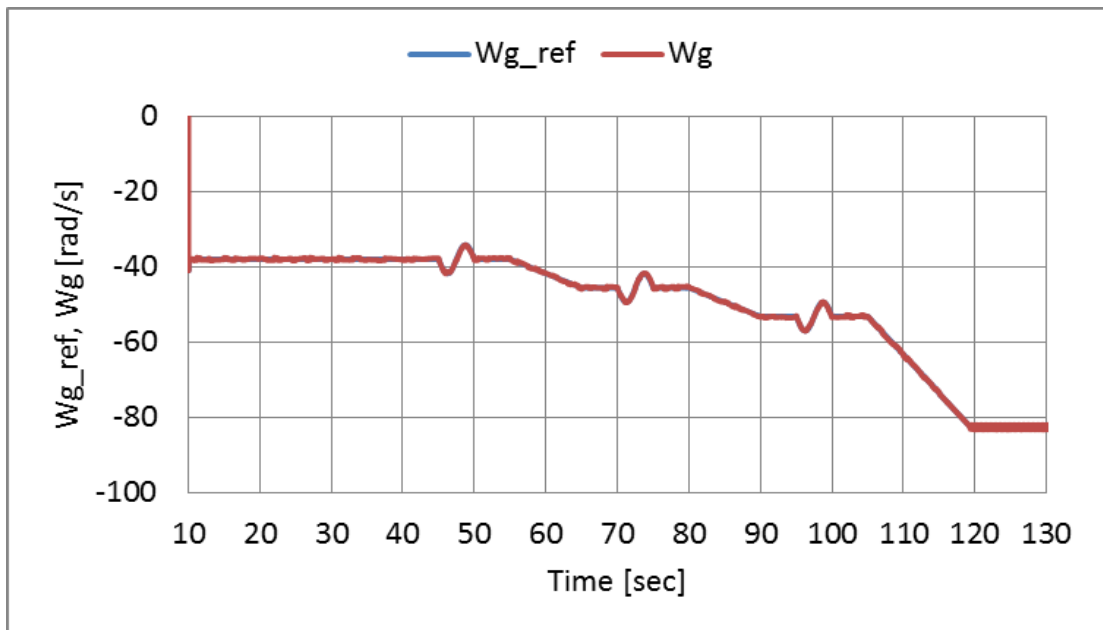


Fig. 5.20. Rotational speed reference and Rotational speed of the PWM converter scheme

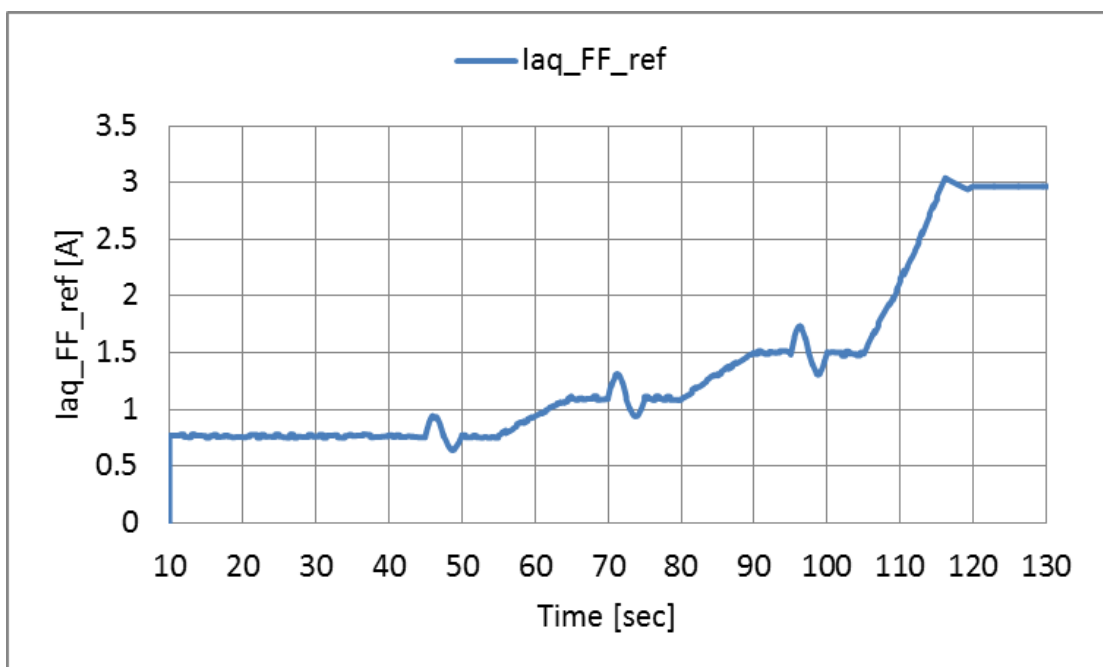


Fig. 5.21. q-axis current reference of feed-forward control of the PWM converter scheme

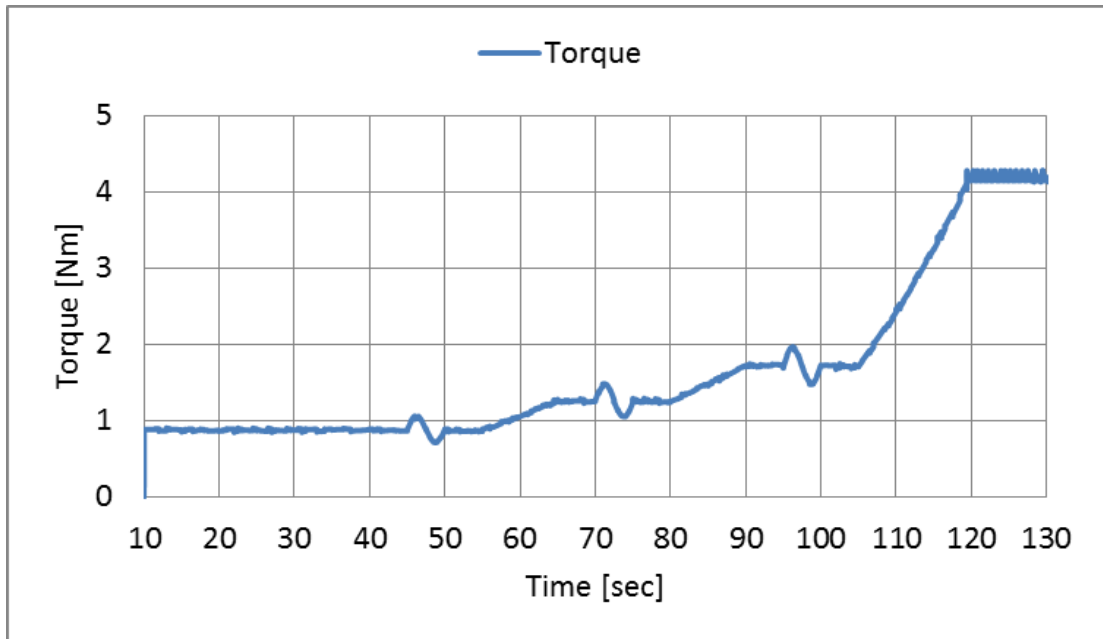


Fig. 5.22. Wind turbine Torque of the PWM converter scheme

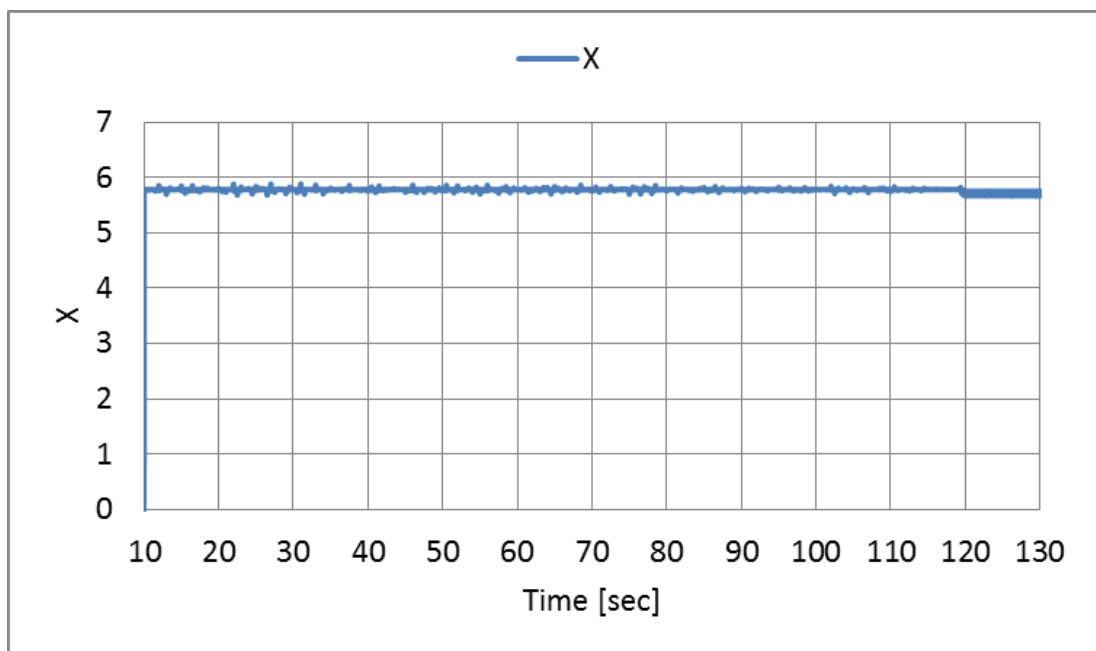


Fig. 5.23. Tip speed ratio of the PWM converter scheme

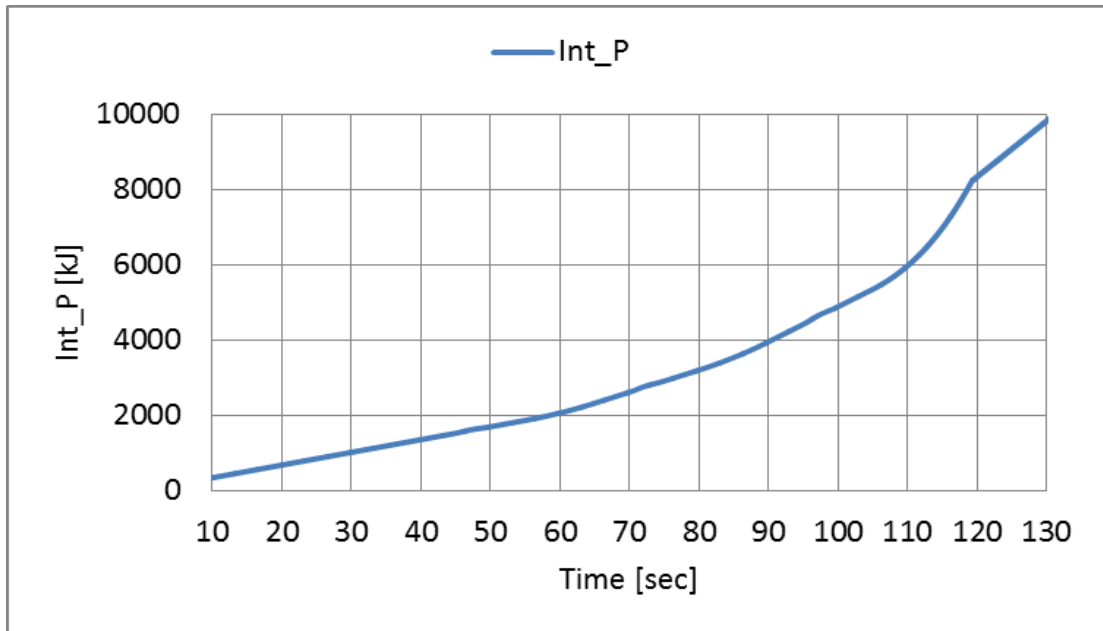


Fig. 5.24. Integrated power system of the PWM converter scheme

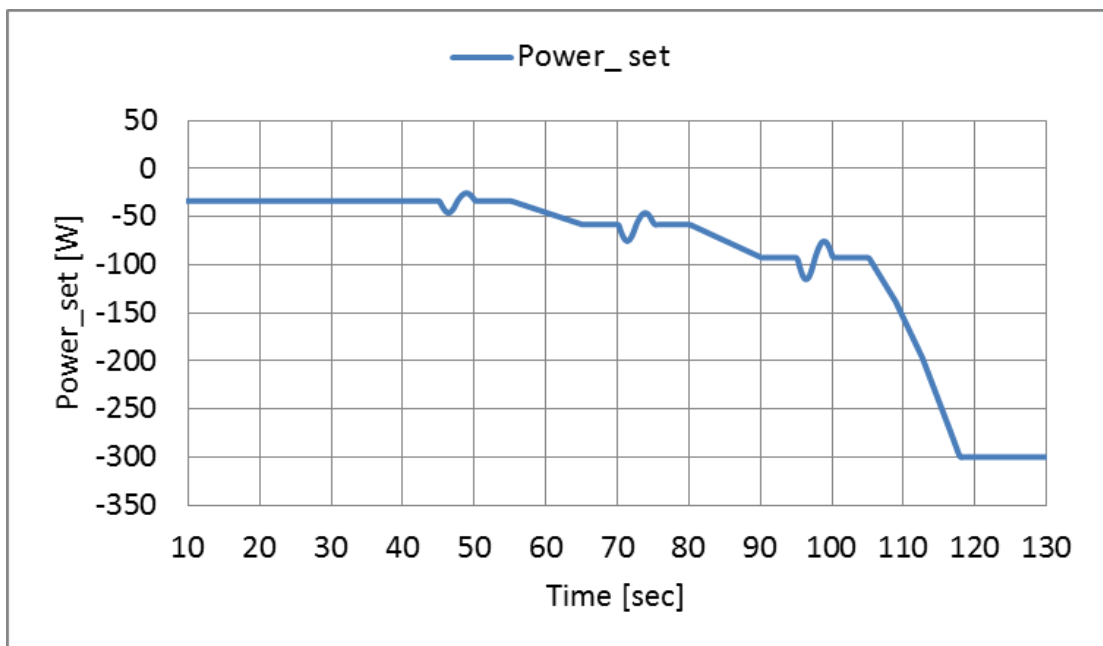


Fig. 5.25. Power set of the PWM converter scheme

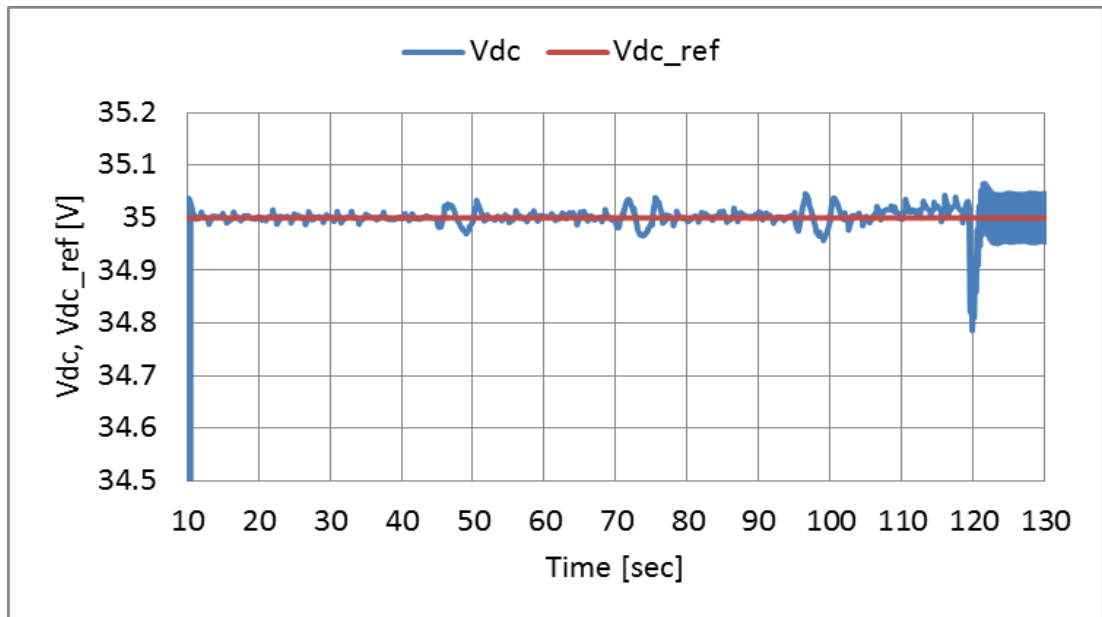


Fig. 5.26. DC link voltage and its reference of the PWM converter scheme

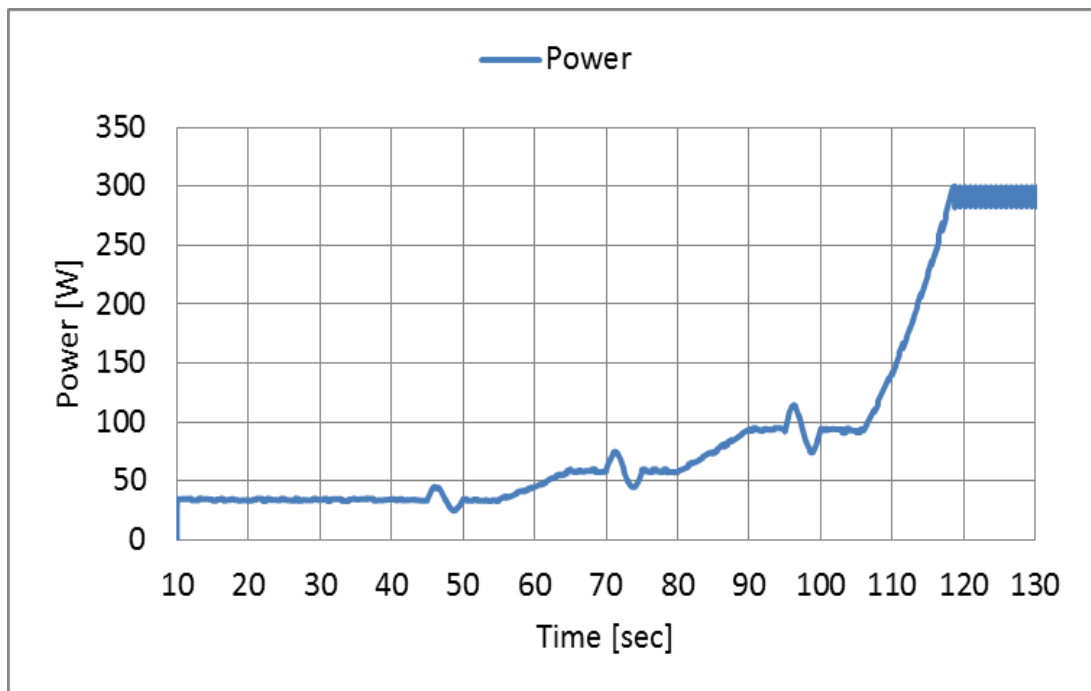


Fig. 5.27. System power of the PWM converter scheme

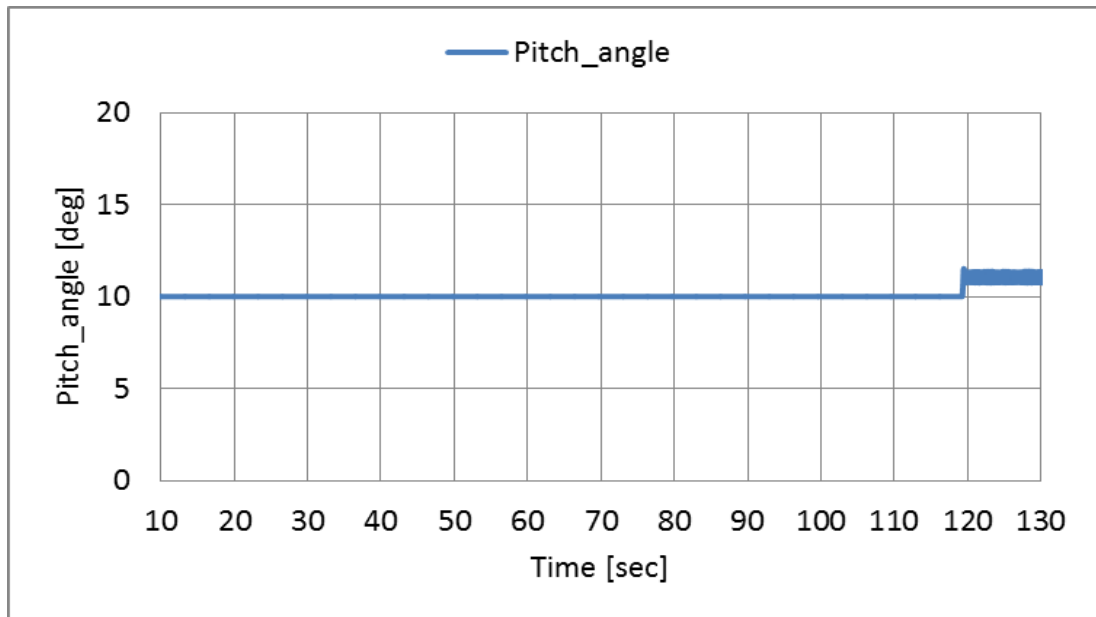


Fig. 5.28. Pitch angle control of the PWM converter scheme

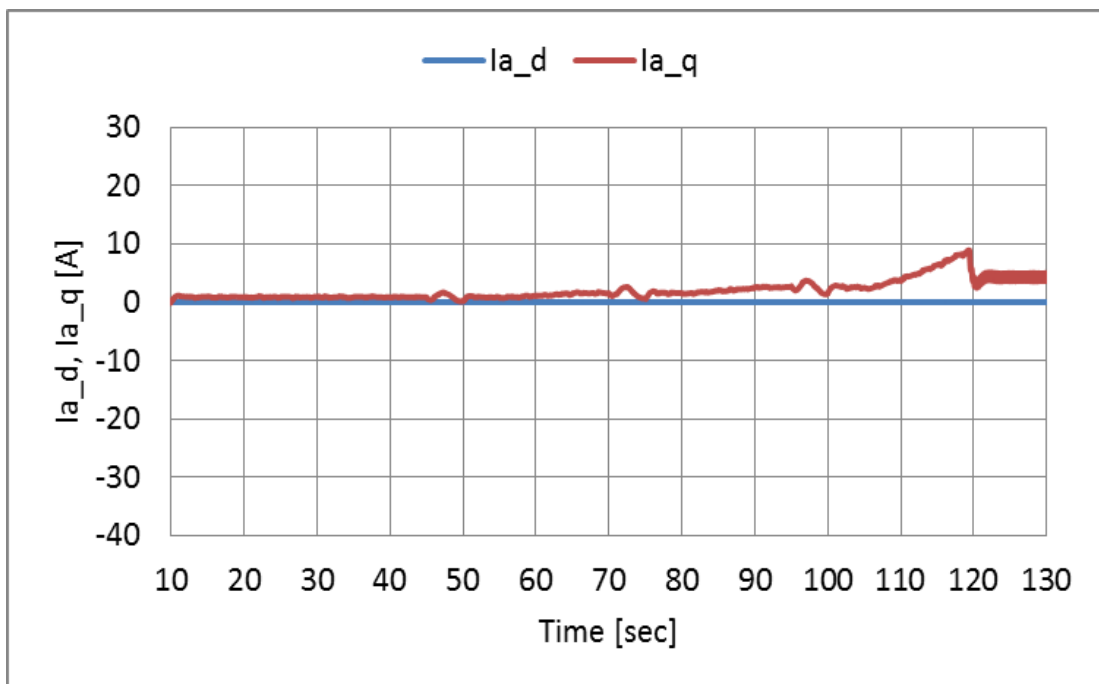


Fig. 5.29. *d*-axis and *q*-axis current for converter side of the PWM converter scheme

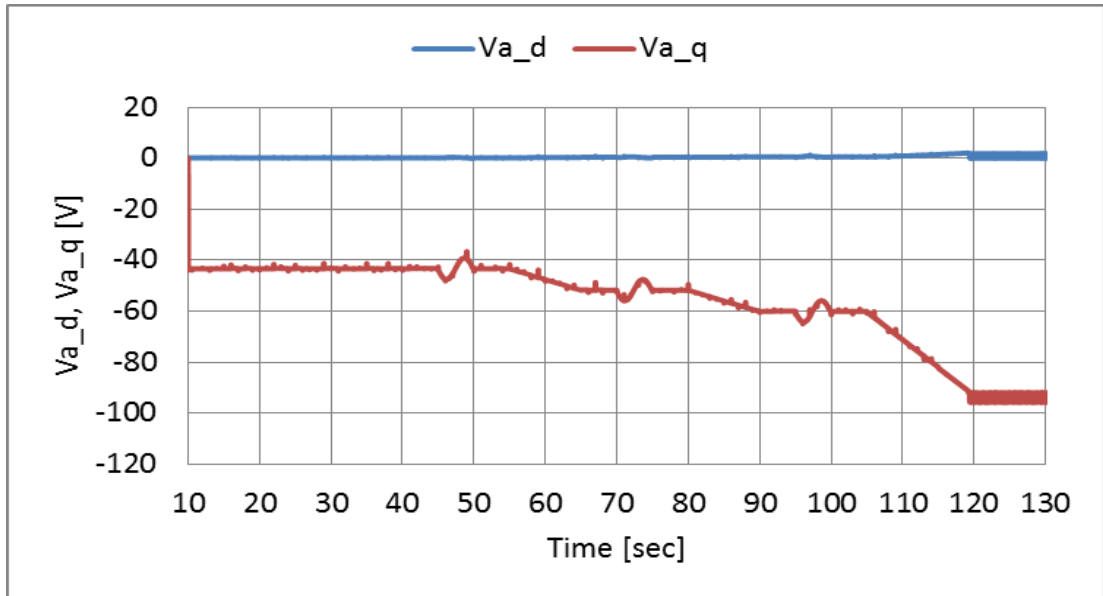


Fig. 5.30. d axis and q axis voltage of the PWM converter scheme

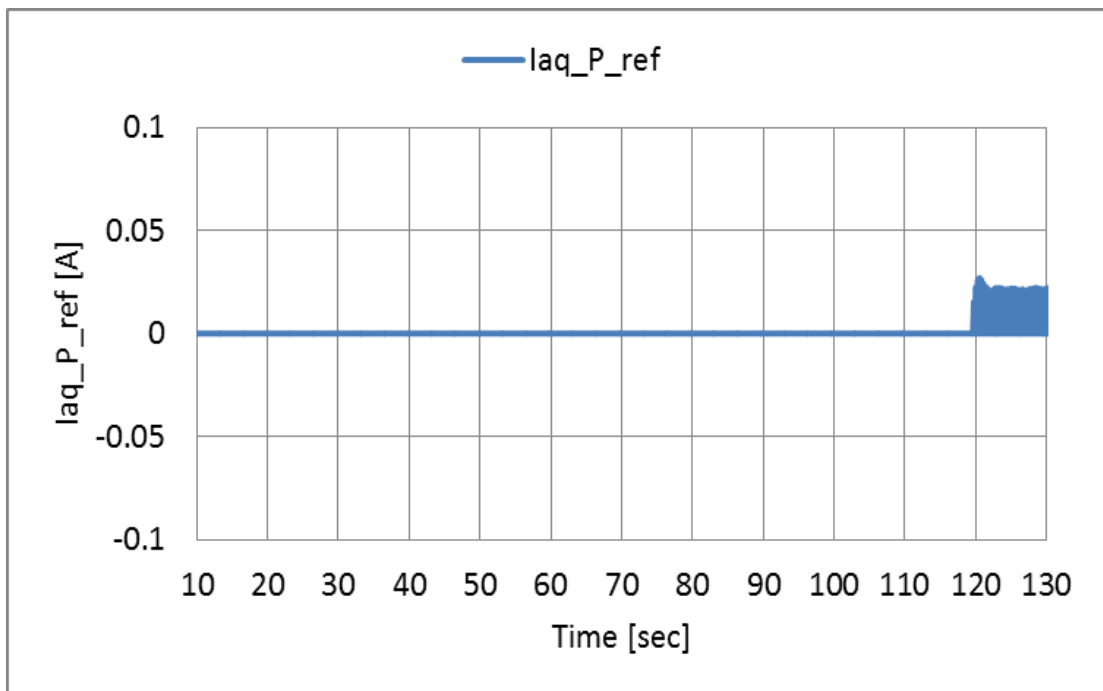


Fig. 5.31. q-axis current reference of power regulator control of the PWM converter scheme

Table 5.1 shows the integrated powers of each mode of the BCC and PWM converter schemes. At 0-55 sec, which corresponds to mode 1, integrated P_s of the BCC scheme decreases compared to the PWM converter scheme, since the tracking characteristic of ω_g for ω_g^{ref} is inferior. At 55-80 sec, which corresponds to the switching point of modes 1 and 2, the BCC scheme uses the hybrid control of the duty control system and speed control of the inverter side. In this operating range, integrated P_s of the BCC scheme decreases, since the tracking characteristic of the speed reference is inferior to the PWM converter scheme. At 80-105 sec, which corresponds to mode 3, the BCC scheme charges the DC link condenser. Therefore, integrated P_s decreases. In this period, the speed control is performed by charging the DC link condenser, since the wind velocity increases. In the operating range of 105-130 sec, which exceeds the rated wind velocity and corresponds to mode 4, there is significant difference between integrated P_s of the BCC scheme and the PWM converter scheme, since the DC link capacitor of BCC scheme discharges. At this operating range, the pitch angle control is activated, the efficiency of the converter of the BCC scheme changes, since the operating circuit changes for the operating modes.

Table 5.1. Integrated power of each mode.

| Mode | Time[sec] | Integrated electric power | Integrated electric power |
|----------------|--------------|-------------------------------------|-----------------------------------|
| | | in kJ for Boost Converter system | in kJ for PWM Converter system |
| mode1 | 0~55[sec] | 0-1647 | 0-1859 |
| mode1 or mode2 | 55~80[sec] | 1647-2861 | 1859-3197 |
| mode3 | 80~105[sec] | 2861-4817 | 3197-5344 |
| mode4 | 105~130[sec] | 4817-9785 | 5344-9813 |

5.10 Experimental system of real wind turbine

(Boost chopper scheme)

Fig. 5.32 shows the experimental system using the real wind turbine of the boost chopper scheme. The wind turbine side, the natural wind velocity data is given by the real time data of anemometer (CYG-5103VM, CLIMATEC Japan). The rotational speed of PMSG is estimated in the DSP by using the signals from the rotary encoder (RE, E6C3-CWZ3XH, Omron Japan). Also, the digital signal processing (DSP) unit calculates the wind turbine torque reference from the wind velocity data and rotational speed of the induction motor (IM). The natural wind velocity data is given by the real data of anemometer from real time. The rotational speed of IM is estimated in the DSP by using the signals from the rotary encoder (RE). The torque of IM is controlled by the off-the-shelf inverter. The IM is operated based on the wind turbine torque reference sent from a DSP through the D/A board (DS2102). After the wind turbine emulator is activated, the PMSG starts to rotate, and the converter control system starts to control the windmill rotational speed for the maximum power point tracking. The Duty and PWM signals for controlling the Duty, and INV are sent from a DSP to the short-circuit prevention circuit (FPGA) through a digital IO board (DS4002). The PWM signals are sent to the CNV and INV through the optical circuit.

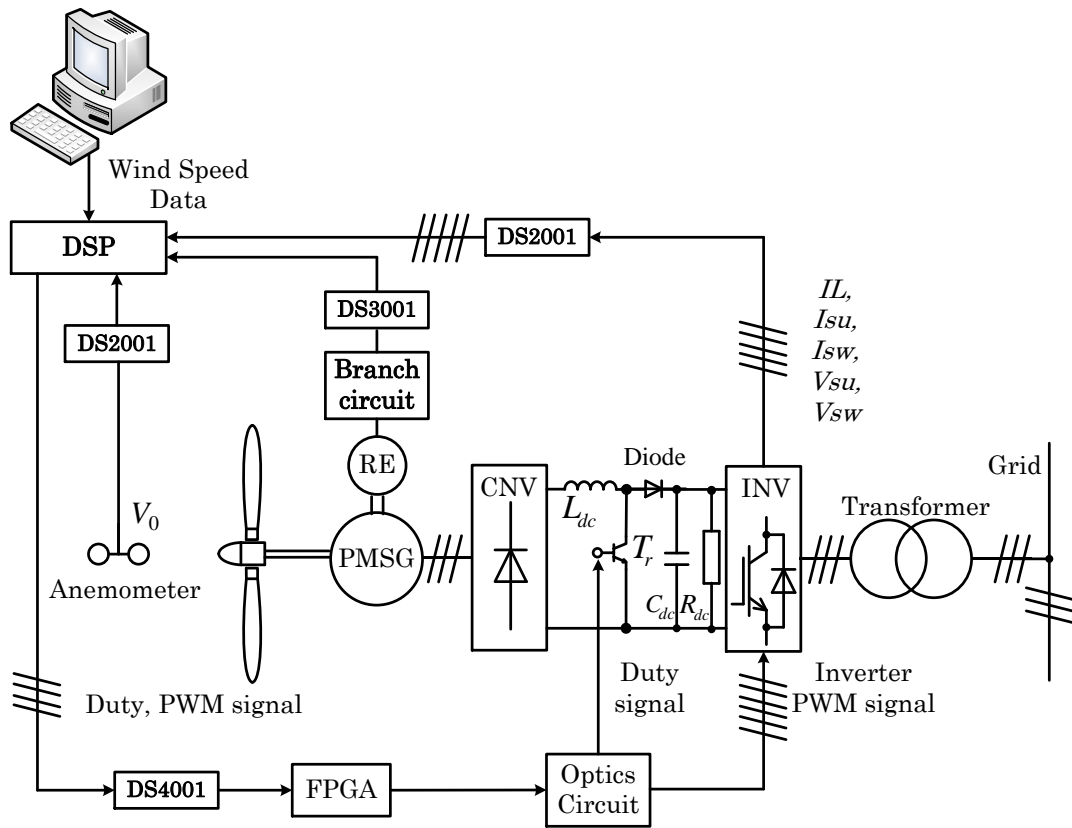


Fig. 5.32. Experimental system using the real wind turbine (Boost chopper scheme)

5.11 Experimental results of real wind turbine.

(Boost chopper scheme)

Fig. 5.33 shows the change of the natural wind velocity V_0 [m/s] user filter is given by the real time data of anemometer (CYG-5103VM, CLIMATEC Japan). The change of natural wind velocity includes the ranges of low wind velocity, middle wind velocity, and high wind velocity. The high wind velocity means the wind velocity that exceeds the rated value. All ranges include the change of wind velocity. The boost chopper scheme (of real wind turbine) and boost chopper scheme (of wind turbine emulator) are tested for the same change of the wind velocity, and the control performances of both schemes are discussed.

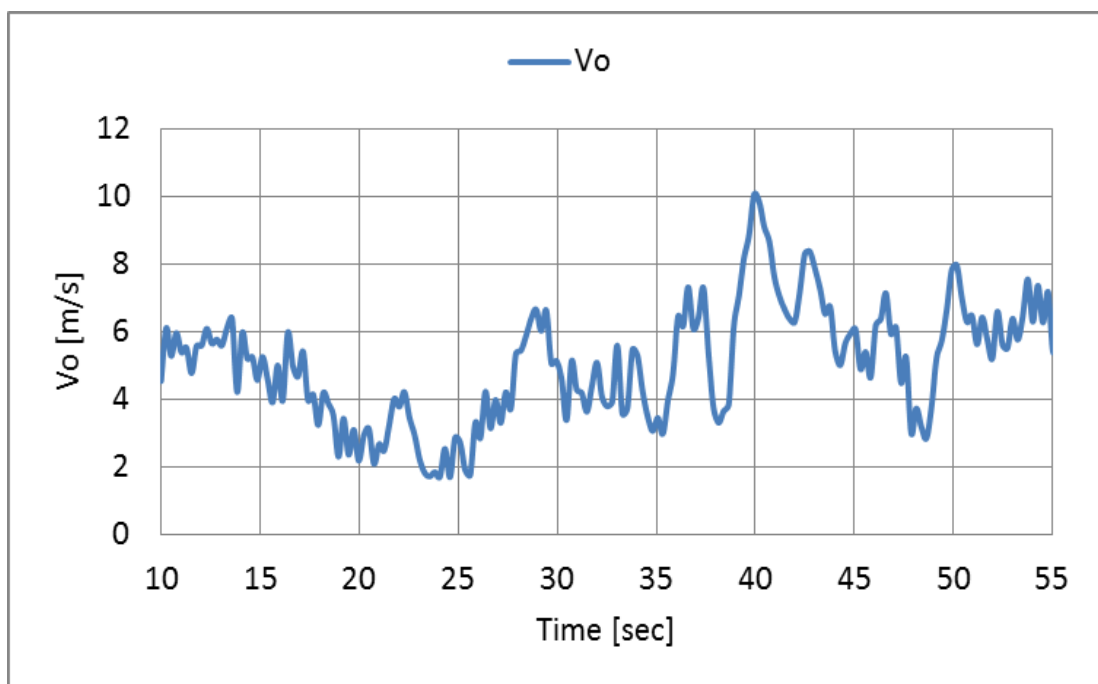


Fig. 5.33. Natural wind velocity of the real wind turbine

Figs. 5.34–5.39 show the experimental results of the boost chopper scheme. The system activates at 5m/s which exceeds cut-in wind velocity of 3m/s, and the power generation has been started after about 10 seconds in which windmill speed ω_g reaches to the windmill rotational speed reference ω_g^{ref} . In the natural wind velocity, at 5 m/s which corresponds to mode1, the speed control is carried out by the duty control system. It can be confirmed by the windmill speed ω_g and Duty shown in fig. 5.34-5.36 that the speed control is well carried out. In the wind velocity of 6m/s which corresponds to the switching point of mode2 and mode3, it can be confirmed by the ω_g , Duty, and DC link voltage V_{dc} shown in fig. 5.37-5.39 that the speed control is carried out while the speed control system is smoothly switched. In the wind velocity of 7m/s which corresponds to mode3, the speed control is carried out by adjusting V_{dc} with the inverter control system. It can be confirmed by the ω_g and V_{dc} that the speed control is well carried out. In wind velocity of 11m/s which corresponds to mode4, the speed control is carried out by the pitch angle control system, and the electric power control is carried out by the inverter control system. It can be confirmed by the ω_g , V_{dc} , and pitch angle θ shown in fig. 5.42, 5.43 and 5.45 that the ω_g is controlled at of the rated speed and the generated power P_s shown in fig. 5.41 is controlled at the rated power of 300W.

The control system similar in Fig. 3.5, Logic for control of wind turbine was described in section 3.2.

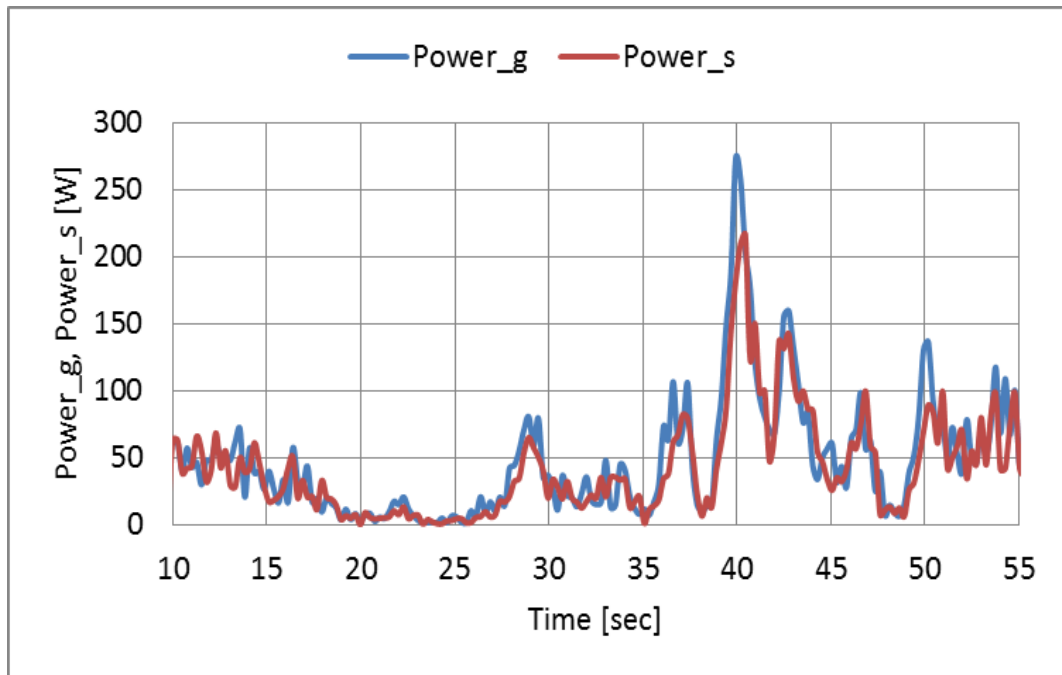


Fig. 5.34. Generated power and system power of the real wind turbine

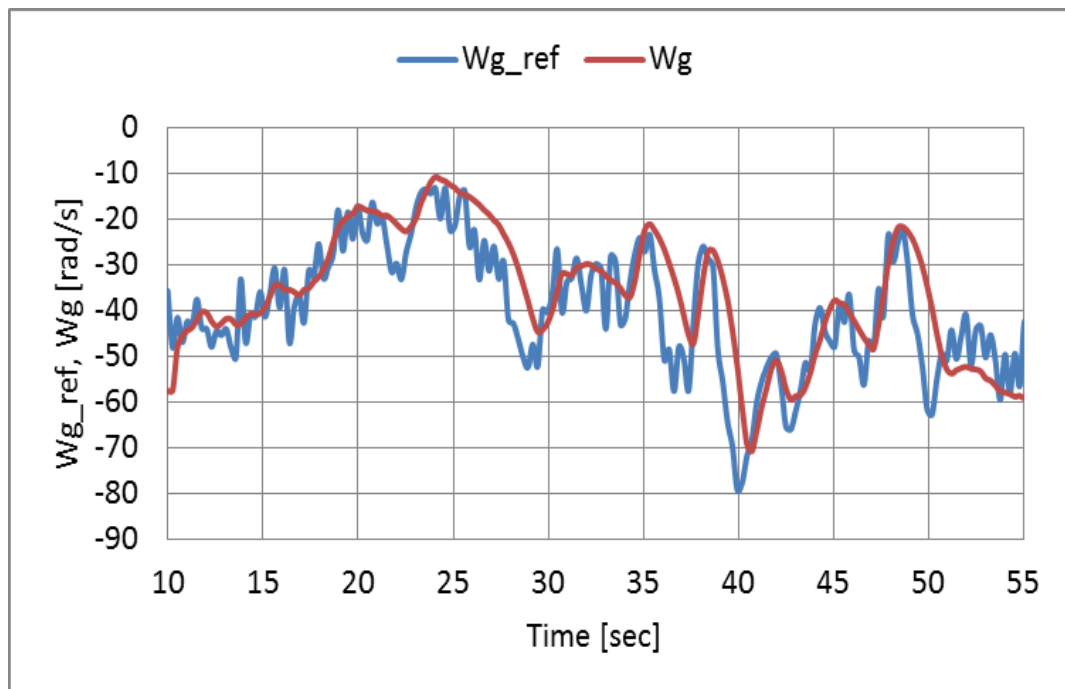


Fig. 5.35. Rotational speed Reference and Rotational speed of the real wind turbine

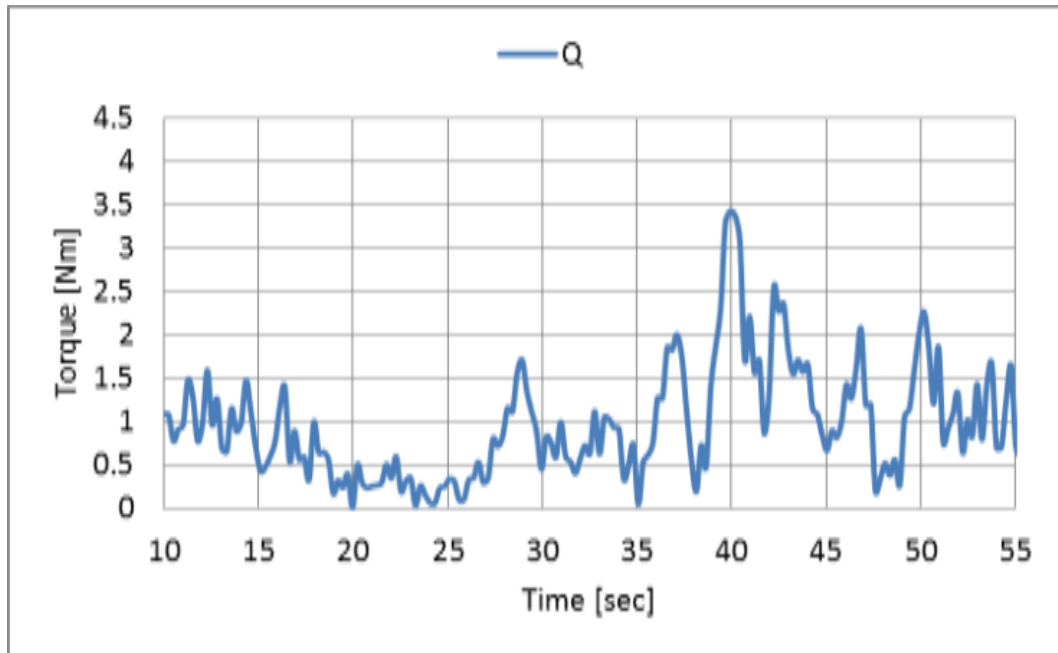


Fig. 5.36. Torque for wind turbine

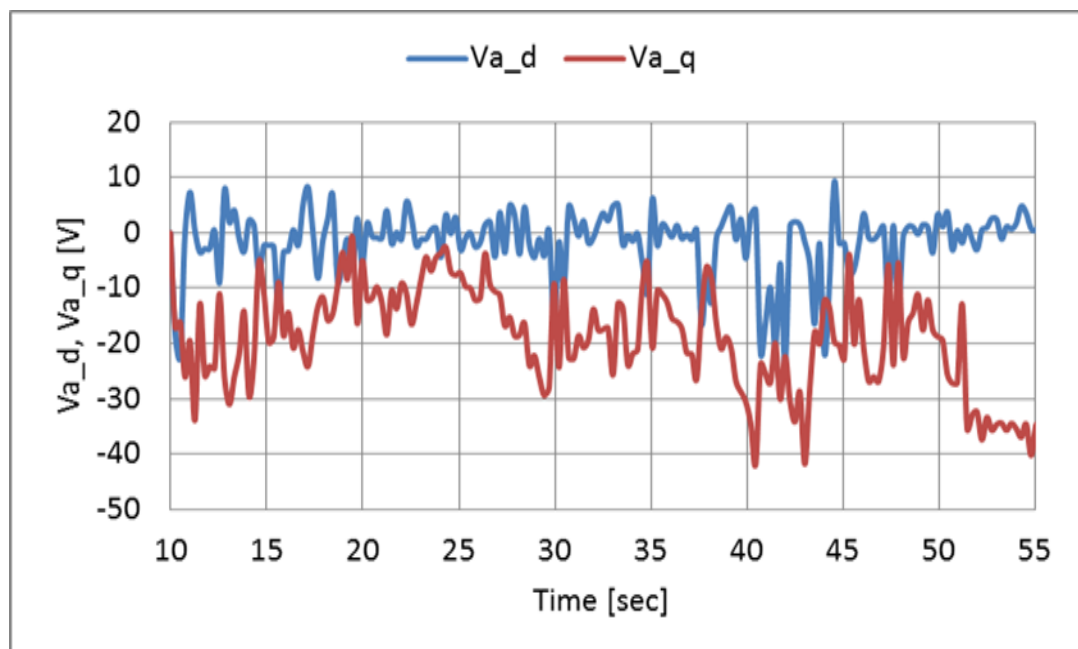


Fig. 5.37. d -axis and q -axis voltage reference for converter side of the real wind turbine

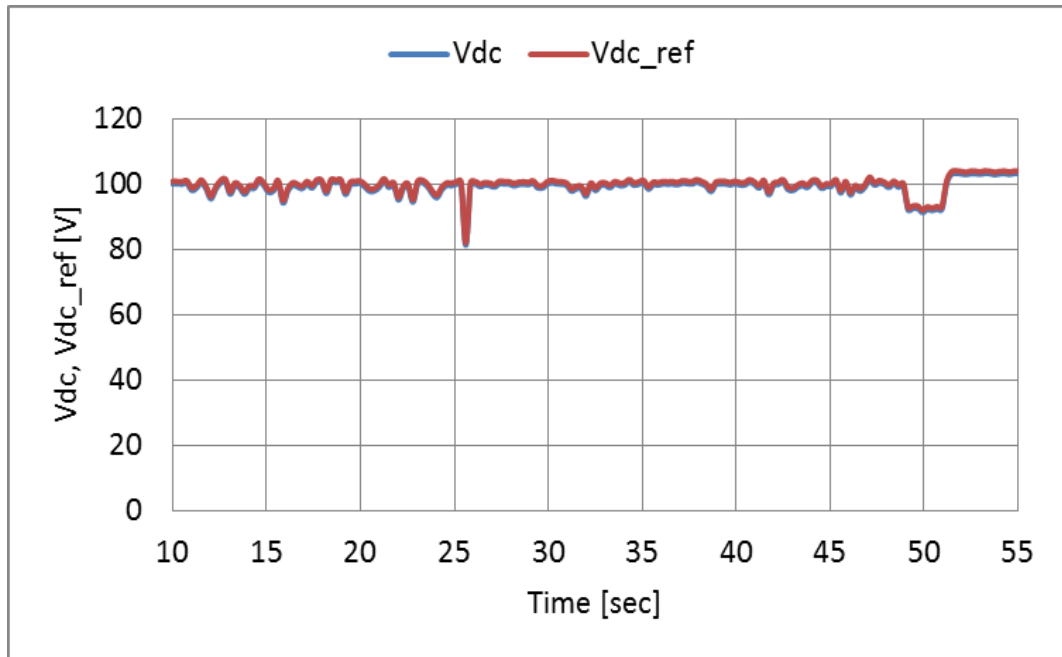


Fig. 5.38. DC link voltage and its reference of the real wind turbine

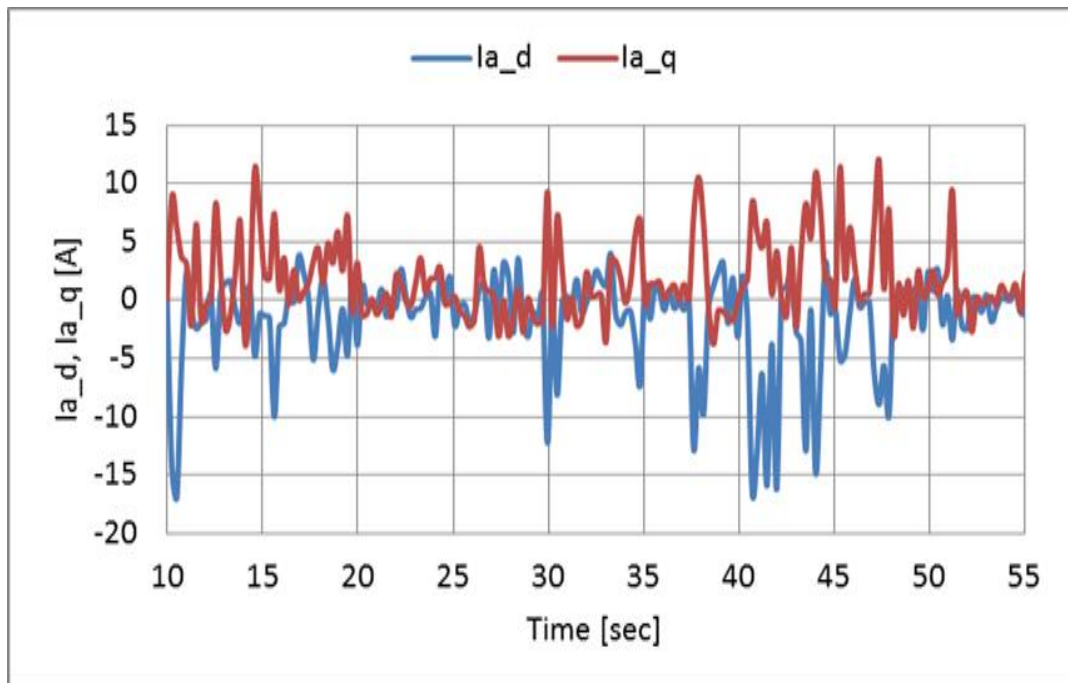


Fig. 5.39. d axis and q axis current for converter side of the real wind turbine

5.12 Experimental results of wind turbine emulator

(Boost chopper scheme)

Fig. 5.40-5.45 shows the experimental results of the variable speed wind power generation system using wind turbine emulator. The same V_0 is used for the wind turbine emulation. All of the results agree very well with the results for the real wind turbine of Fig. 5.34-5.39. It is obvious that the proposed wind turbine emulator can represent the behavior of real wind turbine for arbitrary wind velocities.

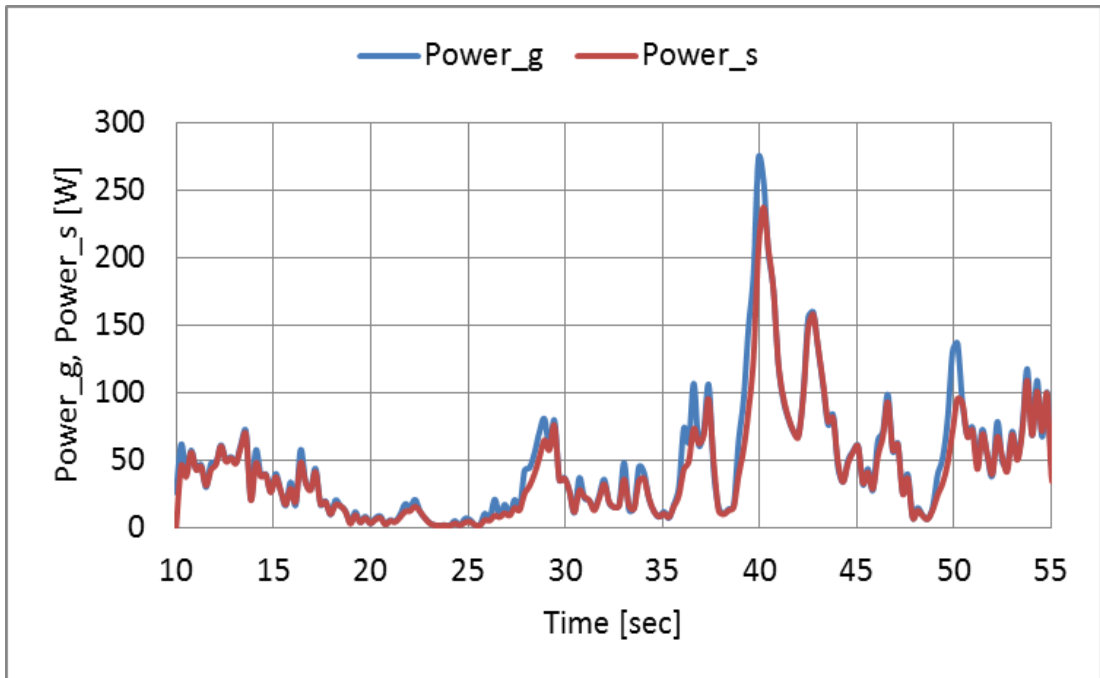


Fig. 5.40. Generated power and system power of the wind turbine emulator

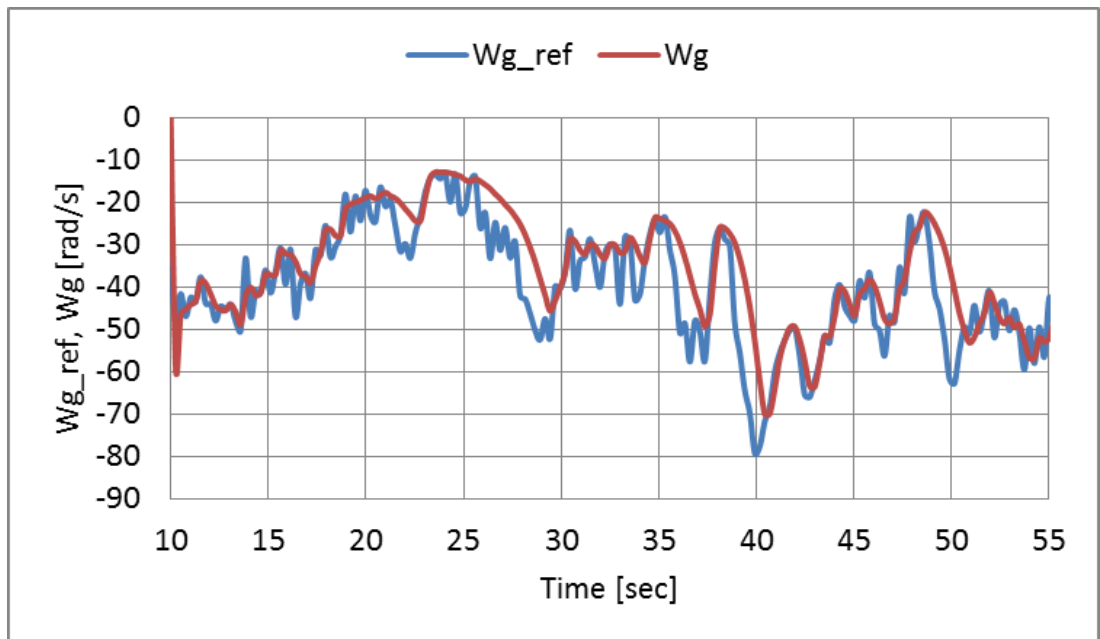


Fig. 5.41. Rotational speed Reference and Rotational speed of the wind turbine emulator

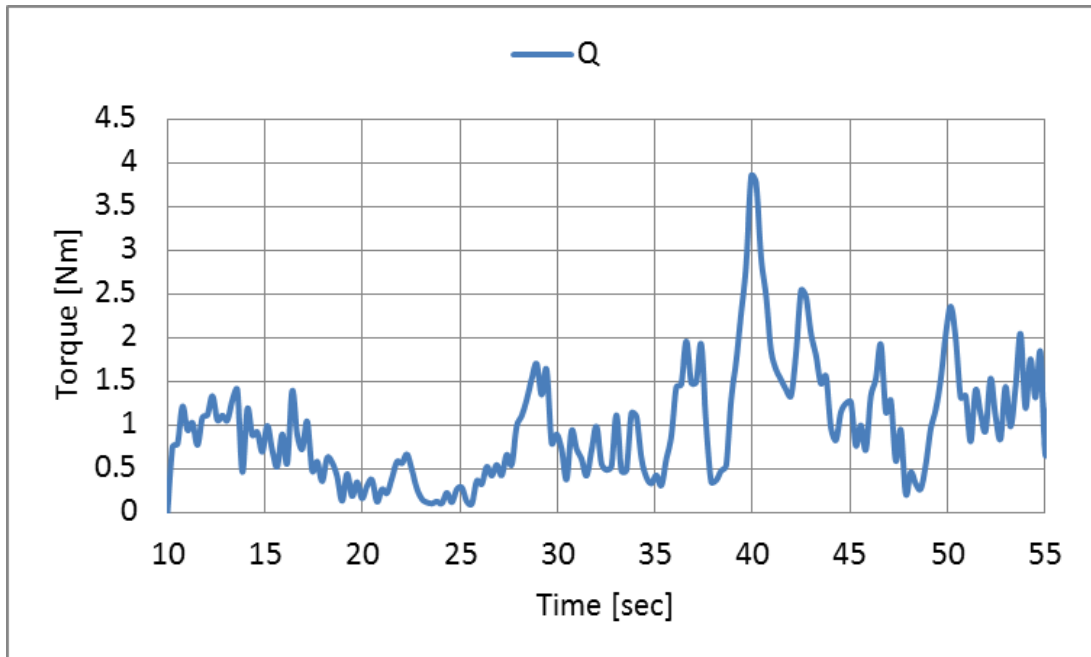


Fig. 5.42. Torque for wind turbine

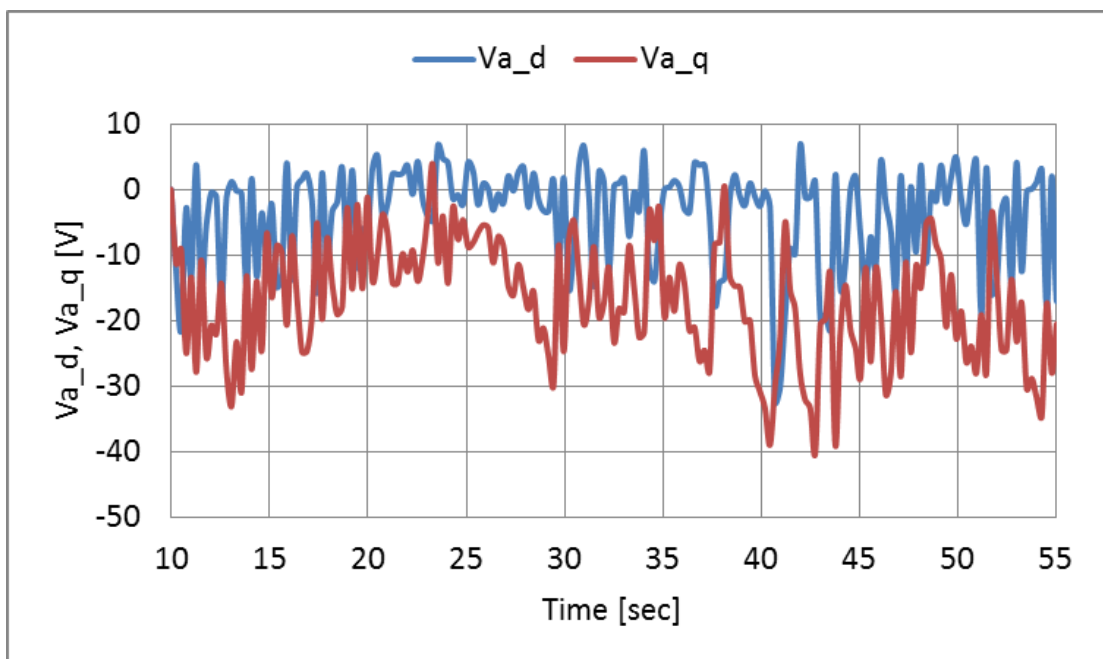


Fig. 5.43. d -axis and q -axis voltage reference for converter side of the wind turbine emulator

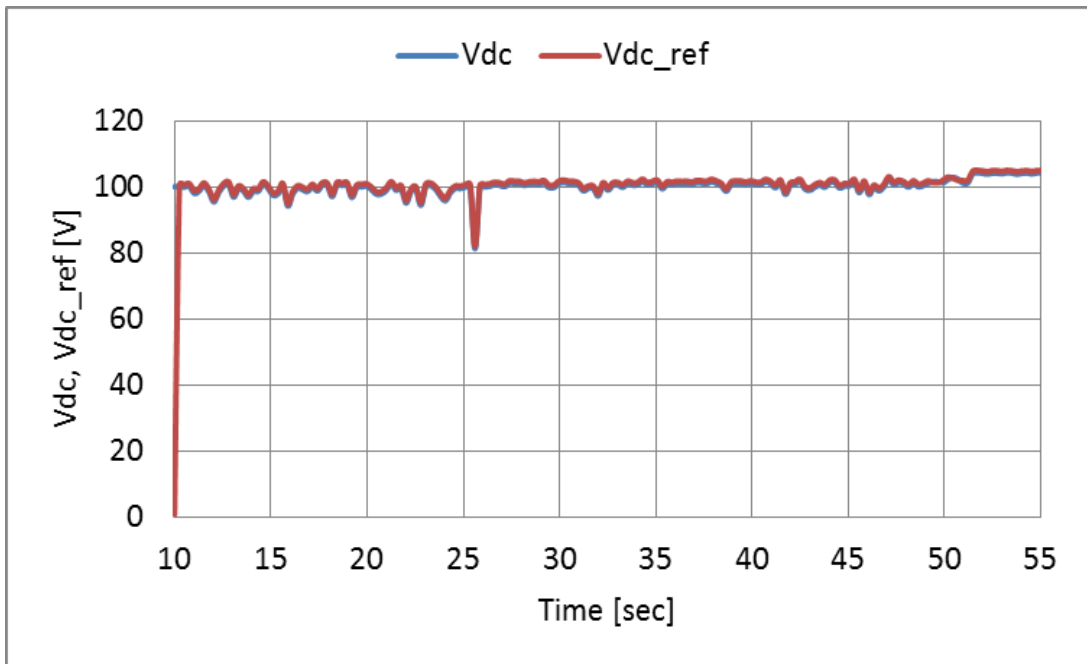


Fig. 5.44. DC link voltage and its reference of the wind turbine emulator

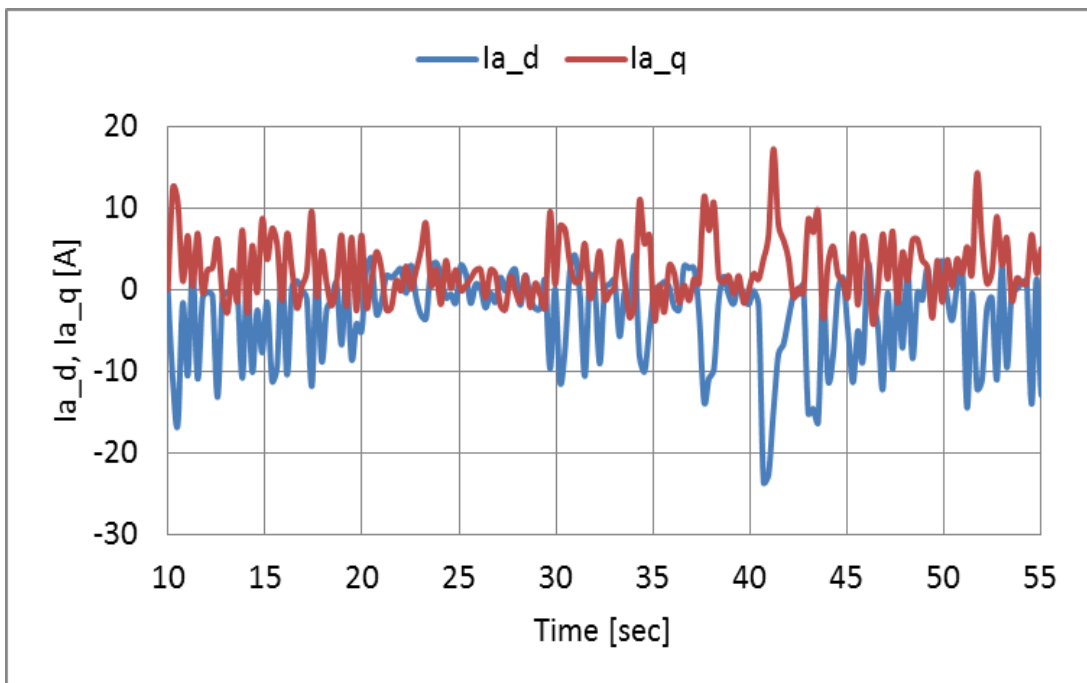


Fig. 5.45. d axis and q axis current for converter side of the wind turbine emulator

5.13 The each element of the system

The each element of the system, which are used for experimental assessments, is discussed.

5.13.1 Boost chopper scheme

The primary characteristic of a boost chopper circuit is to increase the voltage. If the converter configuration consists of diode rectifier bridge and boost chopper circuit, it can reduce the cut-in wind speed for a wind turbine. This allows a low voltage output from the diode rectifier at a low wind speed. The boost circuit also can provide a stable DC voltage for the following inverter circuit. Because the current only flows from the generator to the grid, this configuration is appropriate for the occasions when the wind turbine can start its operation by itself with low wind speed. And in fig 5.1 illustrates a simple topology of a diode rectifier for a wind turbine PMSG with grid-connection with a 3-phase diode bridge rectifier. At the generator side, the rectifier circuit consists of 6 passive diodes. And at the grid side, the full bridge inverter is composed of 6 IGBTs. And the strategy inserts a boost circuit between the rectifier and inverter bridge, and adds a feedback circuit to maintain the DC output voltage. The feedback circuit compares the voltage from the filter capacitor and the reference voltage. The output from the differential amplifier is compared with a triangular wave to produce the PWM signal that will control the switching IGBT, and determines the duty ratio of the PWM signal.

5.13.2 PWM converter scheme

In fig 5.2 shows the rectifier circuit consisting of 6 active switching devices in the topology of a back-to back converter or PWM converter scheme. This arrangement is bi-directional, and both circuits at the generator side and inverter side are symmetrical. At the generator side, in order to stabilise the DC bus voltage, the controller samples the voltage of the DC bus link and generator output, and locks the frequency output from generator to produce firing angle time for each of the switching devices after some calculations. At the inverter side, based on the voltage,

frequency and amplitude of the power grid, the controller produces PWM signals to control the IGBTs conduction.

The advantages of back to back converter are as follows:

- The rectifier is controllable, and
- Both rectifier and inverter bridges are composed of active IGBT devices, with the current be able to flow from either the generator to the grid or the grid to the generator.

The major disadvantage of back-to-back topology is:

- The controller is complex and expensive because it requires 12-channel Pulse Width Modulation (PWM) signals for the rectifier and the inverter. For this reason, in a practical application, the control system requires at least two or more Micro-Controller Units (MCU), Digital Signal Processor (DSP), Field Programmable Gate Array (FPGA), etc. to control the chips on the board.

From the experimental results of a variable-speed wind power generation system using a permanent magnet synchronous generator and a boost chopper circuit, with three speed control modes for wind velocity. The control system is used for the variable-speed wind generator system using the diode bridge rectifier and boost chopper circuit as a converter (boost chopper scheme). The speed control mode of low wind velocity controls the windmill speed by controlling the PMSG torque with the boost chopper circuit. The boost chopper circuit can control the generator torque by adjusting the armature current of the PMSG. The speed control mode of middle wind velocity controls the windmill speed by controlling the PMSG torque with the system interconnection inverter. The system interconnection inverter can control the PMSG torque by adjusting the DC link voltage. The speed control mode over the rated wind velocity controls the windmill speed by controlling the windmill torque with the pitch angle control system. The pitch angle control system can control the windmill torque by adjusting the pitch angle. The extension of the variable-speed range is realized by using the hybrid control of three speed control modes, consequently, the system interconnection for all speed control modes is achieved. Compared to the back to back or PWM converter scheme, the proposed control system has two advantages:

- the cost reduction achieved by reducing the number of switching devices and
- the high reliability achieved by simplifying the main circuits and control circuits.

5.14 Summary

This chapter has discussed the experimental results, the quantitative evaluation of various wind velocities. By the boost chopper scheme and PWM converter scheme are tested for the same change of the wind velocity, the control performances of both schemes, and analyzed both scheme with system advantages and disadvantages.

To summarize by comparison of the detection results, if the integrated powers of each mode of the boost chopper scheme and PWM converter schemes.

Chapter 6

Conclusion and Discussion

6.1 Conclusion and Discussion

First, the whole system framework is illustrated, clarifies the aim of research and describes objects which will be achieved in this project.

Next, the operating principle of the variable-speed wind power generation system, An overview of the fundamental principles relating to wind turbines with grid connection is presented. It briefly summaries what technologies are currently employed in the development of the converter wind turbine, and the achievement made by this project.

Next, the assessment with simulation of the variable-speed wind power generation system, The principles of an inverter based on PWM converter control system are presented in detail, and a number of mathematical models are given. An inverter based PWM converter system has been modelled using MATLAB/Simulink. At specifications of a 300W wind turbine, and the outcomes in chapter 5 demonstrate that the model meets the design parameters.

Next, The wind turbine emulator, The operating principle and the structure of WTE based on the BEMT. Also the structures of the test benches using the WT or WTE are explained. The simulation results of the VSWPGS using PWM converter are compared with the experiment results obtained with the test bench using WTE under the same conditions of low, medium and high wind velocities. Furthermore, under the conditions of natural winds, the experiment results obtained with the bench using WTE or WT for the VSWPGS using PWM converter are shown. The obtained experimental results are validated, and they show that the proposed WTE for the experimental assessment has a sufficient performance.

Finally, The experimental assessment of the VSWPGS using the BCC scheme. The implementation process considering all systems for BCC scheme was proposed to verify the validity. Also the implementation process of the VSWPGS using the PWM converter scheme was described as the benchmark comparison. The experimental systems of both schemes were built to evaluate the performance of the BCC scheme. It was confirmed that the BCC scheme enabled the windmill rotational speed control from the cut-in wind velocity to the over rated wind velocity. Therefore, it was confirmed that the BCC scheme obtained the similar performance to the PWM converter scheme. The developed WTE can be utilized for analyzing various mechanical and electrical characteristics of grid tied PMSG wind power system.

Published Papers

The present work has resulted in four conference papers [75, 78, 79 and 80] and one journal publications [89].

Reference

- [1] T. Ackermann.: “Wind energy technology and current status: a review”, *Renewable and Sustainable Energy Reviews* Vol 4, Issue 4, December 2000, pp. 315–374.
- [2] Orlando, N.A. ; Liserre, M. ; Mastromauro, R.A. ; Dell'Aquila, A.,: “A Survey of Control Issues in PMSG-Based Small Wind-Turbine Systems”, *Industrial Informatics, IEEE Transactions on*, Vol. 9, Issue. 3, Aug. 2013, pp. 1211-1221.
- [3] Muni Prakash, T., and Shakeer Ahhamad, SK., "Direct torque control for doubly fed induction machine-based wind turbines under voltages dips and without crowbar protection," *International Journal of Electrical and Electronics Engineering*, Vol-1 Iss-4, pp. 52-54.(2012).
- [4] J. S. Thongam, P. Bouchard, R. Beguane, A. F.Okou, and A. F. Merabet, “Control of variable speed wind energy conversion system using a wind speed sensorless optimum speedMPPT control method,” in *Proc. 37th Annu. Conf. IEEE Ind. Electron. So., IECON’11, Melbourne, Australia, Nov. 7–10, 2011*, pp. 855–860.
- [5] O. Ozgener, “A small wind turbine system (SWTS) application and its performance analysis,” *Energy Conversion Manag.*, vol. 47, pp. 1326–1337, 2006.
- [6] B. Wilamowski and D. Irwin, *The Industrial Electronics Handbook Power Electron. and Motor Drives*, 2nd ed. Boca Raton, FL, USA: CRC Press, 2011.

-
- [7] A. Mirecki, X. Roboam, and F. Richardeau, "Architecture complexity and energy efficiency of small wind turbines," *IEEE Trans. Ind. Electron.*, vol. 54, no. 1, pp. 660–670, Jan. 2007.
- [8] O. Carranza, E. Figures, G. Carcera, R. Ortega, and D. Velasco, "Low power wind generation system based on variable speed permanent magnet synchronous generators," in *Proc. 2011 IEEE Int. Symp. Ind. Electron., ISIE'11*, Gdansk, Poland, Jun. 27–30, 2011, pp. 1063–1068.
- [9] A. Di Gerlando, G. Foglia, M. F. Iacchetti, and R. Perini, "Analysis and test of diode rectifier solutions in grid-connected wind energy conversion systems employing modular permanent-magnet synchronous generators," *IEEE Trans. Ind. Electron.*, vol. 59, no. 5, pp. 2135, 2146, May 2012.
- [10] B. Wu, Y. Lang, N. Zargari, and S. Kouro, "Power Conversion and Control of Wind Energy Systems," *Hoboken NJ: Wiley*, 2011
- [11] M. P. Kazmierkowski, R. Krishnan, and F. Blaabjerg, "Control in Power Electronics-Selected Problems," *New York: Academic Press*, 2002
- [12] K. H. Kim, Y. C. Jeung, D. C. Lee, and H. G. Kim, "Robust Control of PMSG Wind Turbine Systems with Back-to-Back PWM Converters," *IEEE International Symposium on Power Electronics for Distributed Generation Systems*, 2012
- [13] S. Li, T. A. Haskew, R. P. Swatloski, and W. Gathings, "Optimal and Direct-Current Vector Control of Direct-Driven PMSG Wind Turbines," *IEEE Transactions on Power Electronics*, Vol. 27, No. 5, pp. 2325-2337, May 2012
- [14] F. Kendouli, K. Abed, K. Nabti, H. Benalla, and B. Azoui, "High Performance PWM Converter Control Based PMSG for Variable Speed Wind Turbine," *International Conference on Renewable Energies and Vehicular Technology*, pp. 502-507, 2012
- [15] I. Ushiyama, "Power generation characteristics and system interconnection of wind power generation", *J. IEE Japan*, 120, pp.514-517 (2000-8/9) (in Japanese)
- [16] I. Nagata, K. Hayakawa, S. Arinaga, N. Inomata, "Development of Gearless Variable-Speed Wind Turbine", Vol.38, No.2, pp.100-103 (2001-3) (in Japanese)

-
- [17] H. Chikaraishi, Y. Hayashi, and N. Sato: "A Variable Speed Control of the Induction Generator without Speed Sensor for Wind Generation", T. IEE Japan, Vol. 110-D, No.6, pp.664 - 672 (1990-6) (in Japanese)
- [18] R. Pena, J. C. Clare, G. M. Asher: "Doubly fed induction generator using back-to-buck PWM converters and its application to variable speed wind-energy generation", IEE Proc.-Electr. Power Appl., Vol. 143, No.3, pp.231 - 241 (1996-3)
- [19] M. G. Simoes, B. K. Bose, R. J. Spiegel: "Fuzzy Logic Based Intelligent Control of a Variable Speed Cage Machine Wind Generation System", T. IEEE, Vol. 12, No. 1, pp.87 - 95 (1997-1)
- [20] N. Horiuchi, T. Kawakami, T. Suzuki: "Power Control of Induction Generator by V/F control for Wind Energy Conversion System", T. IEE Japan, Vol. 118-B, No. 10, pp.1170 - 1176 (1998-10) (in Japanese)
- [21] K. Ohyama, S. Arinaga, Y. Yamashita: "Speed Sensorless Vector Controlled Converter for Variable Speed Wind Generation System Using Induction Generator", Proc. of the World Wind Energy Conference and Exhibition (WWECE2002), VC3.11, Berlin, Germany (2002-6)
- [22] T. Senjyu, T. Hamano, N. Urasaki, K. Uezato, T. Funabashi, H. Fujita: "Maximum Power Point Tracking Control for Wind Power Generating System Using Permanent Magnet Synchronous Generator", T. IEE Japan, Vol. 122-B, No. 12, pp.1403 - 1409 (2002-12) (in Japanese)
- [23] G. Poddar, A. Joseph, and A. K. Unnikrishnan: "Sensorless Variable - Speed Controller for Existing Fixed - Speed Wind Generator With Unity - Power - Factor Operation", T. IEEE, Vol. 50, No. 5, pp.1007 - 1015 (2003-10)
- [24] K. Ohyama, S. Arinaga, Y. Yamashita: "Sensorless Vector Controlled Converter for Variable Speed Wind Generation System Using Induction Generator", T. IEE Japan, Vol. 125-D, No. 4, pp.386 - 396 (2005-4) (in Japanese)
- [25] I. Ushiyama, "Introduction to windmill engineering", Morikita Publishing Co., Ltd., ISBN978-4-627-94651-4, pp.87 - 99 (2002) (in Japanese)
-

-
- [26] K. Fujita, N. Ushiki, T. Nakano: “A Evaluation of Wind Generation Control System by Real Time Simulator”, T. IEE Japan, SPC-02-112, pp.93 - 98 (2002) (in Japanese)
- [27] L. Latkovskis, K. Rashevits, L. Rutmanis, J. Stabulnieks: “Maximum Power Transfer in small Wind Energy Converter with Permanent Magnet Generator for Heating Purposes”, Proc. of EPE’99, CD-ROM, Lausanne, Switzerland (1999-9)
- [28] K. Ito, N. Yamamura, M. Ishida, M. Hori: “Maximum Power Control method for Small Wind Power Generation System Using Permanent Magnet Synchronous Generator”, T. IEE Japan, SPC-01-56, pp.41 - 46 (2001) (in Japanese)
- [29] K. Ohyama, T. Yodogawa, S. Arinaga, Y. Yamashita: “Wind Turbine Rotational Frequency Control of Wind Power System Using Diode Bridge Rectification Circuit”, T. IEE Japan, SPC-03-103, pp.87 - 92 (2003) (in Japanese)
- [30] H. Sugimoto, M. Oyama, S. Tamai, “Theory and practical design of AC servo system”, Sougoudenshi publisher, pp.12 - 20, (1990) (in Japanese)
- [31] Y. Takeda, N. Matsui, S. Morimoto, Y. Honda, “Design and control of interior permanent magnet synchronous motor”, Ohmsha, pp.9 - 13 (2001) (in Japanese)
- [32] The Institute of Electrical Engineering of Japan, “Power electronics circuit”, Ohmsha, pp.85 - 92 (2000) (in Japanese)
- [33] D. M. Eggleston, and F. S. Stoddard, “Wind Turbine Engineering Design,” *Van Nostrand Reinhold*, pp. 15-64, 1987
- [34] Kolar, J.W. ; Friedli, T. ; Rodriguez, J. ; Wheeler, P.W.: “Review of Three-Phase PWM AC–AC Converter Topologies”, *Industrial Electronics, IEEE Transactions on*, Vol. 58, Issue. 11, Nov.2011, pp. 4988-5006.
- [35] M. Allagui, O. Hasnaoui, and J. Belhadj. : “A 2MW direct drive wind turbine; vector control and direct torque control techniques comparison,” *Journal of Energy in Southem Africa*, Vol. 25, No. 2, May. 2014.
- [36] Xibo Yuan ; Jianyun Chai ; Yongdong Li,: “A Transformer-Less High-Power Converter for Large Permanent Magnet Wind Generator Systems”, *Sustainable Energy, IEEE Transactions on*, Vol. 3, Issue. 3, July 2012, pp. 318-329.
-

-
- [37] Shuhui Li ; Haskew, T.A.: “Analysis of Decoupled d-q Vector Control in DFIG Back-to-Back PWM Converter”, Power Engineering Society General Meeting, 2007. IEEE, pp. 1-7.
- [38] Xibo Yuan ; Jianyun Chai ; Yongdong Li.: “Control of variable pitch, variable speed wind turbine in weak grid systems”, Energy Conversion Congress and Exposition (ECCE), 2010 IEEE , pp. 3778-3785.
- [39] Henz, G. ; Koch, G. ; Franchi, C.M. ; Pinheiro, H.: “Development of a variable speed wind turbine emulator for research and training”, Power Electronics Conference (COBEP), 2013 Brazilian , pp. 737-742.
- [40] Hardy, T. ; Jewell, W. : “Emulation of a 1.5MW wind turbine with a DC motor”, Power and Energy Society General Meeting, 2011 IEEE, pp. 1-8.
- [41] Weihao Hu ; Zhe Chen ; Yue Wang ; Zhaoan Wang,: “Flicker Mitigation by Active Power Control of Variable-Speed Wind Turbines with Full-Scale Back-to-Back Power Converters”, Vol. 24, Issue. 3, Sept. 2009, pp. 640-649.
- [42] Tao Sun ; Zhe Chen ; Blaabjerg, F.: “Flicker study on variable speed wind turbines with doubly fed induction generators”, Energy Conversion, IEEE Transactions on, Vol. 20, Issue. 4, Dec. 2005, pp.896-905.
- [43] Whaley, D.M. ; Soong, W.L. ; Ertugrul, N.: “Investigation of switched-mode rectifier for control of small-scale wind turbines”, Industry Applications Conference, 2005, Vol. 4. pp. 2849-2856.
- [44] Kyung-Hyun Kim ; Tan Luong Van ; Dong-Choon Lee ; Seung-Ho Song ; Eel-Hwan Kim.: “Maximum Output Power Tracking Control in Variable-Speed Wind Turbine Systems Considering Rotor Inertial Power”, Industrial Electronics, IEEE Transactions on , Vol. 60, Issue. 8, Aug. 2013, pp.3207-3217.
- [45] Shuhui Li ; Haskew, T.A. ; Swatloski, R.P. ; Gathings, W.: “Optimal and Direct-Current Vector Control of Direct-Driven PMSG Wind Turbines”, Power Electronics, IEEE Transactions on, Vol. 27, Issue. 5, May. 2012, pp. 2325-2337.
- [46] Yu Zou ; Elbuluk, M.E. ; Sozer, Y.: “Simulation Comparisons and Implementation of Induction Generator Wind Power Systems”, Industry Applications, IEEE Transactions on, Vol. 49, Issue. 3, May-June. 2013, pp. 1119-1128.
- [47] Shuhui Li ; Haskew, T.A.: “Transient and Steady-State Simulation Study of Decoupled d-q Vector Control in PWM Converter of Variable Speed Wind Turbines”, Industrial Electronics Society, 2007. IECON 2007, pp. 2079-2086.
-

-
- [48] Guoliang Yang Huiguang Li : “Two-Sliding Mode Control for Efficiency Improvement in Variable Speed Small Wind Turbine Systems”, Proceedings of the 2007 IEEE International Conference, pp. 3717-3723.
- [49] Mohod, S.W. ; Aware, M.V.: “Wind energy conversion system simulator using variable speed induction motor”, Power Electronics, Drives and Energy Systems (PEDES) & 2010 Power India, 2010, pp. 1-6.
- [50] Teodorescu, R. ; Blaabjerg, F.: “Flexible control of small wind turbines with grid failure detection operating in stand-alone and grid-connected mode”, Power Electronics, IEEE Transactions on, Vol. 19, Issue. 5, Sept. 2004, pp. 1323-1332.
- [51] dos Reis, F.S. ; Islam, S. ; Tan, K. ; Ale, J.V. ; Adegas, F.D. ; Tonkoski, R.: “Harmonic Mitigation in Wind Turbine Energy Conversion Systems”, Power Electronics Specialists Conference, 2006, pp. 1-7.
- [52] Ki-Hong Kim ; Yoon-Cheul Jeung ; Dong-Choon Lee ; Heung-Geun Kim.: “Robust control of PMSG wind turbine systems with back-to-back PWM converters”, Power Electronics for Distributed Generation Systems (PEDG), 2010, pp. 433-437.
- [53] Zheng Chen ; Xiangning Xiao ; Haitao Wang ; Mengwei Liu.: “Analysis of converter topological structure for direct-drive wind power system with PMSG”, Power System Technology (POWERCON), 2010,
- [54] Kendouli, F. ; Abed, K. ; Nabti, K. ; Benalla, H. ; Azoui, B.: “High performance PWM converter control based PMSG for variable speed wind turbine”, Renewable Energies and Vehicular Technology (REVET), 2012, pp. 502-507.
- [55] Patil, N.S. ; Bhosale, Y.N.: “Small-signal stability of wind turbine by using direct-drive PMSG connected to power grid”, Energy Efficient Technologies for Sustainability (ICEETS), 2013, pp. 635-640.
- [56] Shariatpanah, H. ; Fadaeinedjad, R. ; Rashidinejad, M.: “A New Model for PMSG-Based Wind Turbine with Yaw Control”, Energy Conversion, IEEE Transactions on, Vol. 28, Issue. 4, Dec. 2013, pp. 929-937.
- [57] Mahmoud M. Hussein, Mohamed Orabi, Mahrous E. Ahmed, M. A. Abd El-Wahab, and M.M.Hamada.: “Simple Direct Sensorless Control of Permanent

-
- Magnet Synchronous Generator Wind Turbine”, Proceedings of the 14th International Middle East Power Systems Conference (MEPCON'10), Cairo University, Egypt, December 19-21, 2010,
- [58] Bhende, C.N. ; Mishra, S. ; Malla, S.G.: “Permanent Magnet Synchronous Generator-Based Standalone Wind Energy Supply System”, Sustainable Energy, IEEE Transactions on, Vol. 2, Issue. 4, Oct. 2011, pp. 361-373.
- [59] Barote, L. ; Marinescu, C. ; Cirstea, M.N.: “Control Structure for Single-Phase Stand-Alone Wind-Based Energy Sources”, Industrial Electronics, IEEE Transactions on , Vol. 60, Issue. 2, Feb. 2013, pp. 764-772.
- [60] M.B. Bana Sharifian, Y. Mohamadrezapour, M. Hosseinpour and S. Torabzade,: “Maximum Power Control of Variable Speed Wind Turbine Connected to Permanent Magnet Synchronous Generator Using Chopper Equipped with Superconductive Inductor”, Journal of Applied Science
- [61] Iov, F. ; Ciobotaru, M. ; Blaabjerg, F.: “Power electronics control of wind energy in distributed power systems”, Optimization of Electrical and Electronic Equipment, 2008., May. 2008.
- [62] M. Monfared, G. B. Gharehpetian.: “Application of Boost Converter and Superconductive Coil Combination in Variable Speed Wind Energy System”, Electrical engineering department, Amirkabir University of Technology, Tehran 15914, Iran.
- [63] Shao Zhang ; King-Jet Tseng ; Vilathgamuwa, D.M. ; Trong Duy Nguyen ; Xiao-Yu Wang .: “Design of a Robust Grid Interface System for PMSG-Based Wind Turbine Generators“, Industrial Electronics, IEEE Transactions on, Vol. 58, Issue. 1, Jan. 2011, pp. 316-328.
- [64] Haining Wang ; Nayar, C. ; Jianhui Su ; Ming Ding.: “Control and Interfacing of a Grid-Connected Small-Scale Wind Turbine Generator “, Energy Conversion, IEEE Transactions on, Vol. 26, Issue. 2, June. 2011, pp. 428-434.
- [65] Yuanye Xia ; Ahmed, K.H. ; Williams, B.W.: “Wind Turbine Power Coefficient Analysis of a New Maximum Power Point Tracking Technique”, Industrial

-
- Electronics, IEEE Transactions on , Vol. 60, Issue. 3. March. 2013, pp. 1122-1132.
- [66] Mendis, N. Muttaqi, K.M. ; Sayeef, S. ; Perera, S.: “Standalone Operation of Wind Turbine-Based Variable Speed Generators With Maximum Power Extraction Capability”, Energy Conversion, IEEE Transactions on, Vol. 27, Issue. 4, Dec. 2012, pp. 822-834.
- [67] Hong-Geuk Park ; Seok-Ho Jang ; Dong-Choon Lee ; Heung-Geun Kim.: “Low-cost converters for micro wind turbine systems using PMSG”, Power Electronics, 2007. Pp. 483-487.
- [68] Sangita R Nandurkar, Mini Rajeev,: “Design and Simulation of three phase Inverter for grid connected Photovoltaic systems”, Proceedings of Third Biennial National Conference, NCNTE- 2012,
- [69] Arifujjaman, M.: “Modeling, simulation and control of grid connected Permanent Magnet Generator (PMG)-based small wind energy conversion system”, Electric Power and Energy Conference (EPEC), 2010, pp.1-6.
- [70] Mahmoud M. Hussein, Mohamed Orabi, Mahrous E. Ahmed, M. A. Abd El-Wahab, and M.M.Hamada.: “Simple Direct Sensorless Control of Permanent Magnet Synchronous Generator Wind Turbine”, Proceedings of the 14th International Middle East Power Systems Conference (MEPCON'10), Cairo University, Egypt, December 19-21, 2010.
- [71] Miguel López, Jean-Claude Vannier,: “Stand-alone wind energy conversion system with maximum power transfer control”, Ingeniare. Revista chilena de ingenieria, vol. 17 No 3, 2009, pp. 329-336.
- [72] S. Belakehal, H. Benalla, A. Bentounsi.: “Power maximization control of small wind system using permanent magnet synchronous generator”, Revue des Energies Renouvelables Vol. 12 N°2 (2009) pp. 307–319.
- [73] Koutroulis, E. ; Kalaitzakis, K.: “Design of a maximum power tracking system for wind-energy-conversion applications”, Industrial Electronics, IEEE Transactions on, Vol. 53, Issue. 2, April. 2006, pp. 486-494.

-
- [74] Manju Khare, Ganga Agnihotri, Yogendra Kumar, & V. K. Sethi.: "Performance Analysis of a Grid connected Wind Energy system", Volume-03, Issue-02, pp-204-208.
- [75] S. Tammaruckwattana, and K. Ohyama, "Experimental Verification of Variable Speed Wind Power Generation System Using Permanent Magnet Synchronous Generator by Wind Turbine Emulator," *in Proc. IECON*, pp. 5827-5832, 2012
- [76] K. Ohyama, and T. Nakashima, "Wind Turbine Emulator Using Wind Turbine Model Based on Blade Element Momentum Theory," *International Symposium on Power Electronics, Electrical Drives, Automation and Motion T. SPEEDAM*, pp. 762-765, 2010
- [77] BWEA 2009, *Annual Review 2009*, British Wind Energy Association.
- [78] S. Tammaruckwattana, and K. Ohyama, "Modeling and simulation of permanent magnet synchronous generator wind power generation system using boost converter circuit," *in Proc. EPE*, pp. 1-10, 2013
- [79] S. Tammaruckwattana, and K. Ohyama, "Experimental verification of variable speed wind power generation system using permanent magnet synchronous generator by boost converter circuit," *in Proc. IECON*, pp. 7157-7162, 2013
- [80] S. Tammaruckwattana, Chenxin Yue, Yumi Ikeda, and K. Ohyama, "Comparison of Switching Losses of Matrix Converters for Commutation Methods," *in Proc. EPE*, pp. 1-10, 2014
- [81] Horizon Gitano-Briggs 2010, "Small Wind Turbine Power Controllers," *In Wind Power*, pp. 165-188.
- [82] Von Meier, Alexandra (2006). *Electric Power Systems: A Conception Introduction*. Hoboken, New Jersey: John Wiley & Sons, Inc. pp. 92–95. ISBN 978-0-471--17859-0.
- [83] Bharanikumar R., Yazhini A.C., & Kumar A.N. 2010. Modeling and Simulation of Wind Turbine Driven Permanent Magnet Generator with New MPPT. *Asian Power Electronics Journal*, Vol. 4, (2) 52-58
- [84] Ahmed T., Nishida K., & Nakaoka M. 2004, Wind Energy DC Supply-Based Induction Generator with Static VAR Compensator and AC Voltage Regulator, In INTELEC 2004, 26th Annual International, IEEE, pp. 689-696.

-
- [85] Belakehal S., Benalla H., & Bentounsi A. 2009. Power Maximumization Control of Small Wind System Using Permanent Magnet Synchronous Generator. *Revue des Energies Renouvelables*, 12, (2) 307-319
- [86] Bana Sharifian M.B, Mohamadrezapour Y., Hosseinpour M., & Torabzade S. 2009. Maximum Power Control of Variable Speed Wind Turbine Connected to Permanent Magnet Synchronous Generator Using Chopper Equipped with Superconductive Inductor. *Journal of Applied Sciences*, 9, (4) 777-782
- [87] I. Takahashi and Y. Ohmori, "High-performance direct torque control of an induction motor," *IEEE Trans. Ind. Applicat.*, vol. 25, pp. 257–264, 1989.
- [88] Blaschke, Felix. "The principle of field orientation as applied to the new TRANSVECTOR closed loop control system for rotating field machines." *Siemens review* 34, no. 5 (1972): 217-220.
- [89] S. Tammaruckwattana, K. Ohyama and C. Yue, "Experimental Assessment with Wind Turbine Emulator of Variable-Speed Wind Power Generation System using Boost Chopper Circuit of Permanent Magnet Synchronous Generator," *Journal of Power Electronics*, 2014
- [90] Johnson G.L "Wind Turbine Power, Energy, and Torque," *In Wind Energy System*, Electrical Edition ed. Prentice-Hall Englewood Cliffs (NJ), pp. 4-1-4-54. (2006).

Appendix-A

FPGA control for PWM converter

```
library ieee;
use ieee.std_logic_1164.all;
use ieee.std_logic_unsigned.all;

entity siba is

    port(
        IU,IV,IW,CU,CV,CW,clk : in std_logic;
        IUP,IUN,IVP,IVN,IWP,IWN : out std_logic;
        CUP,CUN,CVP,CVN,CWP,CWN : out std_logic);

end siba;

architecture rtl of siba is

    signal
        counter_IUP,counter_IUN,counter_IVP,counter_IVN,counter_IWP,counter_IWN :
        std_logic_vector(7 downto 0);
    signal
        counter_CUP,counter_CUN,counter_CVP,counter_CVN,counter_CWP,counter_CWN:s
        td_logic_vector(7 downto 0);
    signal IUa,IUb,IUa_r,IUb_r,IUP_s,IUN_s : std_logic;
    signal IVa,IVb,IVa_r,IVb_r,IVP_s,IVN_s : std_logic;
    signal IWa,IWb,IWa_r,IWb_r,IWP_s,IWN_s : std_logic;
```


FPGA CORD

```
signal CUa,CUb,CUa_r,CUb_r,CUP_s,CUN_s : std_logic;
signal CVa,CVb,CVa_r,CVb_r,CVP_s,CVN_s : std_logic;
signal CWA,CWb,CWa_r,CWb_r,CWP_s,CWN_s : std_logic;
```

```
begin
```

```
    --Synchronization of signal--
```

```
    process (clk)
```

```
    begin
```

```
        if (clk'event and clk = '1') then
```

```
            IUa <= IU;
```

```
            IUa_r <= not IUa;
```

```
            IUb <= not IU;
```

```
            IUb_r <=not IUb;
```

```
            IVa <= IV;
```

```
            IVa_r <= not IVa;
```

```
            IVb <= not IV;
```

```
            IVb_r <=not IVb;
```

```
            IWa <= IW;
```

```
            IWa_r <= not IWa;
```

```
            IWb <= not IW;
```

```
            IWb_r <=not IWb;
```

```
            CUa <= CU;
```

```
            CUa_r <= not CUa;
```

```
            CUb <= not CU;
```

```
            CUb_r <=not CUb;
```

```
            CVa <= CV;
```

```
            CVa_r <= not CVa;
```

```
            CVb <= not CV;
```

```
            CVb_r <=not CVb;
```

```
CWa <= CW;
CWa_r <= not CWa;
CWb <= not CW;
CWb_r <=not CWb;
end if;
end process;

--count program--          % Inverter side with reset counter
process (clk)
begin
    --INV--
--IU pulse counter
    if ((IUa and IUa_r) = '1') then
        counter_IUP <= "00000000";
    elsif (clk'event and clk = '1') then
        counter_IUP <= counter_IUP + '1';
    end if;

    if ((IUb and IUb_r) = '1') then
        counter_IUN <= "00000000";
    elsif (clk'event and clk = '1') then
        counter_IUN <= counter_IUN + '1';
    end if;

--IV pulse counter
    if ((IVa and IVa_r) = '1') then
        counter_IVP <= "00000000";
    elsif (clk'event and clk = '1') then
        counter_IVP <= counter_IVP + '1';
    end if;

    if ((IVb and IVb_r) = '1') then
        counter_IVN <= "00000000";
```

```
    elsif (clk'event and clk = '1') then
        counter_IVN <= counter_IVN + '1';
    end if;

--IW pulse counter
    if ((IWa and IWa_r) = '1') then
        counter_IWP <= "00000000";
    elsif (clk'event and clk = '1') then
        counter_IWP <= counter_IWP + '1';
    end if;

    if ((IWb and IWb_r) = '1') then
        counter_IWN <= "00000000";
    elsif (clk'event and clk = '1') then
        counter_IWN <= counter_IWN + '1';
    end if;

        --CNV--                                % Converter side with reset counter
--CU pulse counter
    if ((CUa and CUa_r) = '1') then
        counter_CUP <= "00000000";
    elsif (clk'event and clk = '1') then
        counter_CUP <= counter_CUP + '1';
    end if;

    if ((CUb and CUb_r) = '1') then
        counter_CUN <= "00000000";
    elsif (clk'event and clk = '1') then
        counter_CUN <= counter_CUN + '1';
    end if;

--CV pulse counter
    if ((CVa and CVa_r) = '1') then
```

FPGA CORD

```
        counter_CVP <= "00000000";
    elsif (clk'event and clk = '1') then
        counter_CVP <= counter_CVP + '1';
    end if;

    if ((CVb and CVb_r) = '1') then
        counter_CVN <= "00000000";
    elsif (clk'event and clk = '1') then
        counter_CVN <= counter_CVN + '1';
    end if;

--CW pulse counter
    if ((CWA and CWA_r) = '1') then
        counter_CWP <= "00000000";
    elsif (clk'event and clk = '1') then
        counter_CWP <= counter_CWP + '1';
    end if;

    if ((CWb and CWb_r) = '1') then
        counter_CWN <= "00000000";
    elsif (clk'event and clk = '1') then
        counter_CWN <= counter_CWN + '1';
    end if;
end process;

--Shift proglam(dead time)--
process (clk)
begin
    --INV--                                % Inverter side with Enable registers
--IU pulse
    if (clk'event and clk = '1') then
        if (counter_IUP = "01110011") then
            IUP_s <= IUA;
        elsif (counter_IUN = "01110011") then
```

FPGA CORD

```
        IUN_s <= IUb;
    end if;
end if;

--IV pulse
if (clk'event and clk = '1') then
    if (counter_IVP = "01110011") then
        IVP_s <= IVa;
    elsif (counter_IVN = "01110011") then
        IVN_s <= IVb;
    end if;
end if;

--IW pulse
if (clk'event and clk = '1') then
    if (counter_IWP = "01110011") then
        IWP_s <= IWa;
    elsif (counter_IWN = "01110011") then
        IWN_s <= IWb;
    end if;
end if;

        --CVN--                                % Converter side with Enable registers
--CU pulse
if (clk'event and clk = '1') then
    if (counter_CUP = "01110011") then
        CUP_s <= CUa;
    elsif (counter_CUN = "01110011") then
        CUN_s <= CUb;
    end if;
end if;

--CV pulse
if (clk'event and clk = '1') then
```

FPGA CORD

```
    if (counter_CVP = "01110011") then
        CVP_s <= CVa;
    elsif (counter_CVN = "01110011") then
        CVN_s <= CVb;
    end if;
end if;

--CW pulse
if (clk'event and clk = '1') then
    if (counter_CWP = "01110011") then
        CWP_s <= CWa;
    elsif (counter_CWN = "01110011") then
        CWN_s <= CWb;
    end if;
end if;
end process;

        --Output signal--
--INV                                     % Inverter side output
    IUP <= IUP_s and IUa;
    IUN <= IUN_s and IUb;
    IVP <= IVP_s and IVa;
    IVN <= IVN_s and IVb;
    IWP <= IWP_s and IWa;
    IWN <= IWN_s and IWb;

--CVN                                     % converter side output
    CUP <= CUP_s and CUa;
    CUN <= CUN_s and CUb;
    CVP <= CVP_s and CVa;
    CVN <= CVN_s and CVb;
    CWP <= CWP_s and CWa;
    CWN <= CWN_s and CWb;
end rtl;
```

Appendix-B

FPGA control for Boost chopper converter

```
library ieee;
```

```
use ieee.std_logic_1164.all;
```

```
use ieee.std_logic_unsigned.all;
```

```
entity siba is
```

```
port(
```

```
    IU,IV,IW,CU,clk : in std_logic;
```

```
    IUP,IUN,IVP,IVN,IWP,IWN : out std_logic;
```

```
    CUP : out std_logic);
```

```
end siba;
```

```
architecture rtl of siba is
```

```
    signal counter_IUP,counter_IUN,counter_IVP,counter_IVN,counter_IWP,counter_IWN :
```

```
    std_logic_vector(7 downto 0);
```

```
    signal counter_CUP : std_logic_vector(7 downto 0);
```

```
signal IUa,IUb,IUa_r,IUb_r,IUP_s,IUN_s : std_logic;

signal IVa,IVb,IVa_r,IVb_r,IVP_s,IVN_s : std_logic;

signal IWa,IWb,IWa_r,IWb_r,IWP_s,IWN_s : std_logic;

signal CUa,CUb,CUa_r,CUb_r,CUP_s : std_logic;

begin

    --Synchronization of signal--

    process (clk)

    begin

        if (clk'event and clk = '1') then

            IUa <= IU;

            IUa_r <= not IUa;

            IUb <= not IU;

            IUb_r <=not IUb;

            IVa <= IV;

            IVa_r <= not IVa;

            IVb <= not IV;

            IVb_r <=not IVb;

            IWa <= IW;

            IWa_r <= not IWa;

            IWb <= not IW;
```



```
IWb_r <=not IWb;

CUa <= CU;

CUa_r <= not CUa;

CUb <= not CU;

CUb_r <=not CUb;

end if;

end process;

--count program--           % Inverter side with reset counter
process (clk)

begin

    --INV--

--IU pulse counter

    if ((IUa and IUa_r) = '1') then

        counter_IUP <= "00000000";

    elsif (clk'event and clk = '1') then

        counter_IUP <= counter_IUP + '1';

    end if;

    if ((IUb and IUb_r) = '1') then

        counter_IUN <= "00000000";
```

```
    elsif (clk'event and clk = '1') then

        counter_IUN <= counter_IUN + '1';

    end if;

--IV pulse counter

    if ((IVa and IVa_r) = '1') then

        counter_IVP <= "00000000";

    elsif (clk'event and clk = '1') then

        counter_IVP <= counter_IVP + '1';

    end if;

    if ((IVb and IVb_r) = '1') then

        counter_IVN <= "00000000";

    elsif (clk'event and clk = '1') then

        counter_IVN <= counter_IVN + '1';

    end if;

--IW pulse counter

    if ((IWa and IWa_r) = '1') then

        counter_IWP <= "00000000";

    elsif (clk'event and clk = '1') then

        counter_IWP <= counter_IWP + '1';

    end if;
```

```
if ((IWb and IWb_r) = '1') then

    counter_IWN <= "00000000";

elsif (clk'event and clk = '1') then

    counter_IWN <= counter_IWN + '1';

end if;

--DUTY--                                % Duty ratio side with reset counter
--DUTY pulse counter

if ((CUa and CUa_r) = '1') then

    counter_CUP <= "00000000";

elsif (clk'event and clk = '1') then

    counter_CUP <= counter_CUP + '1';

end if;

end process;

--Shift proglam(dead time)--

process (clk)

begin
```

```
--INV--                                % Inverter side with Enable registers

--IU pulse

if (clk'event and clk = '1') then

    if (counter_IUP = "01110011") then

        IUP_s <= IUa;

    elsif (counter_IUN = "01110011") then

        IUN_s <= IUb;

    end if;

end if;

--IV pulse

if (clk'event and clk = '1') then

    if (counter_IVP = "01110011") then

        IVP_s <= IVa;

    elsif (counter_IVN = "01110011") then

        IVN_s <= IVb;

    end if;

end if;

--IW pulse
```

```
if (clk'event and clk = '1') then

    if (counter_IWP = "01110011") then

        IWP_s <= IWa;

    elsif (counter_IWN = "01110011") then

        IWN_s <= IWb;

    end if;

end if;

--DUTY--                                % Duty ratio side with Enable registers

--DUTY palse

if (clk'event and clk = '1') then

    if (counter_CUP = "01110011") then

        CUP_s <= CUa;

    end if;

end if;

end process;

--Output signal--

--INV                                    % Inverter side output

IUP <= IUP_s and IUa;
```

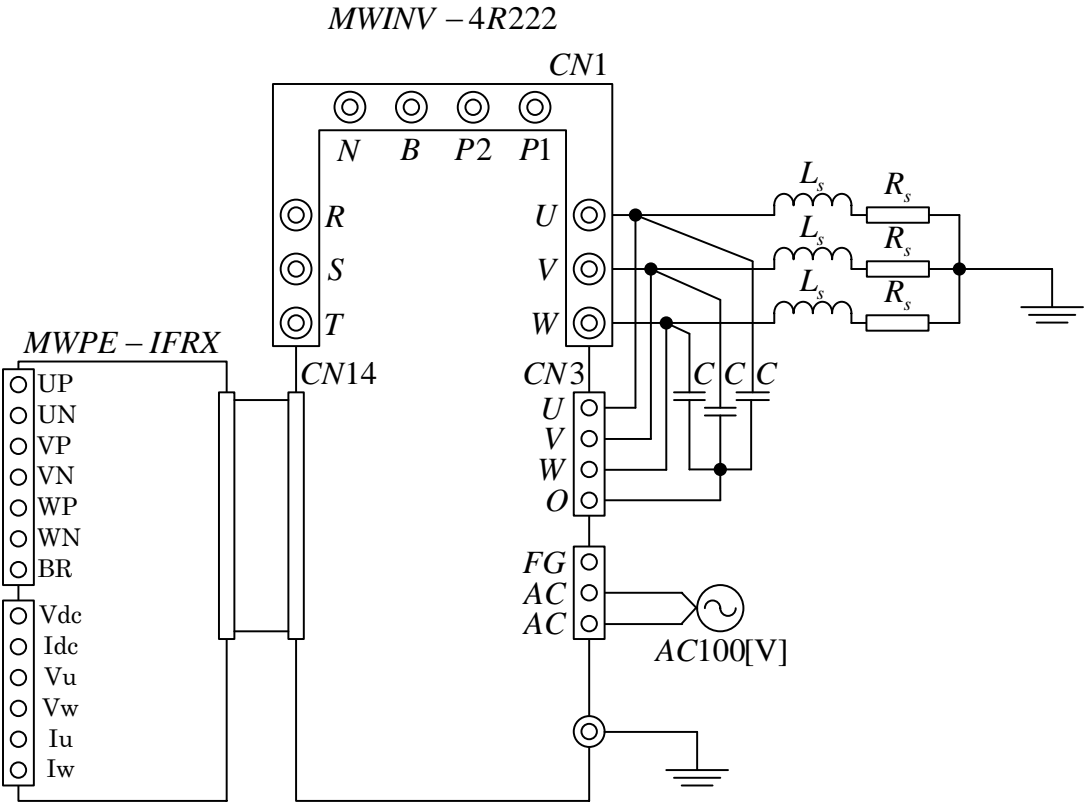
Appendix-C

Rotary Encoder Parameter of omron

| Item/Type | E6C3-CWZ3XH |
|------------------------------|---|
| Supply voltage | 5 to 12 V DC (+10% -5%) |
| Current consumption | 100mA max |
| Output circuit configuration | Line driver output |
| Output capacity | "H" level output voltage : 2.5V min. (at output current : -10mA) |
| | "L" level output voltage : 0.5V max. (at output current : 10mA) |
| | |
| Maximum response frequency | 125kHz |
| Phase difference of output | 90±45° between output A and B |
| Starting torque | 10mH·m |
| Moment of inertia | 2.0×10 ⁻⁶ kg·m ² |
| Slewing speed | 5000r/min |
| Shaft loading | Radial : 80N Axial : 50N |
| Ambient temperature | -10 to +70°C |
| Ambient humidity | 35 to 85%RH |
| Degree of protection | IEC60529 : IP65 |

Appendix-D

MWINV-4R222 (Myway Labs Co., Ltd)



Appendix-E

Anemometer CYG-5103VM

| | |
|-----------------------|--|
| Type equation | CYG-5103VM |
| Feature | Voltage output |
| Recommended use | About 30m distance |
| Wind speed output | 0-1V/0-5V/0-50m/s |
| | 0-1V/0-5V/0-100m/s (optional) |
| Wind direction output | 0-1V/0-5V/0-360 ° |
| Power | 8-24VDC |
| | 5mA @ 12VDC |
| Cable | (LM is ok in a two-core * 2 pairs) outer diameter 7mmφ within 0.5mm ^ 2 2-core twisted pair * 3 sets (6-core) shielded cable recommended weather |